The Large-Time Structure of the Solution to Initial-Value Problems for a Class of Burgers' Equations with Time Dependent Coefficients

by

Faiza Bait Ali Sulaiman

A thesis submitted to
The University of Birmingham
for the degree of
Doctor of Philosophy

School of Mathematics
The University of Birmingham
August 2018

Abstract

In this thesis we use the method of matched asymptotic coordinate expansions to examine in detail the structure of the large-time solution of initial-value problems based on a class of Burgers' equations with time dependent coefficients. The normalized nonlinear paritial differential equation considered is given by

$$u_t + t^{\delta} u u_x = u_{xx}, \quad -\infty < x < \infty, \quad t > 0.$$

where x and t represent dimensionless distance and time respectively, and δ (> -1) is a constant. In particular, we are interested in the emergence of coherent structures (composed of the expansion wave, Taylor shock wave profile, Rudenko-Soluyan wave profile, and the error function wave profile) in the large-time solution of the problems considered.

Acknowledgements

It is great to have this opportunity to express my appreciation to the people who played important roles for completion of this project. First, I want to thank my sponsor, Ministry of Higher Education in Sultanate of Oman (MOHE). I would like to thank my supervisors, Professor John A. Leach, Professor David J. Needham and Professor David Smith for their guidance, advice and patient during my PhD. I would also like to thank my colleagues in the School of Mathematics who I share with them happy and sad moments. I am grateful to Ms Janette Lowe for her help and support throughout my studies. Finally, I would like to sincerely thank my deceased Mum, who died last July, sisters and brothers for their love and encouragement. I want to thank my friend Diaa for her friendship.

List of Figures

1.1 The (α, β) parameter plane for $\alpha, \beta > -1$. We recall that $\delta = \frac{(\alpha-\beta)}{(\beta+1)}$. . . . 10

1.2 Graph of error function profile (1.49) when $u_+ = 1$ and $u_- = -1$. 17

1.3 Graph of the Rudenko-Soluyan implicit solution of (1.55) for $\gamma = 0$ when $\zeta_0 = 0.04,\ 1$ and 2.5. 19

1.4 Graph of the expansion wave profile (1.62) when $u_- = -1$ and $u_+ = 1$. . . 21

1.5 Graph of the Taylor shock profile (1.73) when $u_- = 1$ and $u_+ = -1$ (with translational invariance fixed by taking $\phi_c = 0$). 24

2.1 The (γ, δ) parameter plane. 34

2.2 A graph of $F(\xi)$ against ξ when $\gamma = 2$, $\delta = 1$ and $A_R = -1$. The solid line represents the solution $F(\xi)$ from (2.32) while the dashed line represents the solution $F(\xi) = (\delta + 1)\xi$. 39

2.3 The (F, F') phase plane for (2.37) with fixed A. (a) The case $A < 0$ and (b) the case $A = 0$. 43

2.4 A graph of $F = F^*(\xi)$ when (a) $\delta = 0.1$, $B^* = -3.05$, $C^* = 1.95$, (b) $\delta = 0.5$, $B^* = -2.32$, $C^* = 2.95$, (c) $\delta = 1.0$, $B^* = -1.95$, $C^* = 5.05$ and (d) $\delta = 2.0$, $B^* = -0.25$, $C^* = 7.15$. 44

2.5 A schematic representation of the asymptotic structure of $u(y,t)$ in the (y,u) plane as $t \to \infty$ for **IVP**$^+$ when $\delta > -\frac{1}{2}$. We note that $u = u_+ + O\left(t^{-r}\right)$ as $t \to \infty$ in region IV$^+$, while $u = u_- + O\left(t^{-r}\right)$ as $t \to \infty$ in region IV$^-$ with r given in (2.29). 48

2.7 A schematic representation of the asymptotic structure of $u(y,t)$ in the (y,u) plane as $t \to \infty$ for **IVP**$^+$ when $\delta = -\frac{1}{2}$ and $0 < \gamma < 1$. We recall that $y_l = -y_r = -t^{-\frac{\gamma}{2(1-\gamma)}}\, c(t)$, where $c(t)$ is given by (2.85). 62

2.8 A schematic representation of the asymptotic structure of $u(y,t)$ in the (y,u) plane as $t \to \infty$ for **IVP**$^+$ when $-1 < \delta < -\frac{1}{2}$ and $\gamma \geq 1$. We recall that $y_l = -y_r = -t^{(\delta+\frac{1}{2})}\, c(t)$, where $c(t)$ is given by (2.114). 75

2.9 Graphs of the numerical solution of **IVP**$^+$ in the (y,u) plane when $u_+ = 1$ and $u_- = -1$ at times $t = 5,\ 10,\ 20,\ 30,\ 40$ and 50 with (a) $\delta = 0.01$, $\gamma = 1$ and (b) $\delta = 0.5$, $\gamma = 1$. The graphs illustrate the development of the expansive wave with the solid lines showing the numerically computed solutions and the dash line representing theoretically predicted solution u_E is given by (2.62). 89

2.10 Graphs of the numerical solution of **IVP**$^+$ in the (y,u) plane when $u_+ = 1$ and $u_- = 0$ at times $t = 5,\ 10,\ 20,\ 30,\ 40$ and 50 with (a) $\delta = 0.01$, $\gamma = 1$ and (b) $\delta = 0.5$, $\gamma = 1$. The graphs illustrate the development of the expansive wave with the solid lines showing the numerically computed solutions and the dash line representing theoretically predicted solution u_E is given by (2.62). 91

2.11 Graphs of the numerical solution of **IVP**$^+$ in the (y, u) plane when $u_+ = 0$ and $u_- = -1$ at times $t = 5,\ 10,\ 20,\ 30,\ 40$ and 50 with (a) $\delta = 0.01$, $\gamma = 1$ and (b) $\delta = 0.5$, $\gamma = 1$. The graphs illustrate the development of the expansive wave with the solid lines showing the numerically computed solutions and the dash line representing theoretically predicted solution u_E is given by (2.62). 93

2.12 Graphs of the numerical solution of **IVP**$^+$ in the (y, u) plane when $u_+ = 1$ and $u_- = -1$ at times $t = 5,\ 10,\ 20,\ 30,\ 40$ and 50 with (a) $\delta = -0.5$, $\gamma = 0.5$ and (b) $\delta = -0.5$, $\gamma = 1$. We note that the numerically computed solutions represent the formation of the similarity solution found by Rudenko and Soluyan [32]. 95

2.13 Graphs of the numerical solution of **IVP**$^+$ in the (y, u) plane when $u_+ = 1$ and $u_- = 0$ at times $t = 5,\ 10,\ 20,\ 30,\ 40$ and 50 with (a) $\delta = -0.5$, $\gamma = 0.5$ and (b) $\delta = -0.5$, $\gamma = 1$. We note that the numerically computed solutions represent the formation of the similarity solution found by Rudenko and Soluyan [32] 97

2.14 Graphs of the numerical solution of **IVP**$^+$ in the (y, u) plane when $u_+ = 0$ and $u_- = -1$ at times $t = 5,\ 10,\ 20,\ 30,\ 40$ and 50 with (a) $\delta = -0.5$, $\gamma = 0.5$ and (b) $\delta = -0.5$, $\gamma = 1$. We note that the numerically computed solutions represent the formation of the similarity solution found by Rudenko and Soluyan [32] 99

2.15 Graphs of the numerical solution of **IVP**$^+$ in the (y, u) plane when $u_+ = 1$ and $u_- = -1$ at times $t = 5,\ 10,\ 20,\ 30,\ 40$ and 50 with (a) $\delta = -0.75$, $\gamma = 0.5$ and (b) $\delta = -0.75$, $\gamma = 1$. The graphs illustrate the numerically computed solutions and the theoretically predicted solution (dashed) $u_{\overline{R}}$ at $t = 50$. 101

2.16 Graphs of the numerical solution of $\mathbf{IVP}^+$ in the (y,u) plane when $u_+ = 1$ and $u_- = 0$ at times $t = 5,\ 10,\ 20,\ 30,\ 40$ and 50 with (a) $\delta = -0.75$, $\gamma = 0.5$ and (b) $\delta = -0.75$, $\gamma = 1$. The graphs illustrate the numerically computed solutions and the theoretically predicted solution (dashed) $u_{\overline{R}}$ at $t = 50$. 103

2.17 Graphs of the numerical solution of $\mathbf{IVP}^+$ in the (y,u) plane when $u_+ = 0$ and $u_- = -1$ at times $t = 5,\ 10,\ 20,\ 30,\ 40$ and 50 with (a) $\delta = -0.75$, $\gamma = 0.5$ and (b) $\delta = -0.75$, $\gamma = 1$. The graphs illustrate the numerically computed solutions and the theoretically predicted solution (dashed) $u_{\overline{R}}$ at $t = 50$. 105

3.1 A graph of the Taylor shock profile (3.13) when $u_- = 1$ and $u_+ = -1$ (with translational invariance fixed by taking $\phi_c = 0$). 112

3.2 A schematic representation of the asymptotic structure of $u(y,t)$ in the (y,u) plane as $t \to \infty$ for $\mathbf{IVP}^-$. We recall that region SS is located at $y = \frac{u_+ + u_-}{2(\delta+1)}$ (with thickness $O\left(t^{-(2\delta+1)}\right)$ as $t \to \infty$), while regions $\mathrm{TR}^{\pm}$ are located at $y = \frac{(u_+ + u_-)}{2(\delta+1)} \pm \frac{2\gamma(1+\delta)}{(u_- - u_+)} \frac{\ln t}{t^{2\delta+1}}$ (with thickness $O\left(t^{-(2\delta+1)}\right)$) as $t \to \infty$. 116

3.4 A schematic representation of the asymptotic structure of $u(y,t)$ in the (y,u) plane as $t \to \infty$ for $\mathbf{IVP}^-$ when $\delta = -\frac{1}{2}$ and $0 < \gamma < 1$. We recall that $y_l = -y_r = -t^{-\frac{\gamma}{2(1-\gamma)}}\ c(t)$, where $c(t)$ is given by (2.85). 121

3.5 A schematic representation of the asymptotic structure of $u(y,t)$ in the (y,u) plane as $t \to \infty$ for $\mathbf{IVP}^-$ when $-1 < \delta < -\frac{1}{2}$ and $\gamma \geq 1$. We recall that $y_l = -y_r = -t^{(\delta+\frac{1}{2})}\ c(t)$, where $c(t)$ is given by (2.114). 124

3.6 Graphs of the numerical solution of $\mathbf{IVP}^-$ in the (y,u) plane when $u_+ = -1$ and $u_- = 1$ at times $t = 5,\ 10,\ 20,\ 30,\ 40$ and 50 with (a) $\delta = -0.25$, $\gamma = 1$ and (b) $\delta = 0.01$, $\gamma = 1$. We note that the dashed line represents the theoretically predicted solution u_T is given by (3.24) at $t = 50$. 127

3.7 Graphs of the numerical solution of $\mathbf{IVP}^-$ in the (y, u) plane when $u_+ = 0$ and $u_- = 1$ at times $t = 5,\ 10,\ 20,\ 30,\ 40$ and 50 with (a) $\delta = -0.25$, $\gamma = 1$ and (b) $\delta = 0.5$, $\gamma = 1$. We note that the dashed line represents the theoretically predicted solution u_T is given by (3.24) at $t = 50$. 129

3.8 Graphs of the numerical solution of $\mathbf{IVP}^-$ in the (y, u) plane when $u_+ = -1$ and $u_- = 0$ at times $t = 5,\ 10,\ 20,\ 30,\ 40$ and 50 with (a) $\delta = -0.25$, $\gamma = 1$ and (b) $\delta = 0.5$, $\gamma = 1$. We note that the dashed line represents the theoretically predicted solution u_T is given by (3.24) at $t = 50$. 131

3.9 Graphs of the numerical solution of $\mathbf{IVP}^-$ in the (y, u) plane when $u_+ = -1$ and $u_- = 1$ at times $t = 5,\ 10,\ 20,\ 30,\ 40$ and 50 with (a) $\delta = -0.5$, $\gamma = 0.5$ and (b)$\delta = -0.5$, $\gamma = 1$. We note that the numerically computed solutions represent the formation of the similarity solution found by Rudenko and Soluyan [32]. 133

3.10 Graphs of the numerical solution of $\mathbf{IVP}^-$ in the (y, u) plane when $u_+ = 0$ and $u_- = 1$ at times $t = 5,\ 10,\ 20,\ 30,\ 40$ and 50 with (a) $\delta = -0.5$, $\gamma = 0.5$ and (b) $\delta = -0.5$, $\gamma = 1$. We note that the numerically computed solutions represent the formation of the similarity solution found by Rudenko and Soluyan [32]. 135

3.11 Graphs of the numerical solution of $\mathbf{IVP}^-$ in the (y, u) plane when $u_+ = -1$ and $u_- = 0$ at times $t = 5,\ 10,\ 20,\ 30,\ 40$ and 50 with (a) $\delta = -0.5$, $\gamma = 0.5$ and (b)$\delta = -0.5$, $\gamma = 1$. We note that the numerically computed solutions represent the formation of the similarity solution found by Rudenko and Soluyan [32]. 137

3.12 Graphs of the numerical solution of **IVP**$^-$ in the (y,u) plane when$u_+ = -1$ and $u_- = 1$ at times $t = 5,\ 10,\ 20,\ 30,\ 40$ and 50 with (a) $\delta = -0.75$, $\gamma = 0.5$ and (b) $\delta = -0.75$, $\gamma = 1$. The graphs illustrate the numerically computed solutions and the theoretically predicted solution (dashed) $u_{\overline{R}}$ at $t = 50$. 139

3.13 Graphs of the numerical solution of **IVP**$^-$ in the (y,u) plane when$u_+ = 0$ and $u_- = 1$ at times $t = 5,\ 10,\ 20,\ 30,\ 40$ and 50 with (a) $\delta = -0.75$, $\gamma = 0.5$ and (b) $\delta = -0.75$, $\gamma = 1$. The graphs illustrate the numerically computed solutions and the theoretically predicted solution (dashed) $u_{\overline{R}}$ at $t = 50$. 141

3.14 Graphs of the numerical solution of **IVP**$^-$ in the (y,u) plane when $u_+ = -1$ and $u_- = 0$ at times $t = 5,\ 10,\ 20,\ 30,\ 40$ and 50 with (a) $\delta = -0.75$, $\gamma = 0.5$ and (b) $\delta = -0.75$, $\gamma = 1$. The graphs illustrate the numerically computed solutions and the theoretically predicted solution (dashed) $u_{\overline{R}}$ at $t = 50$. 143

1 Graphs of the numerical solution of **IVP**$^+$ in the (y,u) plane when $u_+ = 1$ and $u_- = -1$ at times $t = 5,\ 10,\ 20,\ 30,\ 40$ and 50 with (a) $\delta = 0.01$, $\gamma = 1$, $\triangle x = 0.5$ and $\triangle t = 0.005$, (b) $\delta = 0.01$, $\gamma = 1$, $\triangle x = 0.25$ and $\triangle t = 0.01$, (c) $\delta = 0.5$, $\gamma = 1$, $\triangle x = 0.5$ and $\triangle t = 0.005$ and (d) $\delta = 0.5$, $\gamma = 1$, $\triangle x = 0.25$ and $\triangle t = 0.01$. We note that the numerically computed solutions represent the expansive wave with the solid lines and the dash line representing theoretically predicted solution u_E is given by (2.62). . . . 152

2 Graphs of the numerical solution of **IVP**$^+$ in the (y, u) plane when $u_+ = 1$ and $u_- = 0$ at times $t = 5,\ 10,\ 20,\ 30,\ 40$ and 50 with (a) $\delta = 0.01$, $\gamma = 1$, $\triangle x = 0.5$ and $\triangle t = 0.005$, (b) $\delta = 0.01$, $\gamma = 1$, $\triangle x = 0.25$ and $\triangle t = 0.01$, (c) $\delta = 0.5$, $\gamma = 1$, $\triangle x = 0.5$ and $\triangle t = 0.005$ and (d) $\delta = 0.5$, $\gamma = 1$, $\triangle x = 0.25$ and $\triangle t = 0.01$. We note that the numerically computed solutions represent the expansive wave with the solid lines and the dash line representing theoretically predicted solution u_E is given by (2.62). . . . 153

3 Graphs of the numerical solution of **IVP**$^+$ in the (y, u) plane when $u_+ = 0$ and $u_- = -1$ at times $t = 5,\ 10,\ 20,\ 30,\ 40$ and 50 with (a) $\delta = 0.01$, $\gamma = 1$, $\triangle x = 0.5$ and $\triangle t = 0.005$, (b) $\delta = 0.01$, $\gamma = 1$, $\triangle x = 0.25$ and $\triangle t = 0.01$, (c) $\delta = 0.5$, $\gamma = 1$, $\triangle x = 0.5$ and $\triangle t = 0.005$ and (d) $\delta = 0.5$, $\gamma = 1$, $\triangle x = 0.25$ and $\triangle t = 0.01$. We note that the numerically computed solutions represent the expansive wave with the solid lines and the dash line representing theoretically predicted solution u_E is given by (2.62). . . . 154

4 Graphs of the numerical solution of **IVP**$^+$ in the (y, u) plane when $u_+ = 1$ and $u_- = -1$ at times $t = 5,\ 10,\ 20,\ 30,\ 40$ and 50 with (a) $\delta = -0.5$, $\gamma = 0.5$, $\triangle x = 0.5$ and $\triangle t = 0.005$, (b) $\delta = -0.5$, $\gamma = 0.5$, $\triangle x = 0.25$ and $\triangle t = 0.01$, (c) $\delta = -0.5$, $\gamma = 1$, $\triangle x = 0.5$ and $\triangle t = 0.005$ and (d) $\delta = -0.5$, $\gamma = 1$, $\triangle x = 0.25$ and $\triangle t = 0.01$. We note that the numerically computed solutions represent the formation of the similarity solution found by Rudenko and Soluyan [32]. 156

5 Graphs of the numerical solution of **IVP**$^+$ in the (y, u) plane when $u_+ = 1$ and $u_- = 0$ at times $t = 5,\ 10,\ 20,\ 30,\ 40$ and 50 with (a) $\delta = -0.5$, $\gamma = 0.5$, $\triangle x = 0.5$ and $\triangle t = 0.005$, (b) $\delta = -0.5$, $\gamma = 0.5$, $\triangle x = 0.25$ and $\triangle t = 0.01$, (c) $\delta = -0.5$, $\gamma = 1$, $\triangle x = 0.5$ and $\triangle t = 0.005$ and (d) $\delta = -0.5$, $\gamma = 1$, $\triangle x = 0.25$ and $\triangle t = 0.01$. We note that the numerically computed solutions represent the formation of the similarity solution found by Rudenko and Soluyan [32]. 157

6 Graphs of the numerical solution of **IVP**$^+$ in the (y, u) plane when $u_+ = 0$ and $u_- = -1$ at times $t = 5,\ 10,\ 20,\ 30,\ 40$ and 50 with (a) $\delta = -0.5$, $\gamma = 0.5$, $\triangle x = 0.5$ and $\triangle t = 0.005$, (b) $\delta = -0.5$, $\gamma = 0.5$, $\triangle x = 0.25$ and $\triangle t = 0.01$, (c) $\delta = -0.5$, $\gamma = 1$, $\triangle x = 0.5$ and $\triangle t = 0.005$ and (d) $\delta = -0.5$, $\gamma = 1$, $\triangle x = 0.25$ and $\triangle t = 0.01$. We note that the numerically computed solutions represent the formation of the similarity solution found by Rudenko and Soluyan [32]. 158

7 Graphs of the numerical solution of **IVP**$^+$ in the (y, u) plane when $u_+ = 1$ and $u_- = -1$ at times $t = 5,\ 10,\ 20,\ 30,\ 40$ and 50 with (a) $\delta = -0.75$, $\gamma = 0.5$, $\triangle x = 0.5$ and $\triangle t = 0.005$, (b) $\delta = -0.75$, $\gamma = 0.5$, $\triangle x = 0.25$ and $\triangle t = 0.01$, (c) $\delta = -0.75$, $\gamma = 1$, $\triangle x = 0.5$ and $\triangle t = 0.005$ and (d) $\delta = -0.75$, $\gamma = 1$, $\triangle x = 0.25$ and $\triangle t = 0.01$. We note that the numerical solution converges to an error function profile as $t \to \infty$ and the dash line representing the theoretically predicted solution $u_{\overline{R}}$ (3.25) at $t = 50$. 160

8 Graphs of the numerical solution of **IVP**$^+$ in the (y, u) plane when $u_+ = 1$ and $u_- = 0$ at times $t = 5,\ 10,\ 20,\ 30,\ 40$ and 50 with (a) $\delta = -0.75$, $\gamma = 0.5$, $\triangle x = 0.5$ and $\triangle t = 0.005$, (b) $\delta = -0.75$, $\gamma = 0.5$, $\triangle x = 0.25$ and $\triangle t = 0.01$, (c) $\delta = -0.75$, $\gamma = 1$, $\triangle x = 0.5$ and $\triangle t = 0.005$ and (d) $\delta = -0.75$, $\gamma = 1$, $\triangle x = 0.25$ and $\triangle t = 0.01$. We note that the numerical solution converges to an error function profile as $t \to \infty$ and the dash line representing the theoretically predicted solution $u_{\overline{R}}$ (3.25) at $t = 50$. 161

9 Graphs of the numerical solution of **IVP**$^+$ in the (y, u) plane when $u_+ = 0$ and $u_- = -1$ at times $t = 5,\ 10,\ 20,\ 30,\ 40$ and 50 with (a) $\delta = -0.75$, $\gamma = 0.5$, $\triangle x = 0.5$ and $\triangle t = 0.005$, (b) $\delta = -0.75$, $\gamma = 0.5$, $\triangle x = 0.25$ and $\triangle t = 0.01$, (c) $\delta = -0.75$, $\gamma = 1$, $\triangle x = 0.5$ and $\triangle t = 0.005$ and (d) $\delta = -0.75$, $\gamma = 1$, $\triangle x = 0.25$ and $\triangle t = 0.01$. We note that the numerical solution converges to an error function profile as $t \to \infty$ and the dash line representing the theoretically predicted solution $u_{\overline{R}}$ (3.25) at $t = 50$. 162

10 Graphs of the numerical solution of **IVP**$^-$ in the (y, u) plane when $u_+ = -1$ and $u_- = 1$ at times $t = 5,\ 10,\ 20,\ 30,\ 40$ and 50 with (a) $\delta = -0.25$, $\gamma = 1$, $\triangle x = 0.5$ and $\triangle t = 0.005$, (b) $\delta = -0.25$, $\gamma = 1$, $\triangle x = 0.25$ and $\triangle t = 0.01$, (c) $\delta = 0.01$, $\gamma = 1$, $\triangle x = 0.5$ and $\triangle t = 0.005$ and (d) $\delta = 0.01$, $\gamma = 1$, $\triangle x = 0.25$ and $\triangle t = 0.01$. We note that the numerical solution converges to Taylor shock wave as $t \to \infty$ and the dash line representing the theoretically predicted solution u_T (3.24) at $t = 50$. 165

11 Graphs of the numerical solution of **IVP**$^-$ in the (y, u) plane when $u_+ = 0$ and $u_- = 1$ at times $t = 5,\ 10,\ 20,\ 30,\ 40$ and 50 with (a) $\delta = -0.25$, $\gamma = 1$, $\triangle x = 0.5$ and $\triangle t = 0.005$, (b) $\delta = -0.25$, $\gamma = 1$, $\triangle x = 0.25$ and $\triangle t = 0.01$, (c) $\delta = 0.01$, $\gamma = 1$, $\triangle x = 0.5$ and $\triangle t = 0.005$ and (d) $\delta = 0.01$, $\gamma = 1$, $\triangle x = 0.25$ and $\triangle t = 0.01$. We note that the numerical solution converges to Taylor shock wave as $t \to \infty$ and the dash line representing the theoretically predicted solution u_T (3.24) at $t = 50$. 166

12 Graphs of the numerical solution of **IVP**$^-$ in the (y, u) plane when $u_+ = -1$ and $u_- = 0$ at times $t = 5,\ 10,\ 20,\ 30,\ 40$ and 50 with (a) $\delta = -0.25$, $\gamma = 1$, $\triangle x = 0.5$ and $\triangle t = 0.005$, (b) $\delta = -0.25$, $\gamma = 1$, $\triangle x = 0.25$ and $\triangle t = 0.01$, (c) $\delta = 0.01$, $\gamma = 1$, $\triangle x = 0.5$ and $\triangle t = 0.005$ and (d) $\delta = 0.01$, $\gamma = 1$, $\triangle x = 0.25$ and $\triangle t = 0.01$. We note that the numerical solution converges to Taylor shock wave as $t \to \infty$ and the dash line representing the theoretically predicted solution u_T (3.24) at $t = 50$. 167

13 Graphs of the numerical solution of **IVP**$^-$ in the (y, u) plane when $u_+ = -1$ and $u_- = 1$ at times $t = 5,\ 10,\ 20,\ 30,\ 40$ and 50 with (a) $\delta = -0.5$, $\gamma = 0.5$, $\triangle x = 0.5$ and $\triangle t = 0.005$, (b) $\delta = -0.5$, $\gamma = 0.5$, $\triangle x = 0.25$ and $\triangle t = 0.01$, (c) $\delta = -0.5$, $\gamma = 1$, $\triangle x = 0.5$ and $\triangle t = 0.005$ and (d)$\delta = -0.5$, $\gamma = 1$, $\triangle x = 0.25$ and $\triangle t = 0.01$. We note that the numerically computed solutions represent the formation of the similarity solution found by Rudenko and Soluyan [32]. 169

14 Graphs of the numerical solution of **IVP**$^-$ in the (y, u) plane when $u_+ = 0$ and $u_- = 1$ at times $t = 5,\ 10,\ 20,\ 30,\ 40$ and 50 with (a) $\delta = -0.5$, $\gamma = 0.5$, $\triangle x = 0.5$ and $\triangle t = 0.005$, (b) $\delta = -0.5$, $\gamma = 0.5$, $\triangle x = 0.25$ and $\triangle t = 0.01$, (c) $\delta = -0.5$, $\gamma = 1$, $\triangle x = 0.5$ and $\triangle t = 0.005$ and (d)$\delta = -0.5$, $\gamma = 1$, $\triangle x = 0.25$ and $\triangle t = 0.01$. We note that the numerically computed solutions represent the formation of the similarity solution found by Rudenko and Soluyan [32]. 170

15 Graphs of the numerical solution of **IVP**$^-$ in the (y, u) plane when $u_+ = -1$ and $u_- = 0$ at times $t = 5,\ 10,\ 20,\ 30,\ 40$ and 50 with (a) $\delta = -0.5$, $\gamma = 0.5$, $\triangle x = 0.5$ and $\triangle t = 0.005$, (b) $\delta = -0.5$, $\gamma = 0.5$, $\triangle x = 0.25$ and $\triangle t = 0.01$, (c) $\delta = -0.5$, $\gamma = 1$, $\triangle x = 0.5$ and $\triangle t = 0.005$ and (d)$\delta = -0.5$, $\gamma = 1$, $\triangle x = 0.25$ and $\triangle t = 0.01$. We note that the numerically computed solutions represent the formation of the similarity solution found by Rudenko and Soluyan [32]. 171

16 Graphs of the numerical solution of **IVP**$^-$ in the (y, u) plane when $u_+ = -1$ and $u_- = 1$ at times $t = 5,\ 10,\ 20,\ 30,\ 40$ and 50 with (a) $\delta = -0.75$, $\gamma = 0.5$, $\triangle x = 0.5$ and $\triangle t = 0.005$, (b) $\delta = -0.75$, $\gamma = 0.5$, $\triangle x = 0.25$ and $\triangle t = 0.01$, (c) $\delta = -0.75$, $\gamma = 1$, $\triangle x = 0.5$ and $\triangle t = 0.005$ and (d)$\delta = -0.75$, $\gamma = 1$, $\triangle x = 0.25$ and $\triangle t = 0.01$. We note that the numerical solution converges to an error function profile as $t \to \infty$ and the dash line representing the theoretically predicted solution $u_{\overline{R}}$ (3.25) at $t = 50$. 173

17 Graphs of the numerical solution of **IVP**$^-$ in the (y, u) plane when $u_+ = 0$ and $u_- = 10$ at times $t = 5,\ 10,\ 20,\ 30,\ 40$ and 50 with (a) $\delta = -0.75$, $\gamma = 0.5$, $\triangle x = 0.5$ and $\triangle t = 0.005$, (b) $\delta = -0.75$, $\gamma = 0.5$, $\triangle x = 0.25$ and $\triangle t = 0.01$, (c) $\delta = -0.75$, $\gamma = 1$, $\triangle x = 0.5$ and $\triangle t = 0.005$ and (d)$\delta = -0.75$, $\gamma = 1$, $\triangle x = 0.25$ and $\triangle t = 0.01$. We note that the numerical solution converges to an error function profile as $t \to \infty$ and the dash line representing the theoretically predicted solution $u_{\overline{R}}$ (3.25) at $t = 50$. 174

18 Graphs of the numerical solution of **IVP**$^-$ in the (y, u) plane when $u_+ = -1$ and $u_- = 0$ at times $t = 5,\ 10,\ 20,\ 30,\ 40$ and 50 with (a) $\delta = -0.75$, $\gamma = 0.5$, $\triangle x = 0.5$ and $\triangle t = 0.005$, (b) $\delta = -0.75$, $\gamma = 0.5$, $\triangle x = 0.25$ and $\triangle t = 0.01$, (c) $\delta = -0.75$, $\gamma = 1$, $\triangle x = 0.5$ and $\triangle t = 0.005$ and (d)$\delta = -0.75$, $\gamma = 1$, $\triangle x = 0.25$ and $\triangle t = 0.01$. We note that the numerical solution converges to an error function profile as $t \to \infty$ and the dash line representing the theoretically predicted solution $u_{\overline{R}}$ (3.25) at $t = 50$. 175

List of Tables

1.1 The type of large-time attractor connecting u_+ to u_- in the solution of initial-value problem (1.74)-(1.77) for $\delta > -1$. 26

2.1 The values of the constants B^* and C^* with the associated values of δ when $\gamma > 2\delta + 1$. 42

2.3 The values of the constants $\mathcal{C}_+$ and $\mathcal{C}_-$ corresponding to Figure 2.6. 57

3.2 The values of the constants $\mathcal{C}_+$ and $\mathcal{C}_-$ corresponding to Figure 3.3. 119

1 Numerical convergence test between the numerical solutions of $\mathbf{IVP}^+$ with $\triangle x = 0.5$, $\triangle t = 0.01$, the numerical solutions of $\mathbf{IVP}^+$ with $\triangle x = 0.5$, $\triangle t = 0.005$ and the numerical solutions of $\mathbf{IVP}^+$ with $\triangle x = 0.25$, $\triangle t = 0.01$, respectively, when $\delta > -\frac{1}{2}$ and $\gamma = 1$ at $t = 50$. Values quoted are root mean square error on holding time and space steps respectively. 155

2 Numerical convergence test between the numerical solutions of $\mathbf{IVP}^+$ with $\triangle x = 0.5$, $\triangle t = 0.01$, the numerical solutions of $\mathbf{IVP}^+$ with $\triangle x = 0.5$, $\triangle t = 0.005$ and the numerical solutions of $\mathbf{IVP}^+$ with $\triangle x = 0.25$, $\triangle t = 0.01$, respectively, when $\delta = -\frac{1}{2}$ at $t = 50$. Values quoted are root mean square error on holding time and space steps respectively. 159

3 Numerical convergence test between the numerical solutions of $\mathbf{IVP}^+$ with $\triangle x = 0.5$, $\triangle t = 0.01$, the numerical solutions of $\mathbf{IVP}^+$ with $\triangle x = 0.5$, $\triangle t = 0.005$ and the numerical solutions of $\mathbf{IVP}^+$ with $\triangle x = 0.25$, $\triangle t = 0.01$, respectively, when $-1 < \delta < -\frac{1}{2}$ at $t = 50$. Values quoted are root mean square error on holding time and space steps respectively. 163

4 Numerical convergence test between the numerical solutions of $\mathbf{IVP}^-$ with $\triangle x = 0.5$, $\triangle t = 0.01$, the numerical solutions of $\mathbf{IVP}^-$ with $\triangle x = 0.5$, $\triangle t = 0.005$ and the numerical solutions of $\mathbf{IVP}^-$ with $\triangle x = 0.25$, $\triangle t = 0.01$, respectively, when $\delta > -\frac{1}{2}$ and $\gamma = 1$ at $t = 50$. Values quoted are root mean square error on holding time and space steps respectively. 168

5 Numerical convergence test between the numerical solutions of $\mathbf{IVP}^-$ with $\triangle x = 0.5$, $\triangle t = 0.01$, the numerical solutions of $\mathbf{IVP}^-$ with $\triangle x = 0.5$, $\triangle t = 0.005$ and the numerical solutions of $\mathbf{IVP}^-$ with $\triangle x = 0.25$, $\triangle t = 0.01$, respectively, when $\delta = -\frac{1}{2}$ at $t = 50$. Values quoted are root mean square error on holding time and space steps respectively. 172

6 Numerical convergence test between the numerical solutions of $\mathbf{IVP}^-$ with $\triangle x = 0.5$, $\triangle t = 0.01$, the numerical solutions of $\mathbf{IVP}^-$ with $\triangle x = 0.5$, $\triangle t = 0.005$ and the numerical solutions of $\mathbf{IVP}^-$ with $\triangle x = 0.25$, $\triangle t = 0.01$, respectively, when $-1 < \delta < -\frac{1}{2}$ at $t = 50$. Values quoted are root mean square error on holding time and space steps respectively. 176

Contents

1 Introduction **1**

1.1 Historical Review of Burgers' Equation 2

1.2 The Classical Burgers' Equation with Constant Coefficients 3

1.3 Discussion of Burgers' Equation when the Coefficients are Functions of Time 6

1.4 The Method of Matched Asymptotic Coordinate Expansions 12

1.5 Large-Time Attractors 13

1.5.1 Error Function 15

1.5.2 Rudenko-Soluyan Similarity Solution 17

1.5.3 Expansion Wave 20

1.5.4 Taylor Shock Wave 22

1.6 An Overview of the Mathematical Problems Considered 24

2 The Initial-Value Problem IVP$^+$ **27**

2.1 Asymptotic solution to **IVP$^+$** as $t \to 0$ 28

2.1.1 $\delta > 0$ 28

2.1.2 $-1 < \delta < 0$ 30

2.2 Asymptotic solution to **IVP$^+$** for $t = O(1)$ as

$|x| \to \infty$ 31

2.3 Asymptotic solution to **IVP$^+$** as $t \to \infty$ 35

2.3.1 $\delta > -\frac{1}{2}$ . . . 35
2.3.2 $\delta = -\frac{1}{2}$ . . . 52
2.3.3 $-1 < \delta < -\frac{1}{2}$ . . . 67
2.4 Numerical Solution to the Initial-Value Problem **IVP**$^+$ . . . 85
2.4.1 $\delta > -\frac{1}{2}, \quad \gamma > 0$ . . . 87
2.4.2 $\delta = -\frac{1}{2}, \quad \gamma > 0$ . . . 94
2.4.3 $-1 < \delta < -\frac{1}{2}, \quad \gamma > 0$ . . . 100
2.5 Summary . . . 106

3 The Initial-Value Problem IVP$^-$ 108

3.1 Asymptotic solution to **IVP**$^-$ as $t \to 0$ . . . 109
3.2 Asymptotic solution to **IVP**$^-$ as $|x| \to \infty$ . . . 109
3.3 Asymptotic solution to **IVP**$^-$ as $t \to \infty$ . . . 109
3.3.1 $\delta > -\frac{1}{2}$ . . . 110
3.3.2 $\delta = -\frac{1}{2}$ . . . 118
3.3.3 $-1 < \delta < -\frac{1}{2}$ . . . 122
3.4 Numerical Solution to the Initial-Value Problem **IVP**$^-$ . . . 125
3.4.1 $\delta > -\frac{1}{2}, \quad \gamma > 0$ . . . 126
3.4.2 $\delta = -\frac{1}{2}, \quad \gamma > 0$ . . . 132
3.4.3 $-1 < \delta < -\frac{1}{2}, \quad \gamma > 0$ . . . 138
3.5 Summary . . . 144

4 Conclusion 147

4.1 Thesis Review . . . 147
4.2 Future Work . . . 150
Appendix A: Convergence Test of Numerical Solution to the Initial-Value Problem **IVP**$^+$ . . . 151

A.1.1 $\delta > -\frac{1}{2}$ 152
A.1.2 $\delta = -\frac{1}{2}$ 156
A.1.3 $-1 < \delta < -\frac{1}{2}$ 160
Appendix B: Convergence Test of Numerical Solution to the Initial-Value Problem **IVP**$^-$ 164
B.2.1 $\delta > -\frac{1}{2}$ 165
B.2.2 $\delta = -\frac{1}{2}$ 169
B.2.3 $-1 < \delta < -\frac{1}{2}$ 173

List of References **176**

References **177**

Chapter 1

Introduction

Nonlinear evolution equations arise in the modelling of a wide range of physical phenomena. However, the vast majority of these nonlinear partial differential equations cannot be solved by existing methods (such as the inverse scattering method). Indeed, issues relating to the global existence and uniqueness of solutions to many important and well-studied nonlinear partial differential equations remain unresolved and are open areas of research. For equations for which no current methods of solution are applicable researchers must approach the initial-value or initial-boundary value problems based on these equations by a combination of numerical and asymptotic methods. This powerful combined approach often leads to a significant understanding of the large-time solution of the problem under investigation, and provides valuable information that analysts can use to develop new methods of solution.

In this thesis, we shall use the method of matched asymptotic coordinate expansions to obtain the complete large-time solution of an initial-value problem based on Burgers' equation when the coefficients are time dependent. Specifically, the case when the coefficients are algebraic functions of time will be discussed in detail. We note that this problem is not tractable by existing methods. Before specifying the problem to be considered in this thesis we begin by a historical review of Burgers' equation followed by reviewing the

classical Burgers' Equation.

1.1 Historical Review of Burgers' Equation

Burgers' equation plays a crucial role in applied mathematics, physics, mechanics and biology. It was first introduced by Bateman [6] in 1915 when he derived the classical Burgers' equation in a physical situation and obtained its steady solutions. In 1948, J.M. Burgers [10] emphasized the importance of this equation as a model in the theory of turbulence. Since then the classical Burgers' equation has found applications in many areas of research (including fluid dynamics [19, 31, 42, 44] and gas dynamics [2, 18]). Consequently many studies have analytically or numerically developed solutions for Burgers' equation. In 1951, Hopf [17] and Cole [11] independently noted the remarkable result that can transform Burgers' equation to the linear heat equation, which is known as the Cole-Hopf transformation. At the same time, Cole [11] found that the solution of Burgers' equation has the typical features of a shock wave, i.e. the nonlinear term of Burgers' equation tends to steepen the wave fronts, while the viscous term of Burgers' equation prevents the formation of actual discontinuities. In 1972, Benton and Platzman [8] presented specific exact solutions of the one dimensional Burgers' equation. At the same time, a Morgan-Michal method was applied to Burgers' equation by Ames [4] to determine the proper groups for Burgers' equation without taking the auxiliary conditions. Subsequently, in 1980, Varoglu and Finn [41] applied a new finite-element method based on the space-time elements and characteristics to solve numerically the Burgers' equation. In 1983, Weiss et al., [45] developed the Painlevé property for partial differential equations and showed how to determine the integrability, the Bäcklund transforms, the linearizing transforms, and the Lax pairs for Burgers' equation. From an applications perspective, Vorus [43] discussed the exact solutions to Burgers' equation on a moving medium with a sinusoidal excitation. Subsequently, in 1993, Peralta-Fabi and Plaschko

[30], studied the stability and the bifurcation of classes of solutions to Burgers' equation after adding an integral term, representing nonlocal behavior, to the normal form of the equation describing flow through porous media. From a computational perspective, in 1999, Kutluay, Bahadir and Ozdes [20] developed explicit and exact-explicit finite difference methods for the one-dimensional Burgers' equation. In 2010, a simple numerical method presented by Asaithambi [5] to compute the solution of the one-dimensional Burgers' equation by marched the solution in time using a Taylor series expansion. In 2012, a collocation method for solving Burgers' equation based on using modified cubic B-splines basis functions was developed by Mittal and Jain [27]. In 2013, Büyükasık and Pashaev [7], found and discussed exact solutions of Burgers' equations with time variable coefficients. In 2015, Hanac [15], studied the large-time solution of an initial-value problem and initial-boundary value problem for Burgers' equation with the constant coefficient by using method of matched asymptotic coordinate expansions. At the same year, a linearization method for Burgers equation with time dependent coefficients and nonlinear forcing term was investigated by Schulze-Halberg [35]. In this paper, the results were compared with the previously reported results in [7]. In 2016, Ali Suliman et al [3] presented the complete structure of the large-time solution of an initial-value problem and initial-boundary value problem for the Burgers' equation with variable coefficients by using method of matched asymptotic coordinate expansions. In this thesis the results that have found in [3] have been explained in detail.

1.2 The Classical Burgers' Equation with Constant Coefficients

Burgers' equation named after Johannes Martinus Burgers (1895 -1981) is given by

$$u_t + uu_x = \mu u_{xx} \tag{1.1}$$

where the parameter μ (> 0) is a measure of viscous diffusion, u is velocity, x and t represent distance and time respectively. Burgers' equation is a canonical equation combining both nonlinear and diffusive effects and as such arises in the modelling of a wide variety of physical phenomena. A short history of Burgers' equation is given in Section 1.1. It is convenient at this stage to non-dimensionalize equation (1.1). On writing

$$x = lx', \quad u = u_0 u', \quad t = \left(\frac{l}{u_0}\right)t', \tag{1.2}$$

where l is a typical length scale and u_0 is a typical scale for u, equation (1.1) becomes (on dropping the primes for convenience),

$$u_t + uu_x = Du_{xx} \tag{1.3}$$

where $D = \frac{\mu}{u_0 l}$ is a dimensionless parameter related to the Reynolds number via $Re = 1/D$.

We further note that the Cole-Hopf transformation (see [11] and [17]) allows the general solution to (1.3) to be obtained explicity. In particular, following [46], the initial-value problem

$$u_t + uu_x - Du_{xx} = 0, \quad -\infty < x < \infty, \quad t > 0, \tag{1.4}$$

$$u(x, 0) = F(x), \quad -\infty < x < \infty, \tag{1.5}$$

has the solution

$$u(x,t) = \frac{\int_{-\infty}^{\infty} (\frac{x-\eta}{t}) e^{-\frac{G}{2D}} d\eta}{\int_{-\infty}^{\infty} e^{-\frac{G}{2D}} d\eta} \tag{1.6}$$

where

$$G(\eta; x, t) = \frac{(x-\eta)^2}{2t} + \int_0^{\eta} F(\eta')d\eta'. \tag{1.7}$$

In the case of discontinuous initial data of the form

$$F(x) = \begin{cases} u_-, & x < 0, \\ u_+, & x > 0, \end{cases} \tag{1.8}$$

where $u_+ < u_-$, the solution can be written as

$$u(x,t) = u_+ + \frac{(u_- - u_+)}{1 + h(x,t)\ e^{\left[\frac{(u_- - u_+)}{2D}\left(x - \frac{(u_- + u_+)}{2}t\right)\right]}} \tag{1.9}$$

where

$$h(x,t) = \frac{\int_{-\frac{(x-u_+t)}{\sqrt{4Dt}}}^{\infty} e^{-\xi^2} d\xi}{\int_{\frac{(x-u_-t)}{\sqrt{4Dt}}}^{\infty} e^{-\xi^2} d\xi}. \tag{1.10}$$

For fixed $\frac{x}{t}$ in the range $u_+ < \frac{x}{t} < u_-$, the function $h(x,t) \to 1$ as $t \to \infty$, and the solution approaches the Taylor shock ([17])

$$u(x,t) = u_+ + \frac{(u_- - u_+)}{1 + \ e^{\left[\frac{(u_- - u_+)}{2D}\left(x - Ut\right)\right]}}, \quad \text{with} \quad U = \frac{(u_- + u_+)}{2}. \tag{1.11}$$

When $D = 0$ equation (1.4) becomes the inviscid Burgers' equation

$$u_t + uu_x = 0. \tag{1.12}$$

This equation is considered a prototype for nonlinear hyperbolic equations and conservation laws in general and it appears in studies of gas dynamics and traffic flow. It is important to note that the solution to equation (1.12) when the initial data has a discontinuous expansive step, given by

$$u(x,0) = \begin{cases} u_-, & x < 0, \\ u_+, & x > 0, \end{cases} \tag{1.13}$$

where $u_+ > u_-$, can be readily obtained (see for example [46])

$$u(x,t) = \begin{cases} u_-, & x < u_- t, \\ \frac{x}{t}, & u_- t < x < u_+ t, \\ u_+, & x > u_+ t. \end{cases} \tag{1.14}$$

which is known as a rarefaction wave.

However, it is important to note that in many applications of acoustic waves (see, for example [12] and [37]) the coefficient of uu_x in equation (1.3) is in fact regularly approximated by a constant when in fact it is a function of time. It is therefore clearly important to extend our knowledge of the classical Burgers' equation by considering Burgers' equation when the coefficients are functions of time.

1.3 Discussion of Burgers' Equation when the Coefficients are Functions of Time

In this thesis we consider an initial-value problem for Burgers' equation with time dependent coefficients [3], namely

$$u_t + \Phi(t) u u_x = \Psi(t) u_{xx}, \quad -\infty < x < \infty, \quad t > 0, \tag{1.15}$$

$$u(x,0) = u_0(x), \quad -\infty < x < \infty, \tag{1.16}$$

$$u(x,t) \to \begin{cases} u_-, & x \to -\infty, \\ u_+, & x \to \infty, \end{cases} \quad t \geq 0, \tag{1.17}$$

where u_- and u_+ ($\neq u_-$) are parameters and the functions $\Phi(t)$ and $\Psi(t)$ are algebraic functions of time t. Further, we consider the situation when the initial data $u_0 : \mathbb{R} \to \mathbb{R}$

is continuously differentiable and has algebraic decay as $|x| \to \infty$. Specifically,

$$u_0(x) = \begin{cases} u_+ + \frac{A_R}{(x)^\gamma} + O(E(|x|)) & \text{as } x \to \infty, \\ u_- + \frac{A_L}{(-x)^\gamma} + O(E(|x|)) & \text{as } x \to -\infty, \end{cases} \tag{1.18}$$

where $E(|x|)$ is linearly exponentially small in x as $|x| \to \infty$, A_R $(\neq 0)$, A_L $(\neq 0)$ and γ (> 0) are constants. We consider the cases when $u_+ > u_-$ and when $u_+ < u_-$ separately, with $A_R < 0$ and $A_L > 0$ when $u_+ > u_-$ and $A_R > 0$ and $A_L < 0$ when $u_+ < u_-$. We henceforth refer to the initial-value problem (1.15), (1.16) and (1.18) as **IVP**$^+$ when $u_+ > u_-$ and **IVP**$^-$ when $u_+ < u_-$. We note that equation (1.15) is related to the generalized Burgers' equation

$$v_\tau + vv_x + f(\tau)v = v_{xx}, \tag{1.19}$$

where $f(\tau) = \frac{d}{d\tau}\left(\ln \frac{\Psi}{\Phi} \right)$, via the transformation

$$v(x,\tau) = \frac{\Phi(t)}{\Psi(t)}\, u(x,t), \quad \tau = \int^t \Psi(s)\mathrm{d}s. \tag{1.20}$$

We observe that when $f(\tau) = 0$, equation (1.19) reduces to the classical Burgers' equation discussed in Section 1.2.

The generalized Burgers' equation (1.19) appears in many applications, (see [9, 22, 33, 34]) and has been discussed in many situations where $f(t) \neq 0$. For example, when $f(t) = -1$, equation (1.19) provides a simple model of nonlinear interaction of long wave pumping with short wave dissipation [16], while when $f(t) = \frac{\lambda}{t}$ (where λ is constant) equation (1.19) describes the propagation of finite-amplitude sound waves in ducts of variable cross sectional area ([13], [14], [29], [36]). However, it has been noted in [28] that there is no Bäcklund transformation for the generalized Burgers' equation (1.19), and

hence it is doubtful that a linearizing transformation such as the Cole-Hopf transformation exists in this case. Therefore, other methods of solution need to be investigated for this important class of equation.

In Leach [23], the complete large-time solution to $\mathbf{IVP}^+$ and $\mathbf{IVP}^-$ have been considered for the cases when

(i) $\Phi(t) = e^t, \qquad \Psi(t) = 1.$

(ii) $\Phi(t) = 1, \qquad \Psi(t) = e^t,$

via the method of matched asymptotic coordinate expansions. This analysis established that in case (i) the form of the large-time solutions of $\mathbf{IVP}^+$ and $\mathbf{IVP}^-$ depends on the problem parameters u_+ and u_-. In particular, when $u_+ > u_-$ the solution to the initial-value problem exhibits the formation of an expansion wave, while when $u_+ < u_-$ the solution to the initial-value problem exhibits the formation of a localized Taylor shock profile. In both cases the large-time attractor connects $u = u_+$ to $u = u_-$. In case (ii), the form of the large-time solution of $\mathbf{IVP}^+$ and $\mathbf{IVP}^-$ are independent of the problem parameters and exhibits the formation of an error function profile connecting $u = u_+$ to $u = u_-$.

In this thesis we extend the analysis presented in [23] and consider the case when

$$\Phi(t) = t^\delta \quad (\delta > -1), \qquad \Psi(t) = 1. \tag{1.21}$$

The objective is to obtain, via the method of matched asymptotic coordinate expansions, a uniform asymptotic approximation to the solution of initial-value problems $\mathbf{IVP}^+$ and $\mathbf{IVP}^-$ as $t \to \infty$. The methodology used follows that given in [25] and [26].

For completeness we note that there is no loss of generality in considering equation (1.15) (with (1.21)). To illustrate this point we consider the more general situation when

$\Phi(t) = t^\alpha$ ($\alpha > -1$) and $\Psi(t) = t^\beta$ ($\beta > -1$) where $\alpha \neq \beta$. In this case equation (1.15) becomes

$$u_t + t^\alpha u u_x = t^\beta u_{xx}. \tag{1.22}$$

On introducing the change of variables

$$u = (\beta+1)^{-\delta}\, U, \quad (\beta+1)\tau = t^{(\beta+1)}, \tag{1.23}$$

where

$$\delta = \frac{(\alpha-\beta)}{(\beta+1)} \quad (\in (-1,\infty)) \tag{1.24}$$

equation (1.22) becomes

$$U_t + \tau^\delta U U_x = U_{xx}, \tag{1.25}$$

where δ (> -1) is a constant. The relationship between the new parameter δ and the original parameters α and β is illustrated graphically in Figure 1.1. We will return to the (α, β) parameter plane given in Figure 1.1 later in this thesis when we relate the results regarding to equation (1.15) (with (1.21)) to equation (1.22).

Finally, as an illustration, it is interesting to consider a specific application [3]. We consider the dynamics of a linearly and weakly compressible viscous fluid, with time dependent viscosity, in one spatial dimension. With $\bar{u}$ being the fluid velocity field, the unidirectional evolution of initial finite amplitude disturbances is governed by the following Burgers' equation,

$$\bar{u}_t + \left(c_0 + \frac{\mu'(t)}{2\rho_0 c_0} + \frac{1}{2}\bar{u} \right) \bar{u}_x = \frac{\mu(t)}{2\rho_0} \bar{u}_{xx} \tag{1.26}$$

as $t > 0$ being time and $x \in \mathbb{R}$ being the spatial coordinate, whilst c_0 is the linearly compressive sound speed, ρ_0 is the ambient fluid density and $\mu(t)$ is the fluid viscosity. In

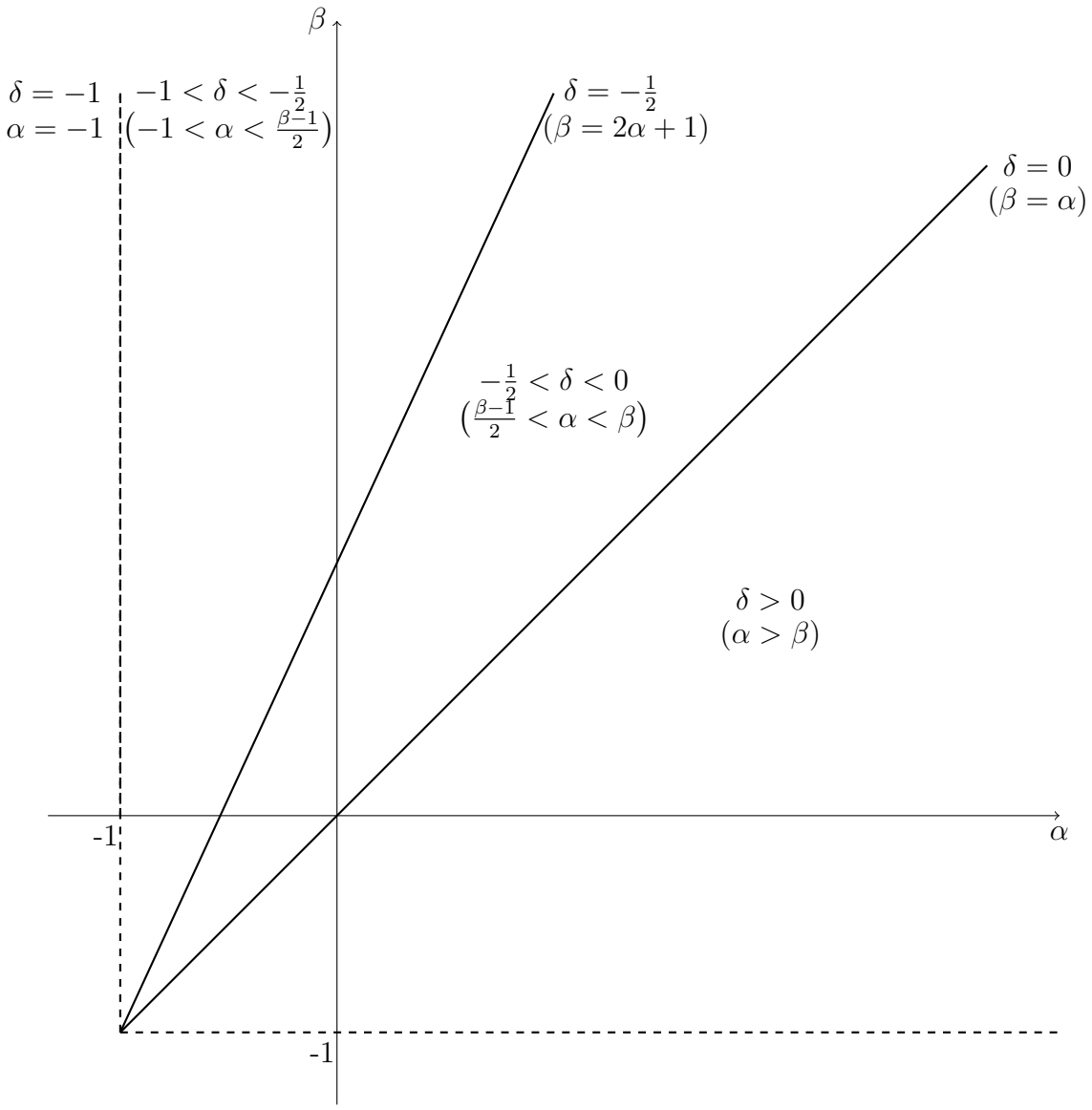

Figure 1.1: The (α, β) parameter plane for $\alpha, \beta > -1$. We recall that $\delta = \frac{(\alpha-\beta)}{(\beta+1)}$.

relation to this thesis, we give attention to the case where the fluid viscosity is time dependent, through, for example, increase or decrease in ambient temperature. In particular, we put,

$$\mu = \mu(t) = \mu_0 t^{\lambda} \tag{1.27}$$

with $\mu_0 > 0$ and $\lambda > -1$. Thus, the fluid viscosity is increasing with $t > 0$ when $\lambda > 1$, but decreasing with $t > 0$ when $-1 < \lambda < 0$. Now, introduce the simple transformation,

$$\begin{aligned} z =& x - \left(c_0 t + \frac{\mu_0 t^{\lambda}}{2\rho_0 c_0} \right), \\ \tau =& \frac{\mu_0}{2(1+\lambda)\rho_0} t^{(1+\lambda)}, \\ u =& (2(1+\lambda))^{-\frac{\lambda}{(1+\lambda)}} \left(\frac{\rho_0}{\mu_0} \right)^{\frac{\lambda}{(1+\lambda)}} \bar{u}. \end{aligned} \tag{1.28}$$

On substitution from (1.28), the partial differential equation (1.26) becomes

$$u_{\tau} + \tau^{-\frac{\lambda}{(1+\lambda)}} u u_z = u_{zz}, \quad -\infty < z < \infty, \quad \tau > 0, \tag{1.29}$$

which is now in the form of the generalized Burgers' equation considered in this thesis, with, for each $\lambda \in (-1, \infty)$,

$$\delta = -\frac{\lambda}{(1+\lambda)} \in (-1, \infty). \tag{1.30}$$

We observe from (1.30) that δ is a monotone decreasing function of λ, with $\delta \to \infty$ as

$\lambda \to -1^+$ and $\delta \to -1$ as $\lambda \to \infty$. In fact,

$$\begin{aligned} &\delta \in \left(-1, -\frac{1}{2}\right) \quad \text{when} \quad \lambda \in (1, \infty), \\ &\delta = -\frac{1}{2} \quad \text{when} \quad \lambda = 1, \\ &\delta \in \left(-\frac{1}{2}, \infty\right) \quad \text{when} \quad \lambda \in (-1, 1). \end{aligned} \tag{1.31}$$

For transition-type initial conditions, the theory developed in this thesis determines the detailed evolution of (1.26). Principally, we will observe that when $\lambda \in (1, \infty)$ an error function profile will develop as $\tau \to \infty$, for any $u_+ \lesseqgtr u_-$. However, for $\lambda = 1$, the Rudenko-Soluyan similarity profile will develop as $\tau \to \infty$, for any $u_+ \lesseqgtr u_-$. However, for $\lambda \in (-1, 1)$, a Taylor shock profile will develop as $\tau \to \infty$, when $u_+ < u_-$, but an expansion wave will develop as $\tau \to \infty$, when $u_+ > u_-$.

1.4 The Method of Matched Asymptotic Coordinate Expansions

Throughout this thesis we use the nomenclature of the theory of matched asymptotic expansions given in Van Dyke [40]. Asymptotic methods applied to nonlinear partial differential equations have a large and rich history, and we do not propose to review the literature on this broad topic here. Rather, we note that we will be primarily concerned with applying the methodology developed by J.A. Leach and D.J. Needham (see [24]) in the context of reaction-diffusion equations to the class of variable coefficient Burgers' equations considered in this thesis. We note that this methodology is far more generic than first thought and has been applied with success to give information about the structure and propagation speed of a wide range of nonlinear evolution equations (both with constant and variable coefficients) for example nonlinear diffusion equations of Fisher-Kolmogorov type. This methodology enables the complete large-time asymptotic structure of the solu-

tion to an initial-value (or initial-boundary value) problem based on a nonlinear evolution equation to be obtained. The methodology requires careful consideration of the asymptotic structure as $t \to 0$ and $|x| \to \infty$ ($t = O(1)$), and links the initial data to the resulting large-time attractor for the initial-value problem.

1.5 Large-Time Attractors

In this section we will review the large-time attractors that we will encounter in the solution to the initial-value problems based on equation (1.15) (with (1.21)) considered in this thesis (which we described in detail in Section 1.6). The specific form of the large-time attractor encountered depends on the problem parameters. We begin by introducing the scaled coordinate z, by

$$z = xt^{-\alpha} \tag{1.32}$$

as $t \to \infty$ with $z = O(1)$ and where α is to be determined, and expand in the form

$$u(z,t) = U(z) + o(1) \tag{1.33}$$

as $t \to \infty$ with $z = O(1)$. On substituting (1.33) into (1.15) with (1.21) (when written in terms of z and t), we find that

$$-\frac{\alpha z}{t}U_z + t^{(\delta-\alpha)}UU_z = t^{-(2\alpha)}U_{zz}. \tag{1.34}$$

To obtain the most structured leading order balance in equation (1.34), we observe immediately that there are three cases to consider depending on the parameters δ and α, namely,

(i) $\alpha = \frac{1}{2}, \quad -1 < \delta < -\frac{1}{2}$.

In this case, the leading order problem is given by

$$U_{zz} + \frac{z}{2}U_z = 0. \tag{1.35}$$

(ii) $\alpha = \frac{1}{2}, \quad \delta = -\frac{1}{2}$.

In this case, the leading order problem is given by

$$U_{zz} + \frac{z}{2}U_z - UU_z = 0. \tag{1.36}$$

(iii) $\alpha = (\delta + 1), \quad \delta > -\frac{1}{2}$.

In this case, the leading order problem is given by

$$(\delta + 1)zU_z - UU_z = 0. \tag{1.37}$$

It is also instructive to introduce the scaled coordinate z, by

$$z = xt^{-\alpha} + At^{-\beta} \tag{1.38}$$

as $t \to \infty$ with $z = O(1)$, where the constants α, β and A are to be determined, and expand in the form

$$u(z,t) = U(z) + o(1) \tag{1.39}$$

as $t \to \infty$ with $z = O(1)$. On substituting (1.39) into equation (1.15) with (1.21) (when written in terms of z and t) we obtain

$$U_z\Big(-\frac{\alpha z}{t} + A(\alpha - \beta)t^{-(\beta+1)}\Big) + t^{(\delta-\alpha)}UU_z = t^{-(2\alpha)}U_{zz}. \tag{1.40}$$

To obtain the most structured leading order balance in (1.40) we require that $\alpha = -\delta$,

$\beta = -(2\delta + 1)$ and $\delta > -\frac{1}{2}$ giving at leading order that

$$U_{zz} - UU_z + A(\delta + 1)U_z = 0. \tag{1.41}$$

The related ordinary differential equations (1.35), (1.36), (1.37), and (1.41) are of fundamental importance in what follows. We now consider each in turn.

1.5.1 Error Function

Here we consider the case when $\alpha = \frac{1}{2}$ and $-1 < \delta < -\frac{1}{2}$. We introduce the scaled coordinate z, by

$$z = xt^{-\frac{1}{2}} \tag{1.42}$$

as $t \to \infty$ with $z = O(1)$, and expand in the form

$$u(z, t) = U(z) + o(1) \tag{1.43}$$

as $t \to \infty$ with $z = O(1)$. On substituting (1.43) into (1.15) with (1.21) (when written in terms of z and t), we obtain at leading order

$$U_{zz} + \frac{z}{2}\, U_z = 0, \quad -\infty < z < \infty. \tag{1.44}$$

We note that this is equation (1.35) mentioned previously. Equation (1.44) is to be solved subject to the boundary conditions

$$U(z) \to \begin{cases} u_+, & z \to \infty, \\ u_-, & z \to -\infty, \end{cases} \tag{1.45}$$

where u_+ and $u_-(\neq u_+)$ are constants. It is straightforward to integrate equation (1.44) once to obtain

$$U_z = Ae^{-\frac{z^2}{4}}, \tag{1.46}$$

where A is a constant of integration. One further integration of (1.46) then yields

$$U(z) = A\int_0^z e^{-\frac{s^2}{4}}\mathrm{d}s + B, \tag{1.47}$$

where B is a constant of integration. Imposing boundary conditions (1.45) then requires that

$$U(z) = \frac{(u_+ - u_-)}{2\sqrt{\pi}}\int_0^z e^{-\frac{s^2}{4}}\mathrm{d}s + \frac{(u_+ + u_-)}{2}, \quad -\infty < z < \infty. \tag{1.48}$$

On rewriting (1.48) in terms of the standard error function (see for example [1]) we obtain

$$U(z) = \frac{(u_+ + u_-)}{2} - \frac{(u_- - u_+)}{2}\,\mathrm{erf}\left(\frac{z}{2}\right), \quad -\infty < z < \infty. \tag{1.49}$$

We note that there is no restriction on the constants u_+ and u_- other then the requirement that $u_+ \neq u_-$. A graph of (1.49) when $u_+ = 1$ and $u_- = -1$ is given for illustration in Figure 1.2.

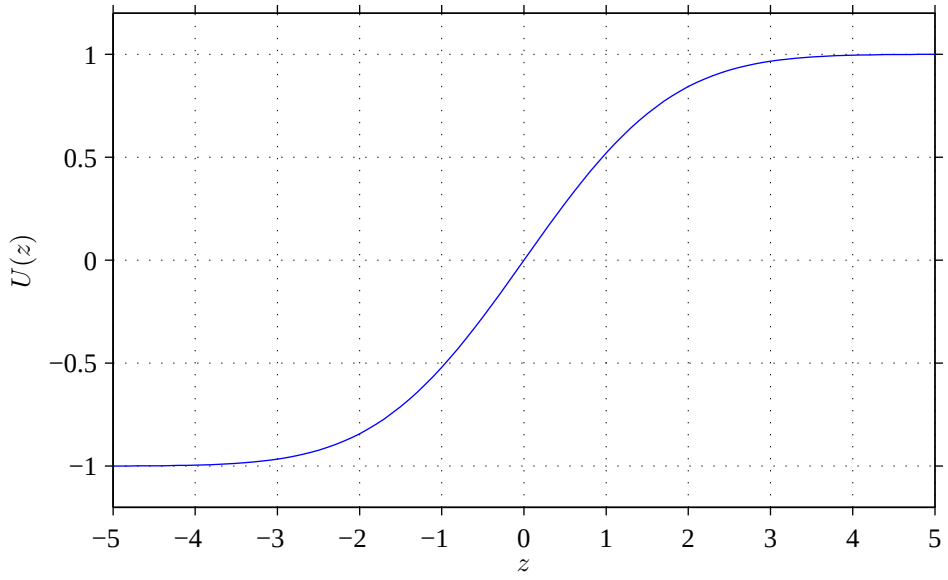

Figure 1.2: Graph of error function profile (1.49) when $u_+ = 1$ and $u_- = -1$.

1.5.2 Rudenko-Soluyan Similarity Solution

When $\alpha = \frac{1}{2}$ and $\delta = -\frac{1}{2}$ equation (1.15) with (1.21) admits the similarity solution

$$u = U(z), \quad z = xt^{-\frac{1}{2}}. \tag{1.50}$$

On substitution of (1.50) into equation (1.15) (when $\delta = -\frac{1}{2}$) we obtain

$$U_{zz} + \left(\frac{z}{2} - U\right) U_z = 0, \quad -\infty < z < \infty. \tag{1.51}$$

We recall that this is equation (1.36) that we encountered earlier. Equation (1.51) is to be solved subject to the boundary conditions

$$U(z) \to \begin{cases} u_+ & \text{as } z \to \infty, \\ u_- & \text{as } z \to -\infty, \end{cases} \tag{1.52}$$

where u_+ and $u_-(\neq u_+)$ are constants. On making the substitution

$$U = \frac{1}{\sqrt{2}}\Omega, \quad z = \sqrt{2}\ Z, \tag{1.53}$$

equation (1.51) becomes

$$\Omega_{ZZ} + (Z - \Omega)\,\Omega_Z = 0, \quad -\infty < Z < \infty, \tag{1.54}$$

which has been analyzed by Rudenko and Soluyan [32]. It is straightforward to establish (see for example [36] and [32]) that the solutions in terms of the similarity variable $Z = \frac{x}{\sqrt{2t}}$ are

$$\left.\begin{aligned} \Omega &= Z - 2F(\zeta), \\ Z &= \gamma + \int_{\zeta_0}^{\zeta} \frac{d\zeta}{F(\zeta)}. \end{aligned}\right\} \ \zeta \geq \zeta_0, \tag{1.55}$$

where

$$F(\zeta) = \pm\left(\zeta - \zeta_0\ e^{-2(\zeta-\zeta_0)}\right)^{\frac{1}{2}}, \tag{1.56}$$

Here ζ is the implicit variable, γ and $\zeta_0(> -\frac{1}{2})$ are constants. The wave profile $\Omega(Z)$ is bounded with constant boundary conditions as $|Z| \to \infty$, and consists of two parts (the plus sign in (1.56) is taken to give $\Omega(Z)$ for $Z \geq \gamma$, while the negative sign is taken in (1.56) to give $\Omega(Z)$ for $Z \leq \gamma$) which smoothly join at $Z = \gamma$. Further, the wave profile $\Omega(Z)$ is monotonically decreasing (increasing) when ζ_0 is positive (negative) respectively. The parameter ζ_0 determines the strength of wave profile $\Omega(Z)$, where the limiting behaviour of (1.55) is given by

$$\Omega(Z) \to \gamma \pm \Delta(\zeta_0) \quad \text{as} \quad Z \to \pm\infty$$

with the height of the wave being $2\Delta(\zeta_0)$, is a function of ζ_0, where $\Delta(\zeta_0)$ can be determined numerically. It was shown by Rudenko and Soluyan [32] that as $\zeta_0 \to 0$, the wave profile $\Omega(Z)$ takes the error function form while when $\zeta_0 \to \infty$ the wave profile $\Omega(Z)$

takes Taylor shock profile. Furthermore, the wave profile $\Omega(Z)$ approaches an expansion wave profile as $\zeta_0 \to -\frac{1}{2}$. In order to satisfy boundary conditions (1.52) we take

$$\gamma = \frac{\sqrt{2}}{2}(u_+ + u_-)$$

and determine ζ_0 such that $\Delta(\zeta_0) = \frac{\sqrt{2}}{2}(u_+ - u_-)$. We observe from (1.53) and (1.55) that

$$U(z) = u_+ + O\left(\frac{1}{z}\exp\left(-\frac{z^2}{4} + u_+ z\right)\right) \quad \text{as} \quad z \to \infty. \tag{1.57}$$

The corresponding asymptotic form for $U(z)$ as $z \to -\infty$ follows (1.57) with u_+ replaced by u_-.

A graph of the implicit solution (1.55) when $\gamma = 0$ for $\zeta_0 = 0.04,\ 1$ and 2.5 is given in Figure 1.3. We note that curves (a), (b), (c) illustrate expansion wave, error function, Taylor shock type profiles respectively.

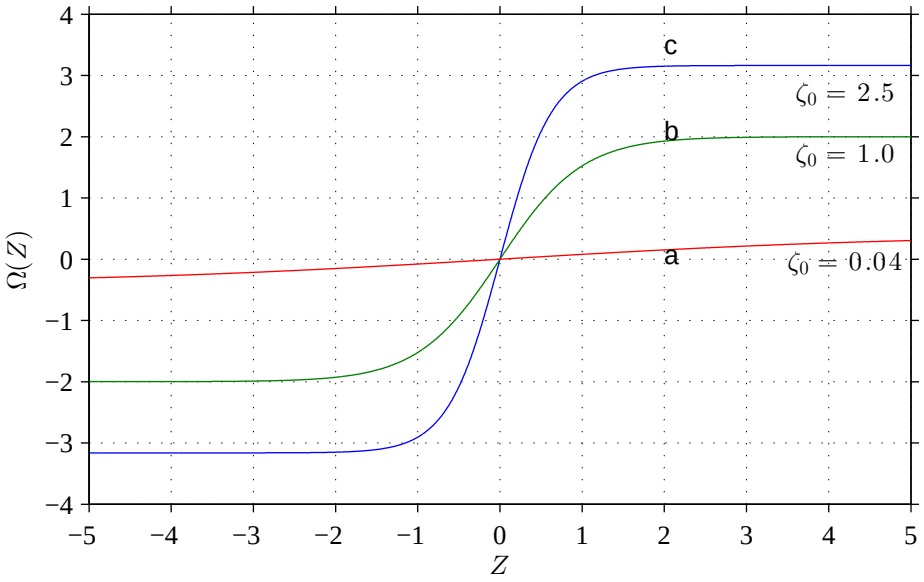

Figure 1.3: Graph of the Rudenko-Soluyan implicit solution of (1.55) for $\gamma = 0$ when $\zeta_0 = 0.04,\ 1$ and 2.5.

1.5.3 Expansion Wave

Here we consider the case when $\alpha = (\delta + 1)$ and $\delta > -\frac{1}{2}$. We introduce the scaled coordinate z, by

$$z = xt^{-(\delta+1)} \tag{1.58}$$

as $t \to \infty$ with $z = O(1)$, and expand in the form

$$u(z,t) = U(z) + o(1) \tag{1.59}$$

as $t \to \infty$ with $z = O(1)$. On substituting (1.59) into (1.15) with (1.21) (when written in terms of z and t), we obtain at leading order

$$-UU_z + z(\delta + 1)U_z = 0, \quad -\infty < z < \infty. \tag{1.60}$$

Therefore, after consideration of (1.60), we have that

$$U = \text{constant} \qquad \text{or} \qquad U = (\delta + 1)z \tag{1.61}$$

are solutions of (1.60). If we further require a solution which satisfies the boundary conditions

$$U(z) \to \begin{cases} u_+, & z \to \infty, \\ u_-, & z \to -\infty, \end{cases}$$

where $u_+ > u_-$, then we require

$$U(z) = \begin{cases} u_+, & z > \frac{u_+}{(\delta+1)}, \\ (\delta + 1)z, & \frac{u_-}{(\delta+1)} \le z \le \frac{u_+}{(\delta+1)}, \\ u_-, & z < \frac{u_-}{(\delta+1)}, \end{cases} \tag{1.62}$$

which is the well known expansion wave solution. A graph of (1.62) when $u_+ = 1$ and $u_- = -1$ is given for illustration in Figure 1.4.

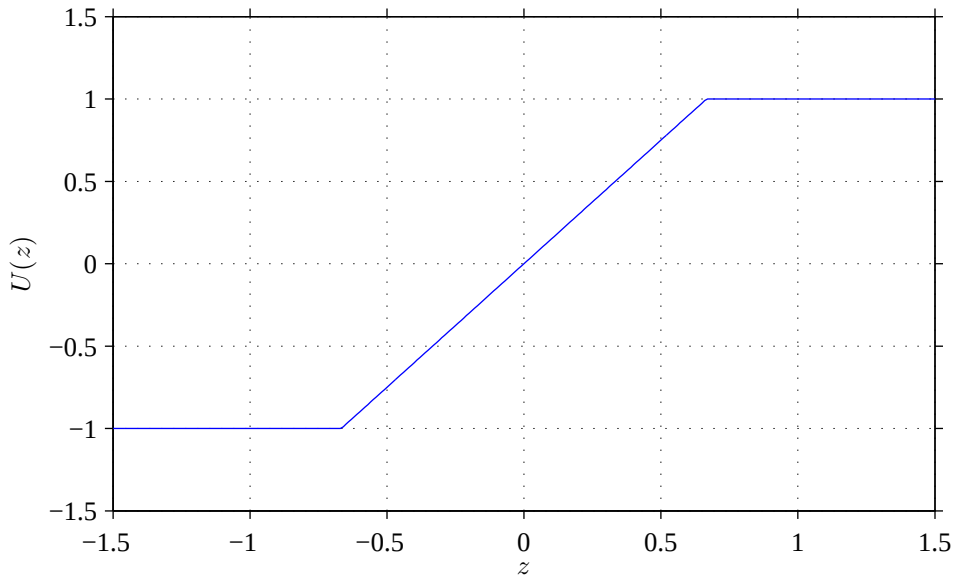

Figure 1.4: Graph of the expansion wave profile (1.62) when $u_- = -1$ and $u_+ = 1$.

1.5.4 Taylor Shock Wave

Here we consider the case when $\alpha = -\delta$, $\beta = -(2\delta + 1)$ and $\delta > -\frac{1}{2}$. We introduce the scaled coordinate z, by

$$z = xt^{\delta} + At^{(2\delta+1)} \tag{1.63}$$

as $t \to \infty$ with $z = O(1)$, and where the constant A is to be determined. We expand in the form

$$u(z,t) = U(z) + o(1) \tag{1.64}$$

as $t \to \infty$ with $z = O(1)$. On substituting (1.64) into (1.15) (when written in terms of z and t), we find at leading order

$$U_{zz} - UU_z + A(\delta + 1)U_z = 0, \quad -\infty < z < \infty. \tag{1.65}$$

Equation (1.65) is to be solved subject to the boundary conditions

$$U(z) \to \begin{cases} u_+, & z \to \infty, \\ u_-, & z \to -\infty. \end{cases} \tag{1.66}$$

On integrating (1.65) once, we obtain

$$U_z = \frac{U^2}{2} - A(\delta + 1)U + c_1, \quad -\infty < z < \infty, \tag{1.67}$$

where c_1 is a constant of integration. On imposing boundary conditions (1.66) we require that

$$A = \frac{u_+ + u_-}{2(\delta + 1)} \quad \text{and} \quad c_1 = \frac{u_+ u_-}{2}.$$

After which we can rewrite (1.67) as

$$U_z = \frac{U^2}{2} - \frac{(u_+ + u_-)}{2}U + \frac{u_+ u_-}{2} = \frac{1}{2}\left(U - u_+\right)\left(U - u_-\right), \tag{1.68}$$

which on separating variables and integrating gives

$$\int \frac{\mathrm{d}U}{\left(U - u_+\right)\left(U - u_-\right)} = \frac{1}{2}z + c_2, \tag{1.69}$$

where c_2 is a constant of integration. We note that $U_z > 0$ for $u_+ < U < u_-$. On using the method of partial fractions we obtain after integration

$$\frac{1}{(u_- - u_+)}\ln\frac{|U - u_-|}{|U - u_+|} = \frac{1}{2}z + c_2. \tag{1.70}$$

Now on restricting attention to $u_+ < U < u_-$ we have that

$$\ln\frac{|U - u_-|}{|U - u_+|} = \frac{1}{2}(u_- - u_+)z + c_2(u_- - u_+). \tag{1.71}$$

On rearranging we obtain

$$U(z) = \frac{u_- + u_+ \mathrm{e}^{\left(\frac{u_- - u_+}{2}\right)z + \Phi_c}}{1 + \mathrm{e}^{\left(\frac{u_- - u_+}{2}\right)z + \Phi_c}}, \quad -\infty < z < \infty, \tag{1.72}$$

where $\Phi_c = c_2(u_- - u_+)$ is a constant. We note that $U(z) \to u_+$ as $z \to \infty$, and that $U(z) \to u_-$ as $z \to -\infty$ (as required).

Finally, we can write (1.72) in terms of the hyperbolic tangent as

$$U(z) = \frac{1}{2}(u_+ + u_-) - \frac{1}{2}\left(u_- - u_+\right)\tanh\left(\frac{1}{4}(u_- - u_+)z + \phi_c\right), \quad -\infty < z < \infty, \tag{1.73}$$

where $\phi_c = \frac{\Phi}{2}$ and $u_+ < u_-$. Equation (1.73) is the well known Taylor shock profile [38]. A graph of (1.73) when $u_+ = -1$ and $u_- = 1$ is given for illustration in Figure 1.5. We note that we have taken $\phi_c = 0$ for convenience.

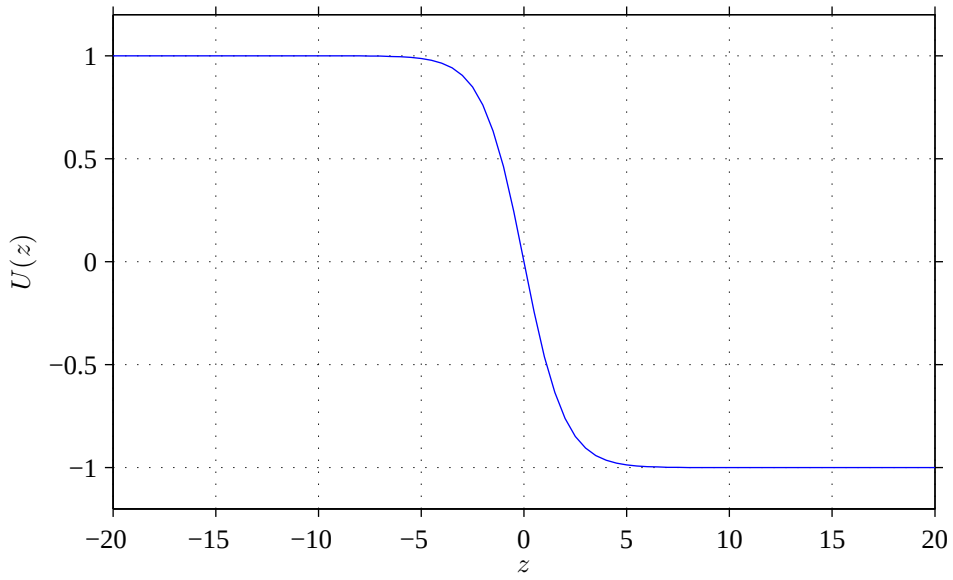

Figure 1.5: Graph of the Taylor shock profile (1.73) when $u_- = 1$ and $u_+ = -1$ (with translational invariance fixed by taking $\phi_c = 0$).

1.6 An Overview of the Mathematical Problems Considered

In Chapter 2 and 3 we consider the initial-value problem

$$u_t + t^\delta u u_x = u_{xx}, \quad -\infty < x < \infty, \quad t > 0, \tag{1.74}$$

$$u(x,0) = u_0(x), \quad -\infty < x < \infty, \tag{1.75}$$

$$u(x,t) \to \begin{cases} u_+, & x \geq -\infty, \\ u_-, & x < \infty, \end{cases} \tag{1.76}$$

where u_+ and u_- ($\neq u_+$) are constants. In particular, we consider the case when the initial data u_0 is continuously differentiable and has algebraic decay as $|x| \to \infty$. Specifically,

$$u_0(x) = \begin{cases} u_+ + \frac{A_R}{(x)^\gamma} + O(E(|x|)) & \text{as } x \to \infty, \\ u_- + \frac{A_L}{(-x)^\gamma} + O(E(|x|)) & \text{as } x \to -\infty. \end{cases} \tag{1.77}$$

where $E(|x|)$ is linearly exponentially small in x as $|x| \to \infty$, A_R ($\neq 0$), A_L ($\neq 0$) and γ (> 0) are constants. In Chapter 2 we consider the case when $u_+ > u_-$. As discussed earlier in this case initial-value problem (1.74)-(1.77) is labelled as $\mathbf{IVP}^+$ and where $A_R < 0$ and $A_L > 0$. We will develop, via the method of matched asymptotic coordinate expansions, the complete large-time asymptotic structure of the solution to $\mathbf{IVP}^+$. The behaviour of the solution depends critically on the problem parameter δ ($\neq 0$). In particular, the large-time attractor of the solution to $\mathbf{IVP}^+$ is

(i) An expansion wave when $\delta > -\frac{1}{2}$.

(ii) The Rudenko-Soluyan Similarity Solution when $\delta = -\frac{1}{2}$.

(iii) The error function when $-1 < \delta < -\frac{1}{2}$.

In Chapter 3 we extend the analysis of Chapter 2 by considering the case when $u_+ < u_-$. In this case initial-value problem (1.74)-(1.77) is labelled as $\mathbf{IVP}^-$ and where $A_R > 0$ and $A_L < 0$. Again we use the method of matched asymptotic coordinate expansions to obtain the complete large-time asymptotic structure of the solution to $\mathbf{IVP}^-$. As in Chapter 2 the behaviour of the solution depends on the problem parameter δ ($\neq 0$). In particular, the large-time attractor of the solution to $\mathbf{IVP}^-$ is

(i) A Taylor shock wave when $\delta > -\frac{1}{2}$.

(ii) The Rudenko-Soluyan Similarity Solution when $\delta = -\frac{1}{2}$.

(iii) The error function when $-1 < \delta < -\frac{1}{2}$.

Table 1.1 provides an overview of the results contained in Chapters 2 and 3, presenting which large-time attractor arises in the solution to initial-value problem (1.74)-(1.77) for the given problem parameters.

	$u_+ < u_-$	$u_+ > u_-$
$\delta > -\frac{1}{2}$	Taylor Shock	Expansion Wave
$\delta = -\frac{1}{2}$	Rudenko-Soluyan Similarity Solution	
$-1 < \delta < -\frac{1}{2}$	Error Function	

Table 1.1: The type of large-time attractor connecting u_+ to u_- in the solution of initial-value problem (1.74)-(1.77) for $\delta > -1$.

We recall that the case when $\delta = -1$ has been considered in [23]; the large-time attractor in this case is of error function type.

Chapter 2

The Initial-Value Problem $\mathbf{IVP}^+$

In this chapter, we consider the initial-value problem for Burgers' equation with a time dependent coefficient [3] , namely,

$$u_t + t^\delta u u_x = u_{xx}, \quad -\infty < x < \infty, \quad t > 0, \tag{2.1}$$

$$u(x,0) = u_0(x), \quad -\infty < x < \infty \tag{2.2}$$

$$u(x,t) \to \begin{cases} u_-, & x \to -\infty, \\ u_+, & x \to \infty, \end{cases} \quad t \geq 0, \tag{2.3}$$

where $\delta > -1$ and $u_+ > u_-$. Further, we consider the situation when the initial data $u_0 : \mathbb{R} \to \mathbb{R}$ is continuously differentiable and has algebraic decay as $|x| \to \infty$. Specifically

$$u_0(x) = \begin{cases} u_+ + \frac{A_R}{(x)^\gamma} + O(E(|x|)) & \text{as } x \to \infty, \\ u_- + \frac{A_L}{(-x)^\gamma} + O(E(|x|)) & \text{as } x \to -\infty, \end{cases} \tag{2.4}$$

where $E(|x|)$ is linearly exponentially small in x as $|x| \to \infty$, $A_R < 0$, $A_L > 0$ and γ (> 0) are constants. We henceforth refer to the initial-value problem (2.1), (2.2) and (2.4) as $\mathbf{IVP}^+$ when $u_+ > u_-$. We develop the structure of the large-time solution to $\mathbf{IVP}^+$ using the method of matched asymptotic coordinate expansions. The large-time solution

is obtained by consideration of the asymptotic structures as $t \to 0$ $(-\infty < x < \infty)$ and as $|x| \to \infty$ with $t = O(1)$. In particular, it is required to obtain

(i) the asymptotic structure of the solution to **IVP**$^+$ as $t \to 0$.

(ii) the asymptotic structure of the solution to **IVP**$^+$ for $t = O(1)$ as $|x| \to \infty$.

(iii) the asymptotic structure of the solution to **IVP**$^+$ as $t \to \infty$.

We begin by examining the asymptotic structure of the solution to **IVP**$^+$ as $t \to 0$.

2.1 Asymptotic solution to IVP$^+$ as $t \to 0$

Consideration of initial data (2.2) (with (2.4)) indicates that the asymptotic solution to **IVP**$^+$ as $t \to 0$ will consist of a single asymptotic region, which we label as region I.

$$\text{Region I}: \; x = O(1).$$

Since $u(x, 0)$ is analytic in region I, with $u = O(1)$ as $t \to 0$, we expand $u(x, t)$ as a regular power series in t and substitute into equation 2.1. However, the cases when $\delta > 0$ and when $-1 < \delta < 0$ need to be considered separately [3]. Further, we note that the case when $\delta = 0$ is classical Burgers' equation. We begin by considering the case when $\delta > 0$.

2.1.1 $\delta > 0$

To examine region I where $x = O(1)$ and $u(x, t) = O(1)$ as $t \to 0$, we look for an expansion of the form

$$u(x, t) = u_0(x) + t^s u_1(x) + o(t^s) \quad \text{as} \quad t \to 0 \tag{2.5}$$

where $x = O(1)$ and $s > 0$ is a constant to be determined. On substituting expansion (2.5) into equation (2.1) we obtain

$$st^{s-1}u_1(x) + t^{\delta}[u_0(x) + t^s u_1(x) + ...][u_0'(x) + t^s u_1'(x) + ...] = [u_0''(x) + t^s u_1''(x) + ...] \quad (2.6)$$

After expanding and grouping terms together in (2.6) we arrive at

$$st^{s-1}u_1(x) + t^{\delta}u_0(x)u_0'(x) + t^{\delta+s}u_0(x)u_1'(x) + t^{\delta+s}u_1(x)u_0'(x) + ... = u_0''(x) + t^s u_1''(x) + ... \quad . \quad (2.7)$$

We now seek values of $s > 0$ which provide possible balances in (2.7). It is straightforward to find that there is only one possible balance, and that requires $s = 1$. Thus, at leading order we obtain

$$u_1(x) = u_0''(x) \quad (2.8)$$

giving, via (2.5)

$$u(x,t) = u_0(x) + tu_0''(x) + O(t^{\beta}) \quad \text{as} \quad t \to 0 \quad (2.9)$$

with $x = O(1)$ and $\beta > 0$ to be determined. The correction term to expansion (2.9) depends upon δ and can readily be obtained on continuing expansion (2.9) on omitting the details for brevity. It follows that in region I, the asymptotic solution to $\mathbf{IVP}^+$ as $t \to 0$, when $\delta > 0$, is given by

$$\begin{aligned} u(x,t) &= u_0(x) + \sum_{i=1}^{\lceil \delta \rceil} \frac{u_0^{(2i)}(x)}{i!} t^i \\ &- \begin{cases} \left(\frac{u_0(x)u_0'(x)}{(\delta+1)} - \frac{u_0^{2(\delta+1)}(x)}{(\delta+1)!} \right) t^{(\delta+1)} + O\left(\frac{t^{(\delta+2)}}{(1+|x|)^{(\gamma+3)}} \right) & \text{when } \delta \in \mathbb{N}, \\ \frac{u_0(x)u_0'(x)}{(\delta+1)} t^{(\delta+1)} + O\left(\frac{t^{(\delta+2)}}{(1+|x|)^{(\gamma+3)}} \right) & \text{when } \delta \notin \mathbb{N}, \end{cases} \end{aligned} \quad (2.10)$$

as $t \to 0$ with $x = O(1)$, where $\lceil \delta \rceil$ is the smallest integer greater than or equal to δ [3]. It is clear that expansion (2.10) when $x = O(1)$ as $t \to 0$, in fact remains uniform for $|x| \gg 1$, and therefore no further asymptotic regions are required in the asymptotic structure of $u(x,t)$ as $t \to 0$. In particular, we have from (2.4) and (2.10), that

$$u(x,t) = \left(u_+ + \frac{A_R}{x^\gamma} + O(E(|x|))\right) + \sum_{i=1}^{\lceil \delta \rceil} \frac{A_R(\gamma+2i-1)!}{i!(\gamma-1)!x^{(\gamma+2i)}}\left(1 + O(E(|x|))\right)t^i$$
$$+ \frac{u_+ A_R \gamma}{(\delta+1)x^{(\gamma+1)}}\left(1 + O(\frac{1}{x^\gamma}, \frac{1}{x^{(2\delta+1)}})\right)t^{(\delta+1)} + O\left(\frac{t^{(\delta+2)}}{(1+|x|)^{(\gamma+3)}}\right) \tag{2.11}$$

as $t \to 0$ uniformly for $x \gg 1$, whilst

$$u(x,t) = \left(u_- + \frac{A_L}{(-x)^\gamma} + O(E(|x|))\right) + \sum_{i=1}^{\lceil \delta \rceil} \frac{A_L(\gamma+2i-1)!}{i!(\gamma-1)!(-x)^{(\gamma+2i)}}\left(1 + O(E(|x|))\right)t^i$$

$$- \frac{u_- A_L \gamma}{(\delta+1)(-x)^{(\gamma+1)}}\left(1 + O(\frac{1}{|x|^\gamma}, \frac{1}{|x|^{(2\delta+1)}})\right)t^{(\delta+1)} + O\left(\frac{t^{(\delta+2)}}{(1+|x|)^{(\gamma+3)}}\right) \tag{2.12}$$

as $t \to 0$ uniformly for $(-x) \gg 1$.

2.1.2 $-1 < \delta < 0$

Following Section 2.1.1 we have in this case that

$$u(x,t) = u_0(x) + \sum_{i=1}^{\lceil \frac{-\delta}{(\delta+1)} \rceil} T_i(x)t^{i(\delta+1)}$$
$$+ \begin{cases} u_0''(x)t + o(t) & \text{when } \frac{-\delta}{(\delta+1)} \notin \mathbb{N}, \\ \left(u_0''(x) + T_{\frac{1}{(\delta+1)}}(x)\right)t + o(t) & \text{when } \frac{-\delta}{(\delta+1)} \in \mathbb{N}, \end{cases} \tag{2.13}$$

as $t \to 0$ with $x = O(1)$, where the functions $T_i(x)$ can be determined in terms of $u_0(x)$ straightforwardly. For example,

$$T_1(x) = \frac{-u_0(x)u_0'(x)}{(\delta+1)}$$

and

$$T_2(x) = \frac{[u_0^2(x)u_0'(x)]'}{2(\delta+1)^2}.$$

Expansion (2.13) (with (2.4)) remains uniform for $x \gg 1$ as $t \to 0$ and for $(-x) \gg 1$ as $t \to 0$. This completes the asymptotic structure as $t \to 0$, with expansion (2.13) of region I providing a uniform approximation to the solution of $\mathbf{IVP}^+$ as $t \to 0$ with $x = O(1)$[3].

2.2 Asymptotic solution to $\mathbf{IVP}^+$ for $t = O(1)$ as $|x| \to \infty$

We now investigate the asymptotic structure of the solution to $\mathbf{IVP}^+$ as $|x| \to \infty$ with $t = O(1)$. We first obtain the structure of the solution to $\mathbf{IVP}^+$ as $x \to \infty$ with $t = O(1)$. The form (2.10) ($\delta > 0$) and (2.13) ($-1 < \delta < 0$) for $x \gg 1$ indicates that in this region, which we label as region II^+, we must expand as

$$u(x,t) = u_+ + \frac{F_0(t)}{x^\gamma} + \frac{F_1(t)}{x^{(\gamma+1)}} + \frac{F_2(t)}{x^r} + \frac{F_3(t)}{x^s} + o\left(\frac{1}{x^s}\right) \quad \text{as} \quad x \to \infty \tag{2.14}$$

with $t = O(1)$, where

$$r = \begin{cases} 2\gamma + 1, & 0 < \gamma \leq 1, \\ \gamma + 2, & \gamma > 1. \end{cases}$$
$$s = \begin{cases} \gamma + 2, & 0 < \gamma < 1, \\ 4 & \gamma = 1, \\ 2\gamma + 1, & \gamma > 1. \end{cases} \tag{2.15}$$

On substituting expansion (2.14) into equation (2.1), expanding, and solving at each order, subject to matching with expansion (2.11) (when $\delta > 0$) and (2.13) (when $-1 < \delta < 0$) in region I as $t \to 0$, we obtain

$$F_0(t) = A_R, \tag{2.16a}$$
$$F_1(t) = \frac{\gamma u_+ A_R t^{(\delta+1)}}{(\delta+1)}, \tag{2.16b}$$
$$F_2(t) = \begin{cases} \frac{\gamma A_R^2}{(\delta+1)} t^{(\delta+1)}, & 0 < \gamma < 1, \\ \frac{A_R^2}{(\delta+1)} t^{(\delta+1)} + 2A_R t, & \gamma = 1, \\ \gamma(\gamma+1) A_R t, & \gamma > 1. \end{cases} \tag{2.16c}$$

and

$$F_3(t) = \frac{\gamma A_R^2}{(\delta+1)} t^{(\delta+1)}, \quad \gamma > 1. \tag{2.16d}$$

The form of $F_3(t)$ when $0 < \gamma \leq 1$ is not required in what follows where it is a small term and will not effect on structure of solution [3]. Thus, the structure of (2.14) depends on the parameters δ and γ, we observe that expansion (2.14) remains uniform for $t \gg 1$

provided that $x \gg \lambda(t)$, but becomes nonuniform when $x = O(\lambda(t))$ for $t \gg 1$, where

$$\lambda(t) = \begin{cases} t^{(\delta+1)}, & \delta > -\frac{1}{2}, \ \gamma > 0, \\ t^{-\delta}, & -1 < \delta \leq -\frac{1}{2}, \ \gamma \geq 1, \\ t^{\frac{\delta}{(\gamma-1)}}, & -1 < \delta \leq -\frac{1}{2}, \ 0 < \gamma < 1. \end{cases} \tag{2.17}$$

For completeness we provide the above information relating to the nonuniformity of expansion (2.14) in Figure 2.1.

We next examine the structure of the solution to $\mathbf{IVP}^+$ as $x \to -\infty$ with $t = O(1)$. The form of expansion (2.12) (when $\delta > 0$) and (2.13) (when $-1 < \delta < 0$) in region I when $(-x) \gg 1$ requires that in region II^- we expand in the form

$$u(x,t) = u_- + \frac{F_0(t)}{(-x)^\gamma} + \frac{F_1(t)}{(-x)^{(\gamma+1)}} + \frac{F_2(t)}{(-x)^r} + \frac{F_3(t)}{(-x)^s} + o\left(\frac{1}{(-x)^s}\right) \quad \text{as} \quad (-x) \to \infty \tag{2.18}$$

with $t = O(1)$, where

$$r = \begin{cases} 2\gamma + 1, & 0 < \gamma \leq 1, \\ \gamma + 2, & \gamma > 1. \end{cases}$$

$$s = \begin{cases} \gamma + 2, & 0 < \gamma < 1, \\ 4 & \gamma = 1, \\ 2\gamma + 1, & \gamma > 1. \end{cases} \tag{2.19}$$

On substituting expansion (2.18) into equation (2.1), expanding, and solving at each order, subject to matching with expansion (2.12) (when $\delta > 0$) and (2.13) (when $-1 < \delta < 0$)

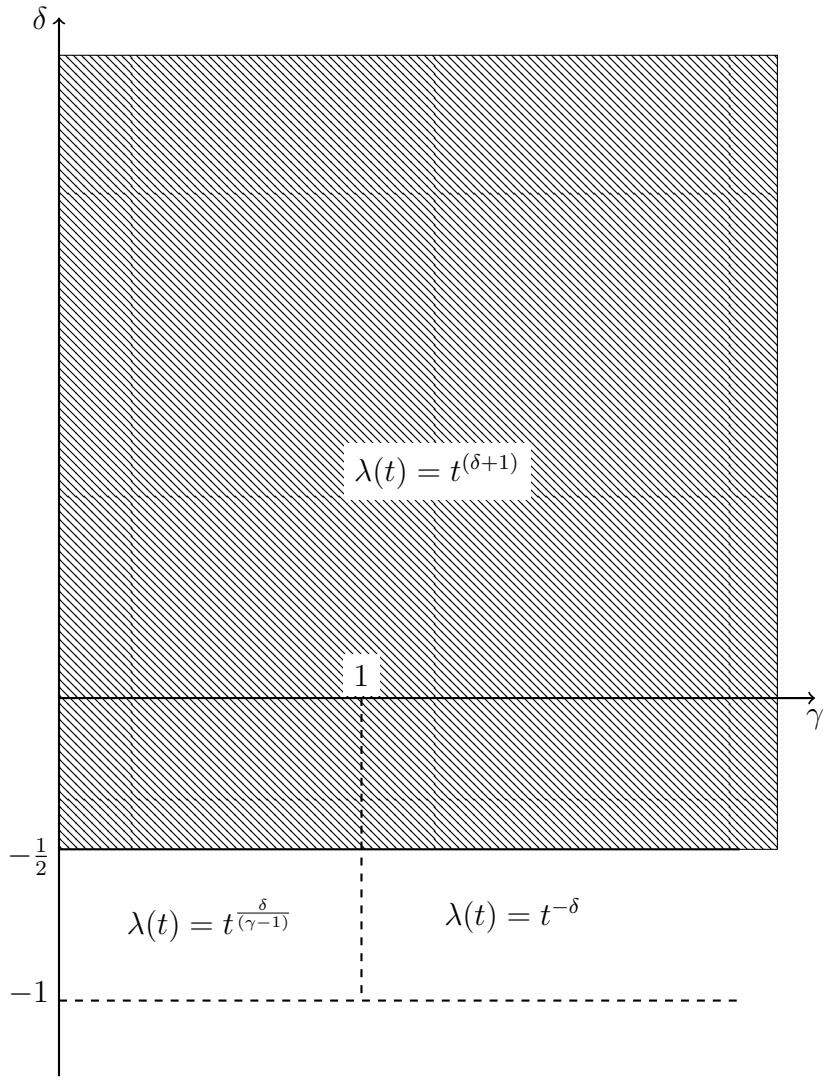

Figure 2.1: The (γ, δ) parameter plane.

in region I as $t \to 0$, we obtain

$$F_0(t) = A_L, \tag{2.20a}$$

$$F_1(t) = -\frac{\gamma u_- A_L}{(\delta+1)} t^{(\delta+1)}, \tag{2.20b}$$

$$F_2(t) = \begin{cases} -\frac{\gamma A_L^2}{(\delta+1)} t^{(\delta+1)}, & 0 < \gamma < 1, \\ -\frac{A_L^2}{(\delta+1)} t^{(\delta+1)} + 2A_L t, & \gamma = 1, \\ \gamma(\gamma+1) A_L t, & \gamma > 1. \end{cases} \tag{2.20c}$$

and

$$F_3(t) = -\frac{\gamma A_L^2}{(\delta+1)} t^{(\delta+1)}, \quad \gamma > 1. \tag{2.20d}$$

The form of $F_3(t)$ when $0 < \gamma \leq 1$ is not required in what follows where it is a small term and will not effect on structure of solution [3]. Thus, the structure of (2.18) depends on the parameters δ and γ. We observe again that expansion (2.18) remains uniform for $t \gg 1$ provided that $(-x) \gg \lambda(t)$, but again becomes nonuniform when $(-x) = O(\lambda(t))$ for $t \gg 1$, with $\lambda(t)$ given by (2.17), This completes the asymptotic structure of $\mathbf{IVP}^+$ as $|x| \to \infty$ with $t = O(1)$.

2.3 Asymptotic solution to $\mathbf{IVP}^+$ as $t \to \infty$

We next consider the asymptotic structure of the solution to $\mathbf{IVP}^+$ as $t \to \infty$. Consideration of expansions (2.14) and (2.18) for $t \gg 1$ in regions $\mathrm{II}^{\pm}$ indicates that there are a number of cases to consider, which are now developed in turn.

2.3.1 $\delta > -\frac{1}{2}$

We now investigate the structure of $\mathbf{IVP}^+$(we recall in this case that $u_+ > u_-$) as $t \to \infty$ when $\delta > -\frac{1}{2}$. We recall from Section 2.2 that expansions (2.14) and (2.18) of regions II^+ $\big(x \to \infty,\ t = O(1)\big)$ and II^- $\big(x \to -\infty,\ t = O(1)\big)$, respectively, continue to remain

uniform provided that $|x| \gg t^{(\delta+1)}$ as $t \to \infty$. We begin by considering the asymptotic structure as $t \to \infty$ moving in from region II$^+$, when $x \gg t^{(\delta+1)}$ as $t \to \infty$. To proceed we introduce a new region labelled as region III$^+$, in which $x = O(t^{(\delta+1)})$ as $t \to \infty$. To examine region III$^+$ it is convenient to introduce the scaled coordinate

$$y = xt^{-(\delta+1)} \tag{2.21}$$

with $y = O(1)$ as $t \to \infty$ [3]. The aim is now to develop an asymptotic approximation to $u(y,t)$ as $t \to \infty$ with $y = O(1)$. We begin in region III$^+$ ***moving in from*** region II$^+$ (when $y \gg 1$) to $y = O(1)$ as $t \to \infty$. The form of the asymptotic expansion for $u(y,t)$ in region III$^+$ follows from the structure of expansion (2.14) in region II$^+$, when written in terms of y and t, and expanded for $y = O(1)$ as $t \to \infty$. This requires that in region III$^+$ we expand in the form

$$u(y,t) = u_+ + g_0(y)t^{-\gamma(\delta+1)} + o\left(t^{-\gamma(\delta+1)}\right) \quad \text{as} \quad t \to \infty \tag{2.22}$$

with $y = O(1)$, and where $g_0(y)$ is a function to be determined. On substitution from (2.22) into equation (2.1) (when written in terms of y and t) we obtain at $O(t^{-\gamma(\delta+1)})$ the following ordinary differential equation for $g_0(y)$, namely

$$g_0' + \left(\frac{\gamma}{y - \frac{u_+}{(\delta+1)}}\right) g_0 = 0, \quad y = O(1). \tag{2.23}$$

Equation (2.23) has to be solved subject to the matching condition with expansion (2.14) in region II$^+$ (when $x = O(t^{(\delta+1)})$), which requires

$$g_0(y) \sim \frac{A_R}{y^\gamma} + \frac{\gamma u_+ A_R}{(\delta+1)y^{\gamma+1}} \quad \text{as} \quad y \to \infty. \tag{2.24}$$

The solution of (2.23) subject to (2.24) is then readily obtained as

$$g_0(y) = A_R\left(y - \frac{u_+}{(\delta+1)}\right)^{-\gamma}, \quad y > \frac{u_+}{(\delta+1)}. \tag{2.25}$$

We observe that $g_0(y)$ develops a singularity as $y \to \left(\frac{u_+}{(\delta+1)}\right)^+$. This anticipates an inner asymptotic region being required when $y = \frac{u_+}{(\delta+1)} + o(1)$ as $t \to \infty$. Thus, the domain for region III$^+$ is restricted now to $y = \frac{u_+}{(\delta+1)} + O(1)$ as $t \to \infty$. To proceed we examine this region of nonuniformity by introducing a new region, which we label as region IV$^+$. In region IV$^+$, we write

$$y = \frac{u_+}{(\delta+1)} + \xi t^{-r} \tag{2.26}$$

where $\xi = O(1)$ as $t \to \infty$, and $r > 0$ to be determined. We look for expansion in region IV$^+$ in the form

$$u(\xi, t) = u_+ + F(\xi)t^{-s} + o\left(t^{-s}\right) \quad \text{as} \quad t \to \infty \tag{2.27}$$

with $\xi = O(1)$, and $s > 0$ is to be determined. On substitution of expansion (2.26) and (2.27) into equation (2.1) (when written in terms of ξ and t) we obtain after some calculation that

$$-sF(\xi) + \xi\Big(r - (\delta+1)\Big)F_\xi + F(\xi)F_\xi t^{(r-s)} = F_{\xi\xi}t^{2(r-(\delta+1))+1}.$$

We now choose r and s to obtain the most structured leading order balance. This requires first that

$$s = r \tag{2.28}$$

and then that

$$r = \begin{cases} \frac{\gamma(\delta+1)}{(\gamma+1)}, & 0 < \gamma < 2\delta + 1, \\ (\delta + \frac{1}{2}), & \gamma \geq 2\delta + 1. \end{cases} \tag{2.29}$$

This delineates three cases $0 < \gamma < 2\delta + 1$, $\gamma > 2\delta + 1$ and $\gamma = 2\delta + 1$, which we consider in turn [3].

(i) $0 < \gamma < 2\delta + 1$

In this case the leading order problem is

$$\left(F - \frac{(\delta+1)}{(\gamma+1)}\xi\right)F_\xi - \frac{\gamma(\delta+1)}{(\gamma+1)}F = 0, \quad -\infty < \xi < \infty. \tag{2.30}$$

Equation (2.30) is to be solved subject to matching with region III^+ as $\xi \to \infty$; that is, we require

$$F(\xi) \sim A_R \xi^{-\gamma} \quad \text{as} \quad \xi \to \infty. \tag{2.31}$$

We observe that equation (2.30) admits the exact solution

$$F(\xi) = (\delta + 1)\xi, \quad -\infty < \xi < \infty.$$

In general, equation (2.30) is of homogeneous type, and admits a quadrature, after which the solution to (2.30) with (2.31) is given implicitly by,

$$\xi = \left(\frac{A_R}{F(\xi)}\right)^{\frac{1}{\gamma}} + \frac{F(\xi)}{(\delta+1)}, \quad -\infty < \xi < \infty. \tag{2.32}$$

It follows from (2.32) that (on recalling that $A_R < 0$),

$$F(\xi) < 0 \quad \text{for all} \quad -\infty < \xi < \infty, \tag{2.33}$$

$$F(\xi) \quad \text{is strictly monotone increasing, with} \quad -\infty < \xi < \infty, \tag{2.34}$$

$$F(\xi) \sim A_R \xi^{-\gamma} + \frac{A_R^2 \gamma}{(\delta+1)} \xi^{-(2\gamma+1)} \quad \text{as} \quad \xi \to \infty, \tag{2.35}$$

$$F(\xi) \sim (\delta+1)\xi - (-A_R)^{\frac{1}{\gamma}}(\delta+1)^{(1-\frac{1}{\gamma})}(-\xi)^{-\frac{1}{\gamma}} \quad \text{as} \quad \xi \to -\infty. \tag{2.36}$$

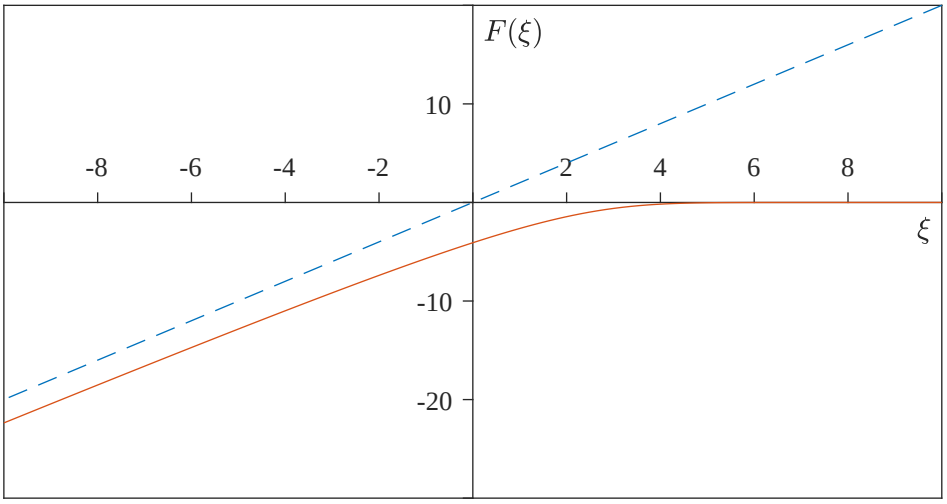

Figure 2.2: A graph of $F(\xi)$ against ξ when $\gamma = 2$, $\delta = 1$ and $A_R = -1$. The solid line represents the solution $F(\xi)$ from (2.32) while the dashed line represents the solution $F(\xi) = (\delta + 1)\xi$.

A graph of $F(\xi)$ against ξ, when $\delta = 1$,$\gamma = 2$ and $A_R = -1$ is given as an illustration in Figure 2.2 [3].

(ii) $\gamma > 2\delta + 1$

In this case the leading order problem is

$$F_{\xi\xi} - \left(F - \frac{1}{2}\xi\right)F_\xi + \left(\delta + \frac{1}{2}\right)F = 0, \quad -\infty < \xi < \infty. \tag{2.37}$$

The principal matching condition with region III$^+$ requires

$$F(\xi) \to 0 \quad \text{as} \quad \xi \to \infty. \tag{2.38}$$

Solutions to (2.37) which satisfy (2.38) have the form

$$F(\xi) \sim A\xi^{-(2\delta+1)} + B\xi^{2\delta}e^{-\frac{1}{4}\xi^2} \quad \text{as} \quad \xi \to \infty, \tag{2.39}$$

with A and B being arbitrary constants. In this case, the expansion in region IV^+ is given by

$$u(\xi, t) \sim u_+ + \left(A\xi^{-(2\delta+1)} + B\xi^{2\delta}e^{-\frac{1}{4}\xi^2} \right) t^{-(\delta+1)} + ... \tag{2.40}$$

as $t \to \infty$. Expansion in region III^+ (2.22) (for $\xi \gg 1$) when written in terms of ξ is gives by

$$u(\xi, t) \sim u_+ + A_R\xi^{-\gamma}\ t^{-\frac{\gamma}{2}} + ... \tag{2.41}$$

as $t \to \infty$. However, we observe immediately that the algebraic power in (2.40) will preclude matching at two-terms with region III^+. A local passive adjustment region is required. This is achieved by requiring $A = 0$ in (2.39) and the passive region is then located at $\xi = \xi_p(t) + O(1)$ as $t \to \infty$, where,

$$\xi_p^2(t) = 2(\gamma - (2\delta + 1)) \ln t + O\left(\ln\left((\gamma - (2\delta + 1)) \ln t \right) \right) \quad \text{as} \quad t \to \infty. \tag{2.42}$$

Thus the leading order problem is now (2.37) with

$$F(\xi) \sim B\xi^{2\delta}e^{-\frac{1}{4}\xi^2} \quad \text{as} \quad \xi \to \infty \tag{2.43}$$

for some constant B. We again note that equation (2.37) admits the exact solution

$$F(\xi) = (\delta + 1)\xi, \quad -\infty < \xi < \infty,$$

and for region IV$^+$ to act as transition region, we require the solution of (2.37) and (2.43) to satisfy

$$F(\xi) \sim (\delta + 1)\xi \quad \text{as} \quad \xi \to -\infty. \tag{2.44}$$

An examination of equation (2.37), with condition (2.39), reveals that for each *fixed* $A \leq 0$, the (F, F') phase portrait of solutions to (2.37) takes the form of Figure 2.3(a) when $A < 0$ and Figure (2.3)(b) when $A = 0$. The local structure of the equilibrium point $(0, 0)$ is obtained via linearization of equation (2.37) (note that although (2.37) is nonautonomous, local phase paths do not intersect because the general form (2.39) is restricted by either fixing $A < 0$ or setting $A = 0$, after which local phase paths are a one parameter family, parameterized by $B \in \mathbb{R}$). The straight line phase path follows from the exact solution $F(\xi) = (\delta + 1)\xi$, with local phase paths to this line again determined by a linearization of (2.37) about this exact solution.The remaining phase paths, and, in particular, the existence of the phase path $\mathcal{H}^*$, and deduced by continuous deformation. In addition, the structure of the phase portrait has been confirmed numerically. Each phase path connecting to $(0, 0)$ corresponds to a unique $B \in \mathbb{R}$. An examination of Figure 2.3 then enables us to conclude that there exists a unique B^*, which corresponds to the phase path $\mathcal{H}^*$, for which (2.37) has a solution $F = F^*(\xi)$, $-\infty < \xi < \infty$, which satisfies conditions (2.43) and (2.44). It is readily established that $B^* < 0$, whilst,

$$\begin{aligned} &F^*(\xi) < 0 \qquad \forall \qquad \xi \in \mathbb{R}, \\ &F^{*'}(\xi) > 0 \qquad \forall \qquad \xi \in \mathbb{R} \\ &F^*(\xi) \sim (\delta + 1)\xi - C^*(-\xi)^{-\frac{1}{(2\delta+1)}} \quad \text{as} \quad \xi \to -\infty, \end{aligned} \tag{2.45}$$

for some constant $C^* > 0$ [3]. A numerical determination of $F = F^*(\xi)$ (using a shooting method, employing (2.43) at large positive ξ) for a range of values of δ is illustrated in Figure 2.4 (*a-d*). The associated values of the constants B^* and C^* are given in Table 2.1.

δ	B^*	C^*
0.1	- 3.05	1.95
0.5	- 2.32	2.95
1.0	- 1.95	5.05
2.0	- 0.25	7.15

Table 2.1: The values of the constants B^* and C^* with the associated values of δ when $\gamma > 2\delta + 1$.

(iii) $\gamma = 2\delta + 1$

In this case the leading order problem is again equation (2.37), but now matching with region III$^+$ is possible with the matching condition requiring that,

$$F(\xi) \sim A_R \xi^{-(2\delta+1)} \quad \text{as} \quad \xi \to \infty. \tag{2.46}$$

Recalling that $A_R < 0$, then it follows from Figure 2.3(a), on taking $A = A_R$, that there exists $B = B^*(A_R)$, such that (2.37) and (2.46) has a solution $F = F_R^*(\xi)$, $-\infty < \xi < \infty$, corresponding to the phase path $\mathcal{H}^*$ in Figure 2.3(a). In particular,

$$\begin{aligned} &F_R^*(\xi) < 0 \qquad \forall \qquad \xi \in \mathbb{R}, \\ &F_R^{*'}(\xi) > 0 \qquad \forall \qquad \xi \in \mathbb{R} \end{aligned} \tag{2.47}$$

$$\begin{aligned} &F_R^*(\xi) \sim A_R \xi^{-(2\delta+1)} + B^*(A_R) \xi^{2\delta} e^{-\frac{1}{4}\xi^2} \quad \text{as} \quad \xi \to \infty, \\ &F_R^*(\xi) \sim (\delta+1)\xi - C^*(A_R)(-\xi)^{-\frac{1}{(2\delta+1)}} \quad \text{as} \quad \xi \to -\infty, \end{aligned} \tag{2.48}$$

for some constant $C^*(A_R) > 0$[3].

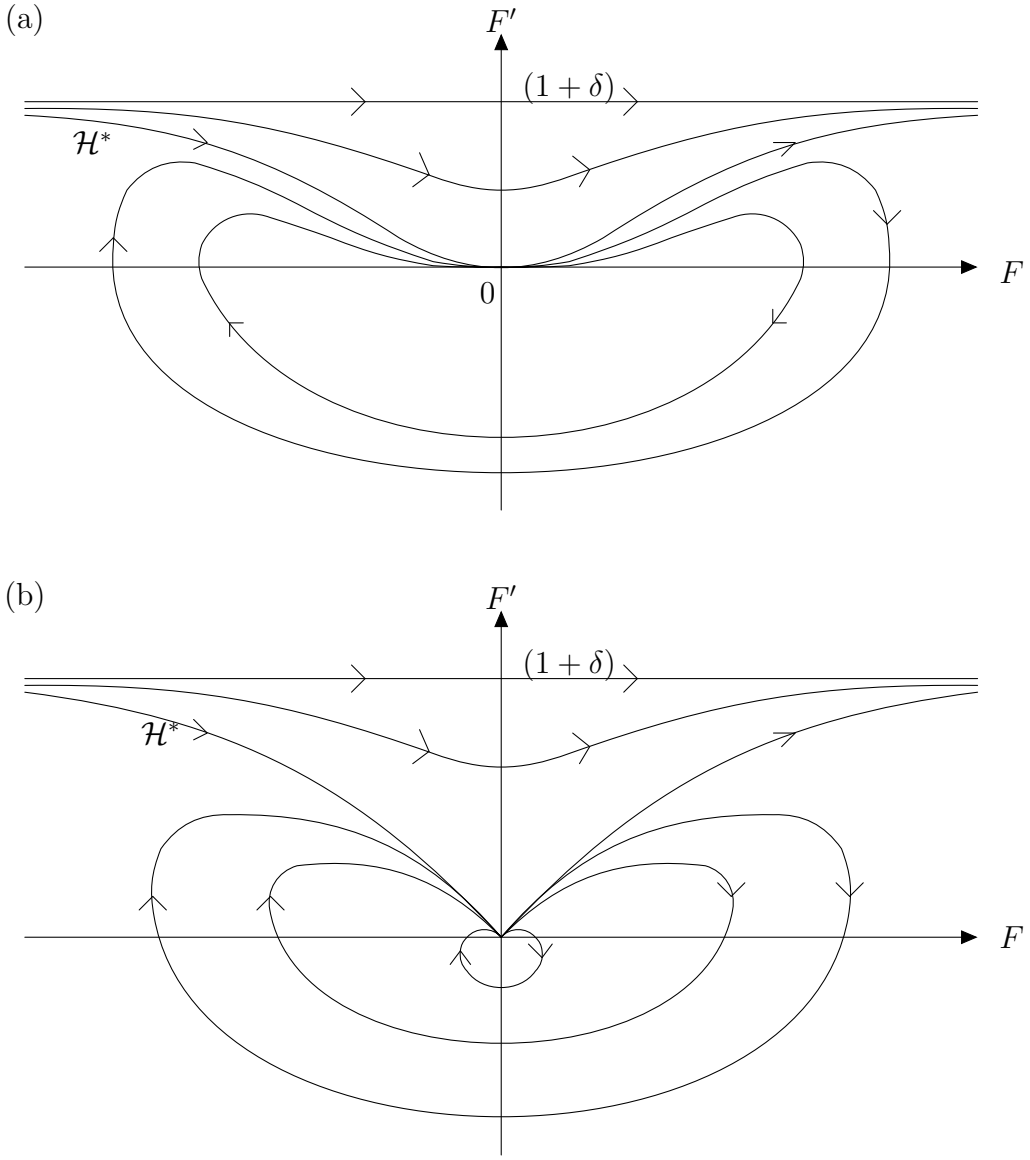

Figure 2.3: The (F, F') phase plane for (2.37) with fixed A. (a) The case $A < 0$ and (b) the case $A = 0$.

As $\xi \to -\infty$, we move out of the localized region IV$^+$ into region V, where now $y = \frac{u_+}{(\delta+1)} - O(1)$. It is convenient as this stage to leave region V until later, and to next develop the asymptotic structure of $u(y,t)$ as $t \to \infty$, ***moving in from*** region II$^-$ (when $(-y) \gg 1$) to $y = O(1)$ as $t \to \infty$. To proceed we introduce a new region, labelled as region III$^-$. The details of this region follow those given for region III$^+$ and are not

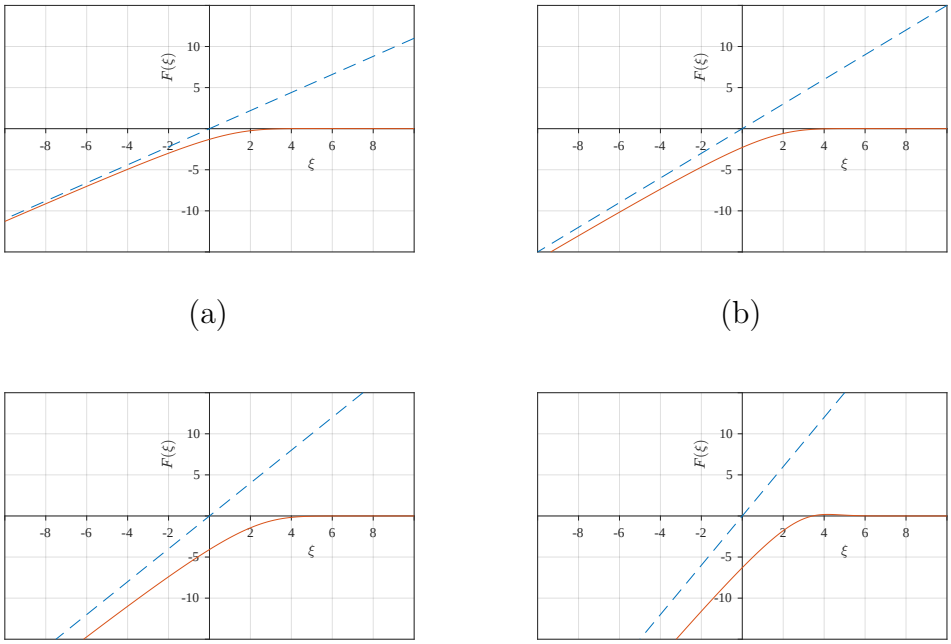

(a) (b)

(c) (d)

Figure 2.4: A graph of $F = F^*(\xi)$ when (a) $\delta = 0.1$, $B^* = -3.05$, $C^* = 1.95$, (b) $\delta = 0.5$, $B^* = -2.32$, $C^* = 2.95$, (c) $\delta = 1.0$, $B^* = -1.95$, $C^* = 5.05$ and (d) $\delta = 2.0$, $B^* = -0.25$, $C^* = 7.15$.

repeated here. In region III$^-$ we have that

$$u(y,t) = u_- + A_L \left(\frac{u_-}{(\delta+1)} - y \right)^{-\gamma} t^{-\gamma(\delta+1)} + o\left(t^{-\gamma(\delta+1)}\right) \quad \text{as} \quad t \to \infty \tag{2.49}$$

with $y = \frac{u_-}{(\delta+1)} - O(1)$. Expansion (2.49) becomes nonuniform when

$$y = \frac{u_-}{(\delta+1)} + O\left(t^{-r}\right) \quad \text{as} \quad t \to \infty$$

with $r > 0$ as given in (2.29). Thus, we examine this region of nonuniformity by introducing region IV$^-$. Accordingly we introduce the scaled variable ξ, via

$$y = \frac{u_-}{(\delta+1)} + \xi t^{-r} \tag{2.50}$$

with $\xi = O(1)$ as $t \to \infty$, and expansion (2.49) dictating that we expand in the form

$$u(\xi,t) = u_- + \hat{F}(\xi) t^{-r} + o\left(t^{-r}\right) \quad \text{as} \quad t \to \infty \tag{2.51}$$

with $\xi = O(1)$. The details are identical to those for region IV$^+$, and are not repeated here. In fact, making the replacement of A_R by $(-A_L)$, we obtain for $\hat{F}(\xi)$, $-\infty < \xi < \infty$, that

$$\hat{F}(\xi) = \begin{cases} -F(-\xi), & 0 < \gamma < 2\delta + 1, \\ -F^*(-\xi), & \gamma > 2\delta + 1, \\ -F_R^*(-\xi), & \gamma = 2\delta + 1. \end{cases}$$

As $\xi \to \infty$, we move out of the localized region IV$^-$ into region V where now $y = \frac{u_-}{(\delta+1)} + O(1)$. To complete the asymptotic structure as $t \to \infty$, it remains to consider region V, where $\frac{u_-}{(\delta+1)} + O(1) \le y \le \frac{u_+}{(\delta+1)} - O(1)$ as $t \to \infty$. The expansions (2.27) and

(2.51) in regions IV^+ and IV^- respectively dictate that we expand in region V as,

$$u(y,t) = G_0(y) + G_1(y)t^{-(1+\delta)} + G_2(y)t^{-2(1+\delta)} + o(t^{-2(1+\delta)}) \quad \text{as} \quad t \to \infty \tag{2.52}$$

with $\frac{u_-}{(\delta+1)} + O(1) \leq y \leq \frac{u_+}{(\delta+1)} - O(1)$. On substitution of expansion (2.52) into equation (2.1) (when written in terms of y and t) we obtain at leading order that

$$G_0'\Big(G_0 - (\delta+1)y\Big) = 0, \quad \frac{u_-}{(\delta+1)} < y < \frac{u_+}{(\delta+1)}. \tag{2.53}$$

We note that we have examined equation (2.53) in Section 1.5.3. Equation (2.53) is to be solved subject to the matching conditions with regions IV^+ and IV^-, namely

$$G_0(y) \sim u_+ + (\delta+1)\left(y - \frac{u_+}{(\delta+1)}\right) \quad \text{as} \quad y \to \left(\frac{u_+}{(\delta+1)}\right)^-, \tag{2.54}$$

and

$$G_0(y) \sim u_- + (\delta+1)\left(y - \frac{u_-}{(\delta+1)}\right) \quad \text{as} \quad y \to \left(\frac{u_-}{\delta+1}\right)^+. \tag{2.55}$$

The solution to (2.53) subject to (2.54) and (2.55) is trivially given by

$$G_0(y) = (\delta+1)\,y, \quad \frac{u_-}{(\delta+1)} < y < \frac{u_+}{(\delta+1)}. \tag{2.56}$$

The function $G_1(y)$ remains undetermined, being a remnant of the global evolution when $t = O(1)$. However, matching to regions $\mathrm{IV}^\pm$ requires

$$G_1(y) \sim \begin{cases} A_L^{\frac{1}{\gamma}}(\delta+1)^{(1-\frac{1}{\gamma})}\left(y - \frac{u_-}{(\delta+1)}\right)^{-\frac{1}{\gamma}} & \text{as } y \to \left(\frac{u_-}{(\delta+1)}\right)^+, \\ -(-A_R)^{\frac{1}{\gamma}}(\delta+1)^{(1-\frac{1}{\gamma})}\left(\frac{u_+}{(\delta+1)} - y\right)^{-\frac{1}{\gamma}} & \text{as } y \to \left(\frac{u_+}{(\delta+1)}\right)^-, \end{cases} \tag{2.57}$$

when $0 < \gamma < (2\delta + 1)$, whilst

$$G_1(y) \sim \begin{cases} C^* \left(y - \frac{u_-}{(\delta+1)} \right)^{-\frac{1}{(2\delta+1)}} & \text{as } y \to \left(\frac{u_-}{(\delta+1)} \right)^+, \\ -C^* \left(\frac{u_+}{(\delta+1)} - y \right)^{-\frac{1}{(2\delta+1)}} & \text{as } y \to \left(\frac{u_+}{(\delta+1)} \right)^-, \end{cases} \tag{2.58}$$

when $\gamma > (2\delta + 1)$, and,

$$G_1(y) \sim \begin{cases} C^*(-A_L) \left(y - \frac{u_-}{(\delta+1)} \right)^{-\frac{1}{(2\delta+1)}} & \text{as } y \to \left(\frac{u_-}{(\delta+1)} \right)^+, \\ -C^*(A_R) \left(\frac{u_+}{(\delta+1)} - y \right)^{-\frac{1}{(2\delta+1)}} & \text{as } y \to \left(\frac{u_+}{(\delta+1)} \right)^-, \end{cases} \tag{2.59}$$

when $\gamma = (2\delta + 1)$. At next order, we obtain

$$G_2(y) = \frac{1}{(\delta + 1)} G_1(y) G_1'(y). \tag{2.60}$$

The asymptotic expansion in region V is then, via (2.52), given by

$$u(y,t) = (\delta + 1)y + G_1(y)t^{-(\delta+1)} + \frac{G_1(y)G_1'(y)}{(\delta + 1)} t^{-2(\delta+1)} + o\left(t^{-2(\delta+1)}\right) \text{ as } t \to \infty \tag{2.61}$$

with $\frac{u_-}{(\delta+1)} + O(1) \leq y \leq \frac{u_+}{(\delta+1)} - O(1)$[3].

The asymptotic structure of $\mathbf{IVP}^+$ as $t \to \infty$ when $\delta > -\frac{1}{2}$ is complete now. A uniform approximation has been given through regions $\mathrm{II}^{\pm}$, $\mathrm{III}^{\pm}$, $\mathrm{IV}^{\pm}$ and V. A schematic representation of the location and thickness of the asymptotic regions as $t \to \infty$ is given in Figure 2.5 (we recall that depending on the problem parameters, there may be passive regions located at $\frac{u_+}{(\delta+1)}$ and $\frac{u_-}{(\delta+1)}$ which allow for the reordering of terms in the expansions in regions III^+ and III^-, respectively). The large-t attractor for solution of $\mathbf{IVP}^+$ is an expansion wave, which allows for the adjustment of the solution from u_+ to u_-.

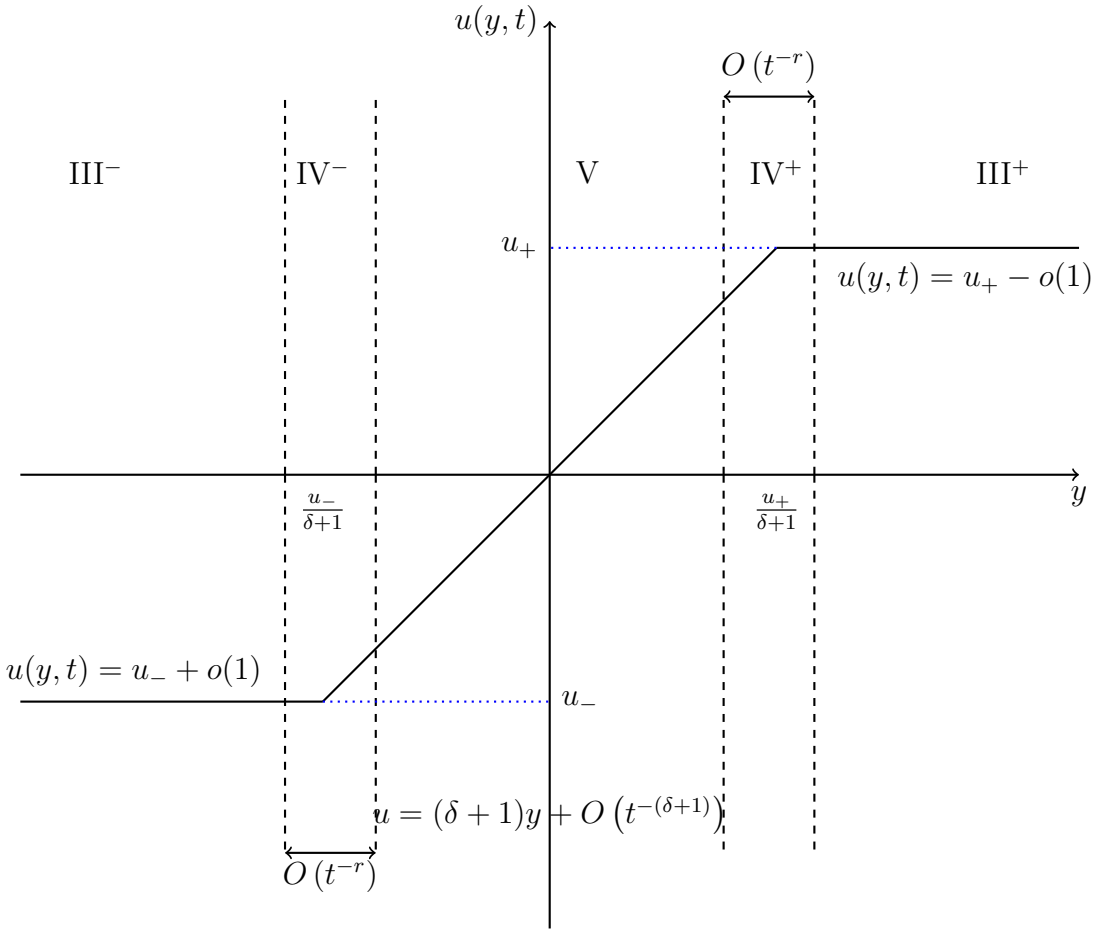

Figure 2.5: A schematic representation of the asymptotic structure of $u(y,t)$ in the (y,u) plane as $t \to \infty$ for **IVP**$^+$ when $\delta > -\frac{1}{2}$. We note that $u = u_+ + O\left(t^{-r}\right)$ as $t \to \infty$ in region IV$^+$, while $u = u_- + O\left(t^{-r}\right)$ as $t \to \infty$ in region IV$^-$ with r given in (2.29).

Finally, the asymptotic structure to the solution of $\mathbf{IVP}^+$ as $t \to \infty$ when $\delta > -\frac{1}{2}$ can be summarized as:

Region II$^+$: $t = O(1)$ as $x \to \infty$

$$u(x,t) = u_+ + \frac{F_0(t)}{x^\gamma} + \frac{F_1(t)}{x^{(\gamma+1)}} + \frac{F_2(t)}{x^r} + \frac{F_3(t)}{x^s} + o\left(\frac{1}{x^s}\right) \text{ as } x \to \infty$$

with $t = O(1)$, with r and s given in (2.15), $F_0(t),\ F_1(t),\ F_2(t)$ and $F_3(t)$ given in (2.16).

Region III$^+$: $y = \frac{u_+}{(1+\delta)} + O(1)$ as $t \to \infty$

$$u(y,t) = u_+ + A_R\left(y - \frac{u_+}{(1+\delta)}\right)^{-\gamma} t^{-\gamma(1+\delta)} + o(t^{-\gamma(1+\delta)}) \text{ as } t \to \infty.$$

with $y = \frac{u_+}{(1+\delta)} + O(1)$.

Region IV$^+$: $y = \frac{u_+}{(1+\delta)} \pm O\left(t^{-r}\right)$ as $t \to \infty$

$$u(\xi,t) = u_+ + F(\xi)\ t^{-r} + o\left(t^{-r}\right) \text{ as } t \to \infty$$

with $\xi = O(1)\Big(\ \in (-\infty,\infty)\Big)$, and where $\xi = \Big(y - \frac{u_+}{(1+\delta)}\Big)t^r$, with r given in (2.29).

Region V: $\frac{u_-}{(1+\delta)} + O(1) \le y \le \frac{u_+}{(1+\delta)} - O(1)$ as $t \to \infty$

$$u(y,t) = (1+\delta)\ y + G_1(y)\ t^{-(1+\delta)} + \frac{G_1(y)G_1'(y)}{(1+\delta)}\ t^{-2(1+\delta)} + o(t^{-2(1+\delta)}) \text{ as } t \to \infty$$

with $\frac{u_-}{(\delta+1)} + O(1) \leq y \leq \frac{u_+}{(\delta+1)} - O(1)$ and where

$$G_1(y) \sim \begin{cases} A_L^{\frac{1}{\gamma}} \, (\delta+1)^{(1-\frac{1}{\gamma})} \Big(y - \dfrac{u_-}{(\delta+1)} \Big)^{-\frac{1}{\gamma}}, & \text{as } y \to \left(\frac{u_-}{(\delta+1)}\right)^+, \\ -(-A_R)^{\frac{1}{\gamma}} \, (\delta+1)^{(1-\frac{1}{\gamma})} \left(\dfrac{u_+}{(\delta+1)} - y \right)^{-\frac{1}{\gamma}} & \text{as } y \to \left(\frac{u_+}{(\delta+1)}\right)^-, \end{cases}$$

when $0 < \gamma < (2\delta+1)$, whilst

$$G_1(y) \sim \begin{cases} C^* \left(y - \dfrac{u_-}{(\delta+1)} \right)^{-\frac{1}{(2\delta+1)}} & \text{as } y \to \left(\frac{u_-}{(\delta+1)}\right)^+, \\ -C^* \left(\dfrac{u_+}{(\delta+1)} - y \right)^{-\frac{1}{(2\delta+1)}} & \text{as } y \to \left(\frac{u_+}{(\delta+1)}\right)^-, \end{cases}$$

when $\gamma > (2\delta+1)$, and,

$$G_1(y) \sim \begin{cases} C^* \, (-A_L) \Big(y - \dfrac{u_-}{(\delta+1)} \Big)^{-\frac{1}{(2\delta+1)}} & \text{as } y \to \left(\frac{u_-}{(\delta+1)}\right)^+, \\ -C^* \, (A_R) \Big(\dfrac{u_+}{(\delta+1)} - y \Big)^{-\frac{1}{(2\delta+1)}} & \text{as } y \to \left(\frac{u_+}{(\delta+1)}\right)^-, \end{cases}$$

when $\gamma = (2\delta+1)$.

Region IV$^-$: $y = \frac{u_-}{(1+\delta)} \pm O\left(t^{-r}\right)$ as $t \to \infty$

$$u(\xi, t) = u_- + \hat{F}(\xi) \, t^{-r} + o\left(t^{-r}\right) \text{ as } t \to \infty$$

with $\xi = O(1)\Big(\in (-\infty, \infty) \Big)$, and where $\xi = \Big(y - \frac{u_-}{(1+\delta)} \Big) t^r$, with r given in (2.29) .

Region III$^-$: $y = \frac{u_-}{(1+\delta)} - O(1)$ as $t \to \infty$

$$u(y, t) = u_- + A_L \left(\frac{u_-}{(1+\delta)} - y \right)^{-\gamma} t^{-\gamma(\delta+1)} + o\left(t^{-\gamma(1+\delta)}\right) \text{ as } t \to \infty$$

with $y = \frac{u_-}{(1+\delta)} - O(1)$.

Region II$^-$: $t = O(1)$ as $x \to \infty$

$$u(x,t) = u_- + \frac{F_0(t)}{(-x)^{\gamma}} + \frac{F_1(t)}{(-x)^{(\gamma+1)}} + \frac{F_2(t)}{(-x)^{r}} + \frac{F_3(t)}{(-x)^{s}} + o\left(\frac{1}{(-x)^{s}}\right) \text{ as } x \to \infty$$

with $t = O(1)$, with r and s given in (2.19), $F_0(t),\ F_1(t),\ F_2(t)$ and $F_3(t)$ given in (2.20).

The above asymptotic structure can be summarized in the following Proposition which has been established via matched asymptotic coordinate expansions. It is first convenient to introduce the function $u_E : \mathbb{R} \to \mathbb{R}$ such that

$$u_E(\lambda) = \begin{cases} u_+, & \lambda > \frac{u_+}{(\delta+1)}, \\ (\delta+1)\lambda, & \frac{u_-}{(\delta+1)} \le \lambda \le \frac{u_+}{(\delta+1)}, \\ u_-, & \lambda < \frac{u_-}{(\delta+1)}, \end{cases} \tag{2.62}$$

We then have,

Proposition 1. *Let $u : \mathbb{R} \times [0, \infty) \to \mathbb{R}$ be the solution to initial-value problem* **IVP**$^+$ *with $\gamma > 0$, $\delta > -\frac{1}{2}$ and $u_+ > u_-$. Then, in terms of the coordinate $y = xt^{-(1+\delta)}$, on writing,*

$$u(y,t) = u_E(y) + R(y,t)$$

for $(y,t) \in \mathbb{R} \times [0,\infty)$, it follows that $R(y,t) \to 0$ as $t \to \infty$ uniformly for $y \in \mathbb{R}$, with the rate of convergence being algebraic in t as $t \to \infty$. In particular,

$$R(y,t) = \begin{cases} O\Big(\dfrac{t^{-\gamma(1+\delta)}}{(1+|y|)^{\gamma}}\Big) & \text{in regions } III^{\pm}, \\ O\Big(t^{-r}\Big) & \text{in regions } IV^{\pm}, \\ O\Big(t^{-(1+\delta)}\Big) & \text{in regions } V, \end{cases}$$

as $t \to \infty$, with r given in (2.29)[3].

2.3.2 $\delta = -\frac{1}{2}$

We recall from Section 2.2 that in this case, we need to consider the cases $\gamma \geq 1$ and $0 < \gamma < 1$ separately. We begin by considering the case $0 < \gamma < 1$ [3].

2.3.2.1 $\delta = -\frac{1}{2}$, $0 < \gamma < 1$:

In this case, expansions (2.14) and (2.18) of regions II$^+$ ($x \to \infty$, $t = O(1)$) and II$^-$ ($x \to -\infty$, $t = O(1)$), respectively, continue to remain uniform provided that $|x| \gg t^{\frac{1}{2(1-\gamma)}}$ as $t \to \infty$. However, a nonuniformity develops when $|x| = O\left(t^{\frac{1}{2(1-\gamma)}}\right)$. We begin by considering the asymptotic structure as $t \to \infty$ by moving in from region II$^+$ when $x \gg t^{\frac{1}{2(1-\gamma)}}$ as $t \to \infty$. To proceed, we introduce a new region, which we label as region III$^+$. To examine region III$^+$, we introduce the scaled coordinate

$$y = x\, t^{-\frac{1}{2(1-\gamma)}} \tag{2.63}$$

where $y = O(1)$ as $t \to \infty$ [3]. The form of the asymptotic expansion for $u(y,t)$ in region III$^+$ follows from the structure of expansion (2.14) in region II$^+$, when written in terms of y and t, and expanded for $y = O(1)$ as $t \to \infty$. This requires that in region III$^+$ we expand in the form

$$u(y,t) = u_+ + F_0(y)t^{-\frac{\gamma}{2(1-\gamma)}} + F_1(y)t^{-\frac{\gamma}{(1-\gamma)}} + F_2(y)t^{-\frac{3\gamma}{2(1-\gamma)}} + o\left(t^{-\frac{3\gamma}{2(1-\gamma)}}\right) \tag{2.64}$$

as $t \to \infty$ with $y = O(1)$, and where $F_0(y)$, $F_1(y)$ and $F_2(y)$ are functions to be determined. On substitution from (2.64) into equation (2.1) (when written in terms of y and t). We obtain after some calculation [1]

$$\begin{aligned}
&\left(-\frac{\gamma}{2(1-\gamma)}F_0(y)t^{-\frac{\gamma}{2(1-\gamma)}} - \frac{\gamma}{(1-\gamma)}F_1(y)t^{-\frac{\gamma}{(1-\gamma)}} - \frac{3\gamma}{2(1-\gamma)}F_2(y)t^{-\frac{3\gamma}{2(1-\gamma)}}\right) \\
&- \frac{y}{2(1-\gamma)}\left(F_0'(y)t^{-\frac{\gamma}{2(1-\gamma)}} + F_1'(y)t^{-\frac{\gamma}{(1-\gamma)}} + F_2'(y)t^{-\frac{3\gamma}{2(1-\gamma)}}\right) + t^{-\frac{\gamma}{2(1-\gamma)}} \\
&\left[\left(u_+ + F_0(y)t^{-\frac{\gamma}{2(1-\gamma)}} + F_1(y)t^{-\frac{\gamma}{(1-\gamma)}} + F_2(y)t^{-\frac{3\gamma}{2(1-\gamma)}}\right)\left(F_0'(y)t^{-\frac{\gamma}{2(1-\gamma)}} + F_1'(y)t^{-\frac{\gamma}{(1-\gamma)}}\right.\right. \\
&\left.\left. + F_2'(y)t^{-\frac{3\gamma}{2(1-\gamma)}}\right)\right] \sim F_0''(y)t^{-\frac{3\gamma}{2(1-\gamma)}} + F_1''(y)t^{-\frac{2\gamma}{(1-\gamma)}} + F_2''(y)t^{-\frac{5\gamma}{2(1-\gamma)}}.
\end{aligned}$$

We now equate at each order in turn and solve to find $F_0(y)$, $F_1(y)$ and $F_2(y)$. Equating at $O(t^{-\frac{\gamma}{2(1-\gamma)}})$ we have the following ordinary differential equation for $F_0(y)$, namely

$$F_0' + \left(\frac{\gamma}{y}\right)F_0 = 0, \quad y = O(1)(> 0). \tag{2.65}$$

[1] $\frac{\partial u}{\partial t} = \left(\frac{\partial u}{\partial t} + \frac{\partial u}{\partial y}\frac{\partial y}{\partial t}\right)$, $\frac{\partial u}{\partial x} = \left(\frac{\partial u}{\partial y}\right)\left(\frac{\partial y}{\partial x}\right)$ and $\frac{\partial^2 u}{\partial x^2} = \left(\frac{\partial^2 u}{\partial y^2}\right)\left(\frac{\partial y}{\partial x}\right)^2$ where $\frac{\partial y}{\partial t} = -\frac{y}{2(1-\gamma)t}$ and $\frac{\partial y}{\partial x} = t^{-\frac{1}{2(1-\gamma)}}$.

Equation (2.65) has to be solved subject to the matching condition with expansion (2.14) in region II$^+$ $\left(\text{when } x = O\left(t^{\frac{\gamma}{2(1-\gamma)}}\right)\right)$, which requires

$$F_0(y) \sim \frac{A_R}{y^\gamma} \quad \text{as} \quad y \to \infty. \tag{2.66}$$

The solution of (2.65) subject to (2.66) is then readily obtained as

$$F_0(y) = A_R\, y^{-\gamma}, \quad y > 0. \tag{2.67}$$

Equating at $O(t^{-\frac{\gamma}{(1-\gamma)}})$ we have the following ordinary differential equation for $F_1(y)$,

$$F_1' + \left(\frac{2\gamma}{y}\right) F_1 = -2A_R u_+ \gamma\,(1-\gamma)\, y^{-(\gamma+2)}, \quad y = O(1)(> 0). \tag{2.68}$$

This is to be solved subject to the corresponding matching condition with expansion (2.14) in region II$^+$ $\left(\text{when } x = O\left(t^{\frac{\gamma}{(1-\gamma)}}\right)\right)$

$$F_1(y) \sim 2u_+\gamma A_R y^{-(\gamma+1)} \quad \text{as} \quad y \to \infty. \tag{2.69}$$

The solution of (2.68) and (2.69) is then readily obtained as

$$F_1(y) = 2u_+\gamma A_R y^{-(\gamma+1)} \quad \text{as} \quad y > 0. \tag{2.70}$$

Equating at $O(t^{-\frac{3\gamma}{2(1-\gamma)}})$ we have the following ordinary differential equation for $F_2(y)$,

$$\begin{aligned} F_2' + \left(\frac{3\gamma}{y}\right) F_2 = -2(1-\gamma)\Big[&\left(\gamma(\gamma+1)A_R + 2\gamma(\gamma+1)A_R u_+^2\right) y^{-(\gamma+3)} \\ &+ \gamma A_R^2 y^{-2(\gamma+1)}\Big], \quad y = O(1)(> 0). \end{aligned} \tag{2.71}$$

This is to be solved subject to the corresponding matching condition with expansion (2.14) in region II^+ $\left(\text{when } x = O\left(t^{\frac{3\gamma}{2(1-\gamma)}}\right)\right)$

$$F_2(y) \sim 2\gamma A_R^2 y^{-(2\gamma+1)} + \gamma(\gamma+1)A_R y^{-(\gamma+2)} \quad \text{as} \quad y \to \infty. \tag{2.72}$$

The solution of (2.71) and (2.72) is then readily obtained as

$$F_2(y) = 2\gamma\ A_R^2\ y^{-(2\gamma+1)} + \left(\gamma(\gamma+1)A_R + 2\gamma(\gamma+1)u_+^2 A_R\right) y^{-(\gamma+2)} \quad \text{as} \quad y > 0. \tag{2.73}$$

In this case the expansion in region III^+ is given by (2.64) with (2.67), (2.70) and (2.73). That is,

$$\begin{aligned} u(y,t) &= u_+ + A_R\ y^{-\gamma}\ t^{-\frac{\gamma}{2(1-\gamma)}} + 2u_+\gamma\ A_R\ y^{-(\gamma+1)} t^{-\frac{\gamma}{(1-\gamma)}} \\ &+ \left(2\gamma\ A_R^2\ y^{-(2\gamma+1)} + \left(\gamma(\gamma+1)A_R + 2\gamma(\gamma+1)u_+^2 A_R\right) y^{-(\gamma+2)}\right) t^{-\frac{3\gamma}{2(1-\gamma)}} + o\left(t^{-\frac{3\gamma}{2(1-\gamma)}}\right) \end{aligned} \tag{2.74}$$

as $t \to \infty$ with $y = O(1)$. We observe that expansion (2.74) becomes nonuniform when

$$y = O\left(t^{-\frac{\gamma}{2(1-\gamma)}}\right) \quad \text{as} \quad t \to \infty\ \left(\text{when } x = O\left(t^{\frac{1}{2}}\right)\ \text{as } t \to \infty\right).$$

We now consider the asymptotic structure as $t \to \infty$ by moving in from region II^- when $(-x) \gg t^{-\frac{\gamma}{2(1-\gamma)}}$. To proceed, we define a new region III^-. The details of this region follow, after minor modification, those given for region III^+ above. We have in region III^-that

$$u(y,t) = u_- + A_L(-y)^{-\gamma} t^{-\frac{\gamma}{2(1-\gamma)}} + O\left(t^{-\frac{\gamma}{(1-\gamma)}}\right) \tag{2.75}$$

as $t \to \infty$ with $y = O(1)$ (< 0). We observe that expansion (2.75) becomes nonuniform when

$$y = O\left(t^{-\frac{\gamma}{2(1-\gamma)}}\right) \quad \text{as} \quad t \to \infty.$$

That is, when $x = O\left(t^{\frac{1}{2}}\right)$. To proceed, we define a new region SS. To examine SS we introduce the scaled coordinate z, via

$$z = x\ t^{-\frac{1}{2}} = y\ t^{\frac{\gamma}{2(1-\gamma)}}, \tag{2.76}$$

as $t \to \infty$ with $z = O(1)$, and expand in the form

$$u(z,t) = U(z) + o(1) \tag{2.77}$$

as $t \to \infty$ with $z = O(1)$. On substituting expansion (2.77) into equation (2.1) (when written in terms of z and t) we obtain at leading order that

$$U_{zz} + \left(\frac{z}{2} - U\right) U_z = 0, \qquad -\infty < z < \infty. \tag{2.78}$$

We note that equation (2.78) has been considered in Section 1.5.2. We recall that equation (2.78) is to be solved subject to the leading order matching conditions with region III$^+$ $(z \to \infty)$ and region III$^-$ $(z \to -\infty)$, namely,

$$U(z) \to \begin{cases} u_+ & \text{as } z \to \infty, \\ u_- & \text{as } z \to -\infty. \end{cases} \tag{2.79}$$

The boundary value problem (2.78) and (2.79) has been examined by Rudenko and Soluyan [32] and Scott [36]. It was established that for each u_+ and u_- $(u_+ \neq u_-)$,

(2.78) and (2.79) have a unique solution $U = u_R(z)$, which is strictly monotone in z, and satisfy

$$u_R(z) \sim \begin{cases} u_+ + \mathcal{C}_+(u_+, u_-) z^{-1} e^{-\frac{1}{4}(z-2u_+)^2} & \text{as } z \to \infty, \\ u_- + \mathcal{C}_-(u_+, u_-) z^{-1} e^{-\frac{1}{4}(z-2u_-)^2} & \text{as } z \to -\infty. \end{cases} \tag{2.80}$$

with $\mathcal{C}_+$ and $\mathcal{C}_-$ globally determined nonzero constants, depending upon u_+ and u_- [3]. A numerical study of (2.78) and (2.80) using a shooting method again reveals that there exists

$$\mathcal{C}_+(u_+, u_-) < 0 \qquad \text{and} \qquad \mathcal{C}_-(u_+, u_-) > 0. \tag{2.81}$$

such that boundary conditions (2.79) are satisfied. A numerical determination of $U = u_R(z)$ for a range of values of u_+ and u_- is illustrated in Figure 2.6. The associated value of $\mathcal{C}_+$ and $\mathcal{C}_-$ are given in Table 2.3.

u_+	u_-	$\mathcal{C}_+$
1	-1	-7.74×10^{16}
1.4	0	-3.47×10^{6}
0	-1	-6.34×10^{16}

u_+	u_-	$\mathcal{C}_-$
1	-1	7.36×10^{3}
1.4	0	3.52×10^{6}
0	-1	6.03×10^{3}

Table 2.3: The values of the constants $\mathcal{C}_+$ and $\mathcal{C}_-$ corresponding to Figure 2.6.

Expansion (2.77) (with (2.80)) (for $z \gg 1$) when written in terms of z is given by

$$u \sim u_+ + \frac{\mathcal{C}_+(u_+, u_-)}{z}\, e^{-\frac{(z-2u_+)^2}{4}} \tag{2.82}$$

as $t \to \infty$. Expansion (2.74) (for $z \gg 1$) when written in terms of z is given by

$$u \sim u_+ + \frac{A_R}{z^\gamma}\, t^{-\frac{\gamma}{2}} \tag{2.83}$$

as $t \to \infty$. However, we observe from (2.77) with (2.80) that expansion (2.77) fails to match at higher order to expansion (2.74) as $z \to \infty$ and expansion (2.75) as $z \to -\infty$.

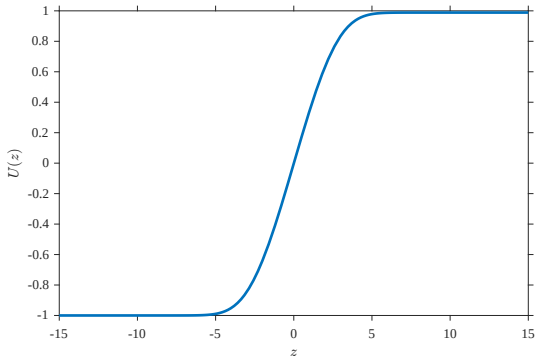

(a)

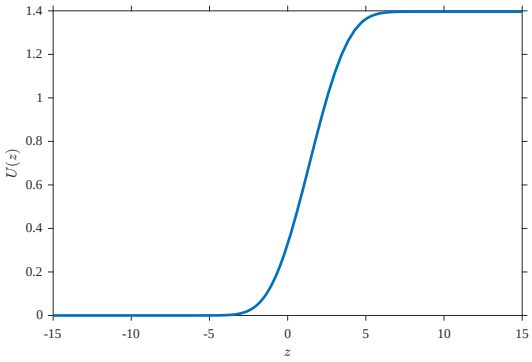

(b)

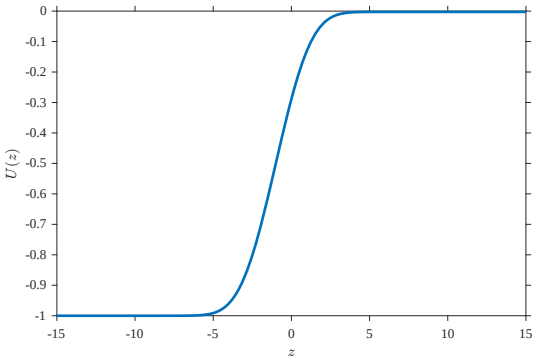

(c)

Figure 2.6: A graph of $U(z)$ when (a) $u_+ = 1$, $u_- = -1$ with $\mathcal{C}_+ = -7.74 \times 10^{16}$ or $\mathcal{C}_- = 7.36 \times 10^3$, (b) $u_+ = 1.4$, $u_- = 0$ with $\mathcal{C}_+ = -3.47 \times 10^6$ or $\mathcal{C}_- = 3.52 \times 10^6$ and (c) $u_+ = 0$, $u_- = -1$ with $\mathcal{C}_+ = -6.34 \times 10^{16}$ or $\mathcal{C}_- = 6.03 \times 10^3$.

We therefore require transition regions , which we label as $\mathrm{TR}^{\pm}$. To examine region TR^{+} we introduce the scaled coordinate ξ , via

$$\xi = (z - c(t))\left(\ln t\right)^{\frac{1}{2}}, \tag{2.84}$$

where the function $c(t)$ is a function to be determined. Comparison of the corrections to u_+ in (2.82) and (2.83) indicates that they are of the same order when $z = c(t)$ as $t \to \infty$. That is

$$\frac{c(t)^2}{4} = \frac{\gamma}{2}\ln t + c(t)u_+ + (\gamma - 1)\ln c(t) - u_+^2$$

which requires

$$c(t) = \sqrt{2\gamma}\,(\ln t)^{\frac{1}{2}} + 2u_+ + \frac{(\gamma-1)}{\sqrt{2\gamma}}\,\frac{\ln(\ln t)}{(\ln t)^{\frac{1}{2}}} + o\left(\frac{\ln(\ln t)}{(\ln t)^{\frac{1}{2}}}\right) \quad \text{as} \quad t \to \infty, \tag{2.85}$$

and it is determined so that matching between regions TR^{+}, III^{+} and SS is possible and in region TR^{+} we look for an expansion of the form

$$u(\xi, t) = u_+ + K(\xi)(\ln t)^{-\frac{\gamma}{2}}t^{-\frac{\gamma}{2}} + o\left((\ln t)^{-\frac{\gamma}{2}}t^{-\frac{\gamma}{2}}\right) \quad \text{as} \quad t \to \infty \tag{2.86}$$

with $\xi = O(1)$ and where $K(\xi)$ is a function to be determined [3]. On substituting expansion (2.86) into equation (2.1) (when equation (2.1) is written in terms of ξ an t),

we obtain after some calculation[2]

$$-\frac{\gamma}{2}K(\xi)(\ln t)^{-(\frac{\gamma}{2}+1)}t^{-\frac{\gamma}{2}} - \frac{\gamma}{2}K(\xi)(\ln t)^{-(\frac{\gamma}{2}+2)}t^{-\frac{\gamma}{2}} + \left(K_\xi(\ln t)^{-(\frac{\gamma}{2}+1)}t^{-(\frac{\gamma}{2}-1)}\right)$$
$$\left[-\frac{c(t)}{2}t^{-1}(\ln t)^{\frac{1}{2}} - \frac{\xi}{2}t^{-1} + \frac{\xi}{2}t^{-1}(\ln t)^{-1} - c'(t)(\ln t)^{\frac{1}{2}} + t^{-\frac{1}{2}}\left(t^{-\frac{1}{2}}(\ln t)^{\frac{1}{2}}\right)\left(u_+ + K(\xi)(\ln t)^{-\frac{\gamma}{2}}t^{-\frac{\gamma}{2}}\right)\right]$$
$$\sim (K_{\xi\xi}(\ln t)^{-\frac{\gamma}{2}}t^{-\frac{\gamma}{2}},$$

which gives at leading order that

$$K_{\xi\xi} + \sqrt{\frac{\gamma}{2}}K_\xi = 0, \quad -\infty < \xi < \infty. \tag{2.87}$$

Equation (2.87) has the solution

$$K(\xi) = A + Be^{-\sqrt{\frac{\gamma}{2}}\xi}, \quad -\infty < \xi < \infty.$$

where A and B are constants to be determined on matching. Matching with region III$^+$ as $\xi \to \infty$ requires that $A = \frac{A_R}{(2\gamma)^{\frac{\gamma}{2}}}$ and matching with region SS as $\xi \to -\infty$ requires that $B = \frac{\mathcal{C}_+(u_+,u_-)}{\sqrt{2\gamma}}$. Therefore, equation (2.87) is to be solved subject to the following matching conditions with region III$^+$ (as $\xi \to \infty$) and region SS (as $\xi \to -\infty$), namely,

$$K(\xi) \sim \begin{cases} \frac{A_R}{(2\gamma)^{\frac{\gamma}{2}}} & \text{as} \quad \xi \to \infty, \\ \frac{\mathcal{C}_+(u_+,u_-)}{\sqrt{2\gamma}}e^{-\sqrt{\frac{\gamma}{2}}\xi} & \text{as} \quad \xi \to -\infty. \end{cases} \tag{2.88}$$

The solution to (2.87) (with(2.88)) is readily obtained as

$$K(\xi) = \frac{A_R}{(2\gamma)^{\frac{\gamma}{2}}} + \frac{\mathcal{C}_+(u_+,u_-)}{\sqrt{2\gamma}}e^{-\sqrt{\frac{\gamma}{2}}\xi}, \quad -\infty < \xi < \infty.$$

[2] $\frac{\partial u}{\partial t} = \left(\frac{\partial u}{\partial t} + \frac{\partial u}{\partial \xi}\frac{\partial \xi}{\partial t}\right)$, $\frac{\partial u}{\partial x} = \left(\frac{\partial u}{\partial \xi}\right)\left(\frac{\partial \xi}{\partial x}\right)$ and $\frac{\partial^2 u}{\partial x^2} = \left(\frac{\partial^2 u}{\partial \xi^2}\right)\left(\frac{\partial \xi}{\partial x}\right)^2$ where $\frac{\partial \xi}{\partial t} = -\frac{c(t)}{2t}(\ln t)^{\frac{1}{2}} - \frac{\xi}{2t} + \frac{\xi}{2t}(\ln t)^{-1} - c'(t)(\ln t)^{\frac{1}{2}}$ and $\frac{\partial \xi}{\partial x} = \sqrt{\frac{\ln t}{t}}$.

Therefore, we have in region TR^+ that

$$u(\xi,t) = u_+ + \left(\frac{A_R}{(2\gamma)^{\frac{\gamma}{2}}} + \frac{\mathcal{C}_+(u_+,u_-)}{\sqrt{2\gamma}} e^{-\sqrt{\frac{\gamma}{2}}\xi} \right) (\ln t)^{-\frac{\gamma}{2}} t^{-\frac{\gamma}{2}} + o\left((\ln t)^{-\frac{\gamma}{2}} t^{-\frac{\gamma}{2}} \right) \tag{2.89}$$

as $t \to \infty$ with $\xi = O(1)$. Finally, we conclude this case by noting that matching expansion (2.77) (as $z \to -\infty$) to expansion (2.75) similarly fails and we require a corresponding transition region, which we label as TR^-. To examine region TR^-we introduce the scaled coordinate $\hat{\xi}$ by

$$\hat{\xi} = (z + c(t)) (\ln t)^{\frac{1}{2}}, \tag{2.90}$$

as $t \to \infty$ with $\hat{\xi} = O(1)$. The details of region TR^- follow, after minor modification, those given above for region TR^+ and summarized here for brevity. Therefore, in region TR^- we have that

$$u(\hat{\xi},t) = u_- + \left(\frac{A_L}{(2\gamma)^{\frac{\gamma}{2}}} + \frac{\mathcal{C}_-(u_+,u_-)}{\sqrt{2\gamma}} e^{\sqrt{\frac{\gamma}{2}}\hat{\xi}} \right) (\ln t)^{-\frac{\gamma}{2}} t^{-\frac{\gamma}{2}} + o\left((\ln t)^{-\frac{\gamma}{2}} t^{-\frac{\gamma}{2}} \right) \tag{2.91}$$

as $t \to \infty$ with $\hat{\xi} = O(1)$. It is again worth noting that higher order matching of expansions (2.89) and (2.91) in regions TR^+ and TR^-, with expansion (2.14) in region SS, requires the correction term in region SS to be $O\left((\ln t)^{-\frac{\gamma}{2}}\ t^{-\frac{\gamma}{2}} \right)$ [3].

The asymptotic structure of $\mathbf{IVP}^+$ as $t \to \infty$ when $0 < \gamma < 1$ and $\delta = -\frac{1}{2}$ is complete now. A uniform approximation has been given through regions $\mathrm{II}^\pm$, $\mathrm{III}^\pm$, $\mathrm{TR}^\pm$ and SS. A schematic representation of the location and thickness of the asymptotic structure as $t \to \infty$ is given in Figure 2.7. The large-time attractor for the solution of $\mathbf{IVP}^+$ in this case is the similarity solution found by Rudenko and Soluyan [32], which allows for the adjustment of the solution from u_+ to u_-. This attractor is in a stretching frame of

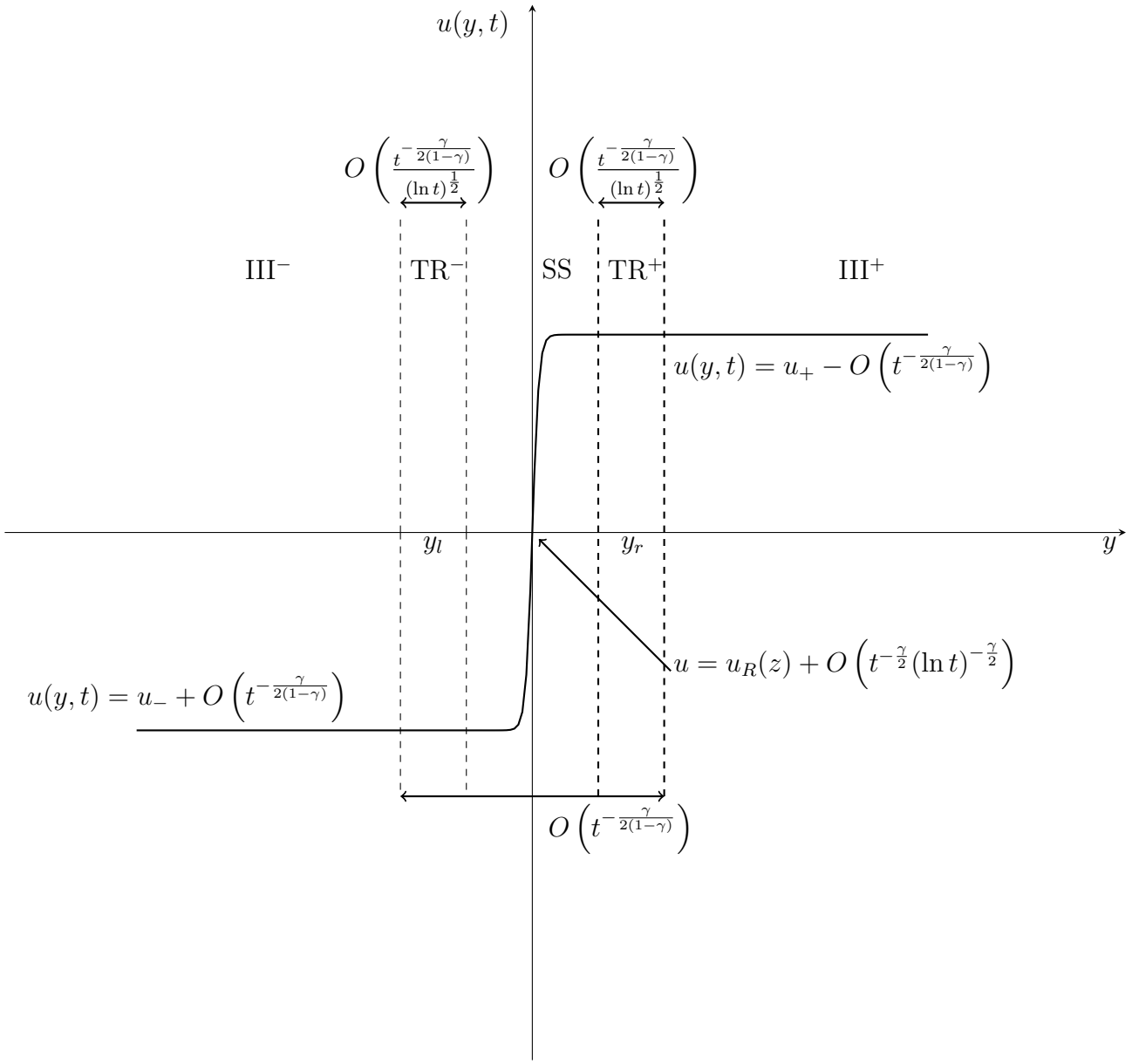

Figure 2.7: A schematic representation of the asymptotic structure of $u(y,t)$ in the (y,u) plane as $t \to \infty$ for **IVP**$^+$ when $\delta = -\frac{1}{2}$ and $0 < \gamma < 1$. We recall that $y_l = -y_r = -t^{-\frac{\gamma}{2(1-\gamma)}}\, c(t)$, where $c(t)$ is given by (2.85).

reference of thickness $|x| = O\left(t^{\frac{1}{2}}\right)$ as $t \to \infty$. Finally, the asymptotic structure to the solution of $\mathbf{IVP}^+$ as $t \to \infty$ when $\delta = -\frac{1}{2}$ and $0 < \gamma < 1$ can be summarized as:

Region II$^+$: $t = O(1)$ as $x \to \infty$

$$u(x,t) = u_+ + \frac{A_R}{x^\gamma} + \frac{\gamma u_+ A_R t^{(\delta+1)}}{(\delta+1)x^{(\gamma+1)}} + \frac{\gamma A_R^2 t^{(\delta+1)}}{(\delta+1)x^{(2\gamma+1)}} + o\left(\frac{1}{x^{(2\gamma+1)}}\right) \text{ as } x \to \infty$$

with $t = O(1)$.

Region III$^+$: $y = O(1)(> 0)$ as $t \to \infty$

$$\begin{aligned} u(y,t) &= u_+ + A_R y^{-\gamma} t^{-\frac{\gamma}{2(1-\gamma)}} + 2u_+\gamma A_R y^{-\gamma-1} t^{-\frac{\gamma}{(1-\gamma)}} \\ &+ \left(2\gamma A_R^2 y^{-(2\gamma+1)} + \left(\gamma(\gamma+1)A_R + 2\gamma(\gamma+1)u_+^2 A_R\right) y^{-(\gamma+2)}\right) t^{-\frac{3\gamma}{2(1-\gamma)}} + o\left(t^{-\frac{3\gamma}{2(1-\gamma)}}\right) \end{aligned}$$

as $t \to \infty$ with $y = O(1)(> 0)$.

Region TR$^+$: $y = \left(c(t) + \frac{\xi}{\sqrt{\ln t}}\right) t^{-\frac{\gamma}{2(1-\gamma)}}$ with $\xi = O(1)$ as $t \to \infty$

$$u(\xi,t) = u_+ + \left(\frac{A_R}{(2\gamma)^{\frac{\gamma}{2}}} + \mathcal{C}_+(u_+,u_-)(2\gamma)^{-\frac{1}{2}} e^{-(\frac{\gamma}{2})^{\frac{1}{2}}\xi}\right) (\ln t)^{-\frac{\gamma}{2}} t^{-\frac{\gamma}{2}} + o\left((\ln t)^{-\frac{\gamma}{2}} t^{-\frac{\gamma}{2}}\right)$$

as $t \to \infty$ with $\xi = O(1)$, and $c(t)$ given in (2.85).

Region SS: $y = zt^{-\frac{\gamma}{2(1-\gamma)})}$ with $z = O(1)$ as $t \to \infty$

$$u(z,t) = u_R(z) + o(1)$$

where

$$u_R(z) \sim \begin{cases} u_+ + \mathcal{C}_+(u_+,u_-)z^{-1}e^{-\frac{1}{4}(z-2u_+)^2} & \text{as } z \to \infty, \\ u_- + \mathcal{C}_-(u_+,u_-)z^{-1}e^{-\frac{1}{4}(z-2u_-)^2} & \text{as } z \to -\infty. \end{cases}$$

with $\mathcal{C}_+$ and $\mathcal{C}_-$ globally determined nonzero constants, depending upon u_+ and u_-, with

$$\mathcal{C}_+(u_+,u_-) < 0 \qquad \text{and} \qquad \mathcal{C}_-(u_+,u_-) > 0$$

as $t \to \infty$ with $z = O(1)$.

Region TR$^-$: $y = \left(-c(t) + \frac{\hat{\xi}}{\sqrt{\ln t}}\right) t^{-\frac{\gamma}{2(1-\gamma)}}$ with $\hat{\xi} = O(1)$ as $t \to -\infty$

$$u(\hat{\xi},t) = u_- + \left(\frac{A_L}{(2\gamma)^{\frac{\gamma}{2}}} + \mathcal{C}_-(u_+,u_-)(2\gamma)^{-\frac{1}{2}}e^{(\frac{\gamma}{2})^{\frac{1}{2}}\hat{\xi}}\right)(\ln t)^{-\frac{\gamma}{2}}t^{-\frac{\gamma}{2}} + o\left((\ln t)^{-\frac{\gamma}{2}}t^{-\frac{\gamma}{2}}\right)$$

as $t \to \infty$ with $\hat{\xi} = O(1)$, and $c(t)$ given in (2.85).

Region III$^-$: $y = O(1)(< 0)$ as $t \to \infty$

$$u(y,t) = u_- + A_L(-y)^{-\gamma}t^{-\frac{\gamma}{2(1-\gamma)}} - 2u_-\gamma A_L(-y)^{-(\gamma+1)}t^{-\frac{\gamma}{(1-\gamma)}}$$
$$+ \left(-2\gamma A_L^2(-y)^{-(2\gamma+1)} + \left(\gamma(\gamma+1)A_L + 2\gamma(\gamma+1)u_-^2A_L\right)(-y)^{-(\gamma+2)}\right)t^{-\frac{3\gamma}{2(1-\gamma)}} + o\left(t^{-\frac{3\gamma}{2(1-\gamma)}}\right)$$

as $t \to \infty$ with $y = O(1)(< 0)$.

Region II$^-$: $t = O(1)$ as $x \to \infty$

$$u(x,t) = u_- + \frac{A_L}{x^\gamma} - \frac{\gamma u_- A_L t^{(\delta+1)}}{(\delta+1)x^{(\gamma+1)}} - \frac{\gamma A_L^2 t^{(\delta+1)}}{(\delta+1)x^{(2\gamma+1)}} + o\left(\frac{1}{x^{(2\gamma+1)}}\right) \text{ as } x \to \infty$$

with $t = O(1)$.

2.3.2.2 $\delta = -\frac{1}{2}$, $\gamma \geq 1$:

In this case, expansions (2.14) and (2.18) of regions II^+ ($x \to \infty,\ t = O(1)$) and II^- ($x \to -\infty,\ t = O(1)$), respectively, continue to remain uniform provided that $|x| \gg t^{\frac{1}{2}}$ as $t \to \infty$. However, a nonuniformity develops when $|x| = O(t^{\frac{1}{2}})$. As in Section 2.3.2.1, we introduce the scaled coordinate

$$z = xt^{-\frac{1}{2}}$$

where $z = O(1)$ as $t \to \infty$. We have established in Section 2.3.2.1 that the solution in region SS, where $|x| \gg t^{\frac{1}{2}}$ as $t \to \infty$, is given by (2.77) with the similarity solution $U = u_R(z)$. Therefore, all that remains in this case is to introduce transition regions TR^+ and TR^- to allow the solution in region SS to match to the far field where $|x| \gg t^{\frac{1}{2}}$ as $t \to \infty$. The details of regions TR^+ and TR^- follow those given in Section 2.3.2.1 [3].

The asymptotic structure of $\mathbf{IVP}^+$ as $t \to \infty$ when $\gamma \geq 1$ and $\delta = -\frac{1}{2}$ is complete now. A uniform approximation has been given through regions $\text{II}^\pm$, $\text{TR}^\pm$ and SS. The large-time attractor for the solution of $\mathbf{IVP}^+$ in this case is the similarity solution found by Rudenko and Soluyan [32], which allows for the adjustment of the solution from u_+ to u_-. This attractor is in a stretching frame of reference of thickness $|x| = O(t^{\frac{1}{2}})$ as $t \to \infty$. Finally, the asymptotic structure to the solution of $\mathbf{IVP}^+$ as $t \to \infty$ when $\delta = -\frac{1}{2}$ and $\gamma \geq 1$ can be summarized as:

Region II^+: $z = O(1)(> 0)$ as $t \to \infty$

$$u(z,t) = u_+ + \left(A_R z^{-\gamma} + 2u_+\gamma A_R z^{-(\gamma+1)} + \gamma(\gamma+1)A_R z^{-(\gamma+2)}\right) t^{-\frac{\gamma}{2}} + o\left(t^{-\frac{\gamma}{2}}\right)$$

as $t \to \infty$ with $z = O(1)(> 0)$.

Region TR$^+$: $z = c(t) + \frac{\xi}{\sqrt{\ln t}}$ with $\xi = O(1)$ as $t \to \infty$

$$u(\xi, t) = u_+ + \left(\frac{A_R}{(2\gamma)^{\frac{\gamma}{2}}} + \mathcal{C}_+(u_+, u_-)(2\gamma)^{-\frac{1}{2}} e^{-(\frac{\gamma}{2})^{\frac{1}{2}}\xi} \right) (\ln t)^{-\frac{\gamma}{2}} t^{-\frac{\gamma}{2}} + o\left((\ln t)^{-\frac{\gamma}{2}} t^{-\frac{\gamma}{2}} \right)$$

as $t \to \infty$ with $\xi = O(1)$, and $c(t)$ given in (2.85).

Region SS: $z = xt^{-\frac{1}{2}}$ with $z = O(1)$ as $t \to \infty$

$$u(z, t) = u_R(z) + o(1)$$

where

$$u_R(z) \sim \begin{cases} u_+ + \mathcal{C}_+(u_+, u_-) z^{-1} e^{-\frac{1}{4}(z-2u_+)^2} & \text{as } z \to \infty, \\ u_- + \mathcal{C}_-(u_+, u_-) z^{-1} e^{-\frac{1}{4}(z-2u_-)^2} & \text{as } z \to -\infty. \end{cases}$$

with $\mathcal{C}_+$ and $\mathcal{C}_-$ globally determined nonzero constants, depending upon u_+ and u_-, with

$$\mathcal{C}_+(u_+, u_-) < 0 \qquad \text{and} \qquad \mathcal{C}_-(u_+, u_-) > 0$$

as $t \to \infty$ with $z = O(1)$.

Region TR$^-$: $z = -c(t) + \frac{\hat{\xi}}{\sqrt{\ln t}}$ with $\hat{\xi} = O(1)$ as $t \to -\infty$

$$u(\hat{\xi}, t) = u_- + \left(\frac{A_L}{(2\gamma)^{\frac{\gamma}{2}}} + \mathcal{C}_-(u_+, u_-)(2\gamma)^{-\frac{1}{2}} e^{(\frac{\gamma}{2})^{\frac{1}{2}}\hat{\xi}} \right) (\ln t)^{-\frac{\gamma}{2}} t^{-\frac{\gamma}{2}} + o\left((\ln t)^{-\frac{\gamma}{2}} t^{-\frac{\gamma}{2}} \right)$$

as $t \to \infty$ with $\hat{\xi} = O(1)$, and $c(t)$ given in (2.85).

Region II$^-$: $z = O(1)(< 0)$ as $t \to \infty$

$$u(z,t) = u_- + \left(A_L(-z)^{-\gamma} - 2u_-\gamma A_L(-z)^{-(\gamma+1)} + \gamma(\gamma+1)A_L(-z)^{-(\gamma+2)}\right) t^{-\frac{\gamma}{2}} + o\left(t^{-\frac{\gamma}{2}}\right)$$

as $t \to \infty$ with $z = O(1)(< 0)$.

2.3.3 $-1 < \delta < -\frac{1}{2}$

We recall from Section 2.2 that in this case, we need to consider the cases $\gamma \geq 1$ and $0 < \gamma < 1$ separately. We begin by considering the case $\gamma \geq 1$ [3].

2.3.3.1 $-1 < \delta < -\frac{1}{2}$, $\gamma \geq 1$:

In this case, expansions (2.14) and (2.18) of regions II$^+(x \to \infty,\ t = O(1))$ and II$^-(x \to -\infty,\ t = O(1))$, respectively, continue to remain uniform provided that $|x| \gg t^{-\delta}$. However, a nonuniformity develops when $|x| = O(t^{-\delta})$. We begin by considering the asymptotic structure as $t \to \infty$ by moving in from region II$^+$ when $x \gg t^{-\delta}$ as $t \to \infty$. To proceed, we introduce a new region, which we label as region III$^+$. To examine region III$^+$, we introduce the scaled coordinate

$$y = xt^{\delta} \tag{2.92}$$

with $y = O(1)$ as $t \to \infty$ [3]. The form of the asymptotic expansion for $u(y,t)$ in region III$^+$ follows from the structure of expansion (2.14) in region II$^+$, when written in terms of y and t, and expanded for $y = O(1)$ as $t \to \infty$. This requires that in region III$^+$ we expand in the form

$$u(y,t) = u_+ + F_0(y)t^{\gamma\delta} + F_1(y)t^{(\delta(\gamma+2)+1)} + o\left(t^{(\delta(\gamma+2)+1)}\right) \tag{2.93}$$

as $t \to \infty$ with $y = O(1)$, and where $F_0(y)$ and $F_1(y)$ are functions to be determined. On substitution from (2.93) into equation (2.1) (when written in terms of y and t). We obtain after some calculation[3]

$$\big((\gamma\delta)\ F_0(y)\ t^{(\gamma\delta)}+(\delta(\gamma+2)+1)F_1(y)\ t^{(\delta(\gamma+2)+1)}\big)+\big(\ F_0'(y)\ t^{(\gamma\delta)-1}+F_1'(y)\ t^{\delta(\gamma+2)}\big)$$
$$\big(\delta y+t^{(2\delta+1)}\big(u_+ + F_0(y)t^{\gamma\delta}+F_1(y)t^{(\delta(\gamma+2)+1)}\big)\big)\sim F_0''(y)\ t^{(\delta(\gamma+2)+1)}+.....$$

We now equate at each order in turn and solve to find $F_0(y)$ and $F_1(y)$. Equating at $O(t^{\gamma\delta})$ we have the following ordinary differential equation for $F_0(y)$, namely

$$F_0' + \left(\frac{\gamma}{y}\right)F_0 = 0, \quad y = O(1)(>0). \tag{2.94}$$

Equation (2.94) has to be solved subject to the matching condition with expansion (2.14) in region II$^+$ $\left(\text{when } x = O\left(t^{-\gamma\delta}\right)\right)$, which requires

$$F_0(y) \sim \frac{A_R}{y^\gamma} \quad \text{as} \quad y \to \infty. \tag{2.95}$$

The solution of (2.94) subject to (2.95) is then readily obtained as

$$F_0(y) = A_R\ y^{-\gamma}, \quad y > 0. \tag{2.96}$$

At $O\left(t^{(\delta(\gamma+2)+1)}\right)$ we obtain the following ordinary differential equation for $F_1(y)$, namely

$$F_1' + \left(\frac{\delta(\gamma+2)+1}{\delta y}\right)F_1 = \left(\frac{A_R\gamma u_+}{\delta}\right)y^{(\gamma+2)} + \left(\frac{A_R\gamma(\gamma+1)}{\delta}\right)y^{(\gamma+3)}, \quad y = O(1)(>0). \tag{2.97}$$

[3] $u_t + u_y\big(y_t + t^\delta u y_x\big) = u_{yy}(y_x)^2$ where $y_x = t^\delta$ and $y_t = \frac{\delta y}{t}$.

This is to be solved subject to the corresponding matching condition

$$F_1(y) \sim \frac{\gamma u_+ A_R}{(\delta+1)y^{(\gamma+1)}} + \frac{A_R\gamma(\gamma+1)}{y^{(\gamma+2)}} \quad \text{as} \quad y \to \infty. \tag{2.98}$$

The solution of (2.97) and (2.98) is then readily obtained as

$$F_1(y) = \frac{u_+ A_R\gamma}{(1+\delta)} y^{-(\gamma+1)} + A_R\gamma(\gamma+1)y^{-(\gamma+2)}, \quad y > 0. \tag{2.99}$$

In this case the expansion in region III$^+$ is given by (2.93) with (2.96) and (2.99). That is,

$$u(y,t) = u_+ + A_R y^{-\gamma} t^{\gamma\delta} + \left(\frac{u_+ A_R\gamma}{(1+\delta)} y^{-(\gamma+1)} + A_R\gamma(\gamma+1)y^{-(\gamma+2)} \right) t^{(\delta(\gamma+2)+1)} + o\left(t^{(\delta(\gamma+2)+1)}\right) \tag{2.100}$$

as $t \to \infty$ with $y = O(1)(> 0)$ [3]. Expansion (2.100) becomes nonuniform when

$$y = O\left(t^{(\delta+\frac{1}{2})}\right) \quad \text{as} \quad t \to \infty \ \left(\text{when } x = O\left(t^{\frac{1}{2}}\right) \text{ as } t \to \infty\right).$$

We now consider the asymptotic structure as $t \to \infty$ by moving in from region II$^-$ when $(-x) \gg t^{-\delta}$. To proceed, we define a new region, which we label as region III$^-$. The details of this region follow, after minor modification, those given for region III$^+$ above. We have in region III$^-$ that

$$u(y,t) = u_- + A_L(-y)^{-\gamma} t^{\gamma\delta} + O\left(t^{(\delta(\gamma+2)+1)}\right) \tag{2.101}$$

as $t \to \infty$ with $y = O(1)(< 0)$. We observe that expansion (2.101) becomes nonuniform when

$$y = O\left(t^{(\delta+\frac{1}{2})}\right) \quad \text{as} \quad t \to \infty,$$

that is, when $x = O\left(t^{\frac{1}{2}}\right)$ as $t \to \infty$ [3]. To proceed, we define a new region, which we label as region SS. To examine region SS, we introduce the scaled coordinate z, via

$$z = xt^{-\frac{1}{2}} = yt^{-(\delta+\frac{1}{2})}, \tag{2.102}$$

with $z = O(1)$ as $t \to \infty$, and expand in the form

$$u(z,t) = U(z) + o(1) \tag{2.103}$$

as $t \to \infty$ with $z = O(1)$ [3]. On substituting expansion (2.103) into equation (2.1) (when written in terms of z and t) we obtain at leading order that

$$U_{zz} + \frac{z}{2}\, U_z = 0, \qquad -\infty < z < \infty. \tag{2.104}$$

We note that we have examined equation (2.104) in Section 1.5.1. The solution to (2.104) is readily obtained as

$$U(z) = A_1 + B_2 \text{ erf}\left(\frac{z}{2}\right), \qquad -\infty < z < \infty, \tag{2.105}$$

where erf(.) is the standard error function[4] (see, for example [1]), A_1 and B_2 are constants to be determined. Equation (2.104) is to be solved subject to the leading order matching

[4] $\text{erf}\,(x) = 1 - \frac{2}{\sqrt{\pi}} \int_x^\infty e^{-s^2} ds$ where

$$\text{erf}\,(x) \sim \begin{cases} 1 - \frac{e^{-x^2}}{x\sqrt{\pi}} & x \gg \infty, \\ 1 + \frac{e^{-x^2}}{(-x)\sqrt{\pi}}, & (-x) \ll -\infty. \end{cases}$$

.

conditions with regions $\text{III}^{\pm}$, namely,

$$U(z) \to \begin{cases} u_+ & \text{as } z \to \infty, \\ u_- & \text{as } z \to -\infty. \end{cases} \tag{2.106}$$

Therefore

$$u_+ = A_1 + B_2 \tag{2.107}$$

and

$$u_- = A_1 - B_2 \tag{2.108}$$

giving

$$A_1 = \frac{(u_+ + u_-)}{2} \qquad \text{and} \qquad B_2 = -\frac{(u_- - u_+)}{2}.$$

The solution to (2.104) and (2.106) is then obtained as

$$U(z) = \frac{(u_+ + u_-)}{2} - \frac{(u_- - u_+)}{2} \operatorname{erf}\left(\frac{z}{2}\right), \qquad -\infty < z < \infty. \tag{2.109}$$

We recall from Section 1.5.1 that (2.109) is an error function of (2.1). Thus in region SS we have that

$$u(z,t) = \frac{(u_+ + u_-)}{2} - \frac{(u_- - u_+)}{2} \operatorname{erf}\left(\frac{z}{2}\right) + o(1) \tag{2.110}$$

as $t \to \infty$ with $z = O(1)$. Expansion (2.110) (for $z \gg 1$) when written in terms of z is given by

$$u \sim u_+ + \frac{(u_- - u_+)}{\sqrt{\pi} z} \exp\left(-\frac{z^2}{4}\right) \tag{2.111}$$

as $t \to \infty$. Expansion (2.100) (for $z \gg 1$) when written in terms of z is given by

$$u \sim u_+ + \frac{A_R}{z^\gamma}\, t^{-\frac{\gamma}{2}} \tag{2.112}$$

as $t \to \infty$. However, we observe that matching expansion (2.111) (as $z \to \infty$) to expansion (2.112) at next order is not possible and we need a transition region, which we label TR^+. To examine region TR^+, we introduce the scaled coordinate η , via

$$\eta = (z - c(t))\,(\ln t)^{\frac{1}{2}} \tag{2.113}$$

where the function $c(t)$ is a function to be determined. Comparison of the corrections to u_+ in (2.111) and (2.112) indicates that they are of the same order when $z = c(t)$ as $t \to \infty$. That is

$$\frac{c(t)^2}{4} = \frac{\gamma}{2}\ln t + (\gamma - 1)\ln c(t)$$

which requires

$$c(t) = \sqrt{2\gamma}\,(\ln t)^{\frac{1}{2}} + \frac{(\gamma-1)}{\sqrt{2\gamma}}\,\frac{\ln(\ln t)}{(\ln t)^{\frac{1}{2}}} + o\left(\frac{\ln(\ln t)}{(\ln t)^{\frac{1}{2}}}\right) \tag{2.114}$$

as $t \to \infty$, and it is determined so that matching between regions TR^+, III^+ and SS is possible. In region TR^+ we look for an expansion of the form

$$u(\eta, t) = u_+ + F(\eta)(\ln t)^{-\frac{\gamma}{2}}\,t^{-\frac{\gamma}{2}} + o\left((\ln t)^{-\frac{\gamma}{2}}\,t^{-\frac{\gamma}{2}}\right) \quad \text{as} \quad t \to \infty \tag{2.115}$$

as $t \to \infty$ with $\eta = O(1)$. On substituting expansion (2.115) into equation (2.1) (when equation (2.1) is written in terms of η and t) we obtain at leading order that

$$F_{\eta\eta} + \sqrt{\frac{\gamma}{2}}F_\eta = 0, \quad -\infty < \eta < \infty. \tag{2.116}$$

The solution to (2.116) is readily obtained as

$$F(\eta) = \bar{A} + \bar{B}e^{-\sqrt{\frac{\gamma}{2}}\xi}, \quad -\infty < \eta < \infty,$$

where $\bar{A}$ and $\bar{B}$ are constants. Matching with region III$^+$as $\eta \to \infty$ requires that $A = \frac{A_R}{(2\gamma)^{\frac{\gamma}{2}}}$ and matching with region SS as $\eta \to -\infty$ requires that $B = \frac{(u_- - u_+)}{\sqrt{2\gamma\pi}}$. Therefore, equation (2.116) is to be solved subject to the following matching conditions with region III$^+$ (as $\eta \to \infty$) and region SS (as $\eta \to -\infty$), namely,

$$F(\eta) \sim \begin{cases} \frac{A_R}{(2\gamma)^{\frac{\gamma}{2}}} & \text{as} \quad \eta \to \infty, \\ \frac{(u_- - u_+)}{\sqrt{2\gamma\pi}} e^{-\sqrt{\frac{\gamma}{2}}\eta} & \text{as} \quad \eta \to -\infty. \end{cases} \tag{2.117}$$

The solution to (2.116) and (2.117) is readily obtained as

$$F(\eta) = \frac{A_R}{(2\gamma)^{\frac{\gamma}{2}}} + \frac{(u_- - u_+)}{\sqrt{2\gamma\pi}} e^{-\sqrt{\frac{\gamma}{2}}\eta}, \qquad -\infty < \eta < \infty. \tag{2.118}$$

Therefore, we have in region TR$^+$ that

$$u(\eta, t) = u_+ + \left(\frac{A_R}{(2\gamma)^{\frac{\gamma}{2}}} + \frac{(u_- - u_+)}{\sqrt{2\gamma\pi}} e^{-\sqrt{\frac{\gamma}{2}}\eta} \right) (\ln t)^{-\frac{\gamma}{2}} \; t^{-\frac{\gamma}{2}} + o\left((\ln t)^{-\frac{\gamma}{2}} \; t^{-\frac{\gamma}{2}} \right) \tag{2.119}$$

as $t \to \infty$ with $\eta = O(1)$. Finally, we conclude this case by noting that matching expansion (2.110) (as $z \to -\infty$) to expansion (2.101) similarly fails and we require a corresponding transition region, which we label TR$^-$. To examine region TR$^-$we introduce the scaled coordinate $\hat{\eta}$ by

$$\hat{\eta} = (z + c(t)) \, (\ln t)^{\frac{1}{2}} \tag{2.120}$$

as $t \to \infty$ with $\hat{\eta} = O(1)$. The details in TR$^-$ follow, after minor modification, those given for region TR$^+$ and are summarized here for brevity. Therefore, in region TR$^-$ we

have that

$$u(\hat{\eta},t) = u_- + \left(\frac{A_L}{(2\gamma)^{\frac{\gamma}{2}}} - \frac{(u_- - u_+)}{\sqrt{2\gamma\pi}} e^{\sqrt{\frac{\gamma}{2}}\hat{\eta}} \right) (\ln t)^{-\frac{\gamma}{2}}\ t^{-\frac{\gamma}{2}} + o\left((\ln t)^{-\frac{\gamma}{2}}\ t^{-\frac{\gamma}{2}} \right) \quad (2.121)$$

as $t \to \infty$ with $\hat{\eta} = O(1)$ [3].

The asymptotic structure of $\mathbf{IVP}^+$ as $t \to \infty$ when $-1 < \delta < -\frac{1}{2}$ and $\gamma \geq 1$ is now complete. A uniform approximation has been given through regions $\mathrm{II}^{\pm}$, $\mathrm{III}^{\pm}$, $\mathrm{TR}^{\pm}$ and SS. A schematic representation of the location and thickness of the asymptotic structure as $t \to \infty$ is given in Figure 2.8. The large-time attractor for the solution of $\mathbf{IVP}^+$ in this case is the error function, which allows for the adjustment of the solution from u_+ to u_-. This attractor is in a stretching frame of reference of thickness $|x| = O\left(t^{\frac{1}{2}}\right)$ as $t \to \infty$. Finally, the asymptotic structure to the solution of $\mathbf{IVP}^+$ as $t \to \infty$ when $-1 < \delta < -\frac{1}{2}$ and $\gamma \geq 1$ can be summarized as:

Region II^+: $t = O(1)$ as $x \to \infty$

$$u(x,t) = u_+ + \frac{A_R}{x^\gamma} + \frac{\gamma u_+ A_R t^{(\delta+1)}}{(\delta+1)x^{(\gamma+1)}} + \frac{\gamma(\gamma+1)A_R t}{x^{(\gamma+2)}} + \frac{\gamma A_R^2 t^{(\delta+1)}}{(\delta+1)x^{(2\gamma+1)}} + o\left(\frac{1}{x^{(2\gamma+1)}}\right) \text{ as } x \to \infty$$

with $t = O(1)$.

Region III^+: $y = O(1)(> 0)$ as $t \to \infty$

$$u(y,t) = u_+ + A_R y^{-\gamma} t^{\gamma\delta} + \left(\frac{u_+ A_R \gamma}{(1+\delta)} y^{-(\gamma+1)} + A_R \gamma(\gamma+1) y^{-(\gamma+2)} \right) t^{(\delta(\gamma+2)+1)} + o\left(t^{(\delta(\gamma+2)+1)}\right)$$

as $t \to \infty$ with $y = O(1)(> 0)$.

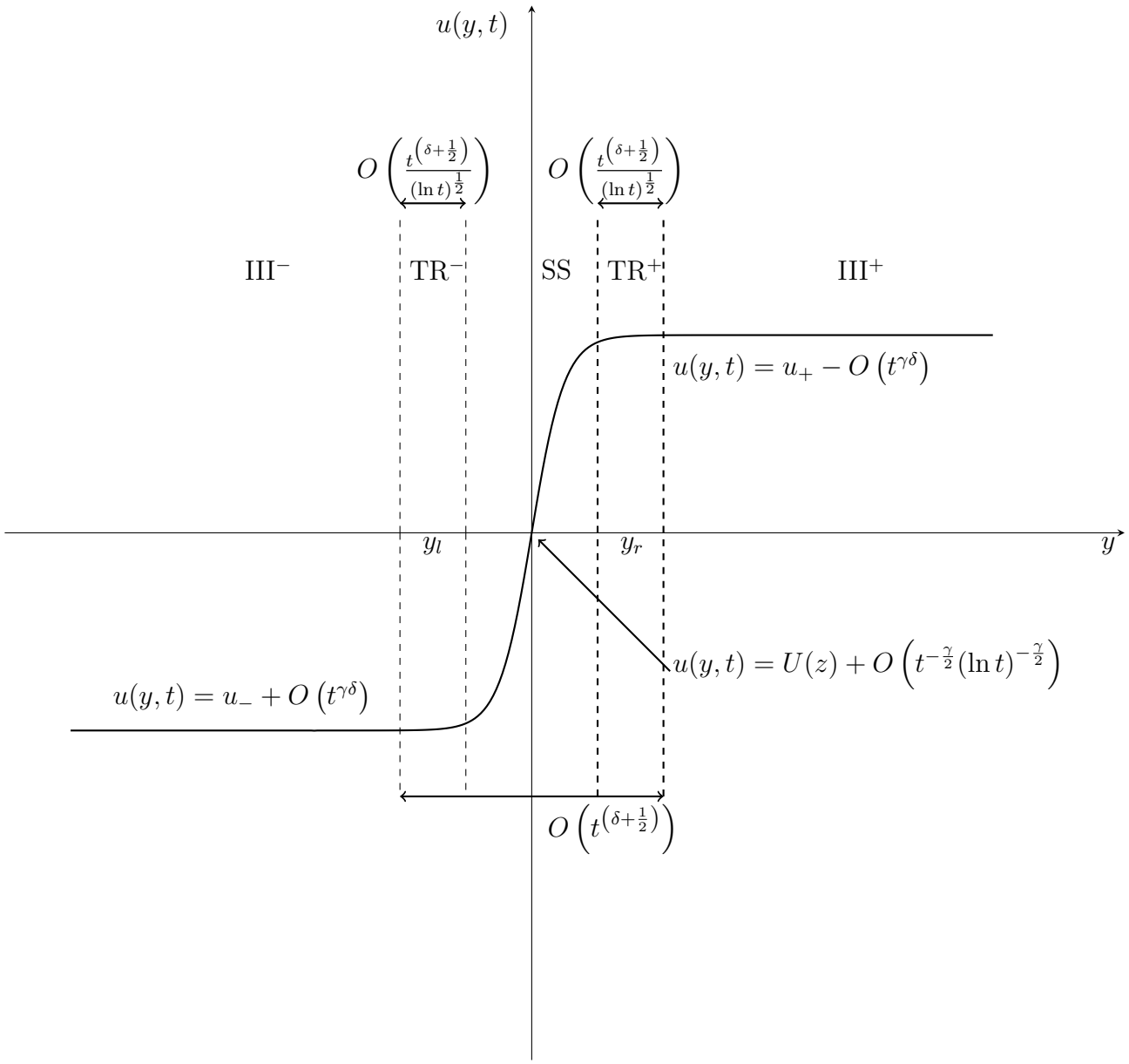

Figure 2.8: A schematic representation of the asymptotic structure of $u(y,t)$ in the (y,u) plane as $t \to \infty$ for $\mathbf{IVP}^+$ when $-1 < \delta < -\frac{1}{2}$ and $\gamma \geq 1$. We recall that $y_l = -y_r = -t^{(\delta+\frac{1}{2})}\, c(t)$, where $c(t)$ is given by (2.114).

Region TR$^+$: $y = \left(c(t) + \frac{\eta}{\sqrt{\ln t}}\right) t^{(\delta+\frac{1}{2})}$ with $\eta = O(1)$ as $t \to \infty$

$$u(\eta, t) = u_+ + \left(\frac{A_R}{(2\gamma)^{\frac{\gamma}{2}}} + \frac{(u_- - u_+)}{\sqrt{2\gamma\pi}} e^{-\sqrt{\frac{\gamma}{2}}\eta}\right) (\ln t)^{-\frac{\gamma}{2}} t^{-\frac{\gamma}{2}} + o\left((\ln t)^{-\frac{\gamma}{2}} t^{-\frac{\gamma}{2}}\right)$$

as $t \to \infty$ with $\eta = O(1)$, and $c(t)$ given in (2.114).

Region SS: $y = zt^{-(\delta+\frac{1}{2})}$ with $z = O(1)$ as $t \to \infty$

$$u(z, t) = \frac{(u_+ + u_-)}{2} - \frac{(u_- - u_+)}{2} \mathrm{erf}\left(\frac{z}{2}\right) + o(1)$$

as $t \to \infty$ with $z = O(1)$.

Region TR$^-$: $y = \left(-c(t) + \frac{\hat{\eta}}{\sqrt{\ln t}}\right) t^{(\delta+\frac{1}{2})}$ with $\hat{\eta} = O(1)$ as $t \to -\infty$

$$u(\hat{\eta}, t) = u_- + \left(\frac{A_L}{(2\gamma)^{\frac{\gamma}{2}}} - \frac{(u_- - u_+)}{\sqrt{2\gamma\pi}} e^{\sqrt{\frac{\gamma}{2}}\hat{\eta}}\right) (\ln t)^{-\frac{\gamma}{2}} t^{-\frac{\gamma}{2}} + o\left((\ln t)^{-\frac{\gamma}{2}} t^{-\frac{\gamma}{2}}\right)$$

as $t \to \infty$ with $\hat{\eta} = O(1)$, and $c(t)$ given in (2.114).

Region III$^-$: $y = O(1)(< 0)$ as $t \to \infty$

$$u(y, t) = u_- + A_L(-y)^{-\gamma} t^{\gamma\delta} + \left(-\frac{u_+ A_L \gamma}{(1+\delta)}(-y)^{-(\gamma+1)} + A_L\gamma(\gamma+1)(-y)^{-(\gamma+2)}\right) t^{(\delta(\gamma+2)+1)}$$
$$+ o\left(t^{(\delta(\gamma+2)+1)}\right)$$

as $t \to \infty$ with $y = O(1)(< 0)$.

Region II$^-$: $t = O(1)$ as $x \to \infty$

$$u(x,t) = u_- + \frac{A_L}{x^\gamma} - \frac{\gamma u_- A_L t^{(\delta+1)}}{(\delta+1)x^{(\gamma+1)}} + \frac{\gamma(\gamma+1)A_L t}{x^{(\gamma+2)}} - \frac{\gamma A_L^2 t^{(\delta+1)}}{(\delta+1)x^{(2\gamma+1)}} + o\left(\frac{1}{x^{(2\gamma+1)}}\right) \text{ as } x \to \infty$$

with $t = O(1)$.

2.3.3.2 $-1 < \delta < -\frac{1}{2}$, $0 < \gamma < 1$:

In this case, expansions (2.14) and (2.18) of regions II$^+$ and II$^-$ with $t = O(1)$, respectively, continue to remain uniform provided that $|x| \gg t^{\frac{\delta}{(\gamma-1)}}$ as $t \to \infty$. However, a nonuniformity develops when $|x| = O\left(t^{\frac{\delta}{(\gamma-1)}}\right)$. We begin by considering the asymptotic structure as $t \to \infty$ by moving in from region II$^+$ when $x \gg t^{\frac{\delta}{(\gamma-1)}}$ as $t \to \infty$. To proceed, we introduce a new region,which we label as region III$^+$. To examine region III$^+$, we introduce the scaled coordinate

$$y = xt^{-\frac{\delta}{(\gamma-1)}} \tag{2.122}$$

with $y = O(1)$ as $t \to \infty$ [3]. The form of the asymptotic expansion for $u(y,t)$ in region III$^+$ follows from the structure of expansion (2.14) in region II$^+$, when written in terms of y and t, and expanded for $y = O(1)$ as $t \to \infty$. This requires that in region III$^+$ we expand in the form

$$u(y,t) = u_+ + F_0(y)t^{-\left(\frac{\gamma\delta}{\gamma-1}\right)} + F_1(y)t^{-\left(\frac{2\delta}{\gamma-1}\right)+1} + F_2(y)t^{-\left(\frac{\delta(\gamma+2)}{\gamma-1}\right)+1} + o\left(t^{-\left(\frac{\delta(\gamma+2)}{\gamma-1}\right)+1}\right) \tag{2.123}$$

as $t \to \infty$ with $y = O(1)$, and where $F_0(y)$, $F_1(y)$ and $F_2(y)$ are functions to be determined. On substitution from (2.123) into equation (2.1) (when written in terms of y and t), we

obtain after some calculation

$$\left(-\frac{\gamma\delta}{\gamma-1}\ F_0(y)\ t^{-\left(\frac{\gamma\delta}{\gamma-1}\right)}-\left(\frac{\delta}{\gamma-1}-1\right)F_1(y)\ t^{-\left(\frac{2\delta}{\gamma-1}\right)+1}-\frac{\delta(\gamma+2)}{\gamma-1}F_2(y)\ t^{-\left(\frac{2\delta}{\gamma-1}\right)+1}\right)$$
$$-\frac{\gamma\delta}{\gamma-1}\left(F_0'(y)t^{-\left(\frac{\gamma\delta}{\gamma-1}\right)}+F_1'(y)t^{-\left(\frac{2\delta}{\gamma-1}\right)+1}+F_2'(y)t^{-\left(\frac{\delta(\gamma+2)}{\gamma-1}\right)+1}\right)+t^{\frac{\delta(\gamma-2)}{\gamma-1}+1}$$
$$\left(u_+ + F_0(y)t^{-\left(\frac{\gamma\delta}{\gamma-1}\right)}+F_1(y)t^{-\left(\frac{2\delta}{\gamma-1}\right)+1}+...\right)\left(F_0'(y)t^{-\left(\frac{\gamma\delta}{\gamma-1}\right)}+F_1'(y)t^{-\left(\frac{2\delta}{\gamma-1}\right)+1}+...\right)$$
$$\sim F_0''(y)\ t^{(\delta(\gamma+2)+1)}+.....$$

We obtain at $O\left(t^{-\frac{\gamma\delta}{\gamma-1}}\right)$ the following ordinary differential equation for $F_0(y)$, namely

$$F_0'+\left(\frac{\gamma}{y}\right)F_0=0,\quad y=O(1)(>0). \tag{2.124}$$

Equation (2.124) has to be solved subject to the matching condition with expansion (2.14) in region II$^+$ $\left(\text{when } x=O\left(t^{\frac{\gamma\delta}{\gamma-1}}\right)\right)$, which requires

$$F_0(y)\sim\frac{A_R}{y^\gamma}\quad \text{as}\quad y\to\infty. \tag{2.125}$$

The solution of (2.124) subject to (2.125) is then readily obtained as

$$F_0(y)=A_R y^{-\gamma},\quad y>0. \tag{2.126}$$

At $O\left(t^{-\frac{2\delta}{\gamma-1}+1}\right)$ we obtain the following ordinary differential equation for $F_1(y)$, namely

$$F_1'+\left(\frac{2\delta-\gamma+1}{\delta y}\right)F_1=-\frac{A_R\gamma(\gamma-1)u_+}{\delta y^{(\gamma+2)}},\quad y=O(1)(>0). \tag{2.127}$$

This is to be solved subject to the corresponding matching condition with expansion (2.14) in region II$^+$ $\left(\text{when } x = O\left(t^{\frac{2\delta}{\gamma-1}-1}\right)\right)$, which requires

$$F_1(y) \sim \frac{u_+ A_R \gamma}{(\delta+1)} y^{-(\gamma+1)} \quad \text{as} \quad y \to \infty. \tag{2.128}$$

The solution of (2.127) and (2.128) is then readily obtained as

$$F_1(y) = \frac{u_+ A_R \gamma}{(\delta+1)} y^{-(\gamma+1)}, \quad y > 0. \tag{2.129}$$

At $O\left(t^{\frac{-\delta(\gamma+2)}{\gamma-1}+1}\right)$ we obtain the following ordinary differential equation for $F_2(y)$, namely

$$F_2' + \left(\frac{\delta(\gamma+2)-(\gamma-1)}{\delta y}\right) F_2 = -\frac{A_R\gamma(\gamma-1)(\gamma+1)u_+}{\delta y^{(\gamma+3)}} - \frac{A_R^2\gamma(\gamma-1)u_+}{\delta y^{(\gamma+3)}},$$
$$y = O(1)(>0). \tag{2.130}$$

This is to be solved subject to the corresponding matching condition with expansion (2.14) in region II$^+$ $\left(\text{when } x = O\left(t^{(\frac{\delta(\gamma+2)}{\gamma-1})-1}\right)\right)$, which requires

$$F_2(y) \sim \frac{u_+ A_R \gamma}{(\delta+1)} y^{-(2\gamma+1)} + A_R\gamma(\gamma+1)y^{-(\gamma+2)} \quad \text{as} \quad y \to \infty. \tag{2.131}$$

The solution of (2.130) and (2.131) is then readily obtained as

$$F_2(y) = \frac{u_+ A_R^2 \gamma}{(\delta+1)} y^{-(2\gamma+1)} + A_R\gamma(\gamma+1)y^{-(\gamma+2)}, \quad y > 0. \tag{2.132}$$

In this case the expansion in region III$^+$ is given by (2.123) with (2.126) , (2.129) and (2.132). That is,

$$u(y,t) = u_+ + A_R y^{-\gamma} t^{-\frac{\gamma\delta}{\gamma-1}} + \frac{u_+ A_R \gamma}{(\delta+1)} y^{-(\gamma+1)} t^{\frac{2\delta}{\gamma-1}+1} + \left(\frac{u_+ A_R^2 \gamma}{(\delta+1)} y^{-(2\gamma+1)} + A_R \gamma(\gamma+1) y^{-(\gamma+2)} \right) t^{-\frac{\delta(\gamma+2)}{\gamma-1}+1} + o\left(t^{\frac{-\delta(\gamma+2)}{\gamma-1}+1} \right) \tag{2.133}$$

as $t \to \infty$ with $y = O(1)(> 0)$ [3]. We observe that expansion (2.133) becomes nonuniform when $y = O\left(t^{-\frac{\delta\gamma}{\gamma-1}}\right)$ as $t \to \infty$. To proceed, we label region III$^+$ as III$^+(a)$ and introduce a new region, labeled as III$^+(b)$. To examine region III$^+(b)$, we introduce the scaled coordinate

$$\hat{y} = y\ t^{\frac{\delta\gamma}{(\gamma-1)}} \tag{2.134}$$

with $\hat{y} = O(1)$ as $t \to \infty$, and look for an expansion of the form

$$u(\hat{y},t) = u_+ + \hat{F}_0(\hat{y}) t^{\gamma\delta} + \hat{F}_1(\hat{y}) t^{(\delta(\gamma+2)+1)} + o\left(t^{(\delta(\gamma+2)+1)}\right) \tag{2.135}$$

as $t \to \infty$ with $\hat{y} = O(1)$, where $\hat{F}_0(\hat{y})$ and $\hat{F}_1(\hat{y})$ are functions to be determined [3]. On substitution from (2.135) into equation (2.1) (when written in terms of $\hat{y}$ and t). We obtain after some calculation

$$\left((\gamma\delta)\ \hat{F}_0(\hat{y}) t^{(\gamma\delta)} + (\delta(\gamma+2)+1)\, \hat{F}_1(\hat{y}) t^{\delta(\gamma+2)+1} \right) + \left(\hat{F}_0'(\hat{y}) t^{(\gamma\delta)} + \hat{F}_1'(\hat{y}) t^{(\delta(\gamma+2)+1)} \right)$$
$$\left[\delta\ \hat{y} + t^{(2\delta+1)} \left(u_+ + \hat{F}_0(\hat{y}) t^{\gamma\delta} + \hat{F}_1(\hat{y}) t^{(\delta(\gamma+2)+1)} \right) \right] \sim \left(\hat{F}_0''(\hat{y}) t^{(\gamma\delta)} + \hat{F}_1''(\hat{y}) t^{(\delta(\gamma+2)+1)} \right) t^{(2\delta+1)}.$$

We now equate at each order in turn and solve to find $F_0(\hat{y})$ and $F_1(\hat{y})$. Equating at $O\left(t^{\gamma\delta}\right)$ we have the following ordinary differential equation for $F_0(y)$, namely

$$F_0' + \left(\frac{\gamma}{\hat{y}}\right) F_0 = 0, \quad \hat{y} = O(1)(> 0). \tag{2.136}$$

Equation (2.136) has to be solved subject to the matching condition with expansion (2.14) in region II$^+$ $\left(\text{when } x = O\left(t^{-\gamma\delta}\right)\right)$, which requires

$$F_0(\hat{y}) \sim \frac{A_R}{\hat{y}^\gamma} \quad \text{as} \quad \hat{y} \to \infty. \tag{2.137}$$

The solution of (2.136) subject to (2.137) is then readily obtained as

$$F_0(\hat{y}) = A_R \hat{y}^{-\gamma}, \quad \hat{y} > 0. \tag{2.138}$$

At $O\left(t^{(\delta(\gamma+2)+1)}\right)$ we obtain the following ordinary differential equation for $F_1(\hat{y})$,

$$F_1' + \left(\frac{(\delta(\gamma+2)+1)}{\delta\hat{y}}\right)F_1 = \frac{u_+ A_R\gamma}{\delta}\hat{y}^{-(\gamma+2)} + \frac{A_R\gamma(\gamma+1)\hat{y}^{-(\gamma+3)}}{\delta}, \quad \hat{y} = O(1)(> 0). \tag{2.139}$$

This is to be solved subject to the corresponding matching condition with expansion (2.14) in region II$^+$ $\left(\text{when } x = O\left(t^{(-\delta(\gamma+2)+1)}\right)\right)$, which requires

$$F_1(\hat{y}) \sim \frac{u_+ A_R\gamma}{(\delta+1)}\hat{y}^{-(\gamma+1)} \quad \text{as} \quad \hat{y} \to \infty. \tag{2.140}$$

The solution of (2.130) and (2.131) is then readily obtained as

$$F_1(\hat{y}) = \frac{u_+ A_R\gamma}{(\delta+1)}\hat{y}^{-(\gamma+1)} + A_R\gamma(\gamma+1)\hat{y}^{-(\gamma+2)}, \quad \hat{y} > 0. \tag{2.141}$$

We find that

$$u(\hat{y},t) = u_+ + A_R\hat{y}^{-\gamma}t^{\gamma\delta} + \left(\frac{u_+ A_R\gamma}{(\delta+1)}\hat{y}^{-(\gamma+1)} + A_R\gamma(\gamma+1)\hat{y}^{-(\gamma+2)}\right)t^{(\delta(\gamma+2)+1)} + o\left(t^{(\delta(\gamma+2)+1)}\right) \tag{2.142}$$

as $t \to \infty$ with $\hat{y} = O(1)(> 0)$ [3]. We observe that expansion (2.142) becomes nonuniform when

$$\hat{y} = O\left(t^{(\delta+\frac{1}{2})}\right) \quad \text{as} \quad t \to \infty.$$

We now consider the asymptotic structure as $t \to \infty$ by moving in from region II$^-$ when $(-x) \gg t^{\frac{\delta}{(\gamma-1)}}$. To proceed, we define a new region, which we label as region III$^-$. we note that region III$^-$ will need to be replaced by region III$^-(a)$ and region III$^-(b)$. The details of these regions follow, after minor modification, those given for regions III$^+(a)$ and III$^+(b)$ above. Therefore, we have in region III$^-(a)$:

$$u(y,t) = u_- + A_L(-y)^{-\gamma} t^{(\frac{\gamma\delta}{\gamma-1})} + O\left(t^{-(\frac{2\delta}{\gamma-1})+1}\right) \tag{2.143}$$

as $t \to \infty$ with $y = O(1)(< 0)$, and in region III$^-(b)$:

$$u(\hat{y},t) = u_- + A_L(-\hat{y})^{-\gamma} t^{\gamma\delta} + o\left(t^{(\delta(\gamma+2)+1)}\right) \tag{2.144}$$

as $t \to \infty$ with $\hat{y} = O(1)(< 0)$. We observe that expansion (2.144) becomes nonuniform when

$$\hat{y} = O\left(t^{(\delta+\frac{1}{2})}\right). \quad \text{as} \quad t \to \infty$$

The remaining asymptotic structure in this case now follows that given in Section 2.3.3.1 for $\gamma \geq 1$.

The asymptotic structure of **IVP**$^+$ as $t \to \infty$ when $-1 < \delta < -\frac{1}{2}$ and $0 < \gamma < 1$ is complete now. A uniform approximation has been given through regions II$^\pm$, III$(a)^\pm$, III$(b)^\pm$,TR$^\pm$ and SS. Finally, the asymptotic structure to the solution of **IVP**$^+$ when $-1 < \delta < -\frac{1}{2}$, $0 < \gamma < 1$ as $t \to \infty$ can be summarized as:

Region II$^+$: $t = O(1)$ as $x \to \infty$

$$u(x,t) = u_+ + \frac{A_R}{x^\gamma} + \frac{\gamma u_+ A_R t^{(\delta+1)}}{(\delta+1)x^{(\gamma+1)}} + \frac{\gamma A_R^2 t^{(\delta+1)}}{(\delta+1)x^{(2\gamma+1)}} + +o\left(\frac{1}{x^{(2\gamma+1)}}\right) \text{ as } x \to \infty$$

with $t = O(1)$.

Region III$^+(a)$: $y = O(1)(> 0)$ as $t \to \infty$

$$u(y,t) = u_+ + A_R y^{-\gamma} t^{-\left(\frac{\gamma\delta}{\gamma-1}\right)} + \frac{u_+ A_R \gamma}{(\delta+1)} y^{-(\gamma+1)} t^{-\left(\frac{2\delta}{\gamma-1}\right)+1}$$
$$+ \left(\frac{u_+ A_R^2 \gamma}{(\delta+1)} y^{-(2\gamma+1)} + A_R\gamma(\gamma+1)y^{-(\gamma+2)}\right) t^{\left(\frac{-\delta(\gamma+2)}{\gamma-1}\right)+1} + o\left(t^{\left(\frac{-\delta(\gamma+2)}{\gamma-1}\right)+1}\right) \quad \text{as} \quad t \to \infty$$

as $t \to \infty$ with $y = O(1)(> 0)$.

Region III$^+(b)$: $\hat{y} = O(1)(> 0)$ as $t \to \infty$

$$u(\hat{y},t) = u_+ + A_R \hat{y}^{-\gamma} t^{\gamma\delta} + \left(\frac{u_+ A_R \gamma}{(\delta+1)} \hat{y}^{-(\gamma+1)} + A_R\gamma(\gamma+1)\hat{y}^{-(\gamma+2)}\right) t^{(\delta(\gamma+2)+1)}$$
$$+ o\left(t^{(\delta(\gamma+2)+1)}\right)$$

as $t \to \infty$ with $\hat{y} = O(1)(> 0)$.

Region TR$^+$: $\hat{y} = \left(c(t) + \frac{\eta}{(\ln t)^{\frac{1}{2}}}\right) t^{(\delta+\frac{1}{2})}$ with $\eta = O(1)$ as $t \to \infty$

$$u(\eta,t) = u_+ + \left(\frac{A_R}{(2\gamma)^{\frac{\gamma}{2}}} + \frac{(u_- - u_+)}{\sqrt{2\gamma\pi}} e^{-\sqrt{\frac{\gamma}{2}}\eta}\right) (\ln t)^{-\frac{\gamma}{2}} t^{-\frac{\gamma}{2}} + o\left((\ln t)^{-\frac{\gamma}{2}} t^{-\frac{\gamma}{2}}\right)$$

as $t \to \infty$ with $\eta = O(1)$, and $c(t)$ given in (2.114).

Region SS: $\hat{y} = zt^{-(\delta+\frac{1}{2})}$ with $z = O(1)$ as $t \to \infty$

$$u(z,t) = \frac{(u_+ + u_-)}{2} - \frac{(u_- - u_+)}{2}\text{erf}\left(\frac{z}{2}\right) + o(1)$$

as $t \to \infty$ with $z = O(1)$.

Region TR$^-$: $\hat{y} = \left(-c(t) + \frac{\hat{\eta}}{(\ln t)^{\frac{1}{2}}}\right) t^{(\delta+\frac{1}{2})}$ with $\hat{\eta} = O(1)$ as $t \to -\infty$

$$u(\hat{\eta},t) = u_- + \left(\frac{A_L}{(2\gamma)^{\frac{\gamma}{2}}} - \frac{(u_- - u_+)}{\sqrt{2\gamma\pi}} e^{\sqrt{\frac{\gamma}{2}}\hat{\eta}}\right)(\ln t)^{-\frac{\gamma}{2}} t^{-\frac{\gamma}{2}} + o\left((\ln t)^{-\frac{\gamma}{2}} t^{-\frac{\gamma}{2}}\right)$$

as $t \to \infty$ with $\hat{\eta} = O(1)$, and $c(t)$ given in (2.114).

Region III$^-(b)$: $\hat{y} = O(1)(< 0)$ as $t \to \infty$

$$u(\hat{y},t) = u_- + A_L(-\hat{y})^{-\gamma} t^{\gamma\delta} + \left(-\frac{u_- A_L \gamma}{(\delta+1)}(-\hat{y})^{-(\gamma+1)} + A_L\gamma(\gamma+1)(-\hat{y})^{-(\gamma+2)}\right) t^{(\delta(\gamma+2)+1)}$$
$$+ o\left(t^{(\delta(\gamma+2)+1)}\right)$$

as $t \to \infty$ with $\hat{y} = O(1)(< 0)$.

Region III$^-(a)$: $y = O(1)(< 0)$ as $t \to \infty$

$$u(y,t) = u_- + A_L(-y)^{-\gamma} t^{-\left(\frac{\gamma\delta}{\gamma-1}\right)} - \frac{u_- A_L \gamma}{(\delta+1)}(-y)^{-(\gamma+1)} t^{-\left(\frac{2\delta}{\gamma-1}\right)+1}$$
$$+ \left(-\frac{u_- A_L^2 \gamma}{(\delta+1)}(-y)^{-(2\gamma+1)} + A_L\gamma(\gamma+1)(-y)^{-(\gamma+2)}\right) t^{\left(\frac{-\delta(\gamma+2)}{\gamma-1}\right)+1} + o\left(t^{\left(\frac{-\delta(\gamma+2)}{\gamma-1}\right)+1}\right)$$

as $t \to \infty$ with $y = O(1)(< 0)$.

Region II$^-$: $t = O(1)$ as $x \to \infty$

$$u(x,t) = u_- + \frac{A_L}{x^\gamma} - \frac{\gamma u_- A_L t^{(\delta+1)}}{(\delta+1)x^{(\gamma+1)}} + \frac{\gamma(\gamma+1)A_L t}{x^{(\gamma+2)}} - \frac{\gamma A_L^2 t^{(\delta+1)}}{(\delta+1)x^{(2\gamma+1)}} + o\left(\frac{1}{x^{(2\gamma+1)}}\right) \text{ as } x \to \infty$$

with $t = O(1)$.

2.4 Numerical Solution to the Initial-Value Problem IVP$^+$

In this Section we develop a numerical solution to **IVP**$^+$. In particular, we adopt the numerical method that is described in [21]. Specifically, to obtain numerical solutions to **IVP**$^+$ we use a explicit finite difference scheme which we briefly summarize below with $N = 100$ where N is the number of grid points time step $\triangle t = 0.1$ and the length $\triangle x = 0.5$ (Further details of the the convergence test of numerical solutions of **IVP**$^+$ are given in Appendix A.1). Following [21], we begin by rewriting equation (2.1) in the form

$$u_t + t^\delta [v(u)]_x = u_{xx}, \quad -\infty < x < \infty, \quad t > 0, \tag{2.145}$$

with

$$v(u) = \frac{u^2}{2}.$$

On integrating equation (2.145) from $x_{j-\frac{1}{2}}$ to $x_{j+\frac{1}{2}}$ we obtain

$$\int_{x_{j-\frac{1}{2}}}^{x_{j+\frac{1}{2}}} u_t dx - \Big[u_x\Big]_{x_{j-\frac{1}{2}}}^{x_{j+\frac{1}{2}}} = -t^\delta \Big[v(u)\Big]_{x_{j-\frac{1}{2}}}^{x_{j+\frac{1}{2}}} \tag{2.146}$$

with $\{x_j\}_{j\in\mathbb{N}}$ being a discretization of the x-axis, with uniform spacing Δx. We now approximate the terms in (2.146) as follows

$$\int_{x_{j-\frac{1}{2}}}^{x_{j+\frac{1}{2}}} u_t dx \approx \frac{du}{dt}(x_j,t) \triangle x,$$

$$-\Big[u_x\Big]_{x_{j-\frac{1}{2}}}^{x_{j+\frac{1}{2}}} = \Big[u_x(x_{j-\frac{1}{2}},t) - u_x(x_{j+\frac{1}{2}},t)\Big] \approx$$

$$\left[\frac{u(x_j,t)-u(x_{j-1},t)}{\triangle x} - \frac{u(x_{j+1},t)-u(x_j,t)}{\triangle x}\right]$$

$$= -\frac{u(x_{j+1},t)-2u(x_j,t)+u(x_{j-1},t)}{\triangle x},$$

and

$$-t^\delta\Big[v(u)\Big]_{x_{j-\frac{1}{2}}}^{x_{j+\frac{1}{2}}} = t^\delta\Big[v(u(x_{j+\frac{1}{2}},t)) - v(u(x_{j-\frac{1}{2}},t))\Big]. \tag{2.147}$$

On substituting (2.147) into (2.146) we obtain the following ordinary differential equation for $U_j(t)$, namely

$$\frac{dU_j}{dt} - \frac{U_{j+1}-2U_j+U_{j-1}}{\Delta x^2} = t^\delta \frac{v(U_{j-\frac{1}{2}}) - v(U_{j+\frac{1}{2}})}{\Delta x} \tag{2.148}$$

where $U_j(t) \approx u(x_j,t)$ and $v(U_{j\pm\frac{1}{2}})$ is the average of $v(U_j)$ and $v(U_{j\pm1})$. Following [21] we then discretize the time derivative in (2.147) by a forward difference to obtain the explicit method

$$U_j^{n+1} = U_j^n + \triangle t\left[\left(\frac{U_{j+1}^n - 2U_j^n + U_{j-1}^n}{\triangle x^2}\right) + t^\delta\left(\frac{v(U_{j-\frac{1}{2}}^n) - v(U_{j+\frac{1}{2}}^n)}{\triangle x}\right)\right] \tag{2.149}$$

where $\{t_n\}_{n\in\mathbb{N}}$ is a discretization of the $t-$axis, with uniform spacing Δt. We anticipate that this explicit numerical method will be stable when $\Delta t < \frac{1}{2}\Delta x^2$, and this has been confirmed by numerical testing [39].

We now use this numerical method to obtain numerical solutions to $\mathbf{IVP}^+$. In par-

ticular, we consider $\mathbf{IVP}^+$ with initial data $u_0 : \mathbb{R} \to \mathbb{R}$ given by,

$$u_0(x) = \begin{cases} u_+ + \dfrac{(0.5\,(u_+ - u_-))A_R}{1 + x^\gamma}, & \text{as } x \geq 0, \\ u_- + \dfrac{(0.5\,(u_+ - u_-))A_L}{1 + (-x)^\gamma}, & \text{as } x < 0, \end{cases}$$

where $\gamma > 0$, $A_R = -1$ and $A_L = 1$. There are three cases to consider, in each of these cases we compare numerical simulation of the solution with of $\mathbf{IVP}^+$ to the theoretically predicted solution. These are:

(i) $\delta > -\frac{1}{2}, \quad \gamma > 0,$

(ii) $\delta = -\frac{1}{2}, \quad \gamma > 0,$

(iii) $-1 < \delta < -\frac{1}{2}, \quad \gamma > 0,$

and we consider each case in turn.

2.4.1 $\delta > -\frac{1}{2}, \quad \gamma > 0$

In this case we have established in Section 2.3.1 that a expansive wave develops in the solution of $\mathbf{IVP}^+$ as $t \to \infty$. We now present numerical evidence to support that the solution $u(y,t)$ of $\mathbf{IVP}^+$ exhibits the formation of expansion wave profile with $\delta > -\frac{1}{2}$ and $\gamma > 0$. In Figures 2.9-2.11 we plot the numerical solution of $\mathbf{IVP}^+$ against y at times $t = 5,\ 10,\ 20,\ 30,\ 40$ and 50 for the cases

(i) $u_+ = 1, \quad u_- = -1,$

(ii) $u_+ = 1, \quad u_- = 0,$

(iii) $u_+ = 0, \quad u_- = -1,$

respectively. The dashed line represents the theoretically predicted solution (2.62) that is

$$u_E(y) = \begin{cases} u_+, & y > \frac{u_+}{(\delta+1)}, \\ (\delta+1)y, & \frac{u_-}{(\delta+1)} \leq y \leq \frac{u_+}{(\delta+1)}, \\ u_-, & y < \frac{u_-}{(\delta+1)}, \end{cases}$$

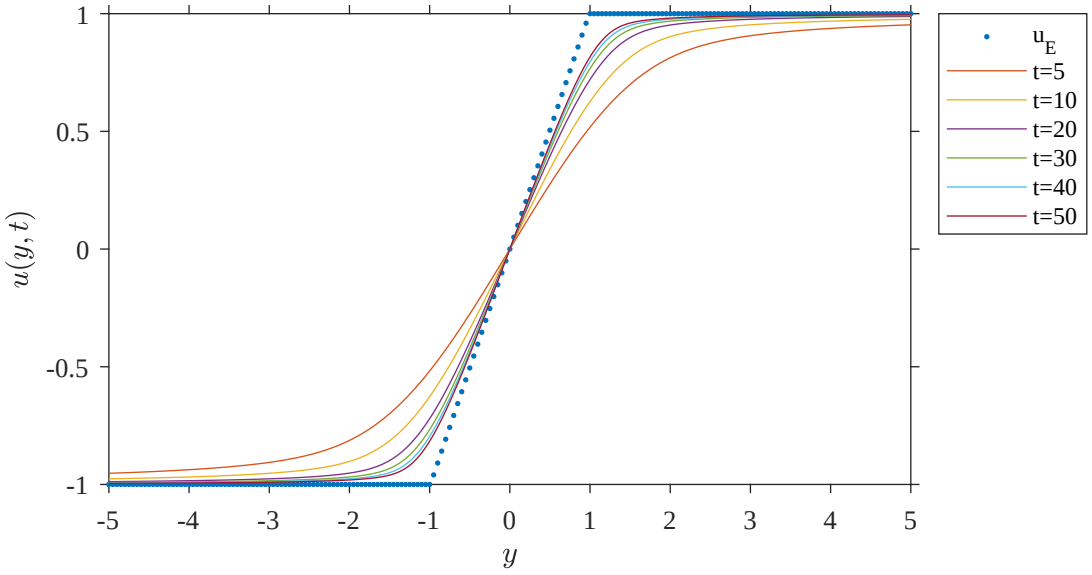

(a)

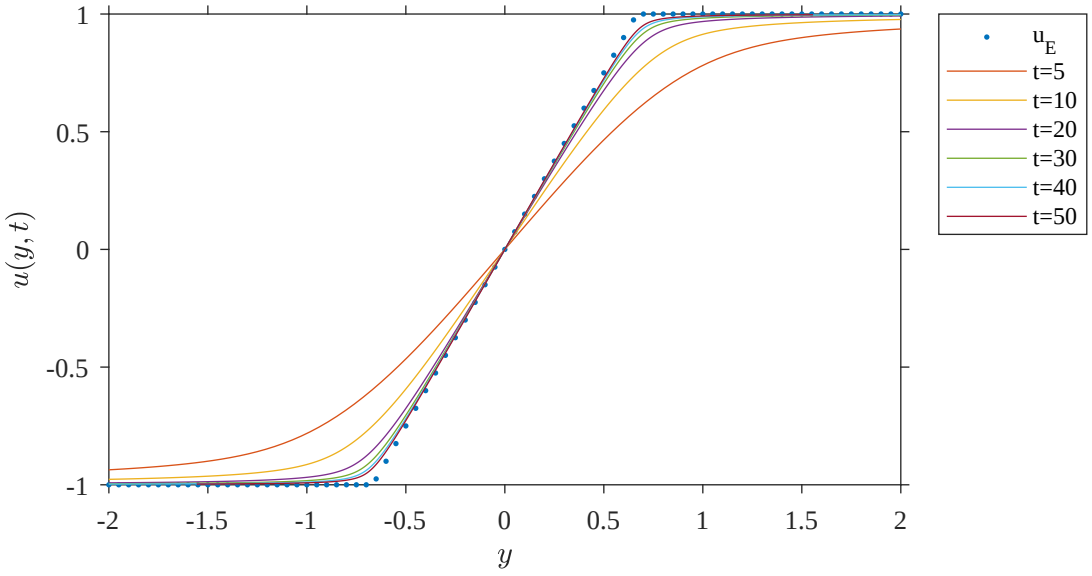

(b)

Figure 2.9: Graphs of the numerical solution of **IVP**$^+$ in the (y,u) plane when $u_+ = 1$ and $u_- = -1$ at times $t = 5,\ 10,\ 20,\ 30,\ 40$ and 50 with (a) $\delta = 0.01$, $\gamma = 1$ and (b) $\delta = 0.5$, $\gamma = 1$. The graphs illustrate the development of the expansive wave with the solid lines showing the numerically computed solutions and the dash line representing theoretically predicted solution u_E is given by (2.62).

In Figure 2.9 we observe that the numerically computed solution of $\mathbf{IVP}^+$ when $u_+ = 1$ and $u_- = -1$ with $\delta > -\frac{1}{2}$ in this approaches the predicted large-time attractor, the expansion wave. This is in line with the Proposition 1 where we expect the numerical solution converges to an expansion wave profile in y as $t \to \infty$. Specifically, at t = 50 and $\delta = 0.5$ we see that the gradient of numerical solution is in good agreement with the theoretically predicted solution given by dashed line.

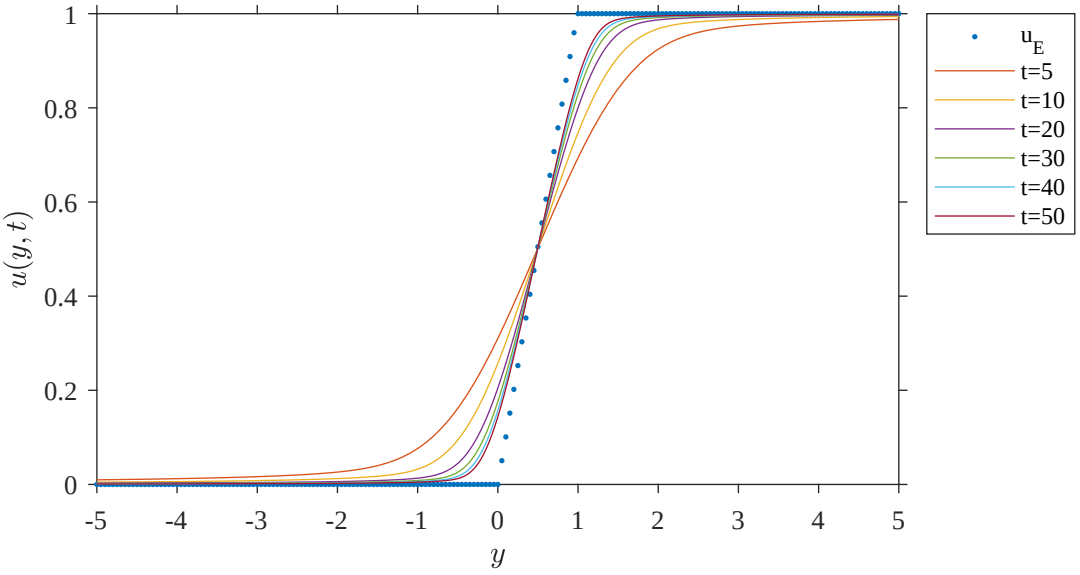

(a)

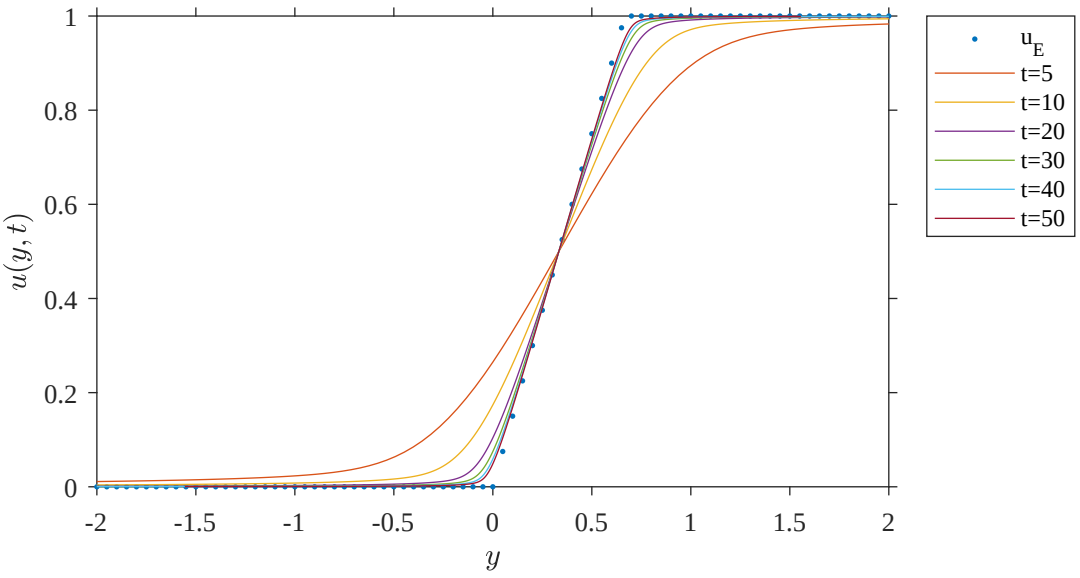

(b)

Figure 2.10: Graphs of the numerical solution of **IVP**$^+$ in the (y, u) plane when $u_+ = 1$ and $u_- = 0$ at times $t = 5,\ 10,\ 20,\ 30,\ 40$ and 50 with (a) $\delta = 0.01$, $\gamma = 1$ and (b) $\delta = 0.5$, $\gamma = 1$. The graphs illustrate the development of the expansive wave with the solid lines showing the numerically computed solutions and the dash line representing theoretically predicted solution u_E is given by (2.62).

In Figure 2.10 we observe that the numerically computed solution of $\mathbf{IVP}^+$when $u_+ = 1$ and $u_- = 0$ with $\delta > -\frac{1}{2}$ in this approaches the predicted large-time attractor, the expansion wave. This is in line with the Proposition 1 where we expect the numerical solution converges to an expansion wave profile in y as $t \to \infty$. Specifically, at t = 50 and $\delta = 0.5$ we see that the gradient of numerical solution is in good agreement with the theoretically predicted solution given by dashed line.

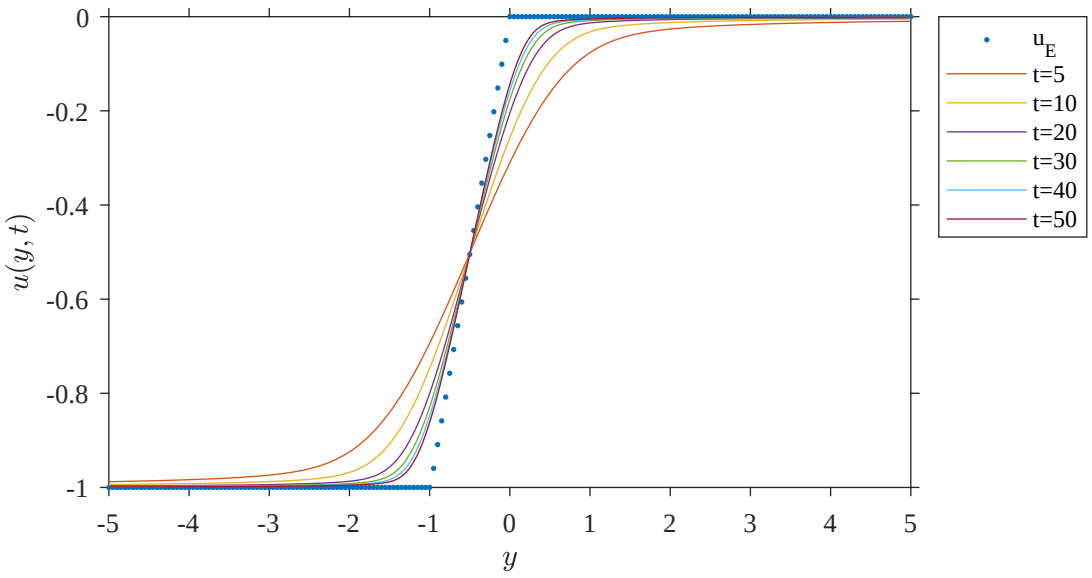

(a)

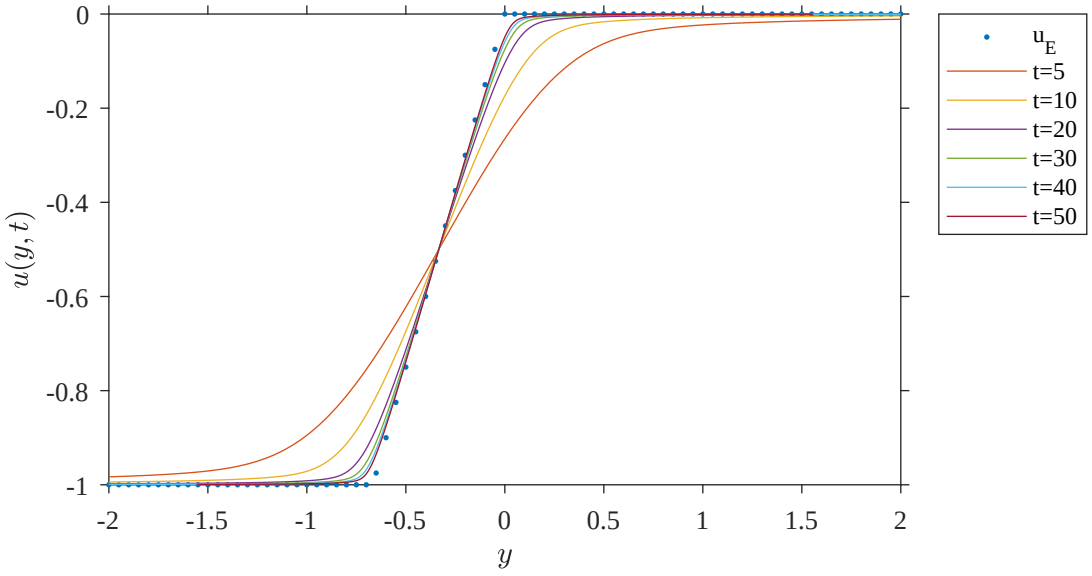

(b)

Figure 2.11: Graphs of the numerical solution of **IVP**$^+$ in the (y, u) plane when $u_+ = 0$ and $u_- = -1$ at times $t = 5,\ 10,\ 20,\ 30,\ 40$ and 50 with (a) $\delta = 0.01$, $\gamma = 1$ and (b) $\delta = 0.5$, $\gamma = 1$. The graphs illustrate the development of the expansive wave with the solid lines showing the numerically computed solutions and the dash line representing theoretically predicted solution u_E is given by (2.62).

In Figure 2.11 we observe that the numerically computed solution of $\mathbf{IVP}^+$ when $u_+ = 0$ and $u_- = -1$ with $\delta > -\frac{1}{2}$ in this approaches the predicted large-time attractor, the expansion wave. This is in line with the Proposition 1 where we expect the numerical solution converges to an expansion wave profile in y as $t \to \infty$. Specifically, at t = 50 and $\delta = 0.5$ we see that the gradient of numerical solution is in good agreement with the theoretically predicted solution given by dashed line.

2.4.2 $\delta = -\frac{1}{2}, \quad \gamma > 0$

In this case we have established in Section 2.3.2 that the similarity solution found by Rudenko and Soluyan [32] develops in the solution of $\mathbf{IVP}^+$ as $t \to \infty$. We now present numerical evidence to support that the solution $u(y,t)$ of $\mathbf{IVP}^+$ exhibits the formation of the similarity solution found by Rudenko and Soluyan when $\delta = -\frac{1}{2}$ and $\gamma > 0$. In Figures 2.12-2.14 we plot the numerical solution of $\mathbf{IVP}^+$ against y at times $t = 5,\ 10,\ 20,\ 30,\ 40$ and 50 for the cases

(i) $u_+ = 1, \quad u_- = -1,$

(ii) $u_+ = 1, \quad u_- = 0,$

(iii) $u_+ = 0, \quad u_- = -1,$

respectively. In this case, the theoretically predicted solution (2.80) that is

$$u_R(y) \sim \begin{cases} u_+ + \mathcal{C}_+(u_+,u_-)y^{-1}e^{-\frac{1}{4}(y-2u_+)^2} & \text{as } y \to \infty, \\ u_- + \mathcal{C}_-(u_+,u_-)y^{-1}e^{-\frac{1}{4}(y-2u_-)^2} & \text{as } y \to -\infty, \end{cases}$$

with $\mathcal{C}_+$ and $\mathcal{C}_-$ globally determined nonzero constants, where

$$\mathcal{C}_+(u_+,u_-) < 0 \qquad \text{and} \qquad \mathcal{C}_-(u_+,u_-) > 0.$$

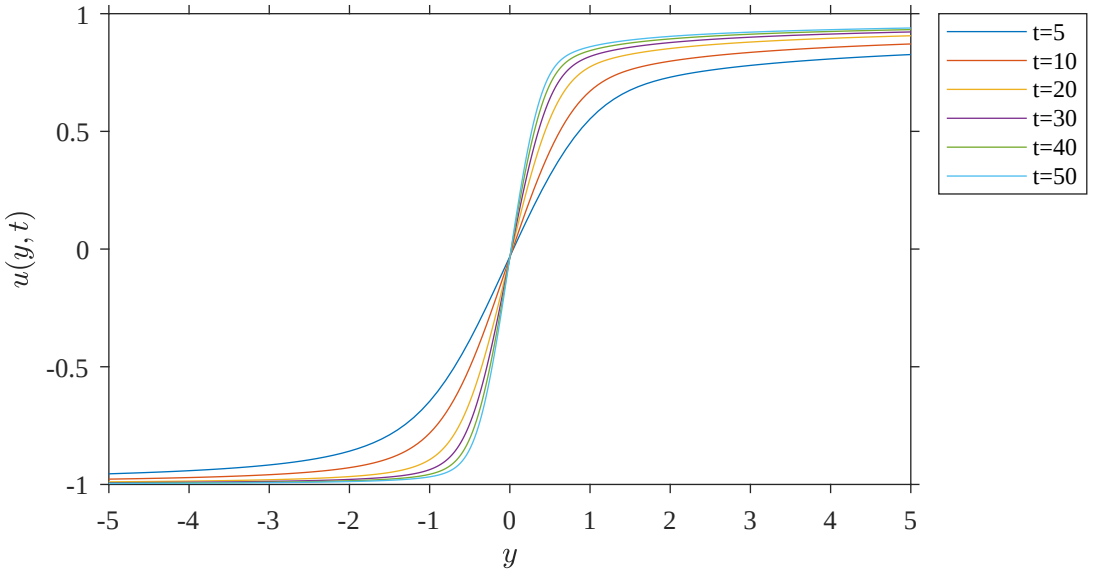

(a)

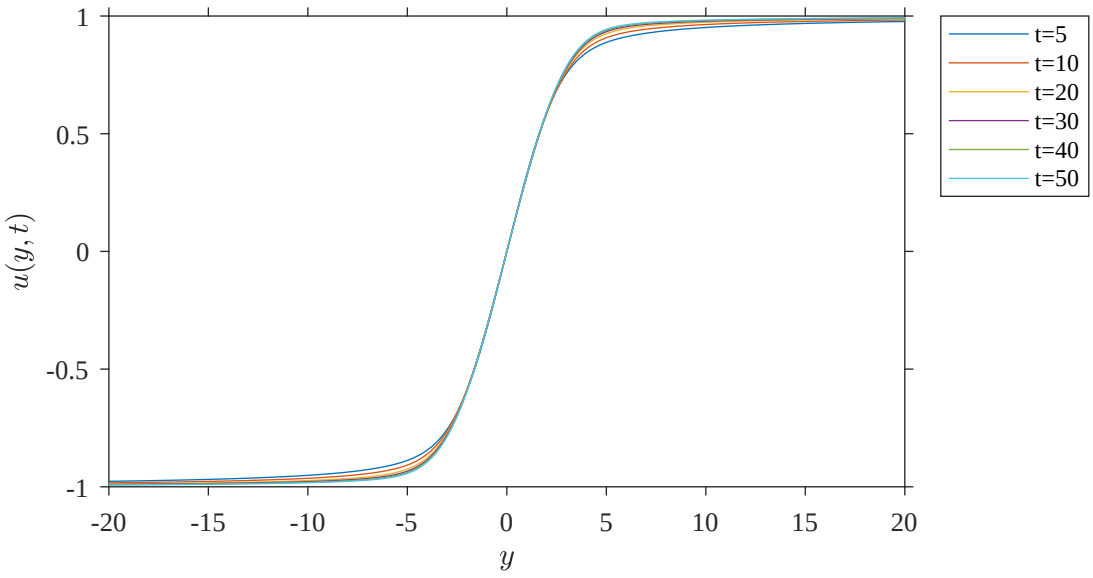

(b)

Figure 2.12: Graphs of the numerical solution of **IVP**$^+$ in the (y,u) plane when $u_+ = 1$ and $u_- = -1$ at times $t = 5,\ 10,\ 20,\ 30,\ 40$ and 50 with (a) $\delta = -0.5$, $\gamma = 0.5$ and (b) $\delta = -0.5$, $\gamma = 1$. We note that the numerically computed solutions represent the formation of the similarity solution found by Rudenko and Soluyan [32].

We observe that in Figure 2.12 the numerically computed solution of $\mathbf{IVP}^+$ when $u_+ = 1$ and $u_- = -1$ with $\delta = -\frac{1}{2}$ approaches the predicted large time attractor which is the similarity solution found by Rudenko and Soluyan [32] as $t \to \infty$. This is in line with the Proposition 3 (later presenting in this thesis) where we expect the numerical solution converges to the similarity solution found by Rudenko and Soluyan [32] as $t \to \infty$. In fact, by $t = 50$ there is already good agreement as can be seen from Figure 2.12.

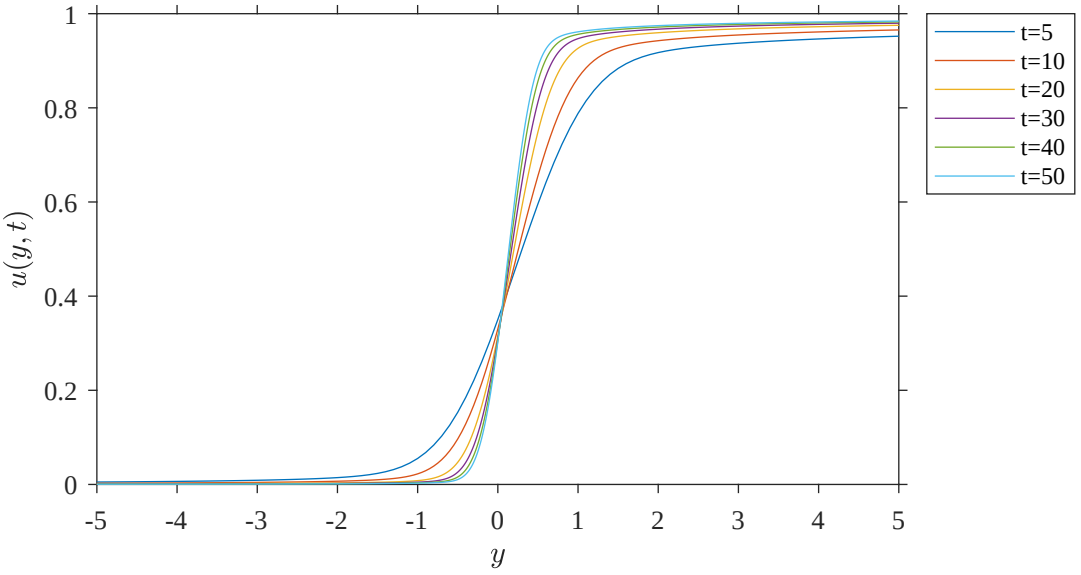

(a)

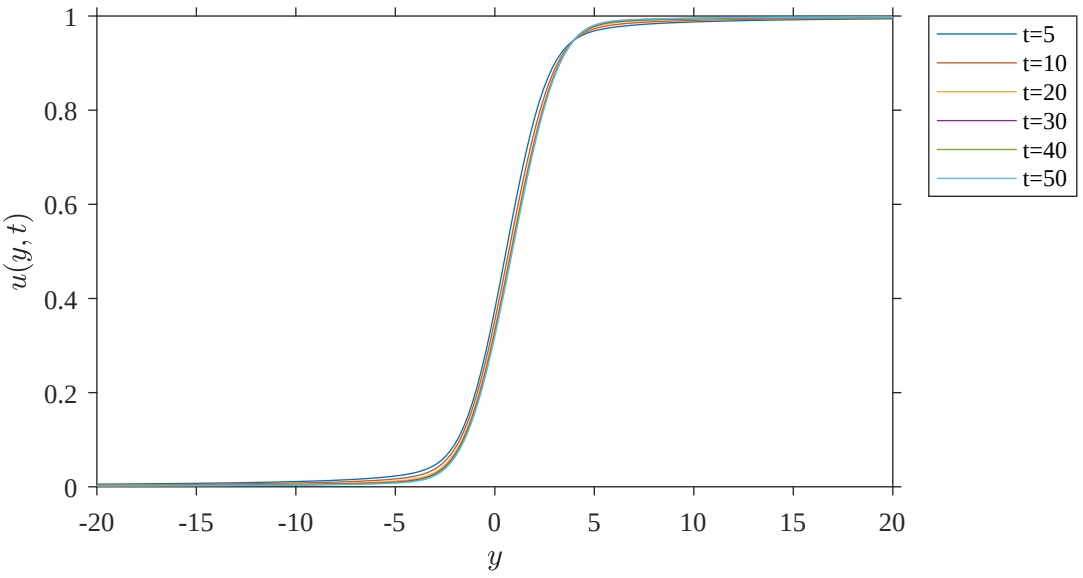

(b)

Figure 2.13: Graphs of the numerical solution of **IVP**$^+$ in the (y,u) plane when $u_+ = 1$ and $u_- = 0$ at times $t = 5,\ 10,\ 20,\ 30,\ 40$ and 50 with (a) $\delta = -0.5$, $\gamma = 0.5$ and (b) $\delta = -0.5$, $\gamma = 1$. We note that the numerically computed solutions represent the formation of the similarity solution found by Rudenko and Soluyan [32] .

We observe that in Figure 2.13 the numerically computed solution of $\mathbf{IVP}^+$ when $u_+ = 1$ and $u_- = 0$ with $\delta = -\frac{1}{2}$ approaches the predicted large time attractor which is the similarity solution found by Rudenko and Soluyan [32] as $t \to \infty$. This is in line with the Proposition 3 (later presenting in this thesis) where we expect the numerical solution converges to the similarity solution found by Rudenko and Soluyan [32] as $t \to \infty$. In fact, by $t = 50$ there is already good agreement as can be seen from Figure 2.13.

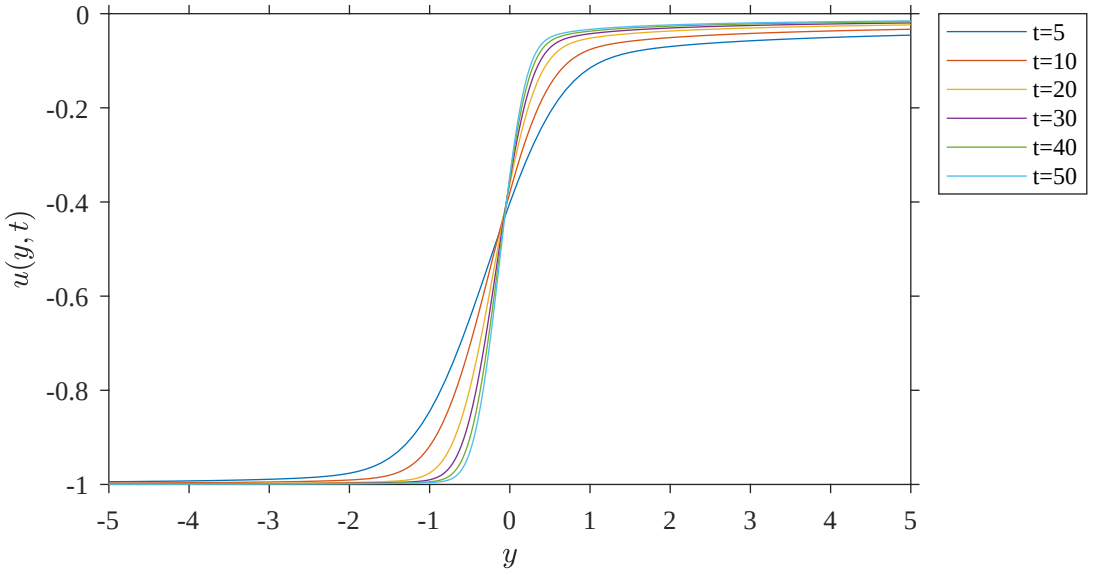

(a)

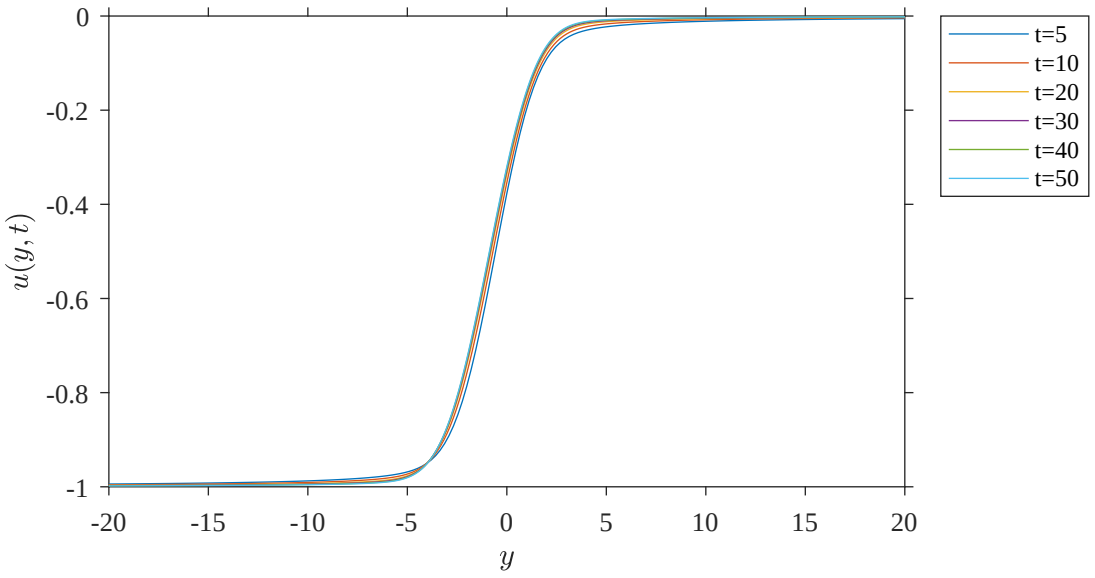

(b)

Figure 2.14: Graphs of the numerical solution of $\mathbf{IVP}^+$ in the (y,u) plane when $u_+ = 0$ and $u_- = -1$ at times $t = 5,\ 10,\ 20,\ 30,\ 40$ and 50 with (a) $\delta = -0.5$, $\gamma = 0.5$ and (b) $\delta = -0.5$, $\gamma = 1$. We note that the numerically computed solutions represent the formation of the similarity solution found by Rudenko and Soluyan [32] .

We observe that in Figure 2.14 the numerically computed solution of $\mathbf{IVP}^+$ when $u_+ = 0$ and $u_- = -1$ with $\delta = -\frac{1}{2}$ approaches the predicted large time attractor which is the similarity solution found by Rudenko and Soluyan [32] as $t \to \infty$.This is in line with the Proposition 3 (later presenting in this thesis) where we expect the numerical solution converges to the similarity solution found by Rudenko and Soluyan [32] as $t \to \infty$. In fact, by $t = 50$ there is already good agreement as can be seen from Figure 2.14.

2.4.3 $-1 < \delta < -\frac{1}{2}, \quad \gamma > 0$

In this case we have established in Section 2.3.3 that the error function profile (2.110) develops in the solution of $\mathbf{IVP}^+$ as $t \to \infty$. We now present numerical evidence to support that the solution $u(y,t)$ of $\mathbf{IVP}^+$ exhibits the formation of an error function profile when $-1 < \delta < -\frac{1}{2}$ and $\gamma > 0$. In Figures 2.15-2.17 we plot the numerical solution of $\mathbf{IVP}^+$ against y at times $t = 5,\ 10,\ 20,\ 30,\ 40$ and 50 for the cases

(i) $u_+ = 1, \quad u_- = -1,$

(ii) $u_+ = 1, \quad u_- = 0,$

(iii) $u_+ = 0, \quad u_- = -1,$

respectively. In this case, the theoretically predicted solution (2.109) that is

$$u_{\overline{R}}(y,t) = \frac{(u_+ + u_-)}{2} - \frac{(u_- - u_+)}{2}\mathrm{erf}(y), \ -\infty < y < \infty. \tag{2.150}$$

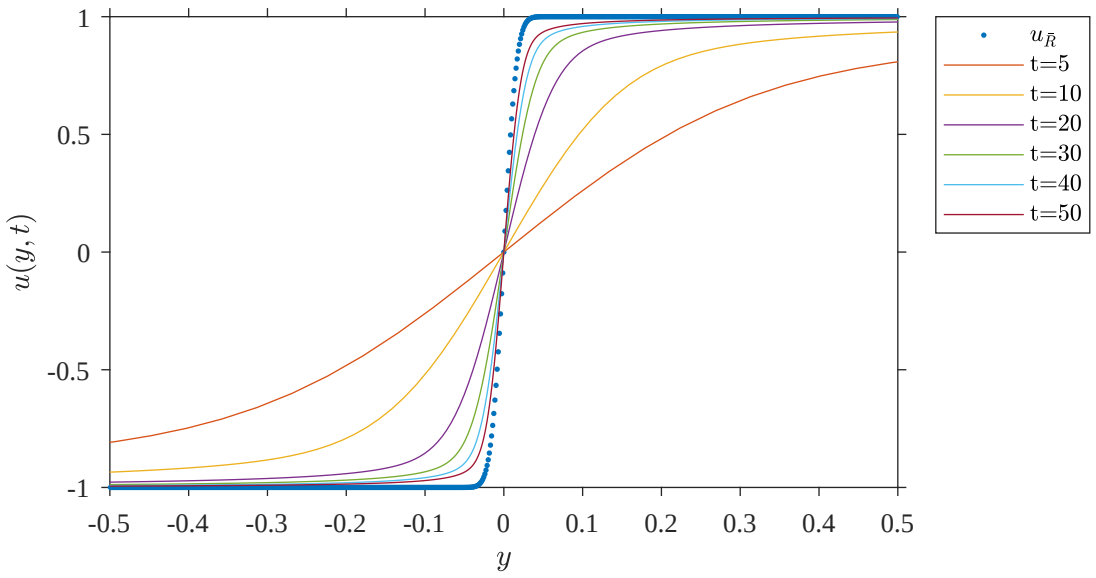

(a)

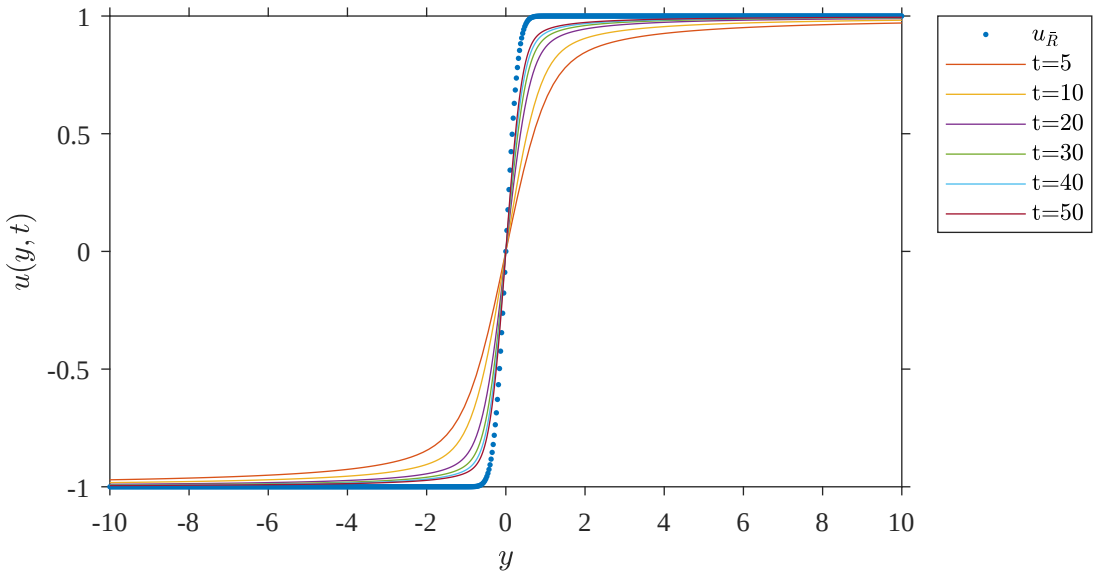

(b)

Figure 2.15: Graphs of the numerical solution of **IVP**$^+$ in the (y,u) plane when $u_+ = 1$ and $u_- = -1$ at times $t = 5,\ 10,\ 20,\ 30,\ 40$ and 50 with (a) $\delta = -0.75$, $\gamma = 0.5$ and (b) $\delta = -0.75$, $\gamma = 1$. The graphs illustrate the numerically computed solutions and the theoretically predicted solution (dashed) $u_{\overline{R}}$ at $t = 50$.

In Figure 2.15 we observe that the numerically computed solution of $\mathbf{IVP}^+$ when $u_+ = 1$ and $u_- = -1$ with $-1 < \delta < -\frac{1}{2}$ in this approaches the predicted large-time attractor, an error function profile. This is in line with the Proposition 4 (later presenting in this thesis) where we expect the numerical solution converges to be an error function profile in y as $t \to \infty$. Specifically, at t = 50 with $\delta = -0.75$ and $\gamma = 1$ we see that the gradient of numerical solution is in good agreement with the theoretically predicted solution given by $u_{\overline{R}}$.

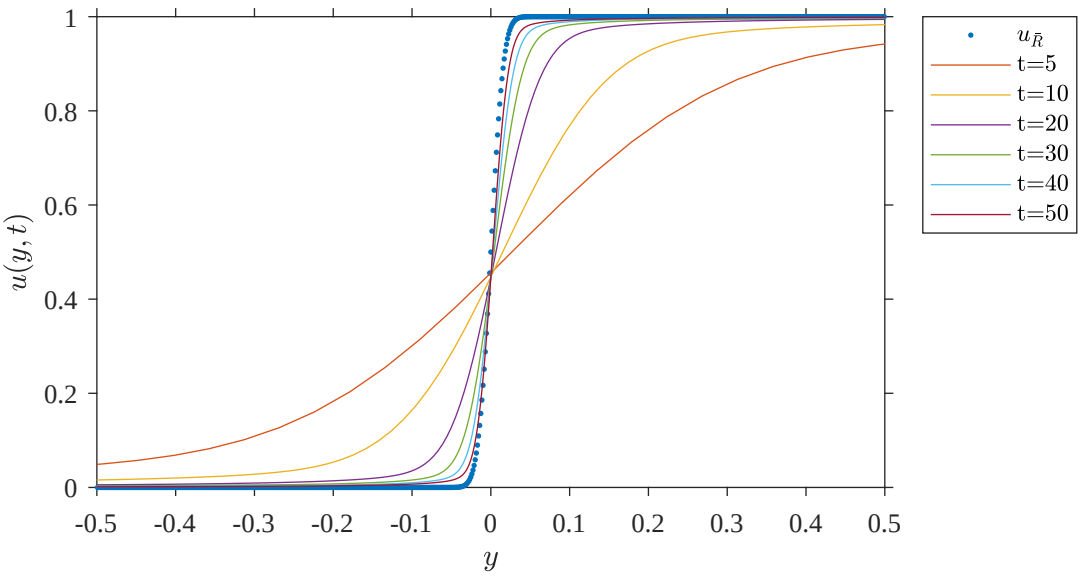

(a)

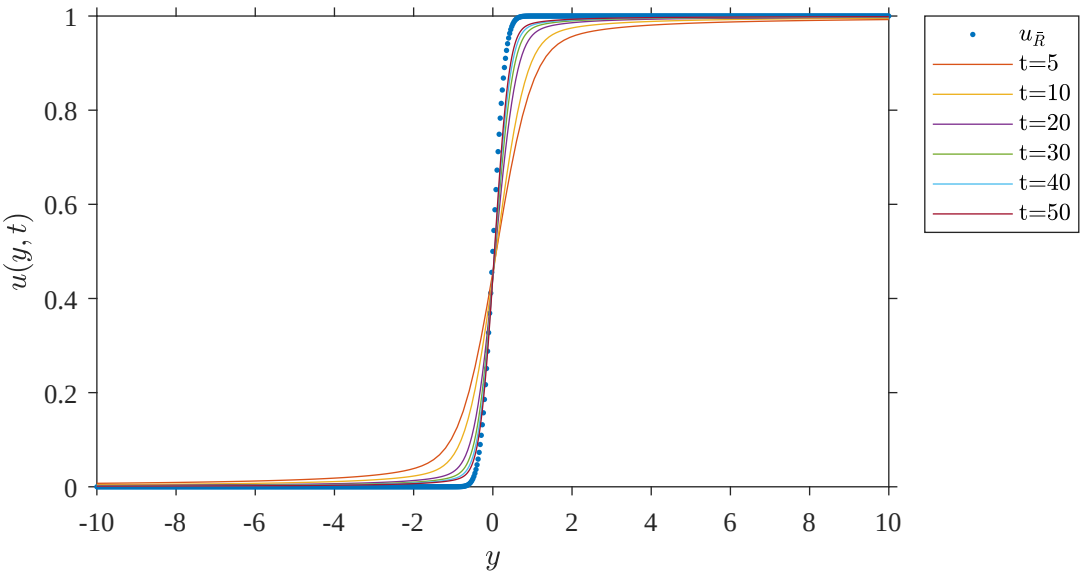

(b)

Figure 2.16: Graphs of the numerical solution of **IVP**$^+$ in the (y,u) plane when $u_+ = 1$ and $u_- = 0$ at times $t = 5,\ 10,\ 20,\ 30,\ 40$ and 50 with (a) $\delta = -0.75$, $\gamma = 0.5$ and (b) $\delta = -0.75$, $\gamma = 1$. The graphs illustrate the numerically computed solutions and the theoretically predicted solution (dashed) $u_{\overline{R}}$ at $t = 50$.

In Figure 2.16 we observe that the numerically computed solution of $\mathbf{IVP}^+$ when $u_+ = 1$ and $u_- = 0$ with $-1 < \delta < -\frac{1}{2}$ in this approaches the predicted large-time attractor, an error function profile. This is in line with the Proposition 4 (later presenting in this thesis) where we expect the numerical solution converges to be an error function profile in y as $t \to \infty$. Specifically, at t = 50 with $\delta = -0.75$ and $\gamma = 1$ we see that the gradient of numerical solution is in good agreement with the theoretically predicted solution given by $u_{\overline{R}}$.

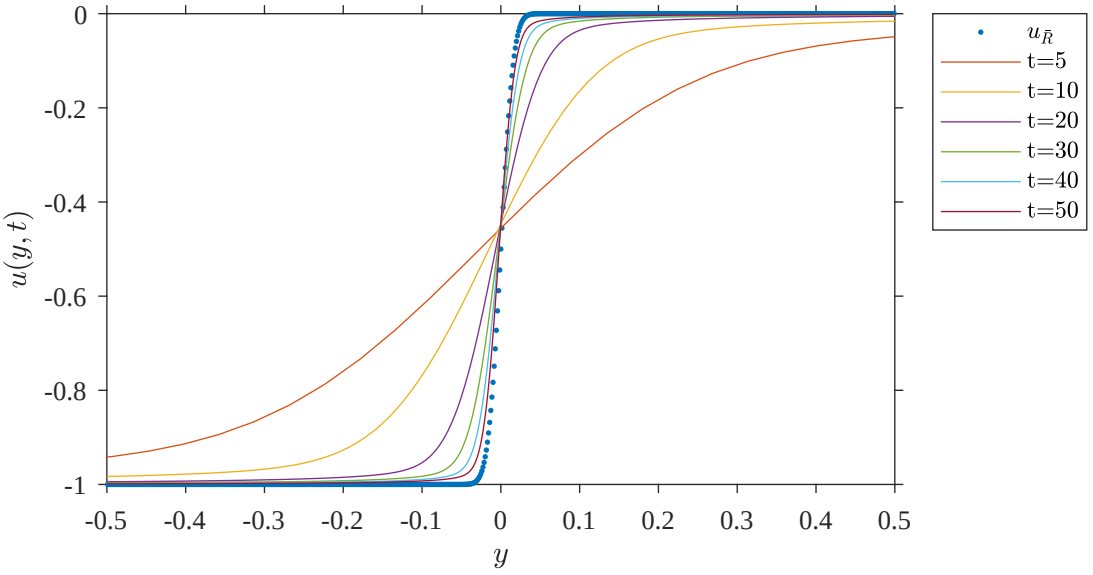

(a)

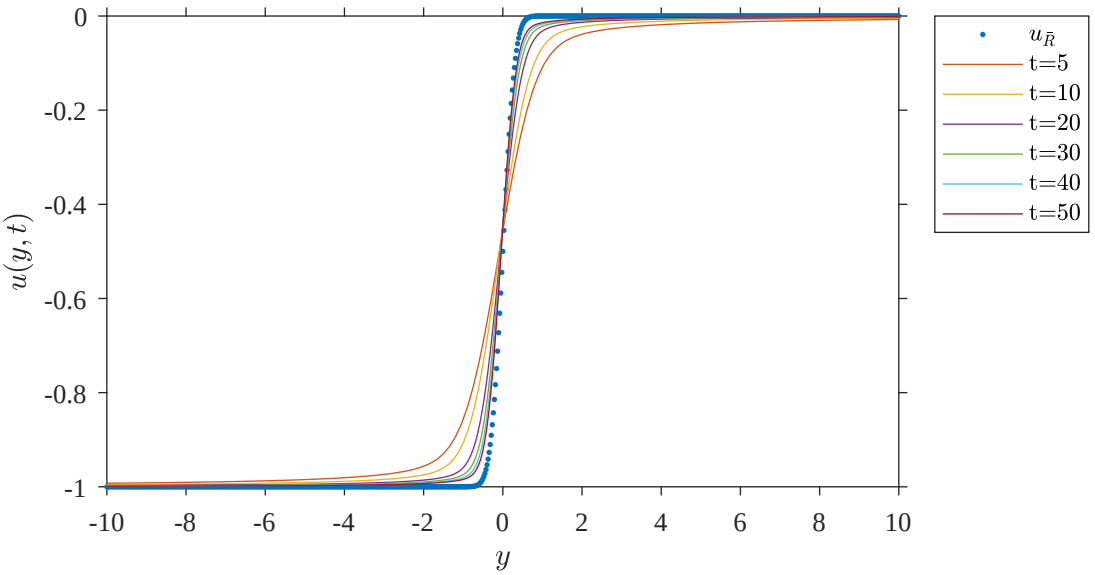

(b)

Figure 2.17: Graphs of the numerical solution of **IVP**$^+$ in the (y,u) plane when $u_+ = 0$ and $u_- = -1$ at times $t = 5,\ 10,\ 20,\ 30,\ 40$ and 50 with (a) $\delta = -0.75$, $\gamma = 0.5$ and (b) $\delta = -0.75$, $\gamma = 1$. The graphs illustrate the numerically computed solutions and the theoretically predicted solution (dashed) $u_{\overline{R}}$ at $t = 50$.

In Figure 2.17 we observe that the numerically computed solution of $\mathbf{IVP}^+$ when $u_+ = 0$ and $u_- = -1$ with $-1 < \delta < -\frac{1}{2}$ in this approaches the predicted large-time attractor, an error function profile. This is in line with the Proposition 4 (later presenting in this thesis) where we expect the numerical solution converges to be an error function profile in y as $t \to \infty$. Specifically, at t = 50 with $\delta = -0.75$ and $\gamma = 1$ we see that the gradient of numerical solution is in good agreement with the theoretically predicted solution given by $u_{\overline{R}}$.

2.5 Summary

In this chapter we have obtained, via the method of matched asymptotic coordinate expansions, the uniform asymptotic structure of $t \to 0$, $t = O(1)$ and the large-t solution to the initial-value problem $\mathbf{IVP}^+$ ($u_+ > u_-$) over all parameter values. The form of the large-t solution to the initial-value problem $\mathbf{IVP}^+$ depends on the problem parameters δ and γ as follows:

(i) When $\delta > -\frac{1}{2}$ and $\gamma > 0$, the solution $u(x,t)$ of $\mathbf{IVP}^+$ exhibits the formation of expansion wave profile, with

$$u\left(yt^{(\delta+1)}, t\right) \to \begin{cases} u_+, & y > \frac{u_+}{(\delta+1)}, \\ (\delta+1)y, & \frac{u_-}{(\delta+1)} \leq y \leq \frac{u_+}{(\delta+1)}, \\ u_-, & y < \frac{u_-}{(\delta+1)}, \end{cases}$$

as $t \to \infty$, uniformly for $y \in \mathbb{R}$. The detailed rate of convergence is given in Proposition 1.

(ii) When $\delta = -\frac{1}{2}$ and $\gamma > 0$, the solution $u(x,t)$ of $\mathbf{IVP}^+$ exhibits the formation of the similarity solution found by Rudenko and Soluyan [32], with

$$u\left(zt^{\frac{1}{2}}, t\right) \to U_R(z)$$

as $t \to \infty$ with $z = O(1)$, where $U_R(z)$ is given by (2.80). We observe that this profile is in a stretching frame of reference of thickness $O\left(t^{\frac{1}{2}}\right)$ as $t \to \infty$.

(iii) When $-1 < \delta < -\frac{1}{2}$ and $\gamma > 0$, the solution $u(x,t)$ of $\mathbf{IVP}^+$ exhibits the formation of an error function profile, with

$$u\left(zt^{\frac{1}{2}}, t\right) \to \left[\frac{(u_+ + u_-)}{2} - \frac{(u_- - u_+)}{2}\ \mathrm{erf}\left(\frac{z}{2}\right)\right]$$

as $t \to \infty$, uniformly for $z = O(1)$. We observe that the error function profile is in a stretching frame of reference of thickness $O\left(t^{\frac{1}{2}}\right)$ as $t \to \infty$.

Chapter 3

The Initial-Value Problem $\mathbf{IVP}^-$

In this chapter, we consider the initial-value problem for Burgers' equation with a time dependent coefficient, namely,

$$u_t + t^\delta u u_x = u_{xx}, \quad -\infty < x < \infty, \quad t > 0, \tag{3.1}$$

$$u(x,0) = u_0(x), \quad -\infty < x < \infty \tag{3.2}$$

$$u(x,t) \to \begin{cases} u_-, & x \to -\infty, \\ u_+, & x \to \infty, \end{cases} \quad t \geq 0, \tag{3.3}$$

where $\delta > -1$ and now $u_- > u_+$. Further, we consider the situation when the initial data $u_0 : \mathbb{R} \to \mathbb{R}$ is continuously differentiable and has algebraic decay as $|x| \to \infty$. Specifically

$$u_0(x) = \begin{cases} u_+ + \frac{A_R}{(x)^\gamma} + O(E(|x|)) & \text{as } x \to \infty, \\ u_- + \frac{A_L}{(-x)^\gamma} + O(E(|x|)) & \text{as } x \to -\infty, \end{cases} \tag{3.4}$$

where $E(|x|)$ is linearly exponentially small in x as $|x| \to \infty$, $A_R > 0$, $A_L < 0$ and $\gamma > 0$ are constants. We henceforth refer to the initial-value problem (3.1), (3.2) and (3.4) as $\mathbf{IVP}^-$ when $u_- > u_+$. We develop the structure of the large-time solution to $\mathbf{IVP}^-$ using the method of matched asymptotic coordinate expansions. The large-time solution

is obtained by consideration of the asymptotic structures as $t \to 0$ $(-\infty < x < \infty)$ and as $t \to \infty$.

We begin by examining the asymptotic structure of the solution to **IVP**$^-$ as $t \to 0$.

3.1 Asymptotic solution to IVP$^-$ as $t \to 0$

Again the consideration of initial data (3.2) (with (3.4)) indicates that the asymptotic solution to **IVP**$^-$ as $t \to 0$ will consist of a single asymptotic region, which we label as region I. We find that the detail of region I in both cases ($\delta > 0$ and $-1 < \delta < 0$) follow those given in Sections 2.1.1 and 2.1.2.

3.2 Asymptotic solution to IVP$^-$ as $|x| \to \infty$

The details of the asymptotic structure of the solution to **IVP**$^-$ as $|x| \to \infty$ with $t = O(1)$ follow those given in Section 2.2 and are not repeated here.

3.3 Asymptotic solution to IVP$^-$ as $t \to \infty$

We now investigate the asymptotic structure of the solution to **IVP**$^-$ as $t \to \infty$. We recall Section 2.2 that expansions (2.14) and (2.18) of regions II$^+$ ($x \to \infty$, $t = O(1)$) and II$^-$ ($x \to -\infty$, $t = O(1)$), respectively, continue to remain uniform provided that $|x| \gg t^{\delta+1}$ as $t \to \infty$. However, as already noted, a nonuniformity develops when $|x| = O\left(t^{\delta+1}\right)$ as $t \to \infty$. As in Section 2.3.1, we introduce the scaled coordinate

$$y = xt^{-(\delta+1)}, \tag{3.5}$$

where $y = O(1)$ as $t \to \infty$, and begin by summarizing the asymptotic structure as $t \to \infty$ in regions III$^{\pm}$, the details of which follow, after minor modification, those given in Section 2.3.1, and are not repeated here.

Region III$^+$:

$$u(y,t) = u_+ + A_R\left(y - \frac{u_+}{(\delta+1)}\right)^{-\gamma} t^{-\gamma(\delta+1)} + o\left(t^{-\gamma(\delta+1)}\right) \tag{3.6}$$

as $t \to \infty$ with $y = \frac{u_+}{(\delta+1)} + O(1)$, and where $A_R > 0$.

Region III$^-$:

$$u(y,t) = u_- + A_L\left(\frac{u_-}{(\delta+1)} - y\right)^{-\gamma} t^{-\gamma(\delta+1)} + o\left(t^{-\gamma(\delta+1)}\right) \tag{3.7}$$

as $t \to \infty$ with $y = \frac{u_-}{(\delta+1)} - O(1)$, and where $A_L < 0$. Consideration of expansions (3.6) and (3.7) for $t \gg 1$ in regions III$^\pm$ indicates that there are a number of cases to consider, which are now developed in turn [3]. We note that, the details of the asymptotic structure of solution to **IVP**$^-$ as $t \to \infty$ in both cases $\delta = -\frac{1}{2}$ and $-1 < \delta < -\frac{1}{2}$ follow those given in Sections 2.3.2 and 2.3.3 respectively. Thus, in order to avoid repetition we give a brief summary of the asymptotic structure of solution to **IVP**$^-$ as $t \to \infty$ in each case.

3.3.1 $\delta > -\frac{1}{2}$

In this case, when $u_- > u_+$ the nonuniformity in expansion (3.6) and (3.7) must occur when $y = \alpha + o(1)$, for some $\alpha \in \left(\frac{u_+}{(\delta+1)}, \frac{u_-}{(\delta+1)}\right)$ which is to be determined. To proceed, we introduce a new region which we label as region SS. To examine region SS we introduce the scaled coordinate z, via

$$z = (y - \alpha)\,\phi(t)^{-1} = O(1), \tag{3.8}$$

where $\phi(t) = o(1)$ as $t \to \infty$, is an as yet undetermined gauge function, and expand in the form

$$u(z,t) = U(z) + o(1) \tag{3.9}$$

as $t \to \infty$ with $z = O(1)$ [3]. On substituting expansion (3.9) into equation (3.1) (when written in terms of z and t) we obtain

$$-\alpha(1+\delta)t^{-1}\phi(t)^{-1}U_z + UU_z t^{-1}\phi(t)^{-1} = U_{zz}t^{-2(1+\delta)}\phi(t)^{-2} + o\left(t^{-2(1+\delta)}\phi(t)^{-2}\right)$$

which simplifies to

$$-\alpha(1+\delta)U_z + UU_z = U_{zz}t^{-(2\delta+1)}\phi(t)^{-1} + o\left(t^{-(2\delta+1)}\phi(t)^{-1}\right). \tag{3.10}$$

We now choose $\phi(t)$ to provide the most structured balance in (3.10).This requires, without loss of generality, taking

$$\phi(t) = t^{-(2\delta+1)}. \tag{3.11}$$

We then obtain at leading order that

$$U_{zz} - UU_z + \alpha(1+\delta)U_z = 0, \qquad -\infty < z < \infty. \tag{3.12}$$

We note that we have examined equation (3.12) in Section 1.5.4. The solution to (3.12) is readily obtained as the standard Taylor shock profile (see [38]) and is given by

$$U(z) = \frac{1}{2}(u_+ + u_-) - \frac{1}{2}(u_- - u_+)\tanh\left(\frac{1}{4}(u_- - u_+)z + \frac{1}{2}\phi_c\right), -\infty < z < \infty, \tag{3.13}$$

where ϕ_c is a globally determined constant. A graph of (3.13) for $u_- = 1$ and $u_+ = -1$ (up to translational invariance in z) is given in Figure 3.1. Therefore the expansion in

region SS is given by

$$u(z,t) = \frac{1}{2}(u_+ + u_-) - \frac{1}{2}(u_- - u_+)\tanh\left(\frac{1}{4}(u_- - u_+)z + \frac{1}{2}\phi_c\right) + o(1), \tag{3.14}$$

with $z = O(1)$ as $t \to \infty$.

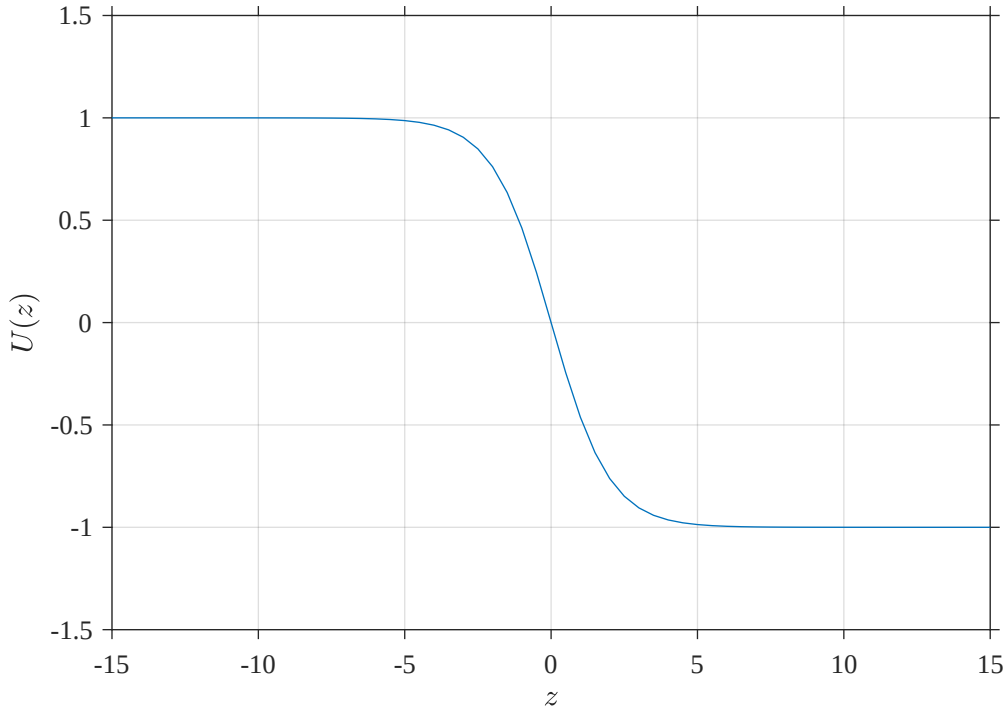

Figure 3.1: A graph of the Taylor shock profile (3.13) when $u_- = 1$ and $u_+ = -1$ (with translational invariance fixed by taking $\phi_c = 0$).

We note that

$$U(z) \sim \begin{cases} u_+ + (u_- - u_+)e^{-\frac{1}{2}(u_- - u_+)z - \phi_c} + O(e^{-(u_- - u_+)z}) & \text{as } z \to \infty, \\ u_- - (u_- - u_+)e^{\frac{1}{2}(u_- - u_+)z + \phi_c} + O(e^{(u_- - u_+)z}) & \text{as } z \to -\infty. \end{cases} \tag{3.15}$$

The similarity solution (3.14) represents a wavefront connecting u_+ (as $z \to \infty$) to u_- (as $z \to -\infty$). Specifically, when $\delta > 0$, the Taylor shock profile is located at $x = \alpha t^{\delta+1}$

and contained in a localized region of thickness $O\left(t^{-\delta}\right)$ as $t \to \infty$ (the profile steepens as $t \to \infty$). The Taylor shock is accelerating in the $+x$ $(-x)$ direction as $t \to \infty$ when $-u_- < u_+ < u_-$ $(u_+ < u_- < -u_+)$, respectively. When $-\frac{1}{2} < \delta < 0$, the Taylor shock profile is located $x = \alpha t^{\delta+1}$ and contained in a localized region of thickness $O\left(t^{|\delta|}\right)$ as $t \to \infty$ (the profile becomes stretched as $t \to \infty$). The Taylor shock is decelerating in the $+x$ $(-x)$ direction as $t \to \infty$ when $-u_- < u_+ < u_-$ $(u_+ < u_- < -u_+)$, respectively. However, we observe that matching expansion (3.9) (as $z \to \infty$) to expansion (3.6) as $y \to \left(\frac{(u_+ + u_-)}{2(\delta+1)}\right)^+$ at next order fails and we require a transition region, which we label TR^+. To examine region TR^+ we introduce the scaled coordinate η by

$$y = \frac{(u_+ + u_-)}{2(\delta+1)} + \Big(\frac{2\gamma(\delta+1)}{(u_- - u_+)} \ln t + \eta\Big) t^{-(2\delta+1)}, \tag{3.16}$$

with $\eta = O(1)$ as $t \to \infty$ in region TR^+ (that is, $z = \frac{2\gamma(1+\delta)}{(u_- - u_+)} \ln t + \eta$). The $t^{-(2\delta+1)} \ln t$ shift in (3.16) is dictated by the matching requirements with regions III^+ and SS, as will be seen. The form of expansion (3.14) (for $z \gg 1$) then suggests that in region TR^+ we expand as

$$u(\eta, t) = u_+ + F(\eta) t^{-\gamma(1+\delta)} + o(t^{-\gamma(1+\delta)}) \tag{3.17}$$

as $t \to \infty$ with $\eta = O(1)$. On substituting expansion (3.17) into equation (3.1)(when equation (3.1) is written in terms of η and t) we obtain at leading order that

$$F_{\eta\eta} + \frac{(u_- - u_+)}{2} F_\eta = 0, \quad -\infty < \eta < \infty. \tag{3.18}$$

Equation (3.18) is to be solved subject to the following matching conditions with region

III$^+$ (as $\eta \to \infty$) and region SS (as $\eta \to -\infty$), namely,

$$F(\eta) \sim \begin{cases} A_R \left(\frac{2(\delta+1)}{(u_- - u_+)} \right)^\gamma & \text{as } \eta \to \infty, \\ (u_- - u_+) e^{-\phi_c} e^{-\frac{1}{2}(u_- - u_+)\eta} & \text{as } \eta \to -\infty. \end{cases} \tag{3.19}$$

The solution to (3.18), (3.19) is readily obtained as

$$F(\eta) = A_R \left(\frac{2(\delta+1)}{u_- - u_+} \right)^\gamma + (u_- - u_+)\ e^{-\phi_c}\ e^{-\frac{1}{2}(u_- - u_+)\eta}, \qquad -\infty < \eta < \infty. \tag{3.20}$$

Therefore, we have in region TR$^+$ that

$$u(\eta, t) = u_+ + \left(A_R \left(\frac{2(\delta+1)}{u_- - u_+} \right)^\gamma + (u_- - u_+)\ e^{-\phi_c}\ e^{-\frac{1}{2}(u_- - u_+)\eta} \right) t^{-\gamma(1+\delta)} + o(t^{-\gamma(1+\delta)}) \tag{3.21}$$

as $t \to \infty$ with $\eta = O(1)$. We also note that matching between region TR$^+$ and region SS, via (3.21) and (3.14), also determines that the correction term in (3.14) must be $O(t^{-\gamma(\delta+1)})$.

Finally, we conclude this case by noting that matching expansion (3.14) (as $z \to -\infty$) to expansion (3.7) $\left(y \to \left[\frac{u_+ + u_-}{2(\delta+1)} \right]^- \right)$ similarly fails at higher order and we require a corresponding transition region, which we label TR$^-$. To examine region TR$^-$ we introduce the scaled coordinate $\hat{\eta}$ by

$$y = \frac{u_+ + u_-}{2(\delta+1)} - \frac{2\gamma(\delta+1)}{u_- - u_+} \ln t\ t^{-(2\delta+1)} + \hat{\eta} t^{-(2\delta+1)} \tag{3.22}$$

so that $\hat{\eta} = O(1)$ as $t \to \infty$ in the region TR$^-$. The details of region TR$^-$ follow, after minor modification, those given for region TR$^+$ and are only summarized here for brevity.

Thus, in region TR^- we have that

$$u(\hat{\eta},t) = u_- + \left(A_L \left(\frac{2(\delta+1)}{u_- - u_+} \right)^{\gamma} - (u_- - u_+)\, e^{\phi_c}\, e^{\frac{1}{2}(u_- - u_+)\hat{\eta}} \right) t^{-\gamma(1+\delta)} + o(t^{-\gamma(1+\delta)}) \quad (3.23)$$

as $t \to \infty$ with $\hat{\eta} = O(1)$ [3].

The asymptotic structure of $\mathbf{IVP}^-$ as $t \to \infty$ when $\delta > -\frac{1}{2}$ is complete now. A uniform approximation has been given through regions $\mathrm{II}^{\pm}$, $\mathrm{III}^{\pm}$, $\mathrm{TR}^{\pm}$ and SS. A schematic representation of the location and thickness of the asymptotic structure as $t \to \infty$ is given in Figure 3.2. The fundamental attractor of the solution is a localized Taylor shock profile. Finally, the asymptotic structure to the solution of $\mathbf{IVP}^-$ when $\delta > -\frac{1}{2}$ as $t \to \infty$ can be summarized as:

Region II^+: $t = O(1)$ as $x \to \infty$

$$u(x,t) = u_+ + \frac{F_0(t)}{x^{\gamma}} + \frac{F_1(t)}{x^{(\gamma+1)}} + \frac{F_2(t)}{x^r} + \frac{F_3(t)}{x^s} + o\left(\frac{1}{x^s}\right) \text{ as } x \to \infty$$

with $t = O(1)$, with r and s given in (2.15), $F_0(t)$, $F_1(t)$, $F_2(t)$ and $F_3(t)$ given in (2.16).

Region III^+: $y = \frac{(u_+ + u_-)}{2(\delta+1)} + O(1)$ as $t \to \infty$

$$u(y,t) = u_+ + A_R \left(y - \frac{u_+}{(\delta+1)} \right)^{-\gamma} t^{-\gamma(\delta+1)} + o\left(t^{-\gamma(\delta+1)}\right)$$

as $t \to \infty$ with $y = \frac{(u_+ + u_-)}{2(\delta+1)} + O(1)$.

Region TR^+: $y = \frac{(u_+ + u_-)}{2(\delta+1)} + \frac{2\gamma(\delta+1)}{(u_- - u_+)} \ln t\; t^{-(2\delta+1)} + \eta\; t^{-(2\delta+1)}$ with $\eta = O(1)$ as $t \to \infty$

$$u(\eta,t) = u_+ + \left(A_R \left(\frac{2(\delta+1)}{(u_- - u_+)} \right)^{\gamma} + (u_- - u_+)\, e^{-\phi_c}\, e^{-\frac{1}{2}(u_- - u_+)\eta} \right) t^{-\gamma(1+\delta)} + o\left(t^{-\gamma(\delta+1)}\right)$$

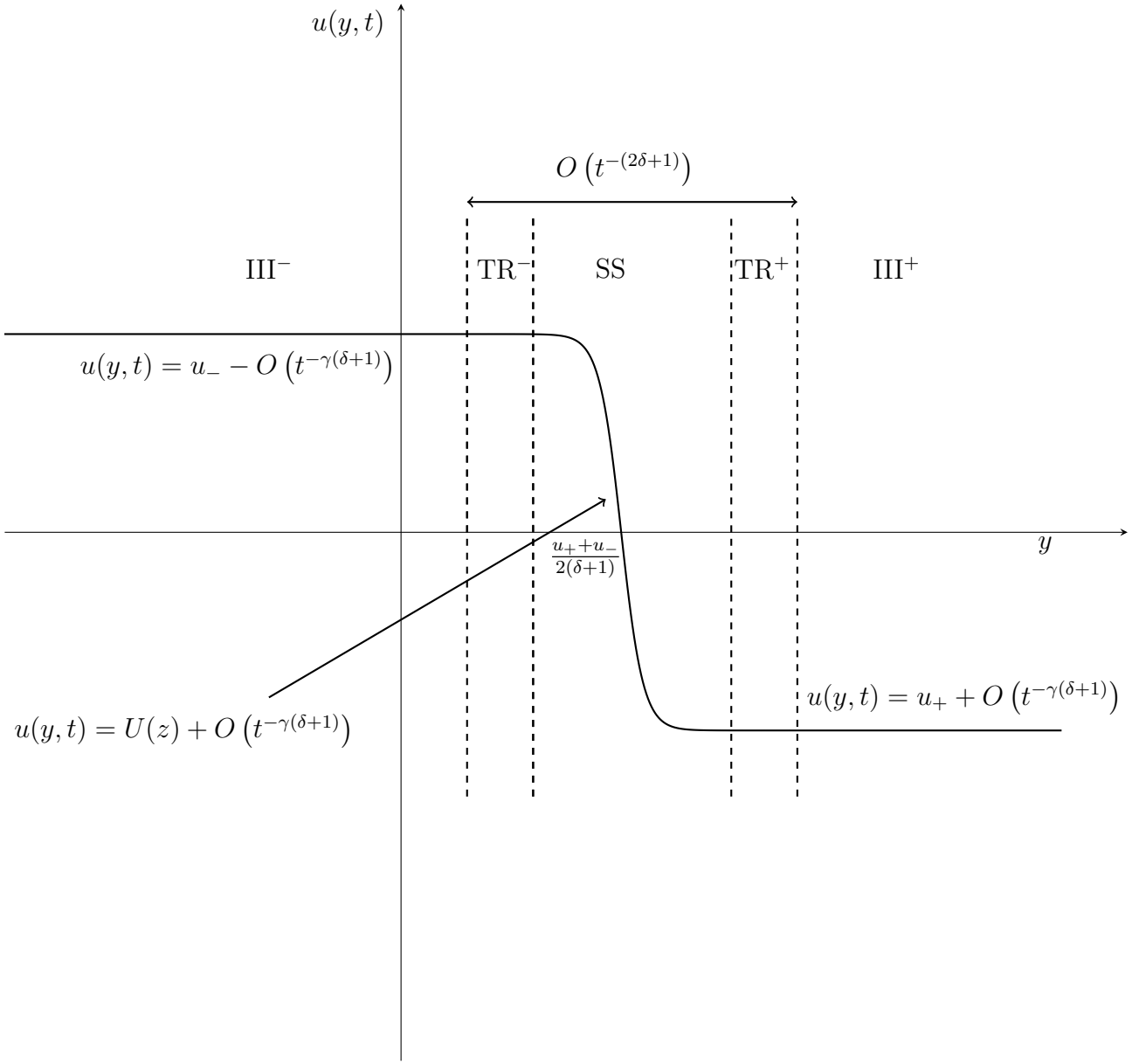

Figure 3.2: A schematic representation of the asymptotic structure of $u(y,t)$ in the (y,u) plane as $t \to \infty$ for $\mathbf{IVP}^-$. We recall that region SS is located at $y = \frac{u_+ + u_-}{2(\delta+1)}$ (with thickness $O\left(t^{-(2\delta+1)}\right)$ as $t \to \infty$), while regions TR$^\pm$ are located at $y = \frac{(u_+ + u_-)}{2(\delta+1)} \pm \frac{2\gamma(1+\delta)}{(u_- - u_+)} \frac{\ln t}{t^{2\delta+1}}$ (with thickness $O\left(t^{-(2\delta+1)}\right)$) as $t \to \infty$.

as $t \to \infty$ with $\eta = O(1)$.

Region SS: $z = \left(y - \frac{(u_+ + u_-)}{2(\delta+1)}\right) t^{(2\delta+1)}$ with $z = O(1)$ as $t \to \infty$

$$u(z,t) = \frac{1}{2}(u_+ + u_-) - \frac{1}{2}(u_- - u_+) \tanh\left(\frac{1}{4}(u_- - u_+)z + \frac{1}{2}\phi_c\right) + o(1)$$

as $t \to \infty$ with $z = O(1)$.

Region TR$^-$: $y = \frac{(u_+ + u_-)}{2(\delta+1)} - \frac{2\gamma(\delta+1)}{(u_- - u_+)} \ln t \; t^{-(2\delta+1)} + \hat{\eta} \; t^{-(2\delta+1)}$ with $\hat{\eta} = O(1)$ as $t \to \infty$

$$u(\hat{\eta}, t) = u_- + \left(A_L \left(\frac{2(\delta+1)}{(u_- - u_+)}\right)^{\gamma} - (u_- - u_+) \; e^{\phi_c} \; e^{\frac{1}{2}(u_- - u_+)\eta}\right) t^{-\gamma(1+\delta)} + o\left(t^{-\gamma(\delta+1)}\right)$$

as $t \to \infty$ with $\hat{\eta} = O(1)$.

Region III$^-$: $y = \frac{(u_+ + u_-)}{2(\delta+1)} - O(1)$ as $t \to \infty$

$$u(y,t) = u_- + A_L \left(\frac{u_-}{\delta+1} - y\right)^{-\gamma} t^{-\gamma(\delta+1)} + o\left(t^{-\gamma(\delta+1)}\right)$$

as $t \to \infty$ with $y = \frac{(u_+ + u_-)}{2(\delta+1)} - O(1)$.

Region II$^-$: $t = O(1)$ as $x \to \infty$

$$u(x,t) = u_- + \frac{F_0(t)}{(-x)^{\gamma}} + \frac{F_1(t)}{(-x)^{(\gamma+1)}} + \frac{F_2(t)}{(-x)^{r}} + \frac{F_3(t)}{(-x)^{s}} + o\left(\frac{1}{(-x)^{s}}\right) \text{ as } x \to \infty$$

with $t = O(1)$, with r and s given in (2.19), $F_0(t)$, $F_1(t)$, $F_2(t)$ and $F_3(t)$ given in (2.20).

The above asymptotic structure can be summarized in the following Proposition 2

which has been established via matched asymptotic coordinate expansions. It is first convenient to introduce the function $u_T : \mathbb{R} \to \mathbb{R}$ such that

$$u_T(\lambda) = \frac{1}{2}(u_+ + u_-) - \frac{1}{2}(u_- - u_+)\tanh\left(\frac{1}{4}(u_- - u_+)\lambda\right) \quad \forall\ \lambda \in \mathbb{R}. \tag{3.24}$$

We then have,

Proposition 2. *Let $u : \mathbb{R} \times [0, \infty) \to \mathbb{R}$ be the solution to initial-value problem* $\mathbf{IVP}^-$ *with $\delta > -\frac{1}{2}$ and $\gamma > 0$. In terms of the coordinate $y = xt^{-(\delta+1)}$, there exists a glolally determined constant ϕ, such that, on writing,*

$$u(y,t) = u_T\left(\left(y - \frac{(u_+ + u_-)}{2(\delta+1)}\right)t^{(2\delta+1)} + \phi\right) + R(y,t)$$

for $(y,t) \in \mathbb{R} \times [0,\infty)$, then $R(y,t) \to 0$ as $t \to \infty$ uniformly for $y \in \mathbb{R}$, with

$$R(y,t) = O\left(\frac{t^{-\gamma(\delta+1)}}{(1+|y|^\gamma)}\right)$$

as $t \to \infty$, uniformly for $y \in \mathbb{R}$ [3]. We remark that the globally determined constant ϕ is a consequence of the evolution over all $t \to \infty$, and as we have seen, is indeterminate through our asymptotic analysis as $t \to \infty$.

3.3.2 $\delta = -\frac{1}{2}$

The details of the asymptotic structure of solution to $\mathbf{IVP}^-$ as $t \to \infty$ when $\delta = -\frac{1}{2}$ in both cases ($0 < \gamma < 1$ and $\gamma \geq 1$) follow those those given in Sections 2.3.2.1 and 2.3.2.2 respectively. A uniform approximation has been given through regions $\mathrm{II}^\pm$, $\mathrm{III}^\pm$, $\mathrm{TR}^\pm$ and SS. The details of regions $\mathrm{II}^\pm$, $\mathrm{III}^\pm$, $\mathrm{TR}^\pm$ follow those given in Section 2.3.2.1 when $0 < \gamma < 1$ and in Section 2.3.2.2 when $\gamma \geq 1$. In The solution in region SS, where

$|x| = O\left(t^{\frac{1}{2}}\right)$ as $t \to \infty$, is given by

$$u(z,t) = u_R(z) + o(1)$$

where

$$u_R(z) \sim \begin{cases} u_+ + \mathcal{C}_+(u_+,u_-)z^{-1}e^{-\frac{1}{4}(z-2u_+)^2} & \text{as } z \to \infty, \\ u_- + \mathcal{C}_-(u_+,u_-)z^{-1}e^{-\frac{1}{4}(z-2u_-)^2} & \text{as } z \to -\infty, \end{cases}$$

with $\mathcal{C}_+$ and $\mathcal{C}_-$ globally determined nonzero constants, depending upon u_+ and u_-, with

$$\mathcal{C}_+(u_+,u_-) > 0 \qquad \text{and} \qquad \mathcal{C}_-(u_+,u_-) < 0,$$

as $t \to \infty$ with $z = O(1)$. A numerical determination of $U = u_R(z)$ for a range of values of u_+ and u_- is illustrated in Figure 3.3. The associated values of $\mathcal{C}_+$ and $\mathcal{C}_-$ are given in Table 3.2. A schematic representation of the location and thickness of the asymptotic

u_+	u_-	$\mathcal{C}_+$
-1	1	4.6×10^{-3}
0	1.4	2.4×10^{-7}
-1	0	5.3×10^{6}

u_+	u_-	$\mathcal{C}_-$
-1	1	-5×10^{10}
0	1.4	-3.4×10^{11}
-1	0	-5.4×10^{6}

Table 3.2: The values of the constants $\mathcal{C}_+$ and $\mathcal{C}_-$ corresponding to Figure 3.3.

structure as $t \to \infty$ is given in Figure 3.4 when $0 < \gamma < 1$. The large-time attractor for the solution of **IVP**$^-$ when $\delta = -\frac{1}{2}$ is the similarity solution found by Rudenko and Soluyan [32], which allows for the adjustment of the solution from u_+ to u_-. This attractor is in a stretching frame of reference of thickness $|x| = O\left(t^{\frac{1}{2}}\right)$ as $t \to \infty$.

Therefore, when $\delta = -\frac{1}{2}$ the asymptotic structure can be summarized in the following Proposition which has been established via matched asymptotic coordinate expansions.

Proposition 3. *Let $u : \mathbb{R} \times [0,\infty) \to \mathbb{R}$ be the solution to initial-value problem* **IVP** *with $\gamma > 0$, $\delta = -\frac{1}{2}$ and any u_+ and u_-. Then, in terms of the coordinate $\overline{y} = xt^{-\frac{1}{2}}$, on*

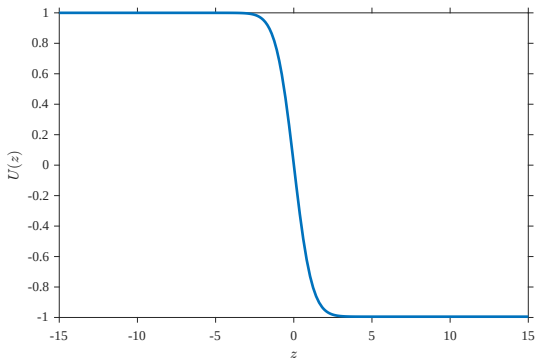

(a)

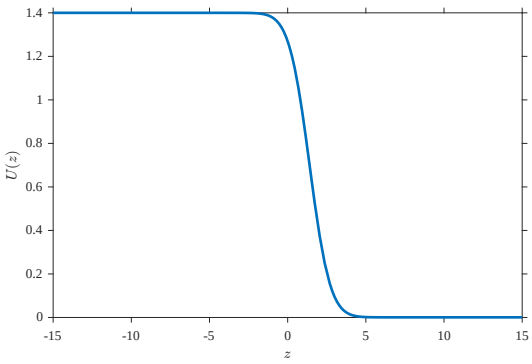

(b)

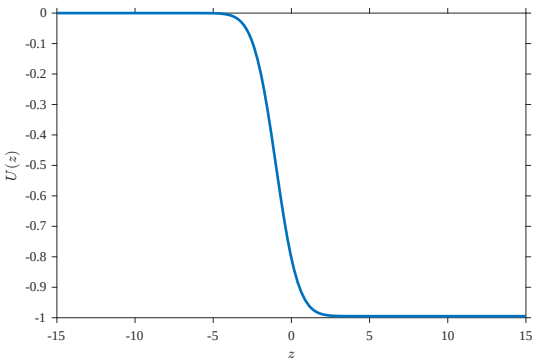

(c)

Figure 3.3: A graph of $U(z)$ when (a) $u_+ = -1$, $u_- = 1$ with $\mathcal{C}_+ = 4.6 \times 10^{-3}$ or $\mathcal{C}_- = -5 \times 10^{10}$, (b) $u_+ = 0$, $u_- = 1.4$ with $\mathcal{C}_+ = 2.4 \times 10^{-7}$ or $\mathcal{C}_- = -3.4 \times 10^{11}$ and (c) $u_+ = -1$, $u_- = 0$ with $\mathcal{C}_+ = 5.3 \times 10^{6}$ or $\mathcal{C}_- = -5.4 \times 10^{6}$.

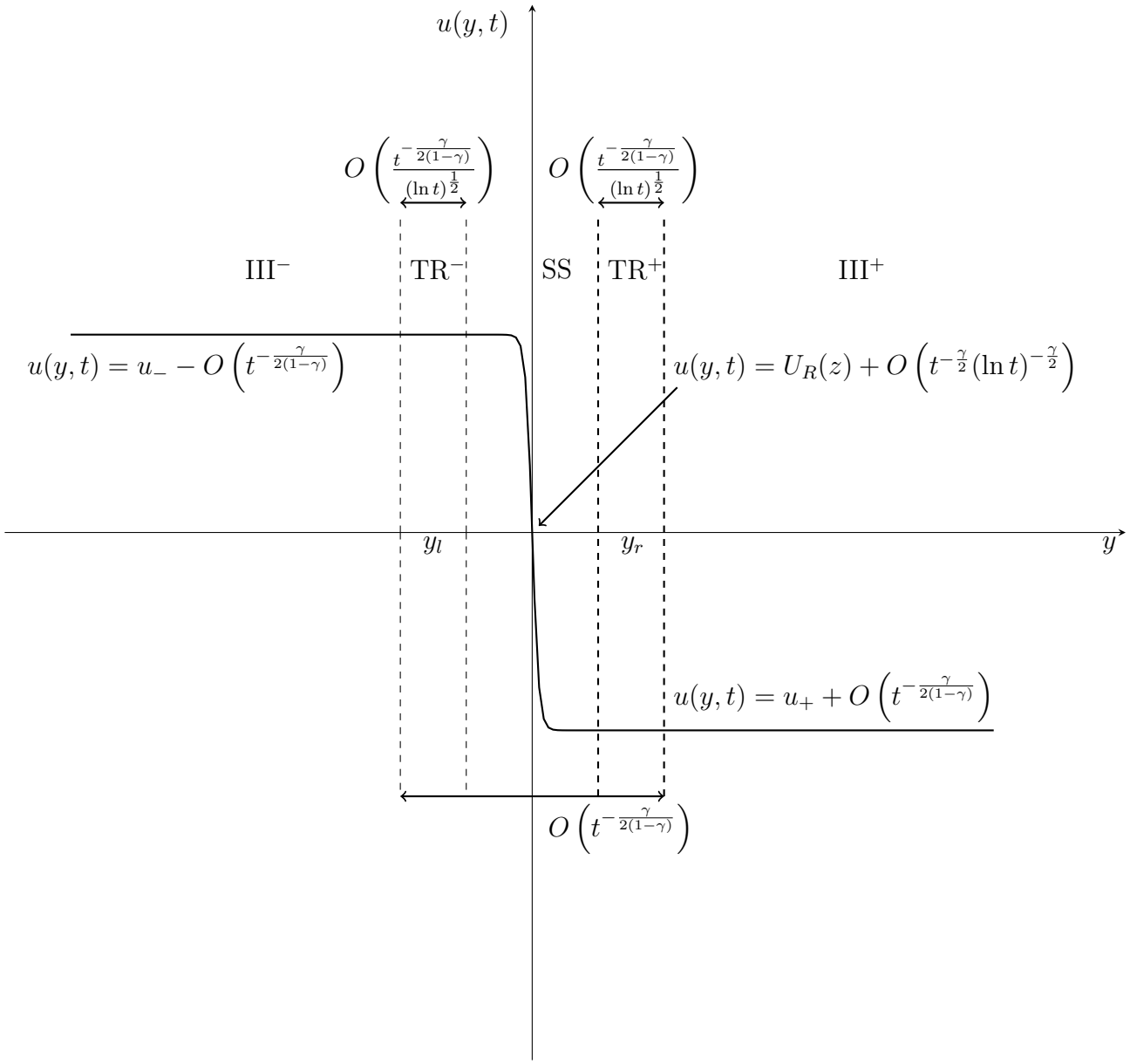

Figure 3.4: A schematic representation of the asymptotic structure of $u(y,t)$ in the (y,u) plane as $t \to \infty$ for **IVP**$^-$ when $\delta = -\frac{1}{2}$ and $0 < \gamma < 1$. We recall that $y_l = -y_r = -t^{-\frac{\gamma}{2(1-\gamma)}}\, c(t)$, where $c(t)$ is given by (2.85).

writing,

$$u(\overline{y},t) = u_R(\overline{y}) + R(\overline{y},t)$$

for $(\overline{y},t) \in \mathbb{R}\times[0,\infty)$*, it follows that* $R(\overline{y},t)\to 0$ *as* $t\to\infty$ *uniformly for* $\overline{y}\in\mathbb{R}$*. In particular, for* $0<\gamma<1$*, as* $t\to\infty$*,*

$$R(\overline{y},t) = \begin{cases} O\Big(\dfrac{t^{-\frac{\gamma}{2(1-\gamma)}}}{(1+|y|)^{\gamma}}\Big) & \textit{in regions } III^{\pm}, \\ O\Big(t^{-\frac{\gamma}{2}}(\ln t)^{-\frac{\gamma}{2}}\Big) & \textit{in regions } TR^{\pm}, \\ O\Big(t^{-\frac{\gamma}{2}}(\ln t)^{-\frac{\gamma}{2}}\Big) & \textit{in regions } SS. \end{cases}$$

where $y = \overline{y}\ t^{-\frac{\gamma}{2(1-\gamma)}}$*, while for* $\gamma\geq 1$

$$R(\overline{y},t) = \begin{cases} O\Big(\dfrac{t^{-\frac{\gamma}{2}}}{(1+|y|)^{\gamma}}\Big) & \textit{in regions } III^{\pm}, \\ O\Big(t^{-\frac{\gamma}{2}}(\ln t)^{-\frac{\gamma}{2}}\Big) & \textit{in regions } TR^{\pm}, \\ O\Big(t^{-\frac{\gamma}{2}}(\ln t)^{-\frac{\gamma}{2}}\Big) & \textit{in regions } SS. \end{cases}$$

as $t\to\infty$ [3].

3.3.3 $-1<\delta<-\frac{1}{2}$

The details of the asymptotic structure of solution to $\mathbf{IVP}^-$ as $t\to\infty$ when $-1<\delta<-\frac{1}{2}$ in both cases ($\gamma\geq 1$ and $0<\gamma<1$) follow those those given in Sections 2.3.3.1 and 2.3.3.2 respectively. A uniform approximation has been given through regions $\mathrm{II}^{\pm}$, $\mathrm{III}^{\pm}$, $\mathrm{III}(a)^{\pm}$, $\mathrm{III}(b)^{\pm}$, $\mathrm{TR}^{\pm}$ and SS. when $\gamma\geq 1$. The details of regions $\mathrm{II}^{\pm}$, $\mathrm{III}^{\pm}$, $\mathrm{TR}^{\pm}$ and SS follow those given in Section 2.3.3.1 when$\gamma\geq 1$. The details of regions $\mathrm{II}^{\pm}$, $\mathrm{III}(a)^{\pm}$, $\mathrm{III}(b)^{\pm}$, $\mathrm{TR}^{\pm}$ and SS follow those given in Section 2.3.3.2 when $0<\gamma<1$. A schematic representation of the location and thickness of the asymptotic structure as $t\to\infty$ is given in Figure 3.5 when $\gamma\geq 1$. The large-time attractor for the solution of $\mathbf{IVP}^-$ when

$-1 < \delta < -\frac{1}{2}$ is the error function, which allows for the adjustment of the solution from u_+ to u_-. This attractor is in a stretching frame of reference of thickness $|x| = O\left(t^{\frac{1}{2}}\right)$ as $t \to \infty$.

Therefore, when $-1 < \delta < -\frac{1}{2}$ the asymptotic structure can be summarized in the following Proposition which has been established via matched asymptotic coordinate expansions. It is first convenient to introduce the function $u_{\overline{R}} : \mathbb{R} \to \mathbb{R}$ such that

$$u_{\overline{R}}(\overline{y}) = \frac{(u_+ + u_-)}{2} - \frac{(u_- - u_+)}{2}\mathrm{erf}(\overline{y}) \tag{3.25}$$

We then have,

Proposition 4. *Let $u : \mathbb{R} \times [0, \infty) \to \mathbb{R}$ be the solution to initial-value problem* **IVP** *with $\gamma > 0$, $-1 < \delta < -\frac{1}{2}$ and any u_+ and u_-. Then, in terms of the coordinate $\overline{y} = xt^{-\frac{1}{2}}$, on writing,*

$$u(\overline{y}, t) = u_{\overline{R}}(\overline{y}) + R(\overline{y}, t)$$

for $(\overline{y}, t) \in \mathbb{R} \times [0, \infty)$, it follows that $R(\overline{y}, t) \to 0$ as $t \to \infty$ uniformly for $\overline{y} \in \mathbb{R}$. In particular, for $\gamma \geq 1$,

$$R(\overline{y}, t) = \begin{cases} O\left(\dfrac{t^{\gamma\delta}}{(1+|y|)^{\gamma}}\right) & \text{in regions } III^{\pm}, \\ O\left(t^{-\frac{\gamma}{2}}(\ln t)^{-\frac{\gamma}{2}}\right) & \text{in regions } TR^{\pm}, \\ O\left(t^{-\frac{\gamma}{2}}(\ln t)^{-\frac{\gamma}{2}}\right) & \text{in regions } SS, \end{cases}$$

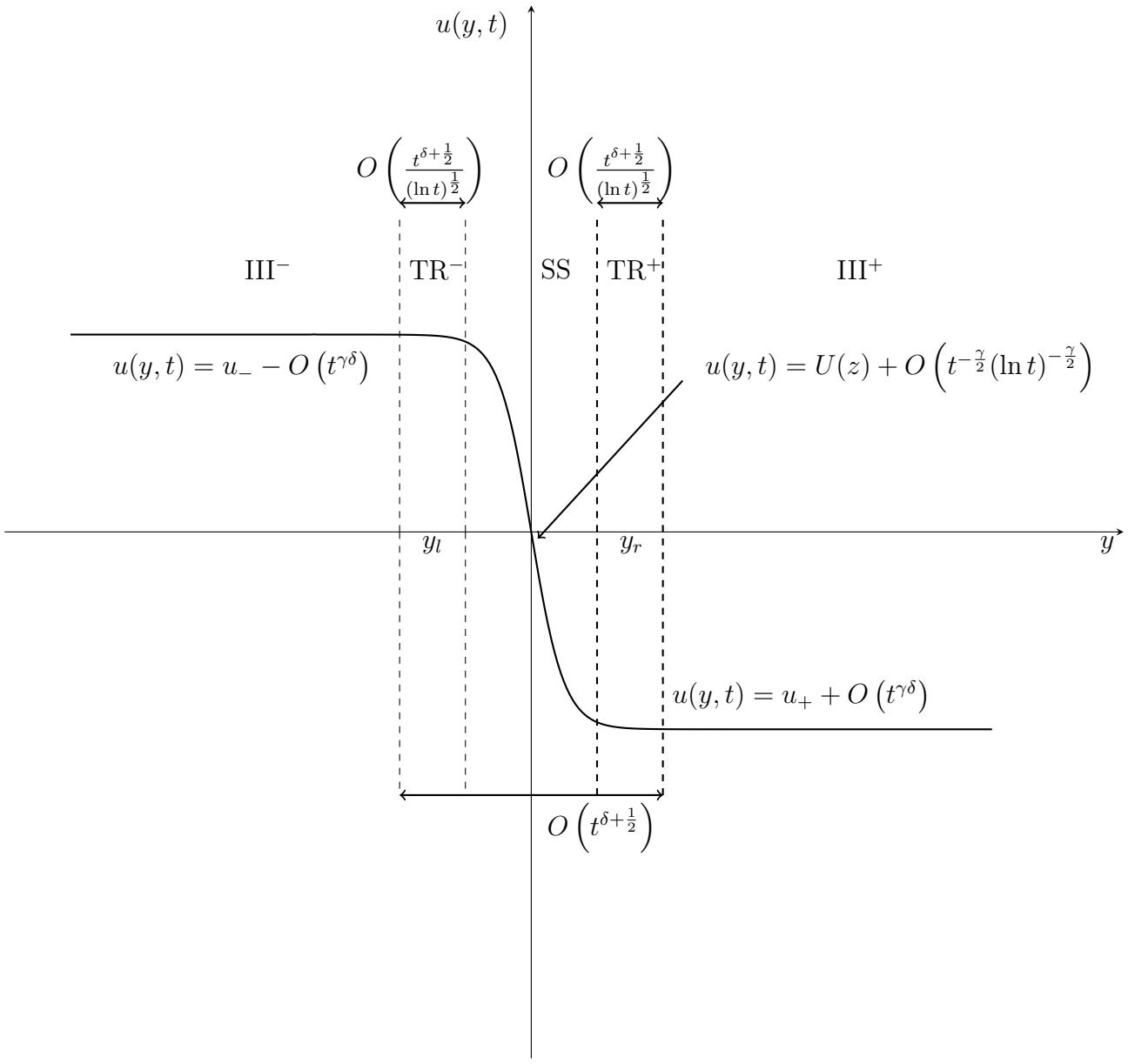

Figure 3.5: A schematic representation of the asymptotic structure of $u(y,t)$ in the (y,u) plane as $t \to \infty$ for $\mathbf{IVP}^-$ when $-1 < \delta < -\frac{1}{2}$ and $\gamma \geq 1$. We recall that $y_l = -y_r = -t^{(\delta+\frac{1}{2})}\, c(t)$, where $c(t)$ is given by (2.114).

as $t \to \infty$*, while for* $0 < \gamma < 1$*,*

$$R(\overline{y},t) = \begin{cases} O\left(\dfrac{t^{\frac{\gamma\delta}{(1-\gamma)}}}{(1+|y|)^{\gamma}}\right) & \textit{in regions III}(a)^{\pm}, \\ O\left(t^{\gamma\delta}\right) & \textit{in regions III}(b)^{\pm}, \\ O\left(t^{-\frac{\gamma}{2}}(\ln t)^{-\frac{\gamma}{2}}\right) & \textit{in regions TR}^{\pm}, \\ O\left(t^{-\frac{\gamma}{2}}(\ln t)^{-\frac{\gamma}{2}}\right) & \textit{in regions SS,} \end{cases}$$

as $t \to \infty$ [3].

3.4 Numerical Solution to the Initial-Value Problem IVP$^-$

In this section we present numerical solutions of **IVP**$^-$ which both support and illustrate the detailed asymptotic analysis given in the above Sections. The details of the numerical method outlined in [21], which follow those given in Section 2.4 for **IVP**$^+$ (Further details of the the convergence test of numerical solutions of **IVP**$^-$ are given in Appendix B.2). In particular, we consider **IVP**$^-$ with initial data $u_0 : \mathbb{R} \to \mathbb{R}$ given by,

$$u_0(x) = \begin{cases} u_+ + \dfrac{0.5\,(u_- - u_+)A_R}{1+x^{\gamma}}, & \text{as } x \geq 0, \\ u_- + \dfrac{0.5\,(u_- - u_+)A_L}{1+(-x)^{\gamma}}, & \text{as } x < 0, \end{cases}$$

where $\gamma > 0$, $A_R = 1$ and $A_L = -1$. There are three cases to consider. These are:

(i) $\delta > -\frac{1}{2}, \quad \gamma > 0,$

(ii) $\delta = -\frac{1}{2}, \quad \gamma > 0,$

(iii) $-1 < \delta < -\frac{1}{2}, \quad \gamma > 0,$

and we consider each case in turn.

3.4.1 $\delta > -\frac{1}{2}, \quad \gamma > 0$

In this case we have established in Section 3.3.1 that the Taylor shock wave develops in the solution of **IVP**$^-$ as $t \to \infty$. We now present numerical evidence to support that the solution $u(y,t)$ of **IVP**$^-$ exhibits the formation of a localized Taylor shock profile when $\delta > -\frac{1}{2}$ and $\gamma > 0$. In Figures 3.6-3.8 we plot the numerical solution of **IVP**$^-$ against y at times $t = 5,\ 10,\ 20,\ 30,\ 40$ and 50 for the cases

(i) $u_- = 1, \quad u_+ = -1,$

(ii) $u_- = 1, \quad u_+ = 0,$

(iii) $u_- = 0, \quad u_+ = -1,$

respectively. In this case, the theoretically predicted solution (3.14) is that

$$u(y,t) = \frac{1}{2}(u_+ + u_-) - \frac{1}{2}(u_- - u_+)\tanh\left(\frac{1}{4}(u_- - u_+)\left(\left(y - \frac{(u_+ + u_-)}{2(\delta+1)}\right)t^{(2\delta+1)}\right)\right).$$

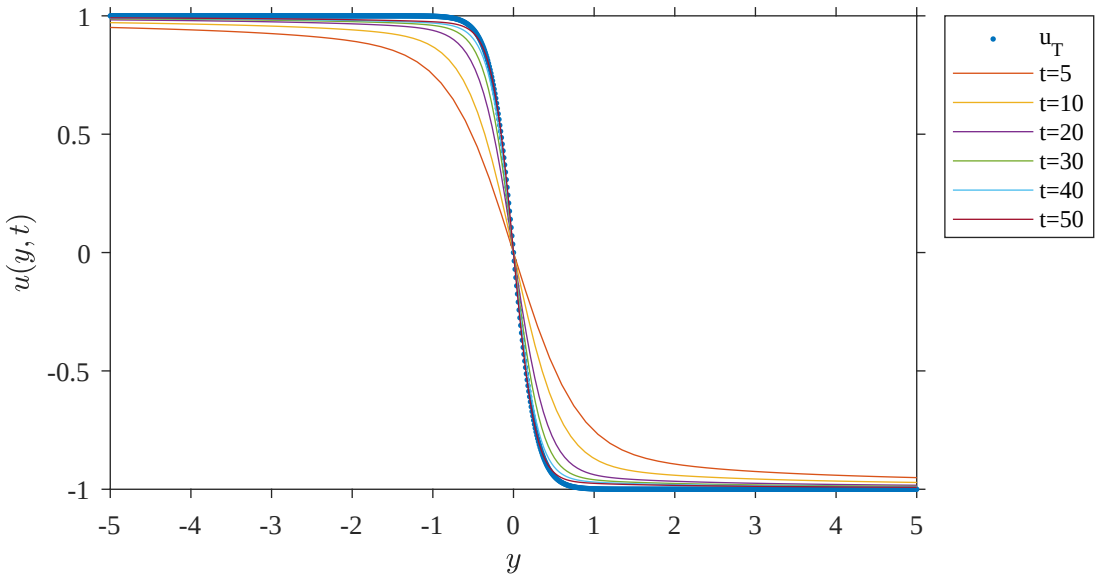

(a)

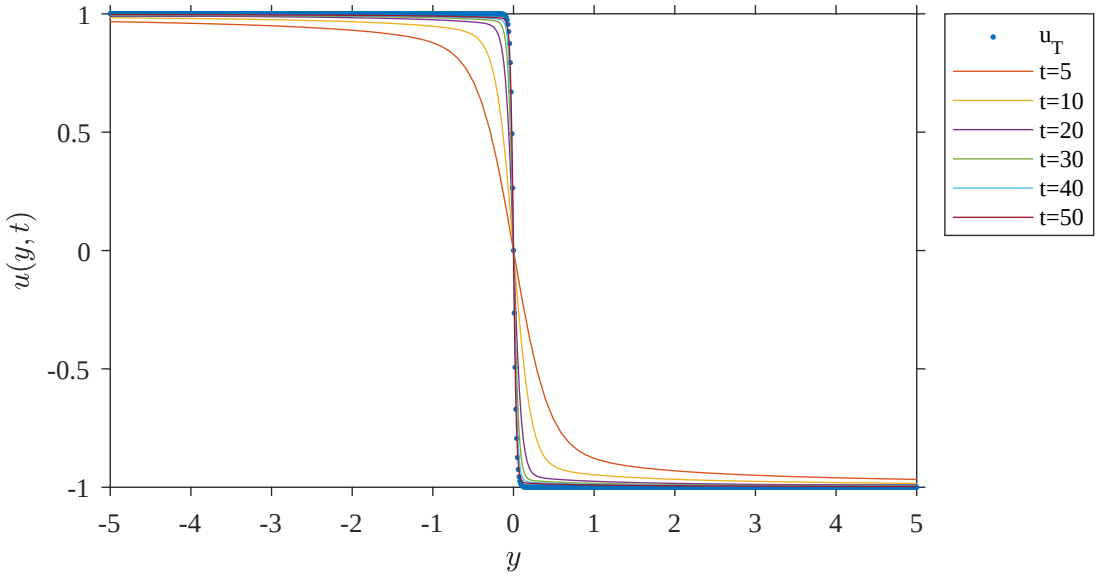

(b)

Figure 3.6: Graphs of the numerical solution of **IVP**$^-$ in the (y, u) plane when $u_+ = -1$ and $u_- = 1$ at times $t = 5,\ 10,\ 20,\ 30,\ 40$ and 50 with (a) $\delta = -0.25$, $\gamma = 1$ and (b) $\delta = 0.01$, $\gamma = 1$. We note that the dashed line represents the theoretically predicted solution u_T is given by (3.24) at $t = 50$.

In Figure 3.6 we observe that the numerically computed solution of $\mathbf{IVP}^-$ when $u_+ = 1$ and $u_- = -1$ with $\delta > -\frac{1}{2}$ in this approaches the predicted large-time attractor, the formation of a localized Taylor shock profile. This is in line with the Proposition 2 where we expect the numerical solution converges to be Taylor shock wave in y as $t \to \infty$. Specifically, at t = 50 and $\delta = 0.5$ we see that the gradient of numerical solution is in good agreement with the theoretically predicted solution u_T given by dashed line.

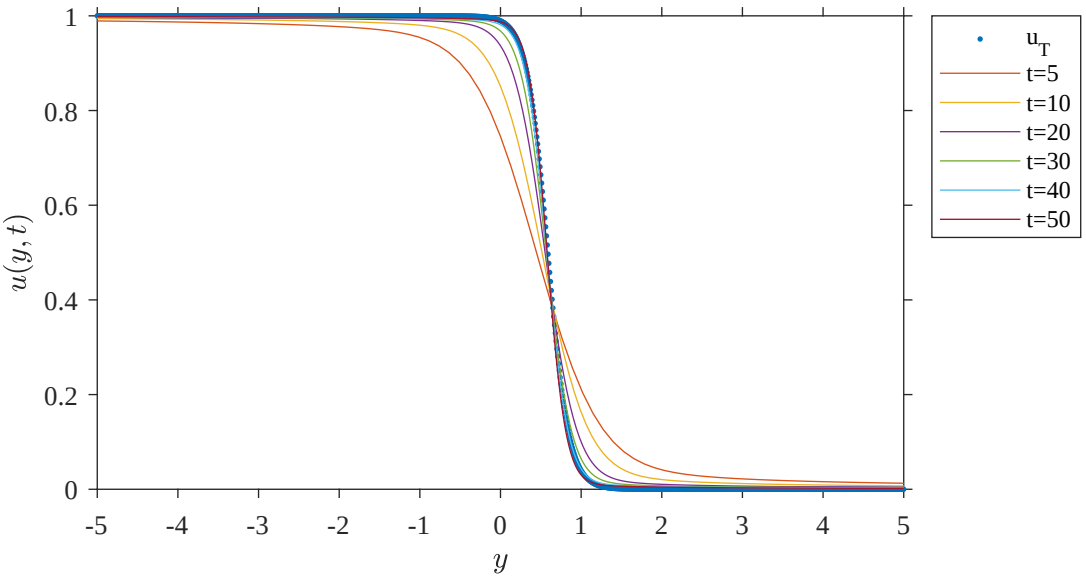

(a)

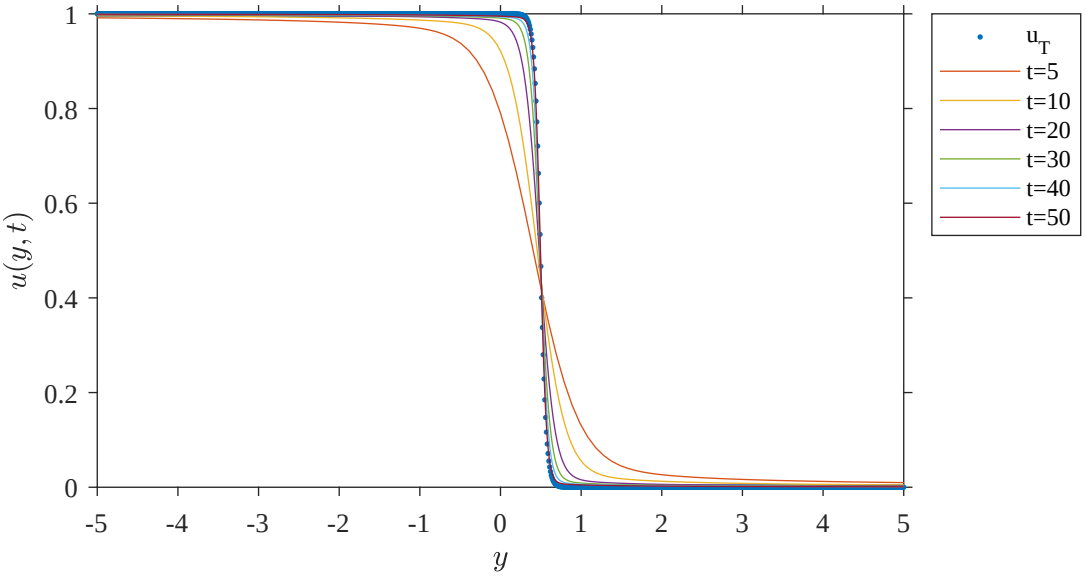

(b)

Figure 3.7: Graphs of the numerical solution of **IVP**$^-$ in the (y,u) plane when $u_+ = 0$ and $u_- = 1$ at times $t = 5,\ 10,\ 20,\ 30,\ 40$ and 50 with (a) $\delta = -0.25$, $\gamma = 1$ and (b) $\delta = 0.5$, $\gamma = 1$. We note that the dashed line represents the theoretically predicted solution u_T is given by (3.24) at $t = 50$.

In Figure 3.7 we observe that the numerically computed solution of $\mathbf{IVP}^-$ when $u_+ = 0$ and $u_- = 1$ with $\delta > -\frac{1}{2}$ in this approaches the predicted large-time attractor, the formation of a localized Taylor shock profile. This is in line with the Proposition 2 where we expect the numerical solution converges to be Taylor shock wave in y as $t \to \infty$. Specifically, at t = 50 and $\delta = 0.5$ we see that the gradient of numerical solution is in good agreement with the theoretically predicted solution u_T given by dashed line.

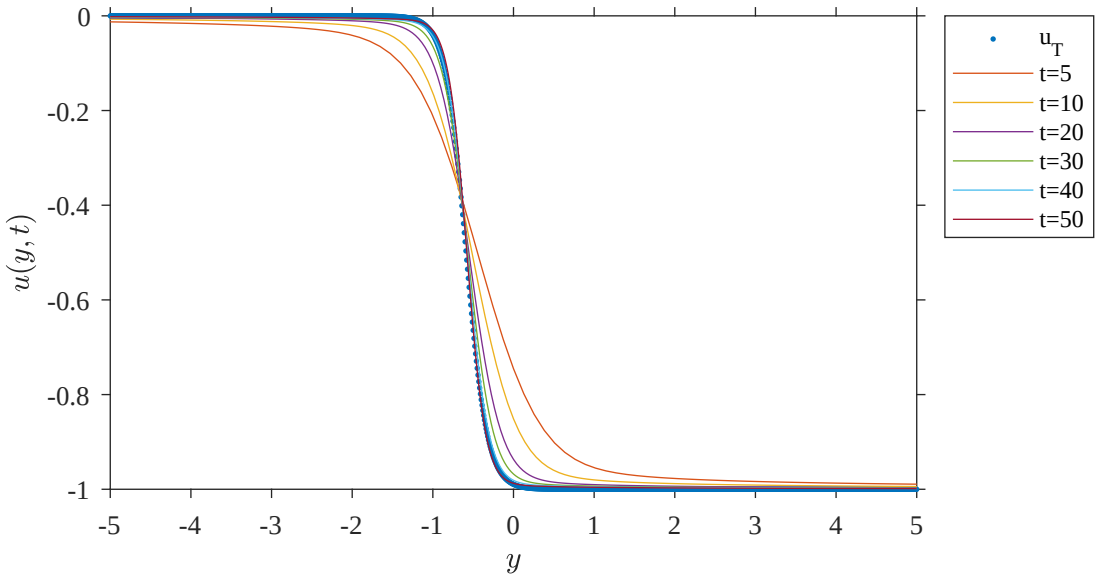

(a)

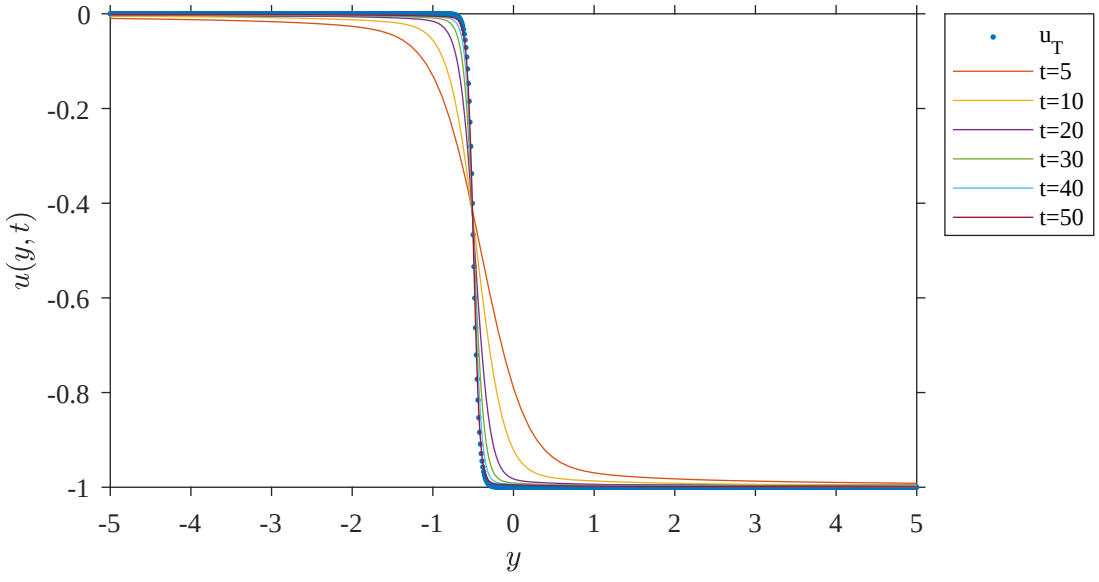

(b)

Figure 3.8: Graphs of the numerical solution of **IVP**$^-$ in the (y,u) plane when $u_+ = -1$ and $u_- = 0$ at times $t = 5,\ 10,\ 20,\ 30,\ 40$ and 50 with (a) $\delta = -0.25$, $\gamma = 1$ and (b) $\delta = 0.5$, $\gamma = 1$. We note that the dashed line represents the theoretically predicted solution u_T is given by (3.24) at $t = 50$.

In Figure 3.8 we observe that the numerically computed solution of **IVP**$^-$ when $u_+ = -1$ and $u_- = 0$ with $\delta > -\frac{1}{2}$ in this approaches the predicted large-time attractor, the formation of a localized Taylor shock profile. This is in line with the Proposition 2 where we expect the numerical solution converges to be Taylor shock wave in y as $t \to \infty$. Specifically, at t = 50 and $\delta = 0.5$ we see that the gradient of numerical solution is in good agreement with the theoretically predicted solution u_T given by dashed line.

3.4.2 $\delta = -\frac{1}{2}, \quad \gamma > 0$

In this case we have established in Section 2.3.2 that the similarity solution found by Rudenko and Soluyan [32] develops in the solution of **IVP**$^-$ as $t \to \infty$. We now present numerical evidence to support that the solution $u(y,t)$ of **IVP**$^-$ exhibits the formation of the similarity solution found by Rudenko and Soluyan when $\delta = -\frac{1}{2}$ and $\gamma > 0$. In Figures 3.9-3.11 we plot the numerical solution of **IVP**$^-$ against y at times $t = 5,\ 10,\ 20,\ 30,\ 40$ and 50 for the cases

(i) $u_+ = 1, \quad u_- = -1,$

(ii) $u_+ = 1, \quad u_- = 0,$

(iii) $u_+ = 0, \quad u_- = -1,$

respectively. In this case, the theoretically predicted solution that is

$$u_R(y) \sim \begin{cases} u_+ + \mathcal{C}_+(u_+,u_-)y^{-1}e^{-\frac{1}{4}(y-2u_+)^2} & \text{as } y \to \infty, \\ u_- + \mathcal{C}_-(u_+,u_-)y^{-1}e^{-\frac{1}{4}(y-2u_-)^2} & \text{as } y \to -\infty. \end{cases}$$

with $\mathcal{C}_+$ and $\mathcal{C}_-$ globally determined nonzero constants, where

$$\mathcal{C}_+(u_+,u_-) > 0 \qquad \text{and} \qquad \mathcal{C}_-(u_+,u_-) < 0.$$

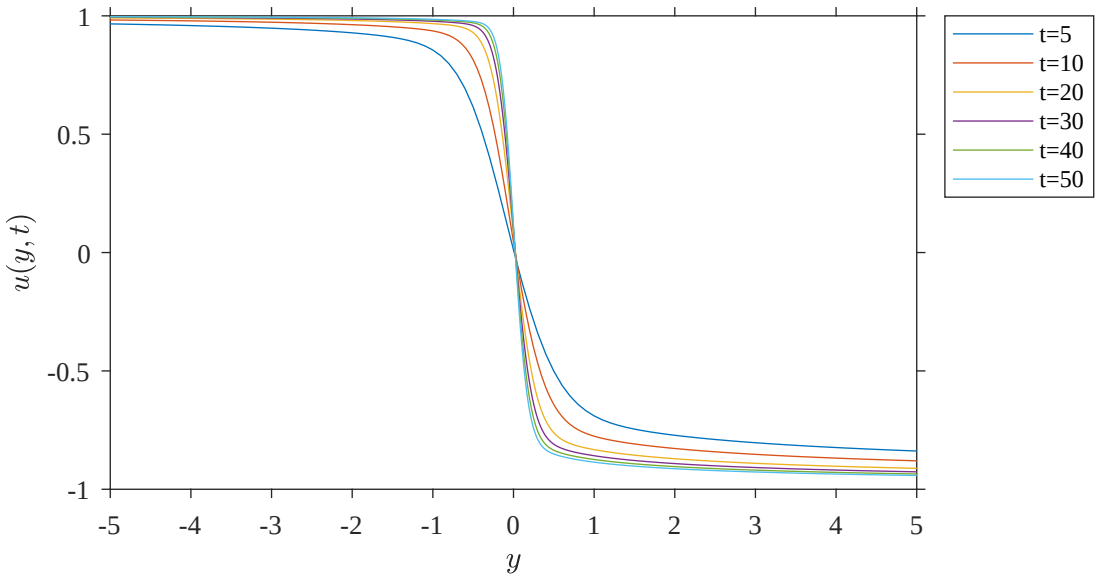

(a)

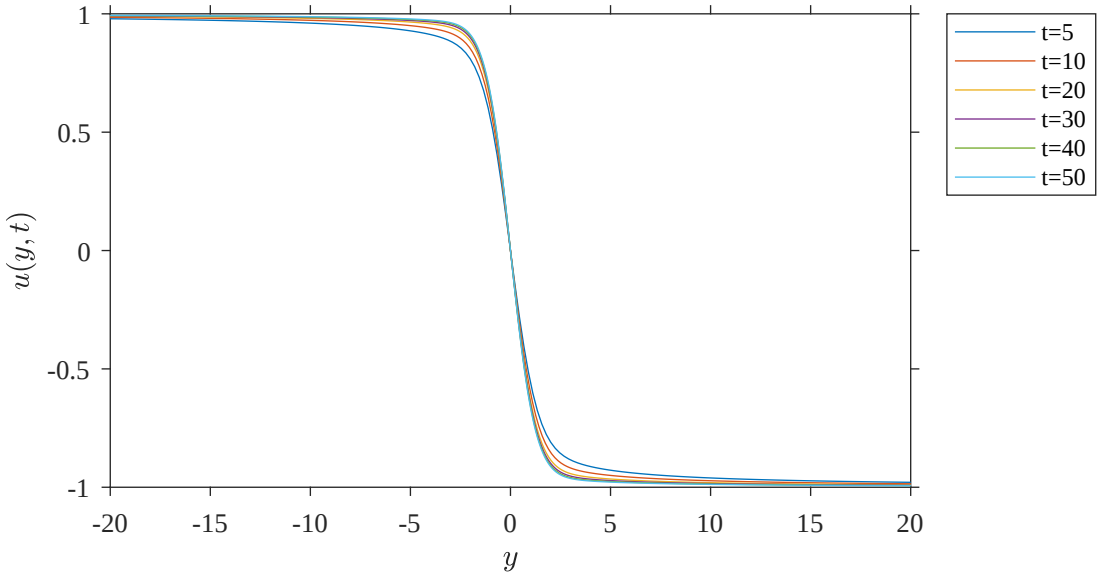

(b)

Figure 3.9: Graphs of the numerical solution of **IVP**$^-$ in the (y, u) plane when $u_+ = -1$ and $u_- = 1$ at times $t = 5,\ 10,\ 20,\ 30,\ 40$ and 50 with (a) $\delta = -0.5$, $\gamma = 0.5$ and (b)$\delta = -0.5$, $\gamma = 1$. We note that the numerically computed solutions represent the formation of the similarity solution found by Rudenko and Soluyan [32].

We observe that in Figure 3.9 the numerically computed solution of $\mathbf{IVP}^-$ when $u_+ = -1$ and $u_- = 1$ with $\delta = -\frac{1}{2}$ approaches the predicted large time attractor which is the similarity solution found by Rudenko and Soluyan [32] as $t \to \infty$. This is in line with the Proposition 3 where we expect the numerical solution converges to the similarity solution found by Rudenko and Soluyan [32] as $t \to \infty$. In fact, by $t = 50$ there is already good agreement as can be seen from Figure 3.9.

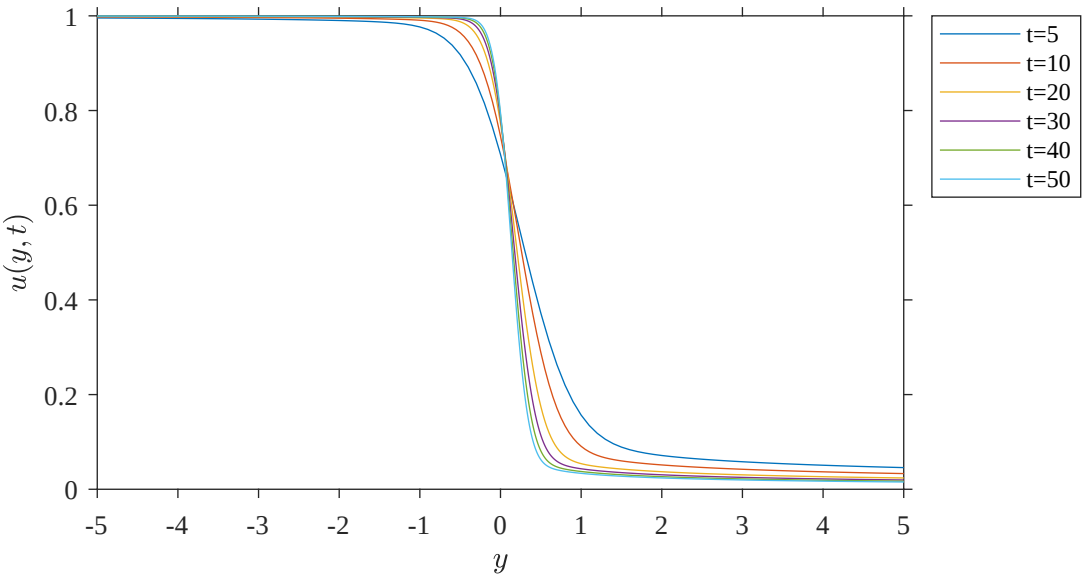

(a)

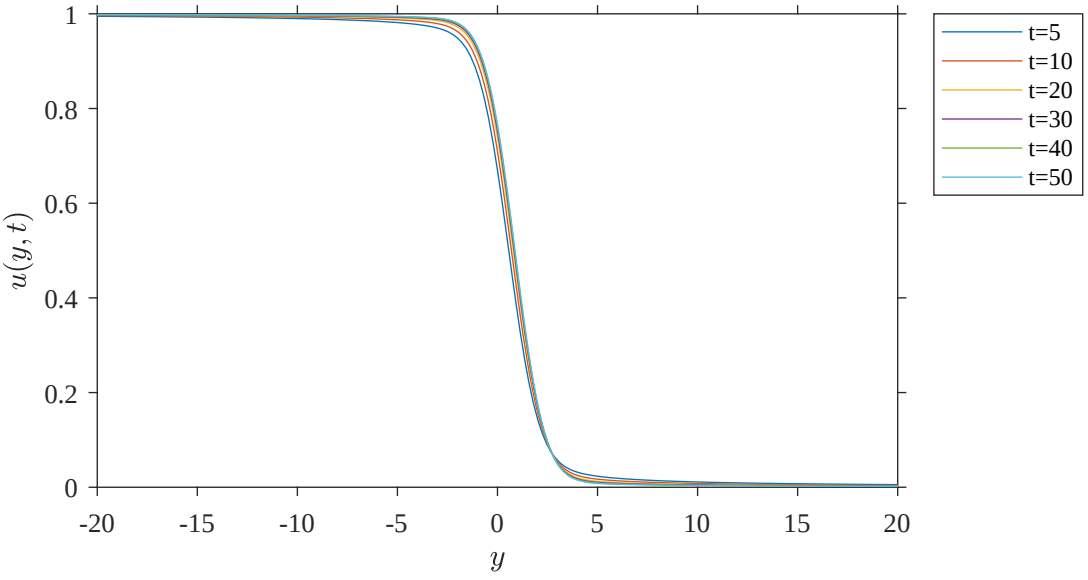

(b)

Figure 3.10: Graphs of the numerical solution of **IVP**$^-$ in the (y, u) plane when $u_+ = 0$ and $u_- = 1$ at times $t = 5,\ 10,\ 20,\ 30,\ 40$ and 50 with (a) $\delta = -0.5$, $\gamma = 0.5$ and (b) $\delta = -0.5$, $\gamma = 1$. We note that the numerically computed solutions represent the formation of the similarity solution found by Rudenko and Soluyan [32].

We observe that in Figure 3.10 the numerically computed solution of $\mathbf{IVP}^-$ when $u_+ = 0$ and $u_- = 1$ with $\delta = -\frac{1}{2}$ approaches the predicted large time attractor which is the similarity solution found by Rudenko and Soluyan [32] as $t \to \infty$. This is in line with the Proposition 3 where we expect the numerical solution converges to the similarity solution found by Rudenko and Soluyan [32] as $t \to \infty$. In fact, by $t = 50$ there is already good agreement as can be seen from Figure 3.10.

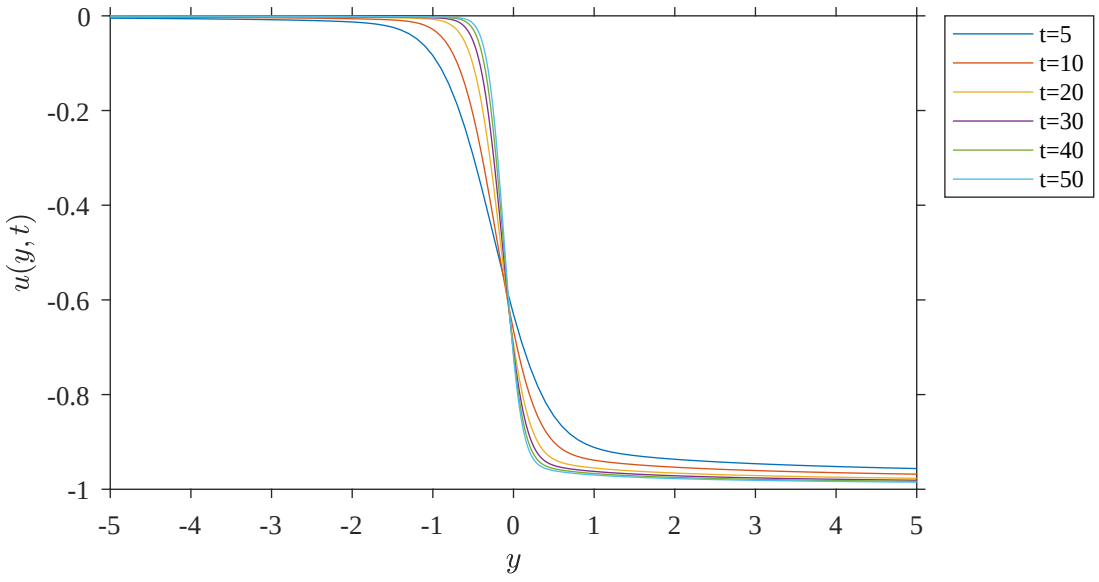

(a)

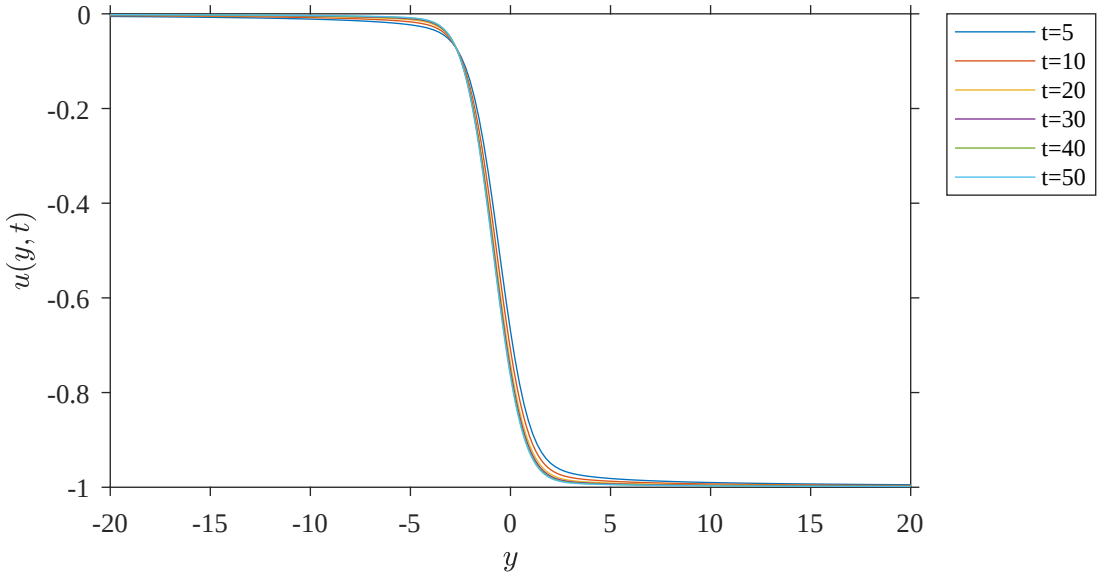

(b)

Figure 3.11: Graphs of the numerical solution of **IVP**$^-$ in the (y,u) plane when $u_+ = -1$ and $u_- = 0$ at times $t = 5,\ 10,\ 20,\ 30,\ 40$ and 50 with (a) $\delta = -0.5$, $\gamma = 0.5$ and (b)$\delta = -0.5$, $\gamma = 1$. We note that the numerically computed solutions represent the formation of the similarity solution found by Rudenko and Soluyan [32].

We observe that in Figure 3.11 the numerically computed solution of **IVP**$^-$ when $u_+ = -1$ and $u_- = 0$ with $\delta = -\frac{1}{2}$ approaches the predicted large time attractor which is the similarity solution found by Rudenko and Soluyan [32] as $t \to \infty$. This is in line with the Proposition 3 where we expect the numerical solution converges to the similarity solution found by Rudenko and Soluyan [32] as $t \to \infty$. In fact, by $t = 50$ there is already good agreement as can be seen from Figure 3.11.

3.4.3 $-1 < \delta < -\frac{1}{2}, \quad \gamma > 0$

In this case we have established in Section 3.3.3 that the error function profile develops in the solution of **IVP**$^-$ as $t \to \infty$. We now present numerical evidence to support that the solution $u(y,t)$ of **IVP**$^-$ exhibits the formation of an error function profile when $-1 < \delta < -\frac{1}{2}$ and $\gamma > 0$. In Figures 3.12-3.14 we plot the numerical solution of **IVP**$^-$ against y at times $t = 5,\ 10,\ 20,\ 30,\ 40$ and 50 for the cases

(i) $u_- = 1, \quad u_+ = -1,$

(ii) $u_- = 1, \quad u_+ = 0,$

(iii) $u_- = 0, \quad u_+ = -1,$

respectively. In this case, the theoretically predicted solution (2.109) that is

$$u_{\overline{R}}(y,t) = \frac{(u_+ + u_-)}{2} - \frac{(u_- - u_+)}{2}\text{erf}(y),\ -\infty < \overline{y} < \infty.$$

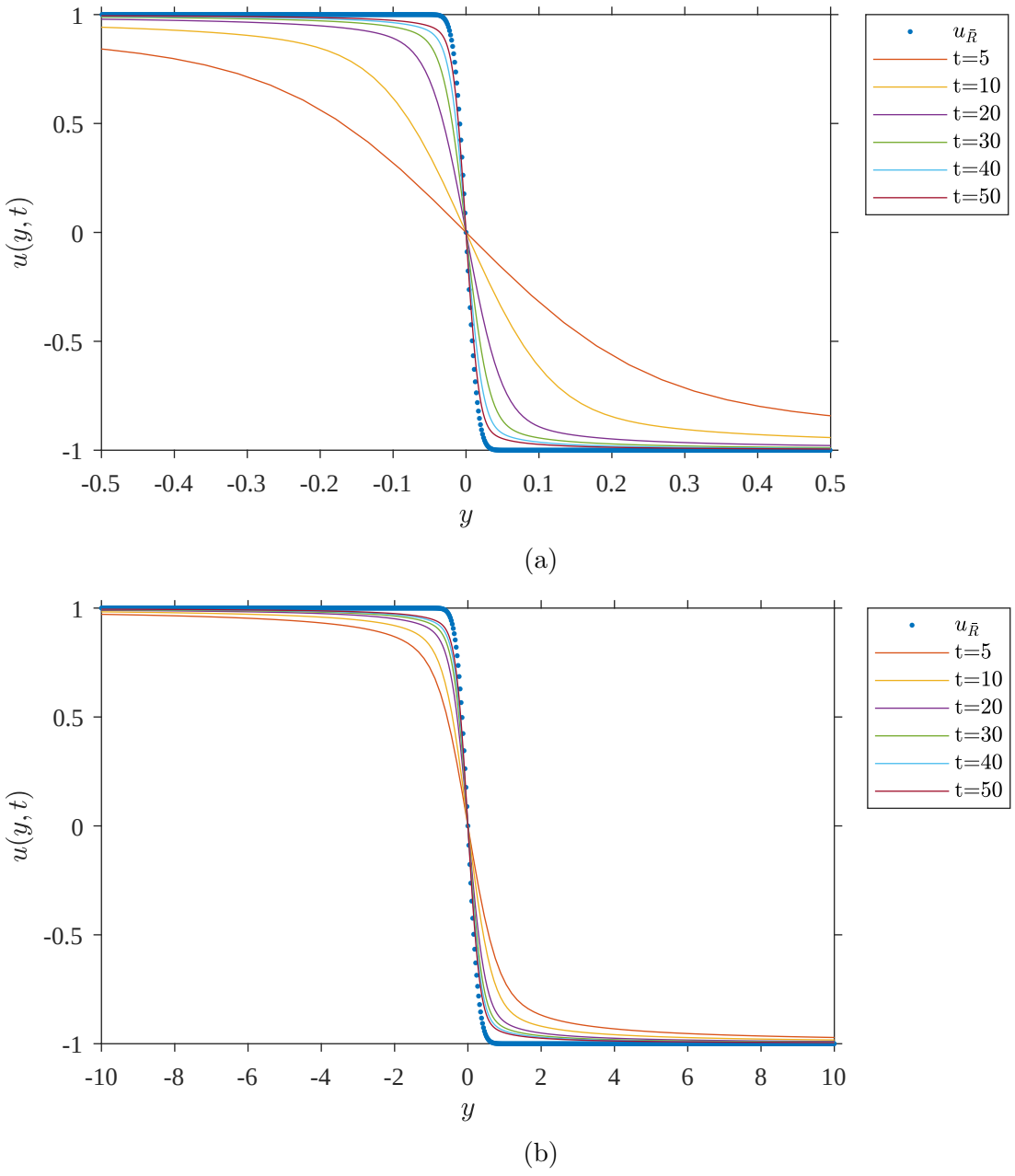

Figure 3.12: Graphs of the numerical solution of **IVP**$^-$ in the (y,u) plane when$u_+ = -1$ and $u_- = 1$ at times $t = 5,\ 10,\ 20,\ 30,\ 40$ and 50 with (a) $\delta = -0.75$, $\gamma = 0.5$ and (b) $\delta = -0.75$, $\gamma = 1$. The graphs illustrate the numerically computed solutions and the theoretically predicted solution (dashed) $u_{\overline{R}}$ at $t = 50$.

In Figure 3.12 we observe that the numerically computed solution of $\mathbf{IVP}^-$ when $u_+ = -1$ and $u_- = 1$ with $-1 < \delta < -\frac{1}{2}$ in this approaches the predicted large-time attractor, an error function profile. This is in line with the Proposition 4 where we expect the numerical solution converges to be an error function profile in y as $t \to \infty$. Specifically, at t = 50 with $\delta = -0.75$ and $\gamma = 1$ we see that the gradient of numerical solution is in good agreement with the theoretically predicted solution given by $u_{\overline{R}}$.

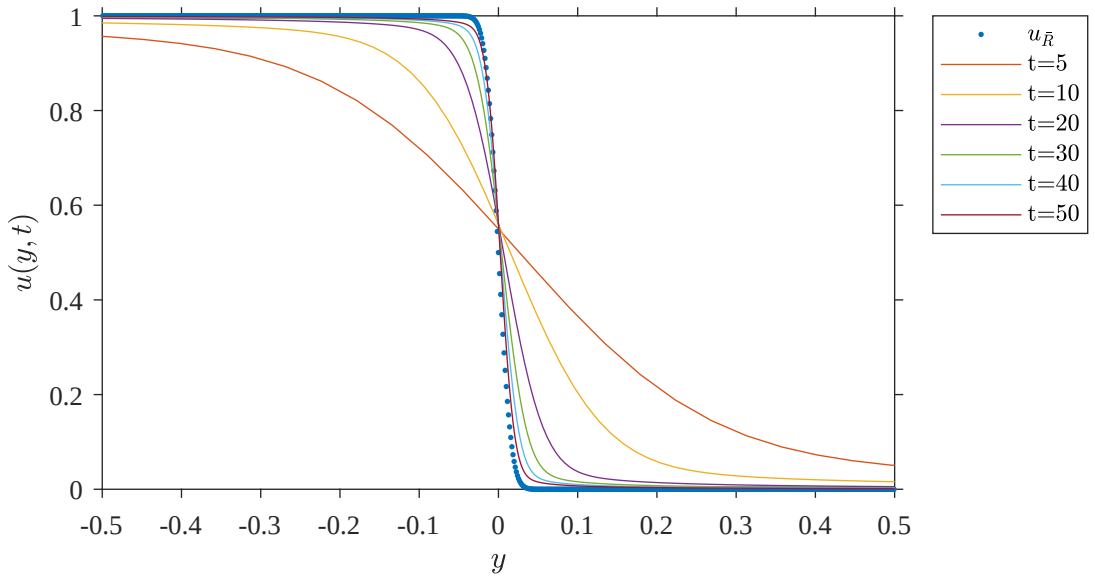

(a)

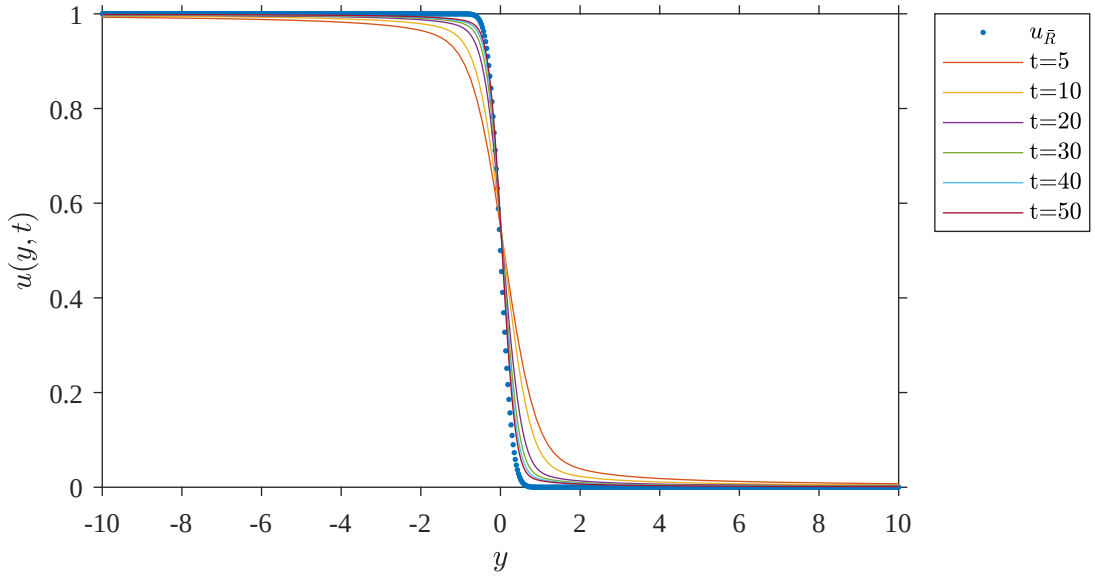

(b)

Figure 3.13: Graphs of the numerical solution of **IVP**$^-$ in the (y,u) plane when$u_+ = 0$ and $u_- = 1$ at times $t = 5,\ 10,\ 20,\ 30,\ 40$ and 50 with (a) $\delta = -0.75$, $\gamma = 0.5$ and (b) $\delta = -0.75$, $\gamma = 1$. The graphs illustrate the numerically computed solutions and the theoretically predicted solution (dashed) $u_{\overline{R}}$ at $t = 50$.

In Figure 3.13 we observe that the numerically computed solution of $\mathbf{IVP}^-$ when $u_+ = 0$ and $u_- = 1$ with $-1 < \delta < -\frac{1}{2}$ in this approaches the predicted large-time attractor, an error function profile. This is in line with the Proposition 4 where we expect the numerical solution converges to be an error function profile in y as $t \to \infty$. Specifically, at t = 50 with $\delta = -0.75$ and $\gamma = 1$ we see that the gradient of numerical solution is in good agreement with the theoretically predicted solution given by $u_{\overline{R}}$.

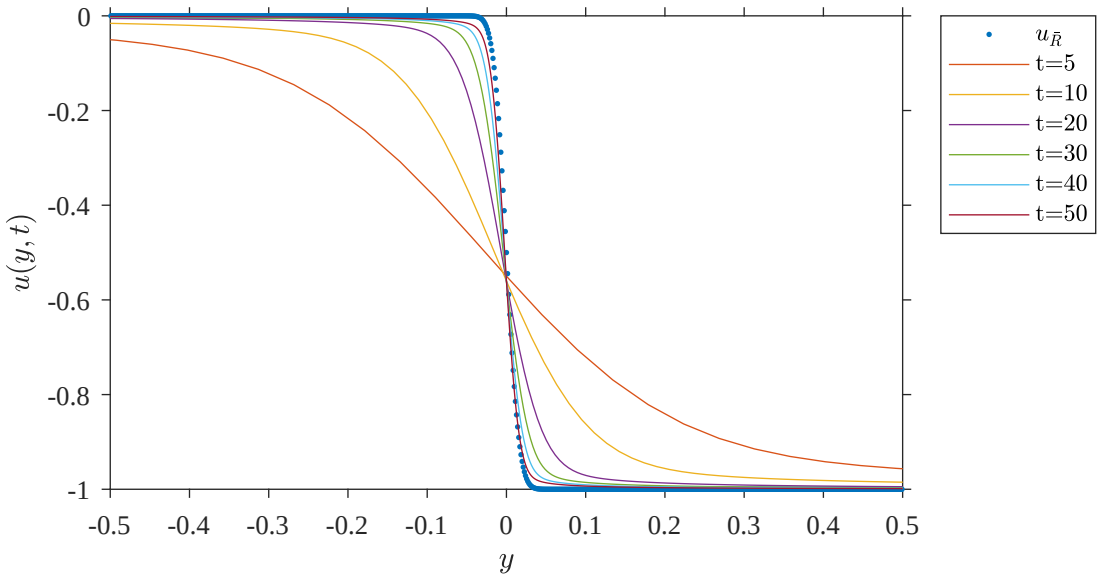

(a)

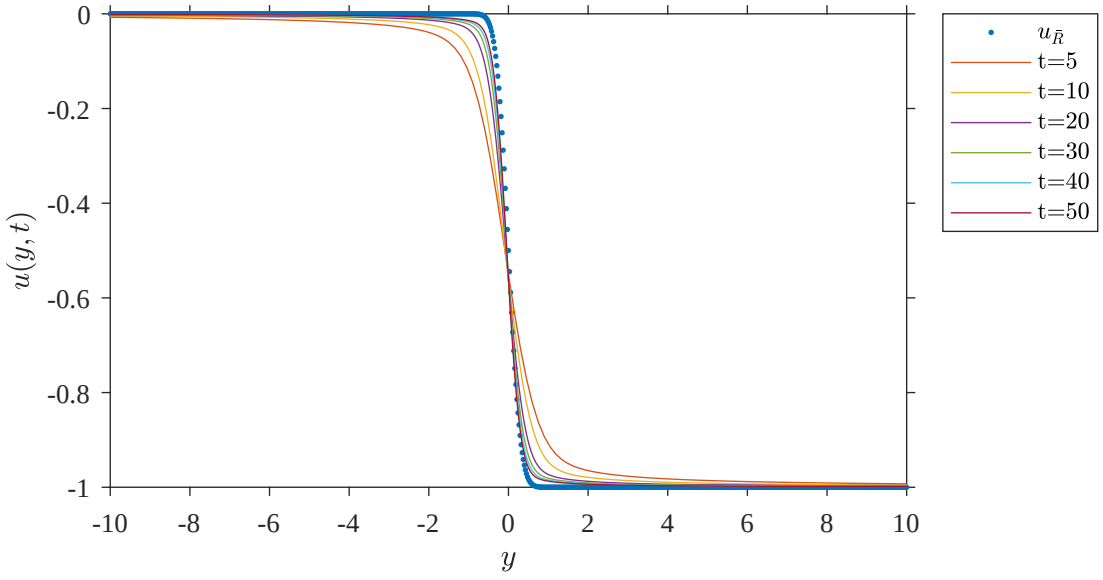

(b)

Figure 3.14: Graphs of the numerical solution of **IVP**$^-$ in the (y,u) plane when $u_+ = -1$ and $u_- = 0$ at times $t = 5,\ 10,\ 20,\ 30,\ 40$ and 50 with (a) $\delta = -0.75$, $\gamma = 0.5$ and (b) $\delta = -0.75$, $\gamma = 1$. The graphs illustrate the numerically computed solutions and the theoretically predicted solution (dashed) $u_{\overline{R}}$ at $t = 50$.

In Figure 3.14 we observe that the numerically computed solution of $\mathbf{IVP}^-$ when $u_+ = -1$ and $u_- = 0$ with $-1 < \delta < -\frac{1}{2}$ in this approaches the predicted large-time attractor, an error function profile. This is in line with the Proposition 4 where we expect the numerical solution converges to be an error function profile in y as $t \to \infty$. Specifically, at t = 50 with $\delta = -0.75$ and $\gamma = 1$ we see that the gradient of numerical solution is in good agreement with the theoretically predicted solution given by $u_{\overline{R}}$.

3.5 Summary

In this chapter we have obtained, via the method of matched asymptotic coordinate expansions, the uniform asymptotic structure of $t \to 0$, $t = O(1)$ and the large-t solution to the initial-value problem $\mathbf{IVP}^-$ $(u_- > u_+)$ over all parameter values. The form of the large-t solution to the initial-value problem $\mathbf{IVP}^-$ depends on the problem parameters δ and γ as follows:

(i) When $\delta > -\frac{1}{2}$ and $\gamma > 0$, the solution $u(x,t)$ of $\mathbf{IVP}^-$ exhibits the formation of a localized Taylor shock profile, with

$$u\left(\frac{(u_+ + u_-)}{2(1+\delta)}t^{(\delta+1)} + zt^{-\delta}, t\right) \to$$

$$\left[\frac{(u_+ + u_-)}{2} - \frac{(u_- - u_+)}{2}\tanh\left(\frac{(u_- - u_+)}{4}z + \frac{1}{2}\phi_c\right)\right]$$

as $t \to \infty$ with $z = O(1)$, and ϕ_c being a globally determined constant. It follows that the Taylor shock wavefront is at $x = s(t)$ where

$$s(t) = \frac{(u_+ + u_-)}{2(\delta+1)}t^{\delta+1} + ct^{-\delta} + o(t^{-\delta})$$

as $t \to \infty$. We note that

$$\frac{(u_+ + u_-)}{2(1+\delta)} \begin{cases} = 0 & when \quad u_+ = -u_- \quad with \quad u_- > 0 \ , \\ < 0 & when \quad u_+ < -u_- \quad with \quad u_+ < 0 \ , \\ > 0 & when \quad u_+ > -u_- \quad with \quad u_- > 0. \end{cases}$$

with c being a globally determined constant, which is a consequence of the evolution over all $t \geq 0$, and is undetermined by our asymptotic analysis as $t \to \infty$. The Taylor shock propagation speed is then

$$\dot{s}(t) = \frac{(u_+ + u_-)}{2} t^{\delta} - \delta c t^{-(\delta+1)} + o\left(t^{-(\delta+1)}\right)$$

as $t \to \infty$. We see that:

(a) $u_+ = -u_-$, the Taylor shock front is decelerating as $t \to \infty$ with $\dot{s}(t) = O\left(t^{-(\delta+1)}\right)$;

$$s(t) \to 0, \quad \text{for} \quad \delta > 0$$

and

$$s(t) \sim c t^{|\delta|}, \quad \text{for} \quad -\frac{1}{2} < \delta < 0.$$

In each case, the Taylor shock profile is contained within a region of thickness $O(t^{-\delta})$, which is a thinning region when $\delta > 0$ and a thickening region when $-\frac{1}{2} < \delta < 0$.

(b) $u_+ < -u_-$, the Taylor shock front has negative acceleration as $t \to \infty$ when $\delta > 0$ ($\dot{s}(t) \to -\infty$ as $t \to \infty$), but negative deceleration when $-\frac{1}{2} < \delta < 0$ ($\dot{s}(t) \to 0^-$ as $t \to \infty$). However, $s(t) \to -\infty$ as $t \to \infty$ for all $\delta > -\frac{1}{2}$. The region containing the Taylor shock front is of thickness $O(t^{-\delta})$ in each case.

(c) $u_+ > -u_-$, the Taylor shock front has positive acceleration as $t \to \infty$ when $\delta > 0$ ($\dot{s}(t) \to \infty$ as $t \to \infty$), but positive deceleration when $-\frac{1}{2} < \delta < 0$ ($\dot{s}(t) \to 0^+$ as $t \to \infty$). However, $s(t) \to \infty$ as $t \to \infty$ for all $\delta > -\frac{1}{2}$. Again the region containing the Taylor shock front is of thickness $O(t^{-\delta})$ in each case.

(ii) When $\delta = -\frac{1}{2}$ and $\gamma > 0$, the solution $u(x,t)$ of $\mathbf{IVP}^-$ exhibits the formation of the similarity solution found by Rudenko and Soluyan [32], with

$$u\left(zt^{\frac{1}{2}}, t\right) \to U_R(z)$$

as $t \to \infty$ with $z = O(1)$, where $U_R(z)$ is given by (2.80). We observe that this profile is in a stretching frame of reference of thickness $O\left(t^{\frac{1}{2}}\right)$ as $t \to \infty$.

(iii) When $-1 < \delta < -\frac{1}{2}$ and $\gamma > 0$, the solution $u(x,t)$ of $\mathbf{IVP}^-$ exhibits the formation of an error function profile, with

$$u\left(zt^{\frac{1}{2}}, t\right) \to \left[\frac{(u_+ + u_-)}{2} - \frac{(u_- - u_+)}{2}\ \mathrm{erf}\left(\frac{z}{2}\right)\right]$$

as $t \to \infty$, uniformly for $z = O(1)$. We observe that the error function profile is in a stretching frame of reference of thickness $O\left(t^{\frac{1}{2}}\right)$ as $t \to \infty$.

Chapter 4

Conclusion

We have now completed the detailed structural analysis of the large-time structure of the solution to initial-value problem of Burgers' equation with a time dependent coefficient. In this chapter we will present a summary of the work completed and the results obtained.

4.1 Thesis Review

In this thesis we have considered an initial-value problem for Burgers' equation with a time dependent coefficient, namely

$$u_t + t^{\delta} u u_x = u_{xx}, \quad -\infty < x < \infty, \quad t > 0, \tag{4.1}$$

$$u(x,0) = \begin{cases} u_+ + \frac{A_R}{(x)^{\gamma}} + O(E(|x|)) & \text{as } x \to \infty, \\ u_- + \frac{A_L}{(-x)^{\gamma}} + O(E(|x|)) & \text{as } x \to -\infty, \end{cases} \tag{4.2}$$

where $E(|x|)$ is linearly exponentially small in x as $|x| \to \infty$, $A_R(\neq 0)$, $A_L(\neq 0)$, $\gamma(> 0)$, u_+ and u_- $(u_+ \neq u_-)$ are constants. The method of asymptotic coordinate expansions is used to obtain the complete uniform large-t solution to the initial-value problem for Burgers' equation with a time dependent coefficient. The complete large-time solution to

the initial-value problem of Burgers' equation with a time dependent coefficient in this thesis is obtained by consideration of the small-time solution ($t \to 0, x = o(1)$) and then the large-time x solution ($|x| \to \infty, t = O(1)$). Although the solution to Burgers' equation can in certain cases (when the coefficient of uu_x in Burgers' equation is a constant) be obtained by the Cole-Hopf transformation (see Section 1.2) it provided a simple model for me to start to develop my understanding of the large-time solution of nonlinear PDEs.

In Chapter 2, we considered the case when $u_+ > u_-$ with $\delta > -\frac{1}{2}$ and $\gamma > 0$. We found that the solution $u(x,t)$ to (4.1) and (4.2) exhibits the formation of an expansion wave profile, that is

$$u(yt^{\delta+1}, t) \to \begin{cases} u_+, & y > \frac{u_+}{(\delta+1)}, \\ (\delta+1)y, & \frac{u_-}{(\delta+1)} \leq y \leq \frac{u_+}{(\delta+1)}, \\ u_-, & y < \frac{u_-}{(\delta+1)}, \end{cases} \tag{4.3}$$

as $t \to \infty$, uniformly for $y \in \mathbb{R}$. The detailed rate of convergence is given in **Proposition 1**. In Section 2.4 we present numerical solutions of (4.1)-(4.2) which confirm and support the asymptotic analysis presented in the Section 2.3.1. In Figures 2.9- 2.11 we see that the numerical simulations are in good agreement with the **Proposition 1** as $t \to \infty$. Similar patterns which corroborate the above results with different values of u_+ and u_- have been depicted in [15].

In Chapter 3, we considered the case when $u_+ < u_-$ with $\delta > -\frac{1}{2}$ and $\gamma > 0$. We found that the solution $u(x,t)$ to (4.1) and (4.2) approaches the formation of the Taylor shock profile, with

$$u\left(\frac{(u_+ + u_-)}{2(\delta+1)}t^{(\delta+1)} + zt^{-\delta}, t\right) \to \frac{1}{2}(u_+ + u_-) - \frac{1}{2}\Big(u_- - u_+\Big)\tanh\Big(\frac{1}{4}(u_- - u_+)z + \phi_c\Big) \tag{4.4}$$

as $t \to \infty$, uniformly for $y \in \mathbb{R}$. The detailed rate of convergence is given in **Proposition**

2. In Section 3.4 we present numerical solutions of (4.1)-(4.2) which confirm and support the asymptotic analysis presented in the Section 3.3.1. In Figures 3.6- 3.8 we see that the numerical simulations are in good agreement with the **Proposition 2** as $t \to \infty$. Similar patterns which corroborate the above results with different values of u_+ and u_- have been depicted in [5, 7, 15, 27].

In Chapter 2 and Chapter 3, we see that for both cases $u_+ > u_-$ and $u_- < u_+$, respectively, with $\delta = -\frac{1}{2}$ and $\gamma > 0$, the large-time solution solution $u(x,t)$ to (4.1) and (4.2) exhibits the formation of the similarity solution found by Rudenko and Soluyan [32], with

$$u\left(zt^{\frac{1}{2}}, t\right) \to \begin{cases} u_+ + \mathcal{C}_+(u_+, u_-) z^{-1} e^{-\frac{1}{4}(z-2u_+)^2} & \text{as } z \to \infty, \\ u_- + \mathcal{C}_-(u_+, u_-) z^{-1} e^{-\frac{1}{4}(z-2u_-)^2} & \text{as } z \to -\infty, \end{cases} \tag{4.5}$$

as $t \to \infty$, uniformly for $y \in \mathbb{R}$. The detailed rate of convergence is given in **Proposition 3**. In Sections 2.4 and 3.4 numerical solutions of (4.1)-(4.2) which confirm and support the asymptotic analysis presented in the Sections 2.3.2 and 3.3.2 are presented for the above cases. In Figures (2.12- 2.14) (when $u_+ > u_-$) and Figures (3.9- 3.11) (when $u_+ < u_-$) we see that the numerical simulations are in good agreement with the **Proposition 3** as $t \to \infty$.

In Chapter 2 and Chapter 3, we see that for both cases $u_+ > u_-$ and $u_- < u_+$, respectively, with $-1 < \delta < -\frac{1}{2}$ and $\gamma > 0$, the large-time solution $u(x,t)$ to (4.1) and (4.2) exhibits the formation of an the error function profile, with

$$u\left(zt^{\frac{1}{2}}, t\right) \to \left[\frac{(u_+ + u_-)}{2} - \frac{(u_- - u_+)}{2} \operatorname{erf}\left(\frac{z}{2}\right)\right] \tag{4.6}$$

as $t \to \infty$, uniformly for $y \in \mathbb{R}$. The detailed rate of convergence is given in **Proposition 4**. In Sections 2.4 and 3.4 numerical solutions of (4.1)-(4.2) which confirm and support the asymptotic analysis presented in the Sections 2.3.3 and 3.3.3 are presented for the above cases. In Figures 2.15- 2.17 (when $u_+ > u_-$) and Figures 3.12- 3.14 (when $u_+ < u_-$)

we see that the numerical simulations are in good agreement with the **Proposition 4** as $t \to \infty$. Similar patterns which corroborate the above results with different values of u_+ and u_- have been depicted in [15].

It is interesting to note that although the parameter γ plays an important role in the development and structure of the large-t solution of the initial-value problems considered in this thesis it does not appear at leading order in expansions 4.3, 4.4, 4.5 and 4.6 (which are dependent only on the constants u_+, u_- and δ).

4.2 Future Work

The theory and results developed in this thesis consider the large-time structure of the solution of Burgers' equation with time dependent coefficients when the initial data is continuously differentiable and has algebraic decay as $|x| \to \infty$. An interesting extension to this thesis would be to investigate the large-time solution of the initial-value problem for the Burgers' equation with space and time dependent coefficients when the initial data is continuously differentiable and has algebraic or exponential decay as $x \to \infty$.

Appendix A: Convergence Test of Numerical Solution to the Initial-Value Problem IVP$^+$

The following figures present the numerical solutions of **IVP**$^+$ which both support and illustrate the detailed asymptotic analysis given in the Sections 2.3.1, 2.3.2 and 2.3.3. The numerical simulations were performed using a numerical method outlined in [21] based on the method of explicit finite difference with $N = 100$ where N is the number of grid points time step $\triangle t = 0.01$ and 0.005, and the length $\triangle x = 0.5$ and 0.25. In order to ensure the reliability of our results in Section 2.4, we compare the numerical simulation of **IVP**$^+$ that presented in Section 2.4 to the numerical solutions of **IVP**$^+$ with $\triangle x = 0.5$, $\triangle t = 0.005$ and the numerical solutions of **IVP**$^+$ with $\triangle x = 0.25$, $\triangle t = 0.01$, respectively, at $t = 50$. As well as, the root mean square error have been computed between the previous cases to obtain the temporal and spatial convergence. The values of the temporal and spatial convergence are reported in Table 1, Table 2 and Table 3 for cases $\delta < -\frac{1}{2}$, $\delta = -\frac{1}{2}$ and $-1 < \delta < -\frac{1}{2}$ respectively. Based on Figure 1-9, we observe that we have similar patterns in Sections 2.4.1, 2.4.2 and 2.4.3 when $\delta < -\frac{1}{2}$, $\delta = -\frac{1}{2}$ and $-1 < \delta < -\frac{1}{2}$ respectively, which corroborate the above results in Section 2.4.

A.1.1 $\delta > -\frac{1}{2}$

(a) $u_+ = 1$ and $u_- = -1$

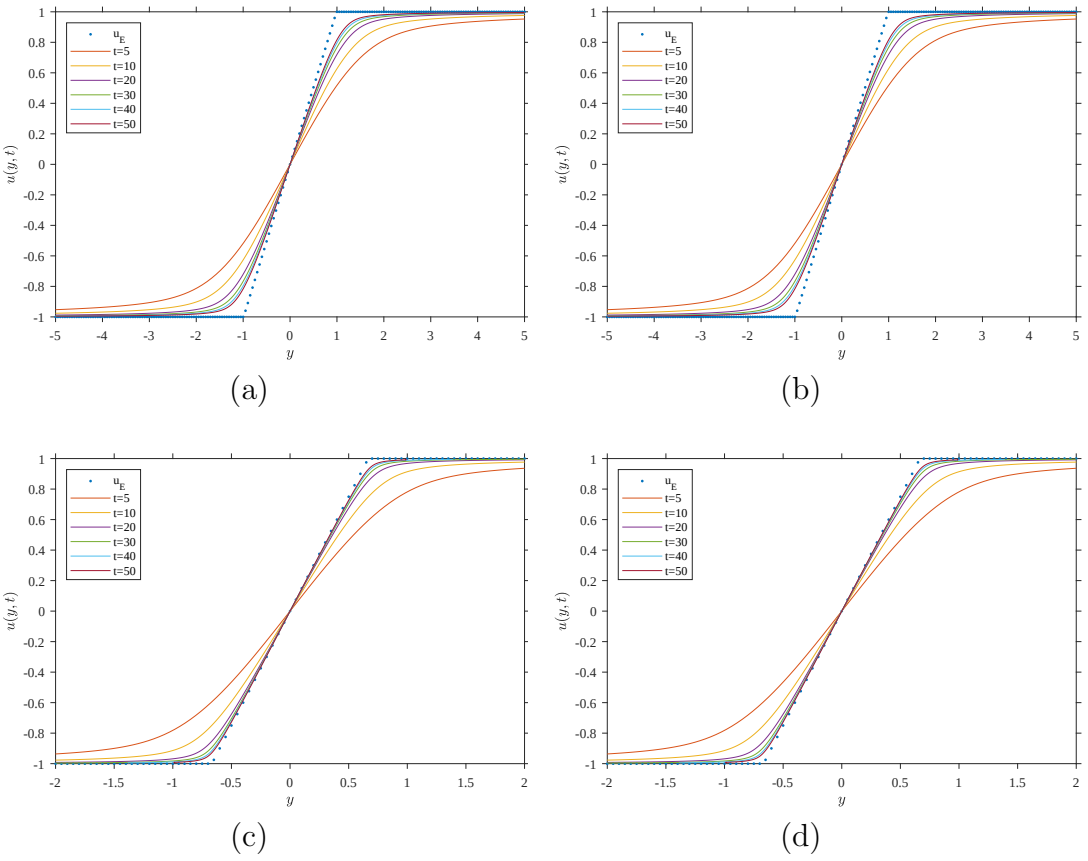

Figure 1: Graphs of the numerical solution of **IVP**$^+$ in the (y, u) plane when $u_+ = 1$ and $u_- = -1$ at times $t = 5,\ 10,\ 20,\ 30,\ 40$ and 50 with (a) $\delta = 0.01$, $\gamma = 1$, $\triangle x = 0.5$ and $\triangle t = 0.005$, (b) $\delta = 0.01$, $\gamma = 1$, $\triangle x = 0.25$ and $\triangle t = 0.01$, (c) $\delta = 0.5$, $\gamma = 1$, $\triangle x = 0.5$ and $\triangle t = 0.005$ and (d) $\delta = 0.5$, $\gamma = 1$, $\triangle x = 0.25$ and $\triangle t = 0.01$. We note that the numerically computed solutions represent the expansive wave with the solid lines and the dash line representing theoretically predicted solution u_E is given by (2.62).

(b) $u_+ = 1$ and $u_- = 0$

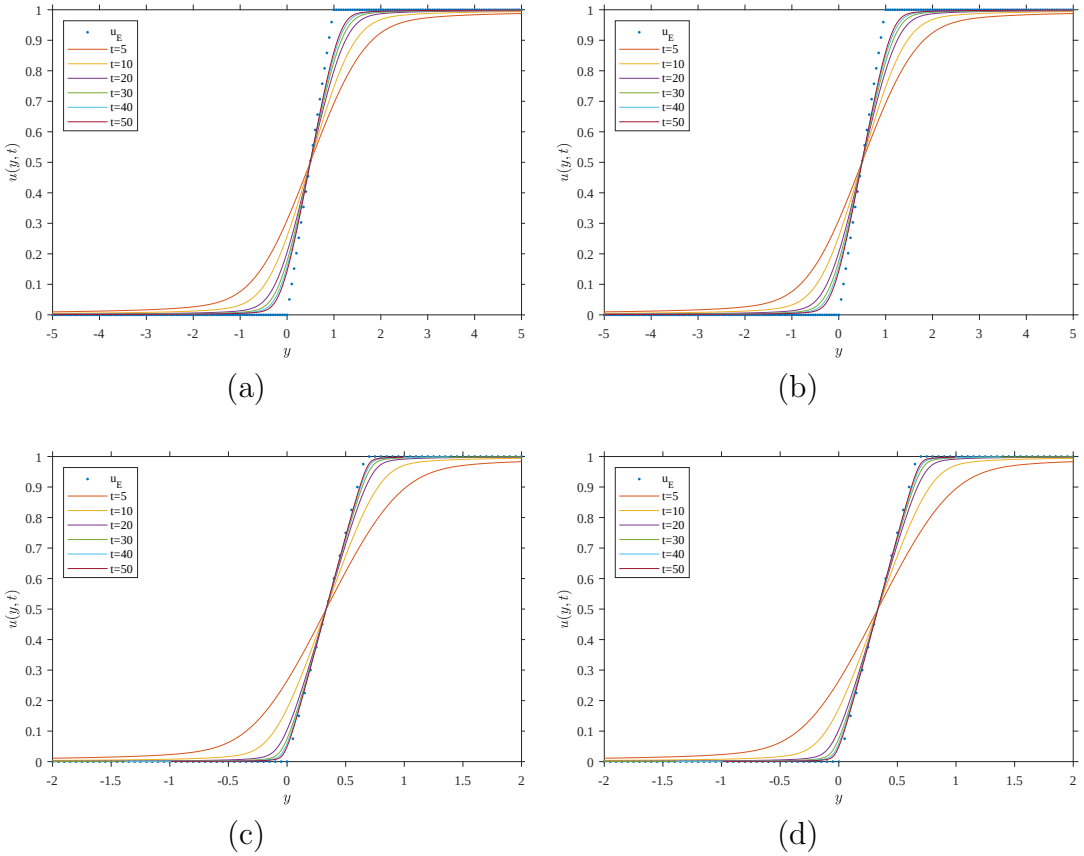

Figure 2: Graphs of the numerical solution of **IVP**$^+$ in the (y, u) plane when $u_+ = 1$ and $u_- = 0$ at times $t = 5,\ 10,\ 20,\ 30,\ 40$ and 50 with (a) $\delta = 0.01$, $\gamma = 1$, $\triangle x = 0.5$ and $\triangle t = 0.005$, (b) $\delta = 0.01$, $\gamma = 1$, $\triangle x = 0.25$ and $\triangle t = 0.01$, (c) $\delta = 0.5$, $\gamma = 1$, $\triangle x = 0.5$ and $\triangle t = 0.005$ and (d) $\delta = 0.5$, $\gamma = 1$, $\triangle x = 0.25$ and $\triangle t = 0.01$. We note that the numerically computed solutions represent the expansive wave with the solid lines and the dash line representing theoretically predicted solution u_E is given by (2.62).

(c) $u_+ = 0$ and $u_- = -1$

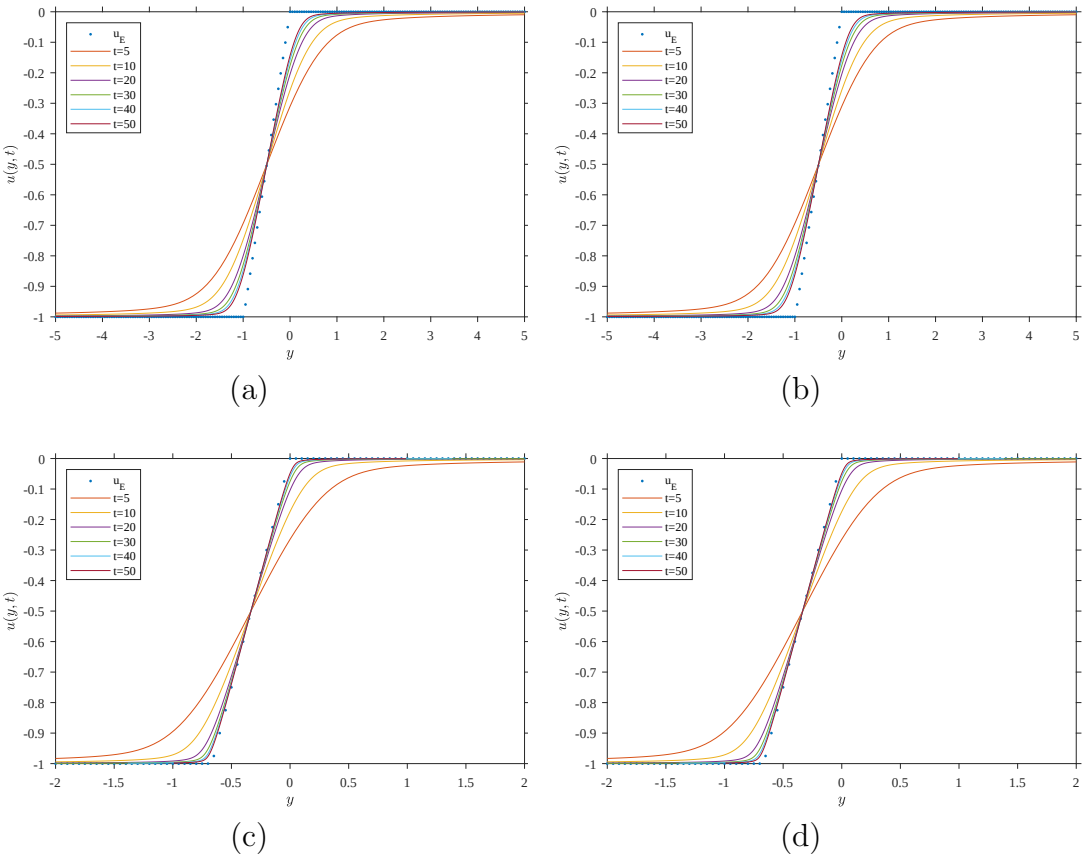

Figure 3: Graphs of the numerical solution of **IVP**$^+$ in the (y, u) plane when $u_+ = 0$ and $u_- = -1$ at times $t = 5,\ 10,\ 20,\ 30,\ 40$ and 50 with (a) $\delta = 0.01$, $\gamma = 1$, $\triangle x = 0.5$ and $\triangle t = 0.005$, (b) $\delta = 0.01$, $\gamma = 1$, $\triangle x = 0.25$ and $\triangle t = 0.01$, (c) $\delta = 0.5$, $\gamma = 1$, $\triangle x = 0.5$ and $\triangle t = 0.005$ and (d) $\delta = 0.5$, $\gamma = 1$, $\triangle x = 0.25$ and $\triangle t = 0.01$. We note that the numerically computed solutions represent the expansive wave with the solid lines and the dash line representing theoretically predicted solution u_E is given by (2.62).

		Temporal convergence	Spatial convergence
	$\gamma = 1$	$\triangle x = 0.5$ and $\triangle t = 0.005$	$\triangle x = 0.25$ and $\triangle t = 0.01$
	$u_+ = 1$ and $u_- = -1$	1.17×10^{-5}	7.74×10^{-5}
$\delta = 0.01$	$u_+ = 1$ and $u_- = 0$	9.04×10^{-6}	5.28×10^{-5}
	$u_+ = 0$ and $u_- = -1$	9.04×10^{-6}	5.28×10^{-5}
	$u_+ = 1$ and $u_- = -1$	6.12×10^{-5}	1.63×10^{-5}
$\delta = 0.5$	$u_+ = 1$ and $u_- = 0$	5.61×10^{-5}	1.17×10^{-5}
	$u_+ = 0$ and $u_- = -0$	5.61×10^{-5}	1.17×10^{-5}

Table 1: Numerical convergence test between the numerical solutions of $\mathbf{IVP}^+$ with $\triangle x = 0.5$, $\triangle t = 0.01$, the numerical solutions of $\mathbf{IVP}^+$ with $\triangle x = 0.5$, $\triangle t = 0.005$ and the numerical solutions of $\mathbf{IVP}^+$ with $\triangle x = 0.25$, $\triangle t = 0.01$, respectively, when $\delta > -\frac{1}{2}$ and $\gamma = 1$ at $t = 50$. Values quoted are root mean square error on holding time and space steps respectively.

A.1.2 $\delta = -\frac{1}{2}$

(a) $u_+ = 1$ and $u_- = -1$

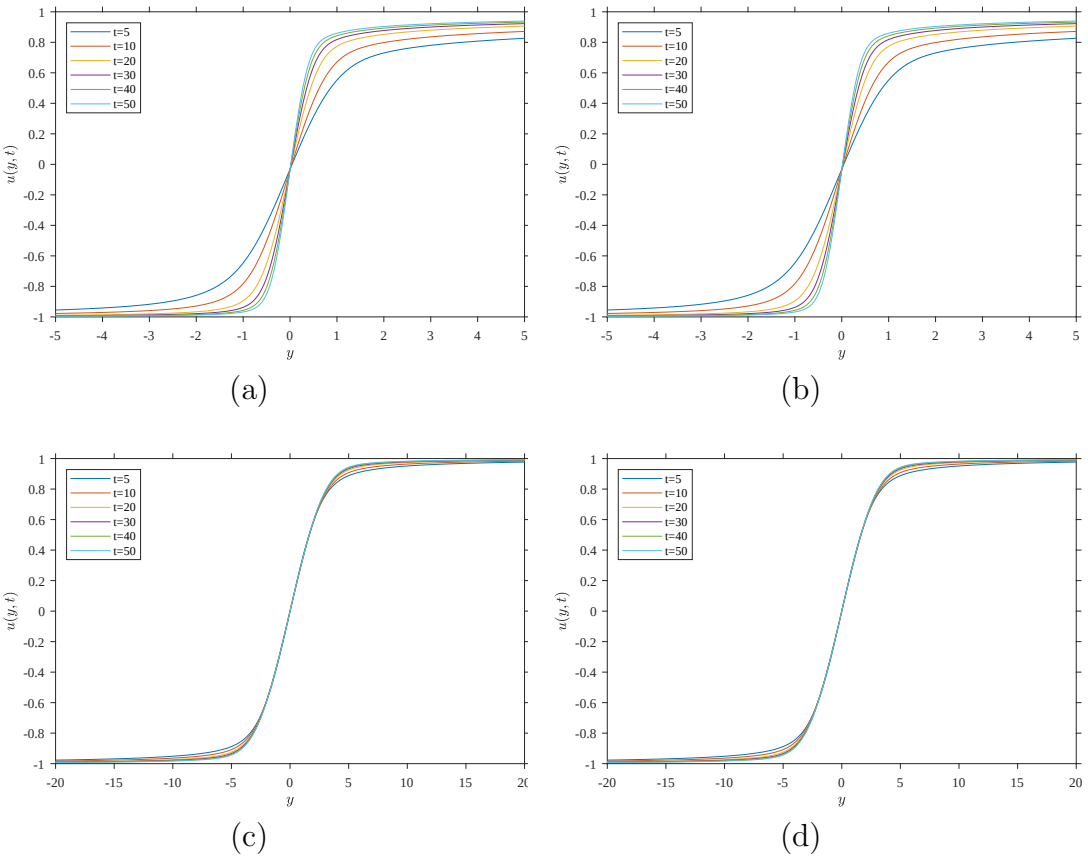

Figure 4: Graphs of the numerical solution of **IVP**$^+$ in the (y, u) plane when $u_+ = 1$ and $u_- = -1$ at times $t = 5,\ 10,\ 20,\ 30,\ 40$ and 50 with (a) $\delta = -0.5$, $\gamma = 0.5$, $\triangle x = 0.5$ and $\triangle t = 0.005$, (b) $\delta = -0.5$, $\gamma = 0.5$, $\triangle x = 0.25$ and $\triangle t = 0.01$, (c) $\delta = -0.5$, $\gamma = 1$, $\triangle x = 0.5$ and $\triangle t = 0.005$ and (d) $\delta = -0.5$, $\gamma = 1$, $\triangle x = 0.25$ and $\triangle t = 0.01$. We note that the numerically computed solutions represent the formation of the similarity solution found by Rudenko and Soluyan [32].

(b) $u_+ = 1$ and $u_- = 0$

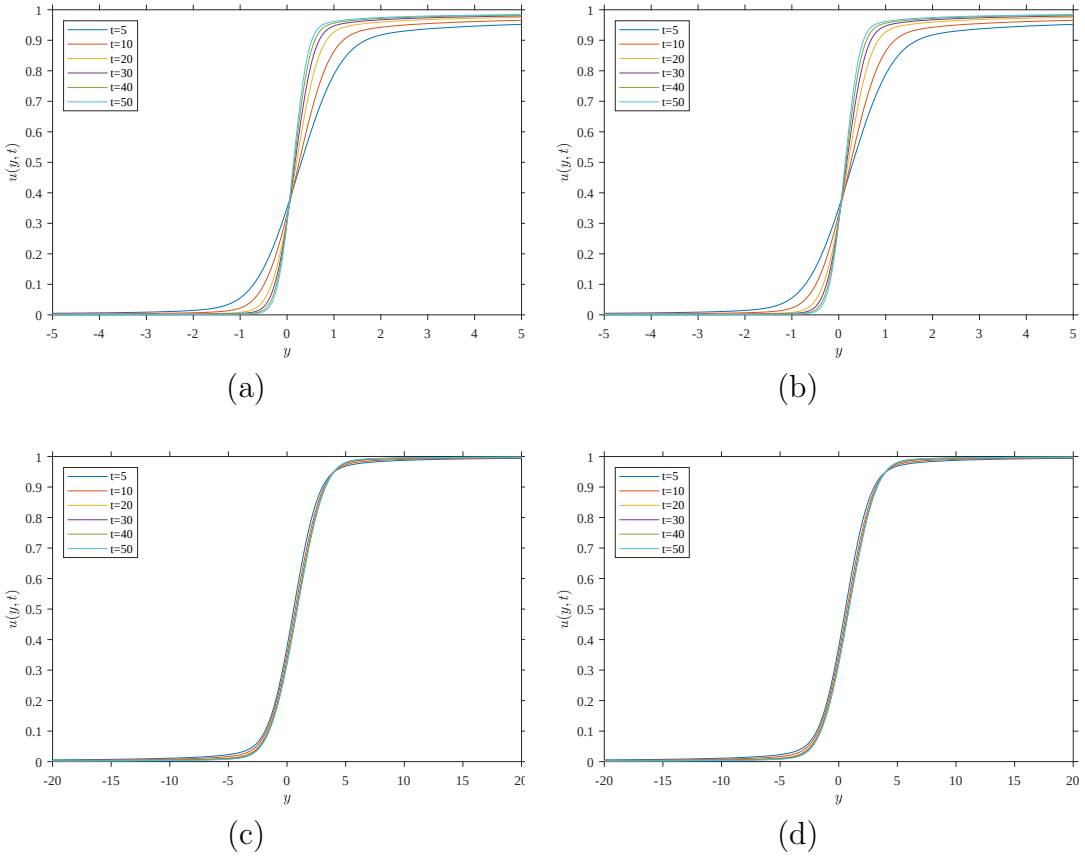

Figure 5: Graphs of the numerical solution of **IVP**$^+$ in the (y, u) plane when $u_+ = 1$ and $u_- = 0$ at times $t = 5,\ 10,\ 20,\ 30,\ 40$ and 50 with (a) $\delta = -0.5$, $\gamma = 0.5$, $\triangle x = 0.5$ and $\triangle t = 0.005$, (b) $\delta = -0.5$, $\gamma = 0.5$, $\triangle x = 0.25$ and $\triangle t = 0.01$, (c) $\delta = -0.5$, $\gamma = 1$, $\triangle x = 0.5$ and $\triangle t = 0.005$ and (d) $\delta = -0.5$, $\gamma = 1$, $\triangle x = 0.25$ and $\triangle t = 0.01$. We note that the numerically computed solutions represent the formation of the similarity solution found by Rudenko and Soluyan [32].

(c) $u_+ = 0$ and $u_- = -1$

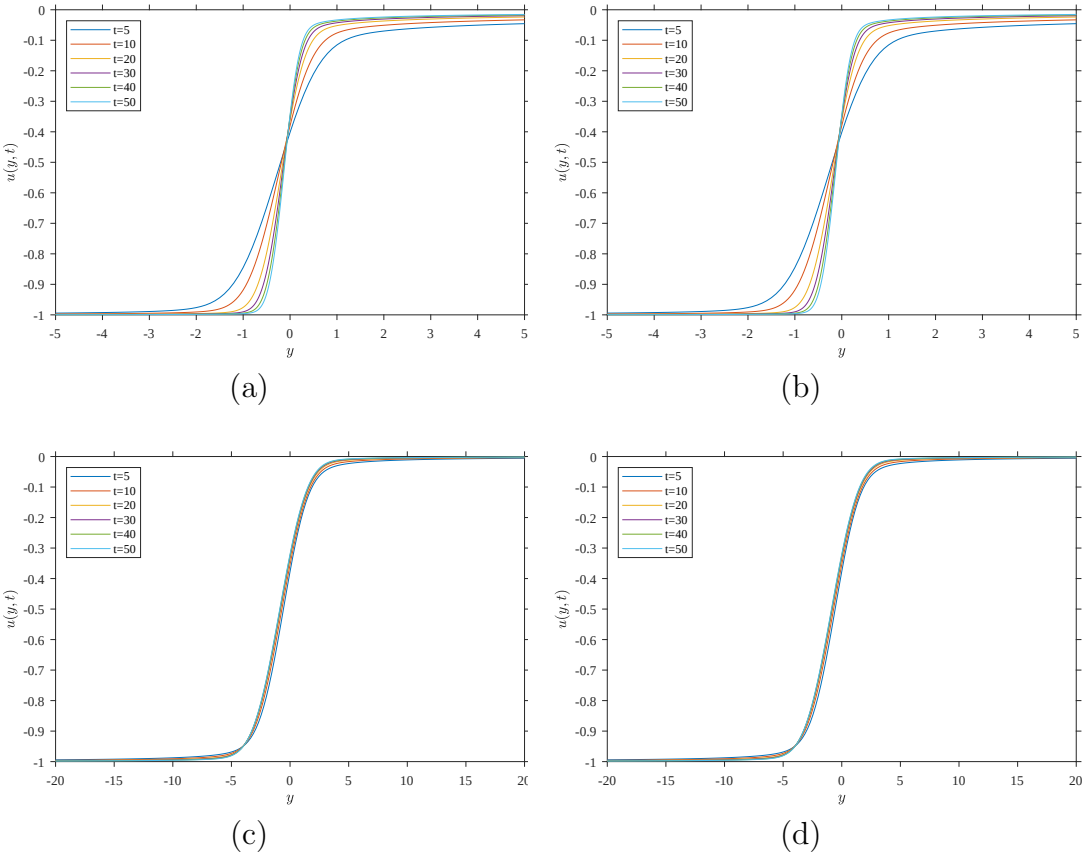

Figure 6: Graphs of the numerical solution of **IVP**$^+$ in the (y, u) plane when $u_+ = 0$ and $u_- = -1$ at times $t = 5,\ 10,\ 20,\ 30,\ 40$ and 50 with (a) $\delta = -0.5$, $\gamma = 0.5$, $\triangle x = 0.5$ and $\triangle t = 0.005$, (b) $\delta = -0.5$, $\gamma = 0.5$, $\triangle x = 0.25$ and $\triangle t = 0.01$, (c) $\delta = -0.5$, $\gamma = 1$, $\triangle x = 0.5$ and $\triangle t = 0.005$ and (d) $\delta = -0.5$, $\gamma = 1$, $\triangle x = 0.25$ and $\triangle t = 0.01$. We note that the numerically computed solutions represent the formation of the similarity solution found by Rudenko and Soluyan [32].

		Temporal convergence	Spatial convergence
	$\delta = -\frac{1}{2}$	$\triangle x = 0.5$ and $\triangle t = 0.005$	$\triangle x = 0.25$ and $\triangle t = 0.01$
	$u_+ = 1$ and $u_- = -1$	1.36×10^{-6}	3.93×10^{-5}
$\gamma = 0.5$	$u_+ = 1$ and $u_- = 0$	2.97×10^{-6}	2.44×10^{-5}
	$u_+ = 0$ and $u_- = -0$	2.97×10^{-6}	2.44×10^{-5}
	$u_+ = 1$ and $u_- = -1$	2.56×10^{-6}	4.36×10^{-6}
$\gamma = 1$	$u_+ = 1$ and $u_- = 0$	3.22×10^{-6}	2.50×10^{-5}
	$u_+ = 0$ and $u_- = -0$	3.22×10^{-6}	2.50×10^{-5}

Table 2: Numerical convergence test between the numerical solutions of $\mathbf{IVP}^+$ with $\triangle x = 0.5$, $\triangle t = 0.01$, the numerical solutions of $\mathbf{IVP}^+$ with $\triangle x = 0.5$, $\triangle t = 0.005$ and the numerical solutions of $\mathbf{IVP}^+$ with $\triangle x = 0.25$, $\triangle t = 0.01$, respectively, when $\delta = -\frac{1}{2}$ at $t = 50$. Values quoted are root mean square error on holding time and space steps respectively.

A.1.3 $-1 < \delta < -\frac{1}{2}$

(a) $u_+ = 1$ and $u_- = -1$

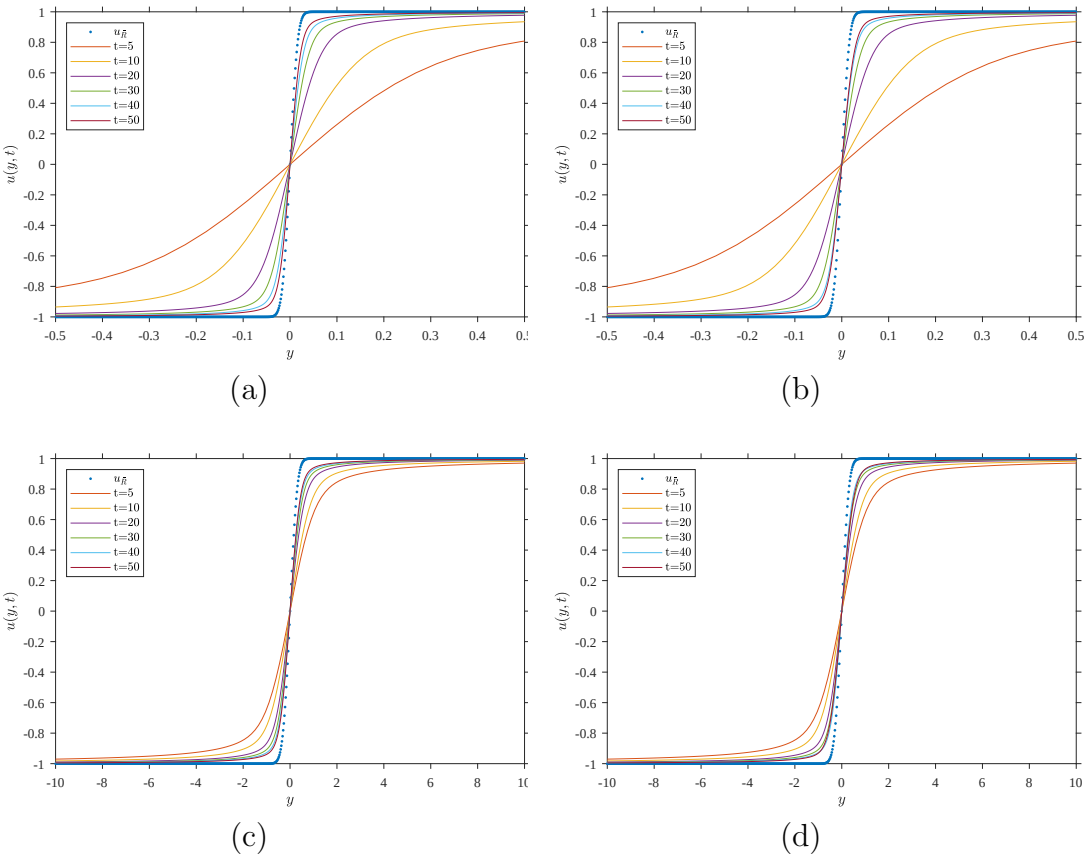

Figure 7: Graphs of the numerical solution of **IVP**$^+$ in the (y, u) plane when $u_+ = 1$ and $u_- = -1$ at times $t = 5,\ 10,\ 20,\ 30,\ 40$ and 50 with (a) $\delta = -0.75$, $\gamma = 0.5$, $\triangle x = 0.5$ and $\triangle t = 0.005$, (b) $\delta = -0.75$, $\gamma = 0.5$, $\triangle x = 0.25$ and $\triangle t = 0.01$, (c) $\delta = -0.75$, $\gamma = 1$, $\triangle x = 0.5$ and $\triangle t = 0.005$ and (d) $\delta = -0.75$, $\gamma = 1$, $\triangle x = 0.25$ and $\triangle t = 0.01$. We note that the numerical solution converges to an error function profile as $t \to \infty$ and the dash line representing the theoretically predicted solution $u_{\overline{R}}$ (3.25) at $t = 50$.

(b) $u_+ = 1$ and $u_- = 0$

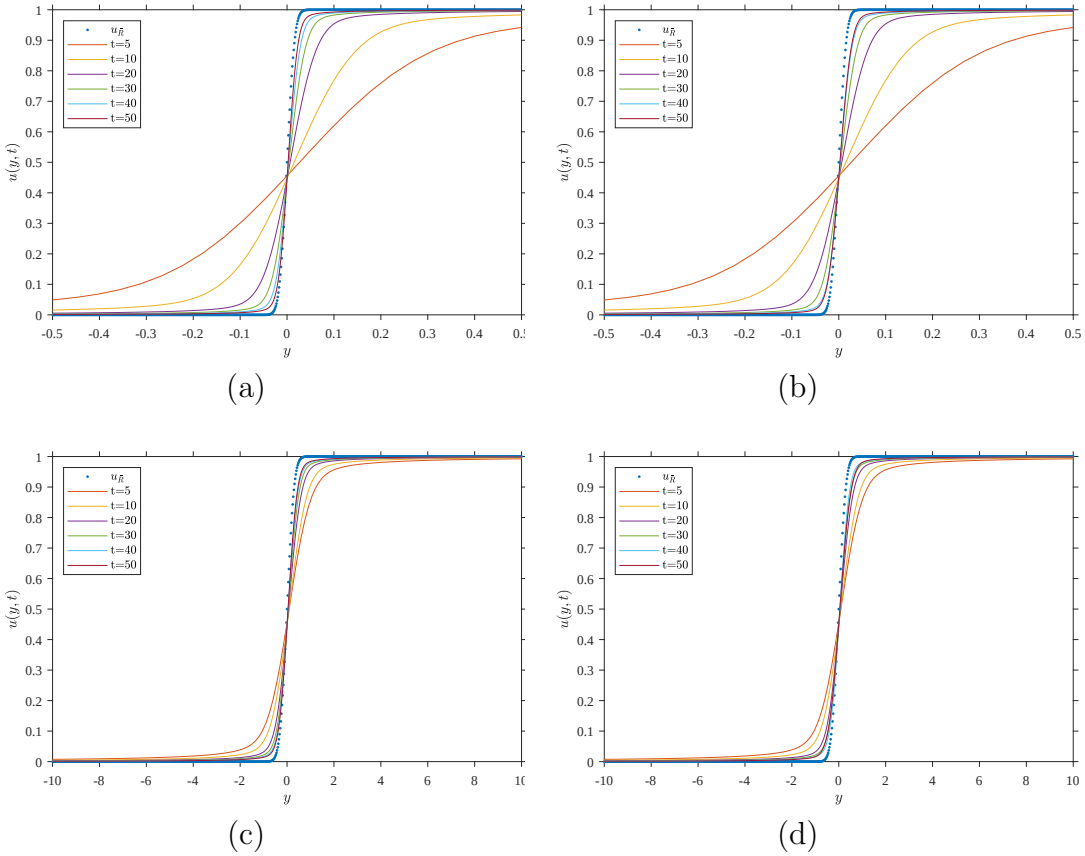

Figure 8: Graphs of the numerical solution of **IVP**$^+$ in the (y, u) plane when $u_+ = 1$ and $u_- = 0$ at times $t = 5,\ 10,\ 20,\ 30,\ 40$ and 50 with (a) $\delta = -0.75$, $\gamma = 0.5$, $\triangle x = 0.5$ and $\triangle t = 0.005$, (b) $\delta = -0.75$, $\gamma = 0.5$, $\triangle x = 0.25$ and $\triangle t = 0.01$, (c) $\delta = -0.75$, $\gamma = 1$, $\triangle x = 0.5$ and $\triangle t = 0.005$ and (d) $\delta = -0.75$, $\gamma = 1$, $\triangle x = 0.25$ and $\triangle t = 0.01$. We note that the numerical solution converges to an error function profile as $t \to \infty$ and the dash line representing the theoretically predicted solution $u_{\overline{R}}$ (3.25) at $t = 50$.

(c) $u_+ = 0$ and $u_- = -1$

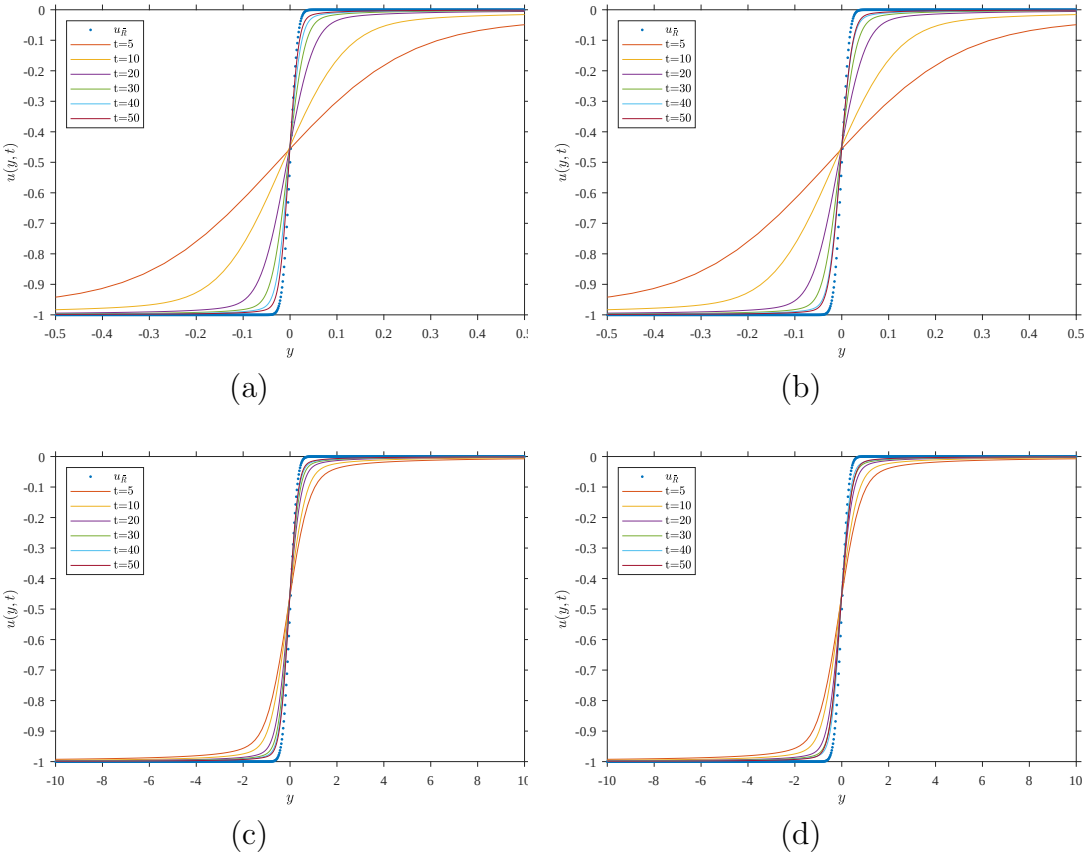

Figure 9: Graphs of the numerical solution of **IVP**$^+$ in the (y, u) plane when $u_+ = 0$ and $u_- = -1$ at times $t = 5,\ 10,\ 20,\ 30,\ 40$ and 50 with (a) $\delta = -0.75$, $\gamma = 0.5$, $\triangle x = 0.5$ and $\triangle t = 0.005$, (b) $\delta = -0.75$, $\gamma = 0.5$, $\triangle x = 0.25$ and $\triangle t = 0.01$, (c) $\delta = -0.75$, $\gamma = 1$, $\triangle x = 0.5$ and $\triangle t = 0.005$ and (d) $\delta = -0.75$, $\gamma = 1$, $\triangle x = 0.25$ and $\triangle t = 0.01$. We note that the numerical solution converges to an error function profile as $t \to \infty$ and the dash line representing the theoretically predicted solution $u_{\overline{R}}$ (3.25) at $t = 50$.

		Temporal convergence	Spatial convergence
	$\delta = -0.75$	$\triangle x = 0.5$ and $\triangle t = 0.005$	$\triangle x = 0.25$ and $\triangle t = 0.01$
	$u_+ = 1$ and $u_- = -1$	1.49×10^{-6}	3.53×10^{-6}
$\gamma = 0.5$	$u_+ = 1$ and $u_- = 0$	3.17×10^{-6}	2.02×10^{-5}
	$u_+ = 0$ and $u_- = -0$	3.42×10^{-6}	2.024×10^{-5}
	$u_+ = 1$ and $u_- = -1$	2.41×10^{-6}	3.86×10^{-6}
$\gamma = 1$	$u_+ = 1$ and $u_- = 0$	3.42×10^{-6}	2.09×10^{-5}
	$u_+ = 0$ and $u_- = -0$	3.42×10^{-6}	2.09×10^{-5}

Table 3: Numerical convergence test between the numerical solutions of $\mathbf{IVP}^+$ with $\triangle x = 0.5$, $\triangle t = 0.01$, the numerical solutions of $\mathbf{IVP}^+$ with $\triangle x = 0.5$, $\triangle t = 0.005$ and the numerical solutions of $\mathbf{IVP}^+$ with $\triangle x = 0.25$, $\triangle t = 0.01$, respectively, when $-1 < \delta < -\frac{1}{2}$ at $t = 50$. Values quoted are root mean square error on holding time and space steps respectively.

Appendix B: Convergence Test of Numerical Solution to the Initial-Value Problem IVP$^-$

The following figures present the numerical solutions of **IVP**$^-$ which both support and illustrate the detailed asymptotic analysis given in the Sections 3.3.1, 3.3.2 and 3.3.3. The numerical simulations were performed using a numerical method outlined in [21] based on the method of explicit finite difference with $N = 100$ where N is the number of grid points time step $\triangle t = 0.01$ and 0.005, and the length $\triangle x = 0.5$ and 0.25. In order to ensure the reliability of our results in Section 3.4, we compare the numerical simulation of **IVP**$^-$ that presented in Section 3.4 to the numerical solutions of **IVP**$^-$ with $\triangle x = 0.5$, $\triangle t = 0.005$ and the numerical solutions of **IVP**$^-$ with $\triangle x = 0.25$, $\triangle t = 0.01$, respectively, at $t = 50$. As well as, the root mean square error have been computed between the previous cases to obtain the temporal and spatial convergence. The values of the temporal and spatial convergence are reported in Table 4, Table 5 and Table 6 for cases $\delta < -\frac{1}{2}$, $\delta = -\frac{1}{2}$ and $-1 < \delta < -\frac{1}{2}$ respectively. Based on Figure 10-18, we observe that we have similar patterns in Sections 3.4.1, 3.4.2 and 3.4.3 when $\delta < -\frac{1}{2}$, $\delta = -\frac{1}{2}$ and $-1 < \delta < -\frac{1}{2}$ respectively, which corroborate the above results in Section 3.4.

B.2.1 $\delta > -\frac{1}{2}$

(a) $u_+ = -1$ and $u_- = 1$

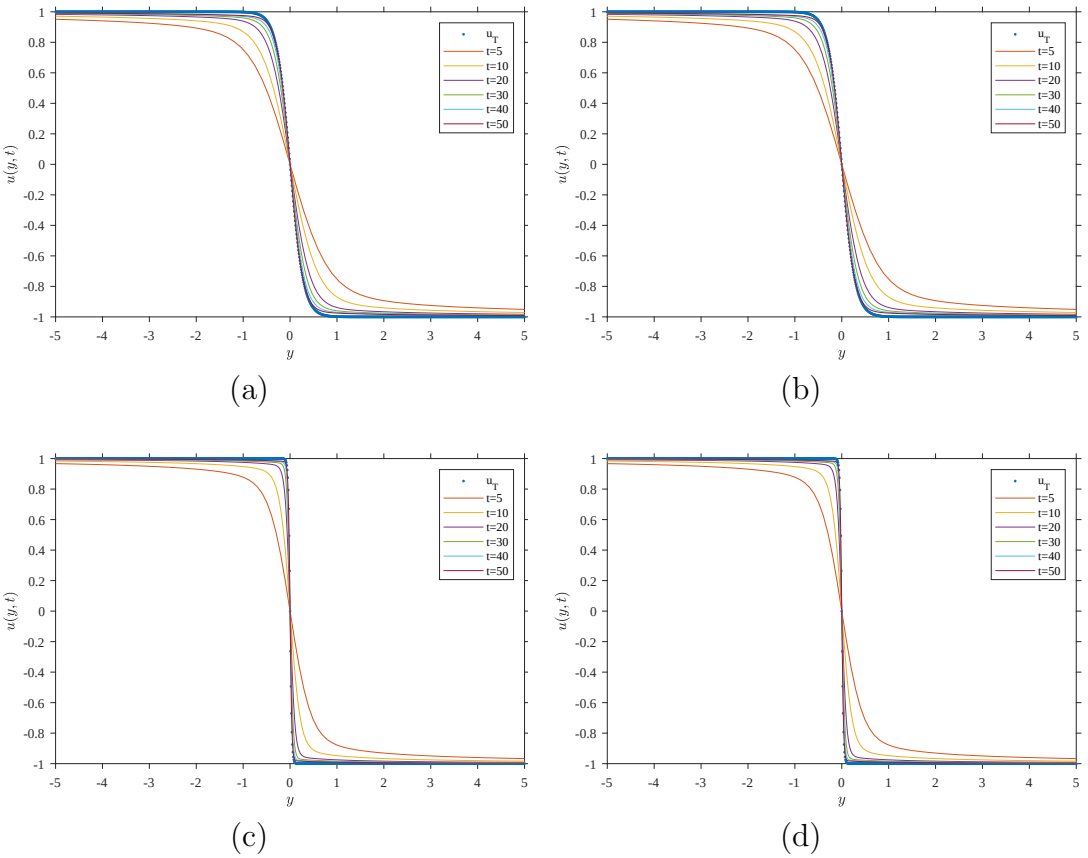

Figure 10: Graphs of the numerical solution of **IVP**$^-$ in the (y, u) plane when $u_+ = -1$ and $u_- = 1$ at times $t = 5,\ 10,\ 20,\ 30,\ 40$ and 50 with (a) $\delta = -0.25$, $\gamma = 1$, $\triangle x = 0.5$ and $\triangle t = 0.005$, (b) $\delta = -0.25$, $\gamma = 1$, $\triangle x = 0.25$ and $\triangle t = 0.01$, (c) $\delta = 0.01$, $\gamma = 1$, $\triangle x = 0.5$ and $\triangle t = 0.005$ and (d) $\delta = 0.01$, $\gamma = 1$, $\triangle x = 0.25$ and $\triangle t = 0.01$. We note that the numerical solution converges to Taylor shock wave as $t \to \infty$ and the dash line representing the theoretically predicted solution u_T (3.24) at $t = 50$.

(b) $u_+ = 0$ and $u_- = 1$

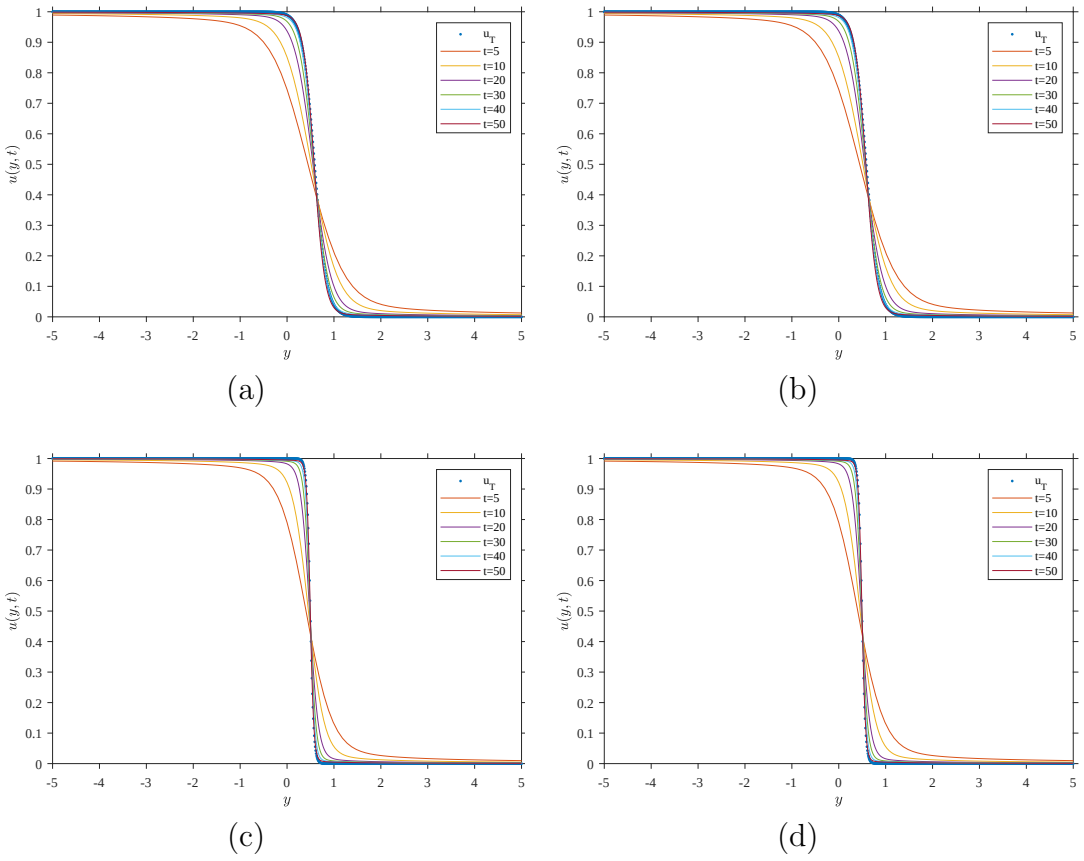

Figure 11: Graphs of the numerical solution of **IVP**$^-$ in the (y, u) plane when $u_+ = 0$ and $u_- = 1$ at times $t = 5,\ 10,\ 20,\ 30,\ 40$ and 50 with (a) $\delta = -0.25$, $\gamma = 1$, $\triangle x = 0.5$ and $\triangle t = 0.005$, (b) $\delta = -0.25$, $\gamma = 1$, $\triangle x = 0.25$ and $\triangle t = 0.01$, (c) $\delta = 0.01$, $\gamma = 1$, $\triangle x = 0.5$ and $\triangle t = 0.005$ and (d) $\delta = 0.01$, $\gamma = 1$, $\triangle x = 0.25$ and $\triangle t = 0.01$. We note that the numerical solution converges to Taylor shock wave as $t \to \infty$ and the dash line representing the theoretically predicted solution u_T (3.24) at $t = 50$.

(c) $u_+ = -1$ and $u_- = 0$

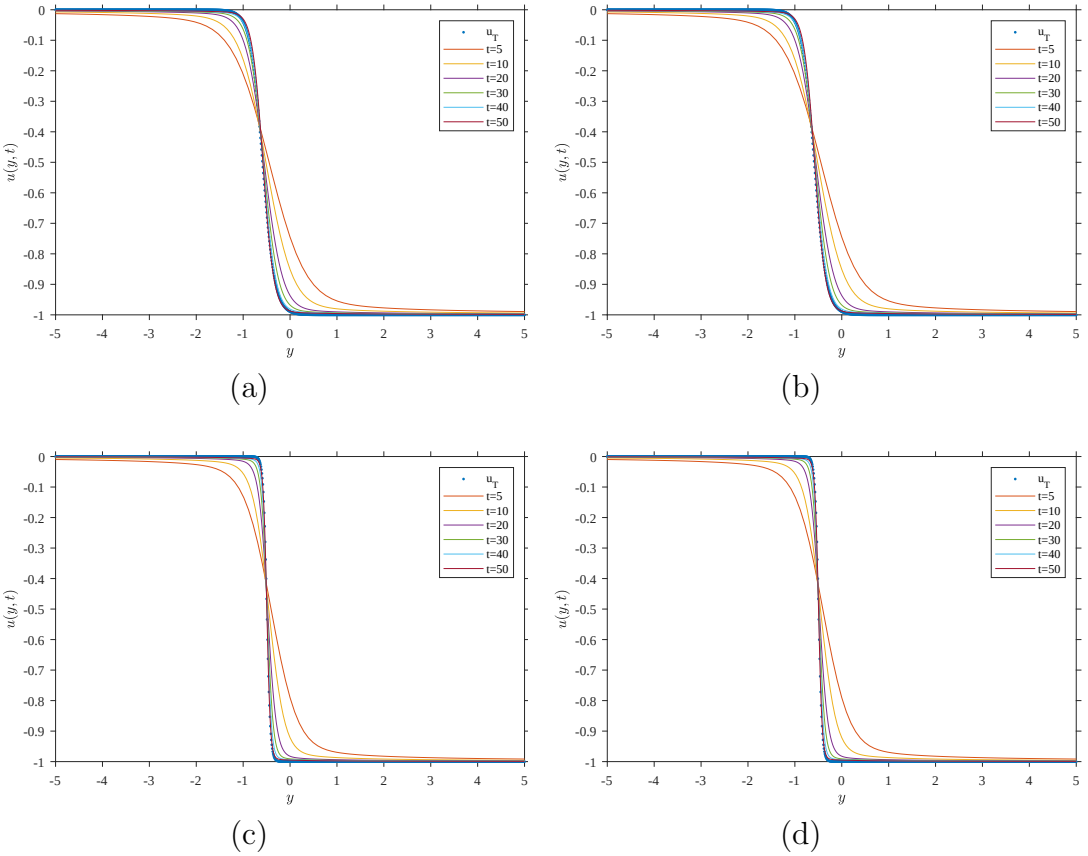

Figure 12: Graphs of the numerical solution of **IVP**$^-$ in the (y, u) plane when $u_+ = -1$ and $u_- = 0$ at times $t = 5,\ 10,\ 20,\ 30,\ 40$ and 50 with (a) $\delta = -0.25$, $\gamma = 1$, $\triangle x = 0.5$ and $\triangle t = 0.005$, (b) $\delta = -0.25$, $\gamma = 1$, $\triangle x = 0.25$ and $\triangle t = 0.01$, (c) $\delta = 0.01$, $\gamma = 1$, $\triangle x = 0.5$ and $\triangle t = 0.005$ and (d) $\delta = 0.01$, $\gamma = 1$, $\triangle x = 0.25$ and $\triangle t = 0.01$. We note that the numerical solution converges to Taylor shock wave as $t \to \infty$ and the dash line representing the theoretically predicted solution u_T (3.24) at $t = 50$.

		Temporal convergence	Spatial convergence
	$\gamma = 1$	$\triangle x = 0.5$ and $\triangle t = 0.005$	$\triangle x = 0.25$ and $\triangle t = 0.01$
	$u_+ = -1$ and $u_- = 1$	3.37×10^{-7}	2.14×10^{-6}
$\delta = -0.25$	$u_+ = 0$ and $u_- = 1$	3.32×10^{-6}	4.14×10^{-5}
	$u_+ = -1$ and $u_- = 0$	3.32×10^{-6}	4.14×10^{-5}
	$u_+ = -1$ and $u_- = 1$	7.09×10^{-8}	1.44×10^{-6}
$\delta = 0.01$	$u_+ = 0$ and $u_- = -1$	8.39×10^{-6}	8.83×10^{-5}
	$u_+ = -1$ and $u_- = 0$	8.39×10^{-6}	8.83×10^{-5}

Table 4: Numerical convergence test between the numerical solutions of $\mathbf{IVP}^-$ with $\triangle x = 0.5$, $\triangle t = 0.01$, the numerical solutions of $\mathbf{IVP}^-$ with $\triangle x = 0.5$, $\triangle t = 0.005$ and the numerical solutions of $\mathbf{IVP}^-$ with $\triangle x = 0.25$, $\triangle t = 0.01$, respectively, when $\delta > -\frac{1}{2}$ and $\gamma = 1$ at $t = 50$. Values quoted are root mean square error on holding time and space steps respectively.

B.2.2 $\delta = -\frac{1}{2}$

(a) $u_+ = -1$ and $u_- = 1$

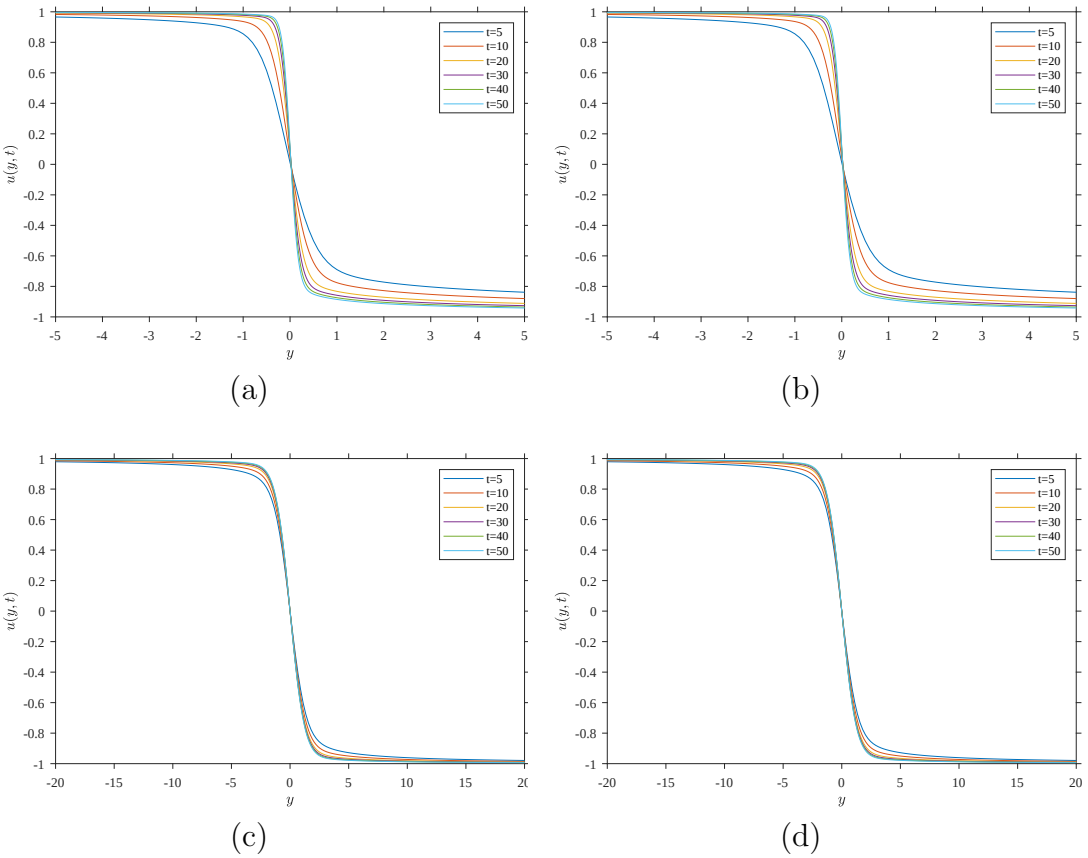

Figure 13: Graphs of the numerical solution of **IVP**$^-$ in the (y, u) plane when $u_+ = -1$ and $u_- = 1$ at times $t = 5,\ 10,\ 20,\ 30,\ 40$ and 50 with (a) $\delta = -0.5$, $\gamma = 0.5$, $\triangle x = 0.5$ and $\triangle t = 0.005$, (b) $\delta = -0.5$, $\gamma = 0.5$, $\triangle x = 0.25$ and $\triangle t = 0.01$, (c) $\delta = -0.5$, $\gamma = 1$, $\triangle x = 0.5$ and $\triangle t = 0.005$ and (d)$\delta = -0.5$, $\gamma = 1$, $\triangle x = 0.25$ and $\triangle t = 0.01$. We note that the numerically computed solutions represent the formation of the similarity solution found by Rudenko and Soluyan [32].

(b) $u_+ = 0$ and $u_- = 1$

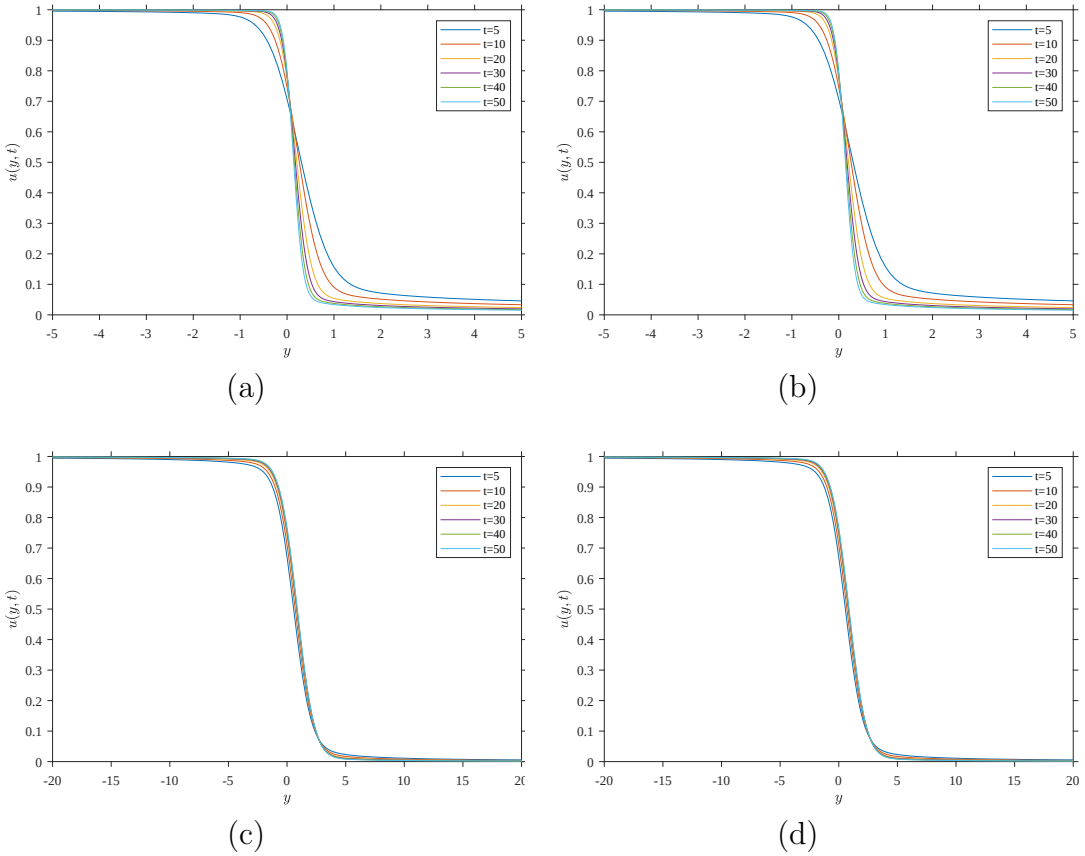

Figure 14: Graphs of the numerical solution of **IVP**$^-$ in the (y, u) plane when $u_+ = 0$ and $u_- = 1$ at times $t = 5,\ 10,\ 20,\ 30,\ 40$ and 50 with (a) $\delta = -0.5$, $\gamma = 0.5$, $\triangle x = 0.5$ and $\triangle t = 0.005$, (b) $\delta = -0.5$, $\gamma = 0.5$, $\triangle x = 0.25$ and $\triangle t = 0.01$, (c) $\delta = -0.5$, $\gamma = 1$, $\triangle x = 0.5$ and $\triangle t = 0.005$ and (d)$\delta = -0.5$, $\gamma = 1$, $\triangle x = 0.25$ and $\triangle t = 0.01$. We note that the numerically computed solutions represent the formation of the similarity solution found by Rudenko and Soluyan [32].

(c) $u_+ = -1$ and $u_- = 0$

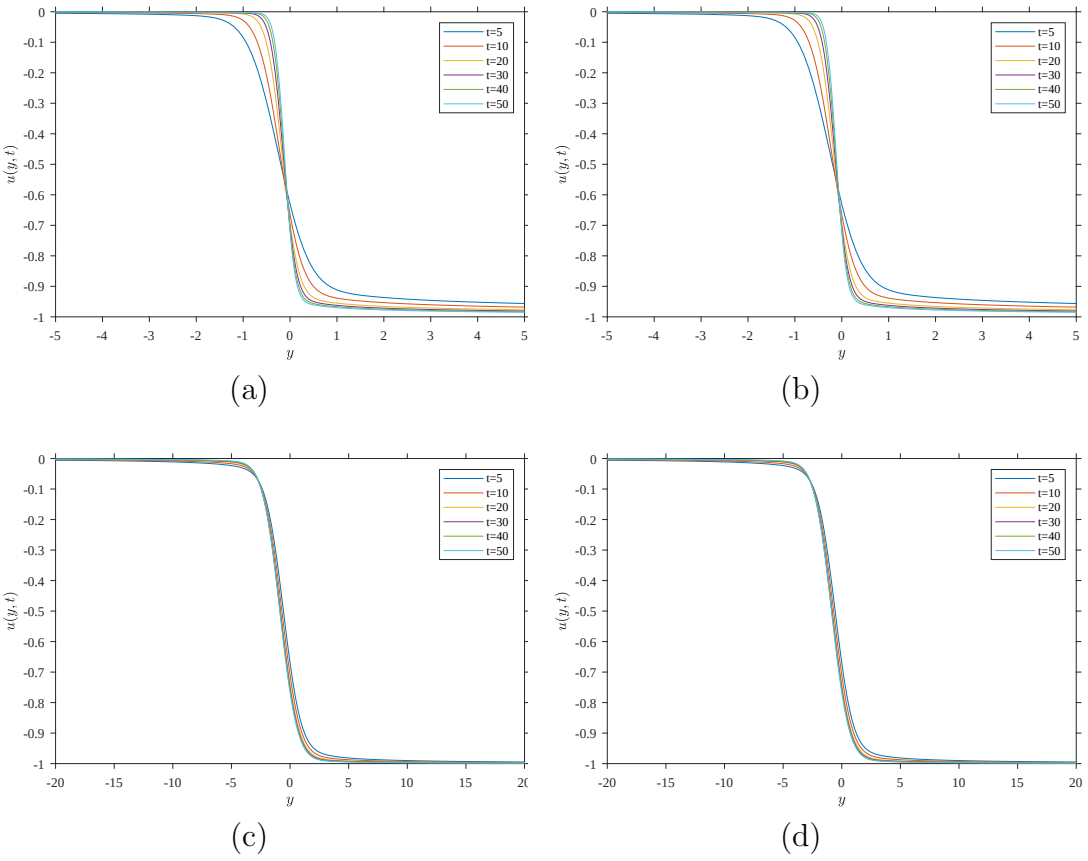

Figure 15: Graphs of the numerical solution of **IVP**$^-$ in the (y, u) plane when $u_+ = -1$ and $u_- = 0$ at times $t = 5,\ 10,\ 20,\ 30,\ 40$ and 50 with (a) $\delta = -0.5$, $\gamma = 0.5$, $\triangle x = 0.5$ and $\triangle t = 0.005$, (b) $\delta = -0.5$, $\gamma = 0.5$, $\triangle x = 0.25$ and $\triangle t = 0.01$, (c) $\delta = -0.5$, $\gamma = 1$, $\triangle x = 0.5$ and $\triangle t = 0.005$ and (d)$\delta = -0.5$, $\gamma = 1$, $\triangle x = 0.25$ and $\triangle t = 0.01$. We note that the numerically computed solutions represent the formation of the similarity solution found by Rudenko and Soluyan [32].

		Temporal convergence	Spatial convergence
	$\delta = -\frac{1}{2}$	$\triangle x = 0.5$ and $\triangle t = 0.005$	$\triangle x = 0.25$ and $\triangle t = 0.01$
	$u_+ = -1$ and $u_- = 1$	4.28×10^{-7}	2.49×10^{-6}
$\gamma = 0.5$	$u_+ = 0$ and $u_- = 1$	3.26×10^{-6}	2.37×10^{-5}
	$u_+ = -1$ and $u_- = 0$	2.99×10^{-6}	2.37×10^{-5}
	$u_+ = -1$ and $u_- = 1$	4.52×10^{-7}	2.77×10^{-6}
$\gamma = 1$	$u_+ = 0$ and $u_- = 1$	3.24×10^{-6}	2.41×10^{-5}
	$u_+ = -1$ and $u_- = 0$	3.24×10^{-6}	2.41×10^{-5}

Table 5: Numerical convergence test between the numerical solutions of $\mathbf{IVP}^-$ with $\triangle x = 0.5$, $\triangle t = 0.01$, the numerical solutions of $\mathbf{IVP}^-$ with $\triangle x = 0.5$, $\triangle t = 0.005$ and the numerical solutions of $\mathbf{IVP}^-$ with $\triangle x = 0.25$, $\triangle t = 0.01$, respectively, when $\delta = -\frac{1}{2}$ at $t = 50$. Values quoted are root mean square error on holding time and space steps respectively.

B.2.3 $-1 < \delta < -\frac{1}{2}$

(a) $u_+ = -1$ and $u_- = 1$

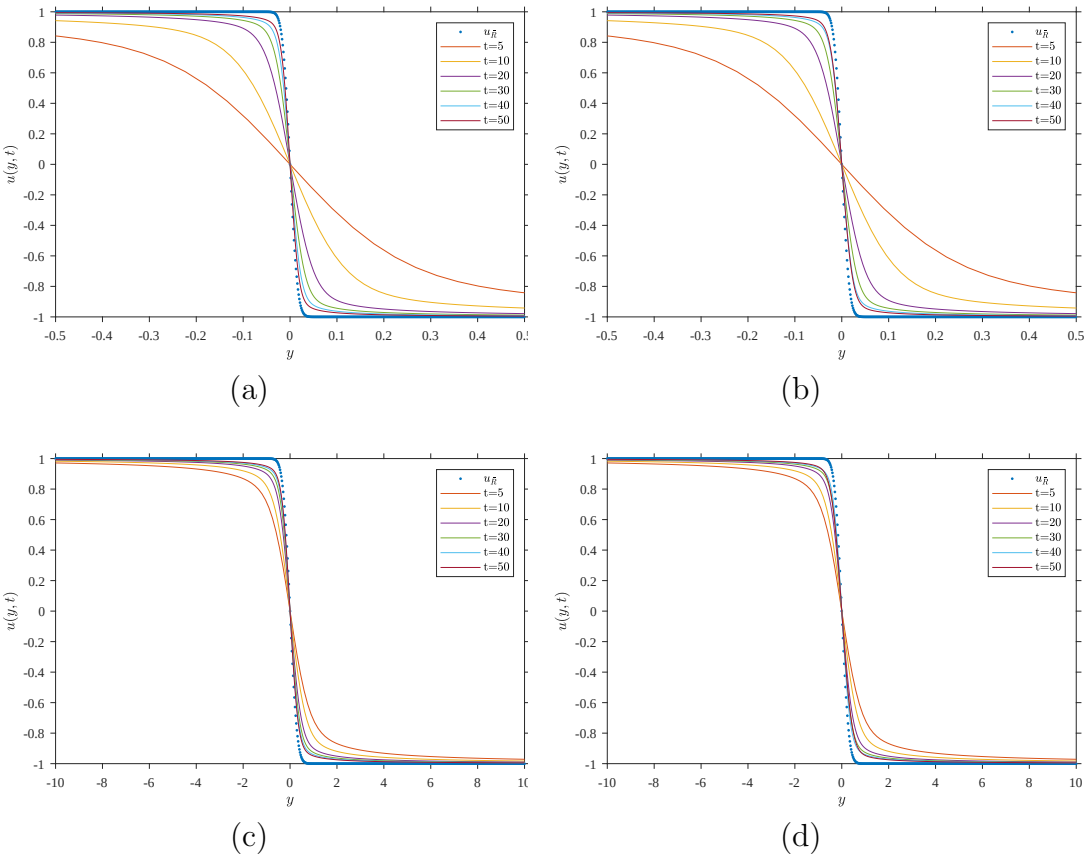

Figure 16: Graphs of the numerical solution of **IVP**$^-$ in the (y, u) plane when $u_+ = -1$ and $u_- = 1$ at times $t = 5,\ 10,\ 20,\ 30,\ 40$ and 50 with (a) $\delta = -0.75$, $\gamma = 0.5$, $\triangle x = 0.5$ and $\triangle t = 0.005$, (b) $\delta = -0.75$, $\gamma = 0.5$, $\triangle x = 0.25$ and $\triangle t = 0.01$, (c) $\delta = -0.75$, $\gamma = 1$, $\triangle x = 0.5$ and $\triangle t = 0.005$ and (d)$\delta = -0.75$, $\gamma = 1$, $\triangle x = 0.25$ and $\triangle t = 0.01$. We note that the numerical solution converges to an error function profile as $t \to \infty$ and the dash line representing the theoretically predicted solution $u_{\overline{R}}$ (3.25) at $t = 50$.

(a) $u_+ = 0$ and $u_- = 1$

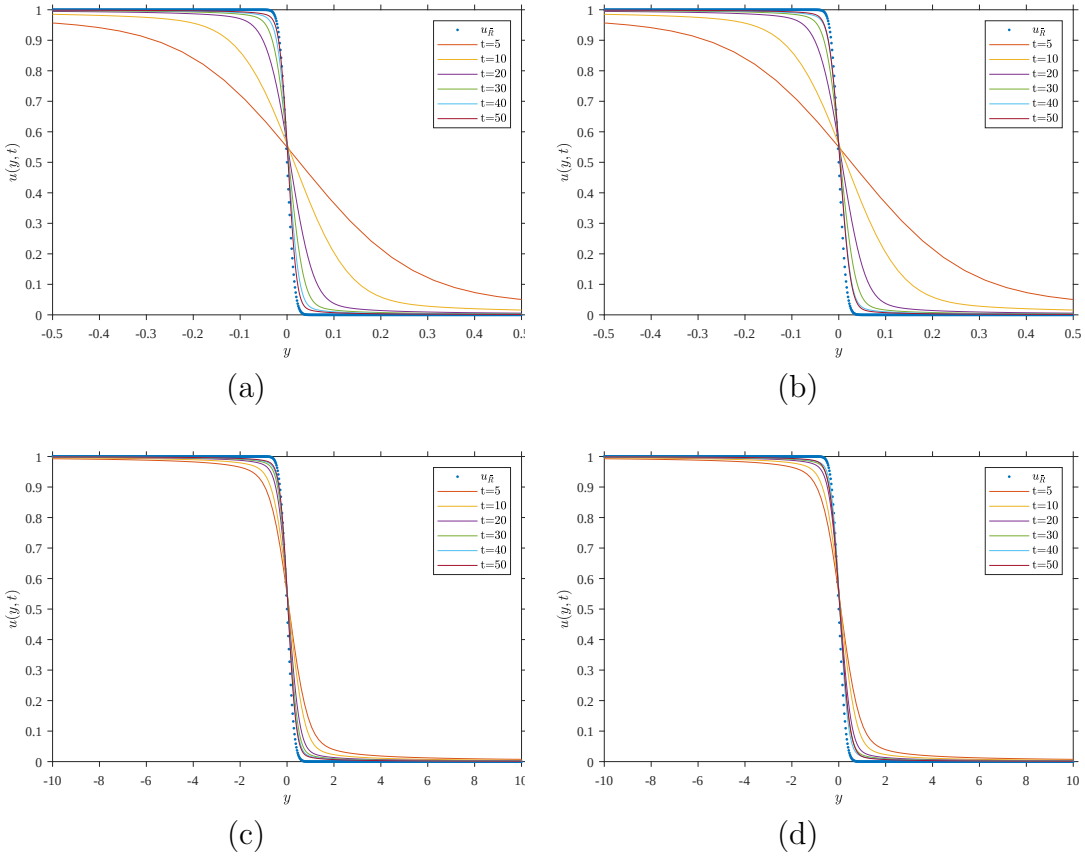

Figure 17: Graphs of the numerical solution of **IVP**$^-$ in the (y, u) plane when $u_+ = 0$ and $u_- = 10$ at times $t = 5,\ 10,\ 20,\ 30,\ 40$ and 50 with (a) $\delta = -0.75$, $\gamma = 0.5$, $\triangle x = 0.5$ and $\triangle t = 0.005$, (b) $\delta = -0.75$, $\gamma = 0.5$, $\triangle x = 0.25$ and $\triangle t = 0.01$, (c) $\delta = -0.75$, $\gamma = 1$, $\triangle x = 0.5$ and $\triangle t = 0.005$ and (d)$\delta = -0.75$, $\gamma = 1$, $\triangle x = 0.25$ and $\triangle t = 0.01$. We note that the numerical solution converges to an error function profile as $t \to \infty$ and the dash line representing the theoretically predicted solution $u_{\overline{R}}$ (3.25) at $t = 50$.

(a) $u_+ = -1$ and $u_- = 0$

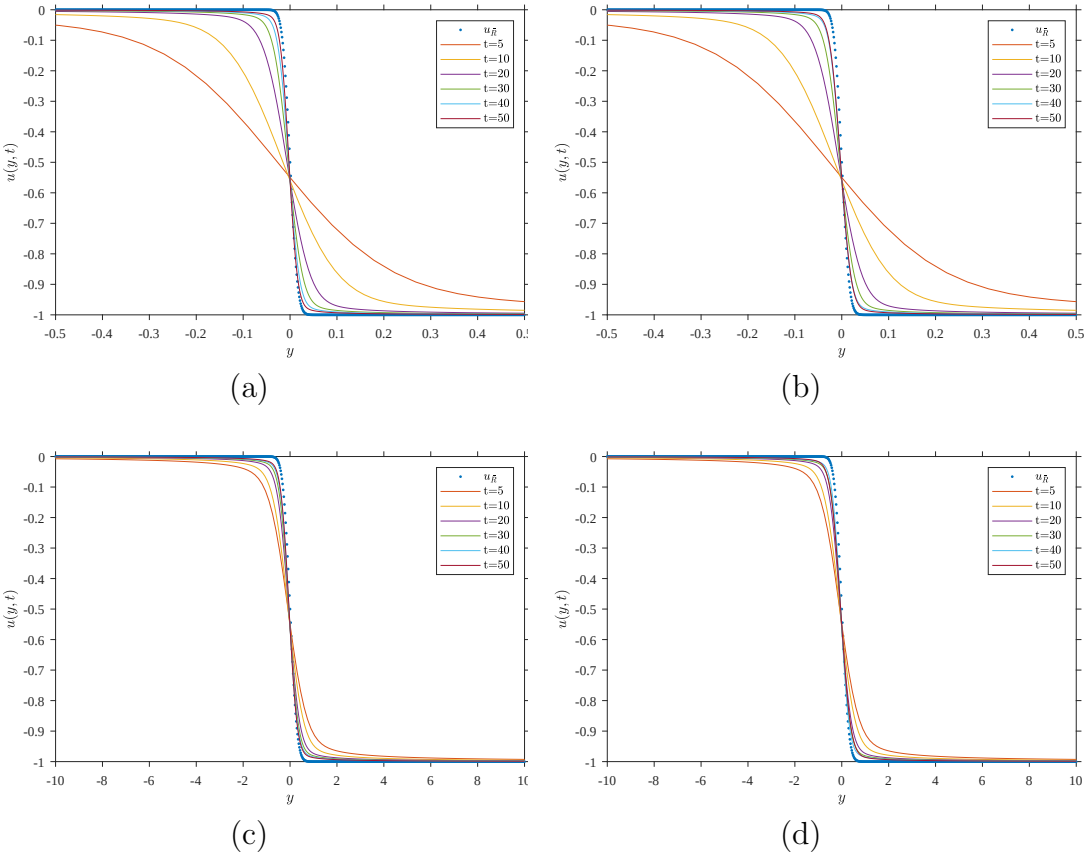

Figure 18: Graphs of the numerical solution of **IVP**$^-$ in the (y, u) plane when $u_+ = -1$ and $u_- = 0$ at times $t = 5,\ 10,\ 20,\ 30,\ 40$ and 50 with (a) $\delta = -0.75$, $\gamma = 0.5$, $\triangle x = 0.5$ and $\triangle t = 0.005$, (b) $\delta = -0.75$, $\gamma = 0.5$, $\triangle x = 0.25$ and $\triangle t = 0.01$, (c) $\delta = -0.75$, $\gamma = 1$, $\triangle x = 0.5$ and $\triangle t = 0.005$ and (d)$\delta = -0.75$, $\gamma = 1$, $\triangle x = 0.25$ and $\triangle t = 0.01$. We note that the numerical solution converges to an error function profile as $t \to \infty$ and the dash line representing the theoretically predicted solution $u_{\overline{R}}$ (3.25) at $t = 50$.

		Temporal convergence	Spatial convergence
	$\delta = -0.75$	$\triangle x = 0.5$ and $\triangle t = 0.005$	$\triangle x = 0.25$ and $\triangle t = 0.01$
	$u_+ = -1$ and $u_- = 1$	3.44×10^{-7}	2.87×10^{-6}
$\gamma = 0.5$	$u_+ = 0$ and $u_- = -1$	3.55×10^{-6}	1.9×10^{-5}
	$u_+ = -1$ and $u_- = 0$	3.28×10^{-6}	1.9×10^{-5}
	$u_+ = -1$ and $u_- = 1$	6.85×10^{-7}	3.12×10^{-6}
$\gamma = 1$	$u_+ = 0$ and $u_- = -1$	3.54×10^{-6}	1.95×10^{-5}
	$u_+ = -1$ and $u_- = 0$	3.54×10^{-5}	1.95×10^{-5}

Table 6: Numerical convergence test between the numerical solutions of $\mathbf{IVP}^-$ with $\triangle x = 0.5$, $\triangle t = 0.01$, the numerical solutions of $\mathbf{IVP}^-$ with $\triangle x = 0.5$, $\triangle t = 0.005$ and the numerical solutions of $\mathbf{IVP}^-$ with $\triangle x = 0.25$, $\triangle t = 0.01$, respectively, when $-1 < \delta < -\frac{1}{2}$ at $t = 50$. Values quoted are root mean square error on holding time and space steps respectively.

References

[1] M Abramowitz and I Stegun. *Handbook of Mathematical Functions*. National Bureau of Standards, New York, 1965.

[2] S Albeverio, A Korshunova, and O Rozanova. A probabilistic model associated with the pressureless gas dynamics. *Bull. Sci. Math.*, 137:902–922, 2013.

[3] FB Ali Suliman, JA Leach, and DJ Needham. The large-time solution of Burgers' equation with time- dependent coefficients II. algebraic coefficients. *Studies in Applied Mathematics*, 137(3):273–305, 2016.

[4] WF Ames. *Nonlinear Partial Differential Equations*. Academic Press, New York, 1972.

[5] A Asaithambi. Numerical solution of the Burgers' equation by automatic differentiation. *Applied Mathematices and Computation*, 137:2700–2708, 2010.

[6] H Bateman. Some recent researches on the motion of fluids. *Mon. Weather Rev.*, 43:163–170, 1915.

[7] SA Büyükasık and OK Pashaev. Exact solutions of forced Burgers' equations with time variable coefficients. *Communications in Nonlinear Science and Numerical Simulation*, 18(7):1635–1651, 2013.

[8] E Benton and GW Platzman. A table of solutions of the one-dimensional Burgers' equations. *Quart. Appl. Math.*, 30(1):195–212, 1972.

[9] H Berestycki, S Kamin, and G Sivashinsky. Nonlinear dynamics and metastability in a Burgers type equation (for upward propagating flames). *C. R. Acad. Sci. Paris Sér. I Math.*, 321(2):185–190, 1995.

[10] JM Burgers. A mathematical model illustrating the theory of turbulence. *Adv. Appl. Mech.*, 1:171–199, 1948.

[11] JD Cole. On a quasi-linear parabolic equations occurring in aerodynamics. *Quart. Appl. Math.*, 9(3):225–236, 1951.

[12] DG Creighton. *Basic theoretical nonlinear acoustics, Frontiers in Physical Acoustics (D. Sette, ed).* North-Holland, Amsterdam, 1986.

[13] DG Creighton and JF Scott. : Asymptotic solutions of model equations in nonlinear acoustics. *Phil. Trans. R. Soc. Lond*, A292:101–134, 1979.

[14] BO Enflo and OV Rudenko. To the theory of generalized Burgers' equations. *Acta. Acust.*, 88:1–8, 2004.

[15] E HANAÇ. *The Large-Time Solution Of Nonlinear Evolution Equations.* University of Birmingham, Ph.D Thesis, 2015.

[16] N Hayashi and PI Naumkin. Asymptotics for the Burgers equation with pumping. *Comm. Math. Phys.*, 239:287–307, 2003.

[17] E Hopf. The partial differential equation $u_t + uu_x = \mu u_{xx}$. *Comm. Pure App. Math.*, 3:201–230, 1950.

[18] M Kardar, G Parisi, and YC Zhang. Dynamical scaling of growing interfaces. *Phys. Rev. Lett.*, 56:889–892, 1986.

[19] L Kofman and AC Raga. Modeling structures of knots in jet flows with the Burgers equation. *Astrophysical Journal*, 390:359–364, 1992.

[20] S Kutluay, AR Bahadir, and A Ozdes. Numerical solution of one-dimensional Burgers equation: explicit and exact-explicit finite difference methods. *J. Comput. Appl. Math.*, 103:251–261, 1999.

[21] M Landajuela. *Burgers Equation, BCAM intership report.* Basque center for applied mathematics, 2011.

[22] RW Lardner and JC Arya. Two generalisations of Burgers' equation. *Acta Mech.*, 37:179–190, 1980.

[23] JA Leach. The large-time solution of Burgers' equation with variable coefficients. I: Exponential coefficients. *Stud. App. Math.*, 136:163–188, 2015.

[24] JA Leach and DJ Needham. *Matched Asymptotic Expansions in Reaction-Diffusion Theory*. Springer Monographs in Mathematics, New York, 2003.

[25] JA Leach and DJ Needham. The large-time development of the solution to an initial-value problem for the Korteweg-de Vries equation: I. Initial data has a discontinuous expansion step. *Nonlinearity*, 21:2391–2408, 2008.

[26] JA Leach and DJ Needham. The large-time development of the solution to an initial-value problem for the Korteweg-de Vries equation: II. Initial data has a discontinuous compress step. *Mathematika*, 60:391–414, 2014.

[27] DJ Mittal and RK Jain. Numerical solutions of nonlinear Burgers' equation with modified cubic b-splines collocation method. *Applied Mathematices and Computation*, 218:7839–7855, 2012.

[28] JJC Nimmo and DG Crighton. Backlund transformations for nonlinear parabolic equations: The general results. *Proc. R. Soc. Lond.*, 37:179–190, 1980.

[29] JJC Nimmo and DG Crighton. Geometrical and diffusive effects in nonlinear acoustic propagation over long ranges. *Proc. R. Soc. Lond.*, A320:1–35, 1986.

[30] R Peralta-Fabi and P Plaschko. Bifurcation of solutions to the controlled Burgers' equation. *Acta Mechanica*, 96:155–161, 1993.

[31] LA Pospelov. Propagation of finite-amplitude elastic waves. *Sov. Phys.*, 11:302–304, 1966.

[32] OV Rudenko and SI Soluyan. *Theoretical Foundations of Nonlinear acoustics (English translation by Robert T. Beyer)*. Consultants Bureau, Plenum, New York, 1977.

[33] PL Sadchev, KRC Nair, and VG Tikekar. Generalized Burgers equations and Eule-Painleve transcendents I. *J. Math. Phys.*, 27(6):1506–1522, 1986.

[34] PL Sadchev, KRC Nair, and VG Tikekar. Generalized Burgers equations and Eule-Painleve transcendents II. *J. Math. Phys.*, 28(5):997–1004, 1987.

[35] A Schulze-Halberg. Burgers' equation with time-dependent coefficients and nonlinear forcing term: Linearization and exact solvability. *Commun Nonlinear Sci Numer Simulat*, 22:1068–1083, 2015.

[36] JF Scott. The long time asymptotics of solutions to the generalized Burgers equation. *Proc. R. Soc. Lond. A*, 373(1755):443–456, 1981.

[37] PN Sionoid and AT Cates. The generalized Burgers and Zabolotskaya-Khokhlov equations: Transformations, exact solutions and qualitative properties. *Proc. R. Soc. Lond.*, A447:253–270, 1994.

[38] GI Taylor. The conditions necessary for discontinuous motion in gases. *Proc. Roy. Soc.*, 84:371–377, 1910.

[39] JW Thomas. *Numerical Partial Differential Equations: Finite Difference Methods.* Springer Science+ Business Media, USA, 1995.

[40] M Van Dyke. *Perturbation Methods in Fluid Mechanics.* Parabolic Press, Stanford CA, 1975.

[41] E Varoglu and WDL Finn. Space-time finite elements incorporating characteristics for the Burgers' equation. *Int. J. Numer. Methods Eng.*, 16:171–184, 1980.

[42] RM Velasco and P Saavedra. A first order model in traffic flow. *Physica D: Nonlinear Phenomena,*, 228(2):153–158, 2007.

[43] WS Vorus. The solution of Burgers' equation for sinusoidal excitation at the up-stream boundary. *Eng. Math.*, 23:219–237, 1989.

[44] S Watanabe, S Ishiwata, K Kawamura, and HG Oh. Higher order solution of nonlinear waves. II. shock wave described by Burgers equation. *J. Phys. Soc. Jpn.*, 66:984–987, 1997.

[45] JM Weiss, JM Tabor, and G Carnevale. The Painleve property of partial differential equations. *J. Math. Phys.*, 24:522–526, 1983.

[46] GB Whitham. *Linear and Nonlinear Waves*. Wiley-Interscience, New York, 1975.